AHMADU BELLO UNIVERSITY, ZARIA

DEPARTMENT OF ELECTRICAL ENGINEERING

STUDY OF NTV - JOS SIGNAL RECEPTION IN ZARIA

BY

ONYEDI DAVID OYEDUM

B.Sc. (HONS)

Being a thesis presented in partial fulfillment
for the award of M.Sc. (Eng.) Degree.

June, 1982

D E D I C A T I O N

To all those who deny self in research
for the benefit of mankind.

ACKNOWLEDGEMENT

The contribution of Dr. E.B. Ojeba (my supervisor) and his personal involvement in this programme is too much for even a modest appraisal to be contained in the limited space here; one can only concede, without reservations, that without him this work would neither have been started, nor see a worthy completion. The opportunity to work with him will always remain an inspiration, and I look forward to making the best use of same.

Also impressive is the role played by Dr. M.F. Bracey, who assisted in the supervision of this research project. His down-to-earth approach to giving me the necessary background for the development of the amplifier, his efforts to secure some of the components used, and his most energetic editting of the first draft of this thesis are all appreciated.

I would like, too, to appreciate the administrative steps taken by Professor B.G. Bajoga (the Head of Department) to see me successfully through this programme, and without excessive financial burden. And Mr. M.L. Okupe who typed this thesis will always be remembered for a job well done.

Also appreciated are the ever ready assistance of Mr. P.F.U. Taylor, Mr. L. Adikwu, Messrs E.O. Okoro and Mr. W.N. Ekemezie of the Computer Centre (A.B.U.), and the provision of funds for the purchase of the research equipment

by the Ahmadu Bello University Board of Research Grant; the co-operation of the Nigerian Meteorological Office, Lagos, for furnishing the rainfall data for Jos and Zaria, and that of the NTV Jos management, for providing the daily transmitted power data. Messrs O.T. Ifedigbo and R. Okeakpu will also be remembered for their help towards alleviating my problems during this exercise.

In all,the sacrifice made by my closest relations (especially my aged parents and my elder brother - Mr. N.A. Oyedum) in connection with this exercise remains supreme, and I look forward to its vindication which will signify the triumph of my MIND over my flesh.

- O.D. Oyedum.

TABLE OF CONTENTS

		Page
Title/Approval Page	... ...	i
Dedication ...	... ...	ii
Acknowledgement	... ...	iii
Table of Contents	... ...	v
List of Tables	... ...	viii
List of Figures	... ...	ix
Appendices and Plates	... ...	xii
Introduction	... ...	1
Chapter One: Propagation of TV and FM Signals	...	4
1.1 The Earth's Surface	... ...	4
1.2 The Troposphere ...	... ...	8
1.3 Some Characteristics and Potential Use of the V.H.F./U.H.F. Bands for TV and FM Transmission		10
Chapter Two: Propagation of Television Signals Beyond The Horizon	... ...	12
2.1 Effect of Terrain on Transhorizon Propagation		15
2.2 Effect of The Troposphere on Transhorizon Propagation	... ...	21
2.2.1 Tropospheric Refraction	... ...	23
2.2.2 Tropospheric Scattering	... ...	23
2.2.3 Tropospheric Reflection	... ...	26
2.2.4 Some Other Factors Relating to Transhorizon Propagation	... ...	31

		Page
Chapter Three:	Data Collection and Compilation ...	33
3.1	Data Compilation	33
3.1.1	Instruments Used For Field Strength Measurements	33
3.1.2	Recording of Field Strength	35
3.1.3	Data Transcription From Analogue to Digital Form	36
3.1.4	Rainfall And Transmitter Power Data ...	39
3.2	Data Compilation Into The Computer ...	40
3.2.1	The Computer Input Format	40
3.2.2.	Data Standardization	41
Chapter Four:	The Analysis of Field Strength Data Collected July 1979 - July 1980 ...	44
4.1	Hourly Median of Signal Level	45
4.2	Daily Median of Signal Level	64
4.3	Monthly Median of Signal Level	82
4.4	Cumulative Distribution of Signal Levels ...	82
4.5	Some Implications of The Computed Results ...	108
4.5.1	Useful Transhorizon Signal	114
4.5.2	Interference Problems	114
Chapter Five:	The Design And Construction of a V.H.F. Pre-amplifier Using S - parameters ...	119
5.1	Introduction	119
5.2	Transistor S - parameters	120
5.3	The Design Theory	127
5.3.1	Stability Factor and Stability Circles ...	133
5.3.2	Graphical Method of Impedance Matching ...	133
5.4	The Design	142

		Page
5.4.1	The Output Matching Network of The Second Stage	145
5.4.2	The Input Matching Network of The Second Stage	148
5.4.3	The Input Matching Network of The First Stage	153
5.4.4	The Inter-stage Coupling Network ...	157
5.4.5	Tuning The Output And Input Networks ...	158
5.4.6	Input Filter For First Stage	161
5.5	The D.C. Bias	161
5.6	The Construction	166
5.6.1	Designing V.H.F. Inductors	169
5.6.2	Choice Of Components And Assemblage ...	172
5.7	Testing The Amplifier	174
5.7.1	The D.C. Measurements	174
5.7.2	Frequency Response	176
5.7.3	Stability And Other Performance Considerations	180
Chapter Six:	Conclusion	184
Appendix A	... ...	189
Appendix B	... ...	196
Appendix C	... ...	198
Appendix D	... ...	200
References	... ...	201

LIST OF TABLES

Table	Description	Page
4.1 (A)	Computed numerical values of hourly median ..	46
4.1 (B)	Computed mean, mean deviation and standard deviation based on hourly median ...	65
4.2	Computed monthly mean Jos - Zaria rainfall	66
4.3	Computed numerical values of Daily Median ...	67
4.4	Computed numerical values of monthly median	83
4.5	Computed daily mean Jos - Zaria Rainfall ...	84
4.6	Cumulative frequency distribution of the 1.25 minutely medians of signal level ...	85 - 86
4.7	Monthly variation of cumulative frequency distribution	91
4.8	Probability distribution of 1.25 minutely median	109
5.1	Transistor data	163
5.2	List of designed trial inductors ...	171
5.3	Initial numerical results of amplifier frequency response measurements	178
5.4	Numerical results of amplifier frequency response with improved gain	182

Figure		Page
20(A)-(P)	Cumulative frequency distributions of the 1.25 minutely medians	92 - 107
21	Normal distribution tendency of the probability distribution	110
22	Part of map of Nigeria showing planned and existing TV channels in the N.Central Area	115
23	A linear two-port network	121
24(A)-(B)	Stability circles on the output plane ...	129
25	Unconditional stability	134
26	Two-port network with input and output matching network	135
27	Input matching network for maximum power transfer and zero reflection coefficient...	137
28	A superimposition of rectangular and orthogonal impedance co-ordinate systems ...	139
29(A)-(D)	Illustrative approaches to impedance transformation	141
30	Determining R_{MS}, R_{ML} and the 20 dB gain circle on a Smith chart	146
31 (A)	A.C. circuit of the second stage (of amplifier) showing the output matching network	150
31 (B)	Output network of second stage showing tuning components	151
31 (C)	Modified A.C. output circuit diagram for the second stage.	151
32	Transformation chart for the source-first stage, and the inter-stage impedance matching	155
33(A)	Theoretical design of the input matching network for first stage	156
33(B)	Modified A.C. network for the input of first stage	156

LIST OF FIGURES

Figure	Description	Page
1	Definition of the parameter Δh ...	7
2	Optical and Radio horizons ...	13
3	Profile map showing relative positions of Jos and Zaria	14
4	Variation of diffraction loss with obstacle clearance	16
5(A)-(B)	Knife-edge diffraction	18
6	Smooth-sphere diffraction	20
7	Comparing the effects of the ground and the troposphere on transhorizon path loss	22
8	Definition of scattering angle and scattering volume	24
9	Specular, Diffuse and Partial Reflections and Scattering	27
10	The Rayleigh Criterion	28
11(A)-(B)	Variation of reflection/scattering loss with distance and frequency ...	30
12	Block diagram of Field Strength Measurement Instrument Set-up ...	34
13(A)-(C)	Typical Field Strength recordings ...	37
14	The dB Scale	38
15(A)-(M)	Graphical Plots of hourly medians ...	47 - 59
16	Initial rise rate of the hourly medians	61
17	Monthly variation of hourly medians ...	62
18(A)-(M)	Graphical Plots of daily medians ...	68 - 80
19(A)-(C)	Variation of monthly medians compared with variation of monthly mean rainfall...	87 - 89

		Page
34	Theoretical design of the inter-stage coupling network	159
35	The D.C. circuit and the Thevenin equivalent	164
36	The A.C. equivalent circuit	167
37	The complete amplifier circuit ...	168
38	Block diagram of amplifier test equipment set-up	176
39	Initial frequency response curves ...	179
40	Frequency response curves of amplifier with improved gain	183

APPENDICES

Appendix	Description	Page
A	The Computer Programs ...	... 189 - 195
B	The Rainfall Data ...	... 196 - 197
C	The NTV Jos Transmitter Power Data	... 198 - 199
D	List of Amplifier Components (with value and type specifications)	... 200

PLATES

Plate	Description	Page
I (A)	The Amplifier - External View	... 173
I (B)	The Amplifier - Internal View	... 173

"..... that it may never seem that I have lived in vain".

- Kepler.

INTRODUCTION

In accordance with the scientific spirit which calls for continuous research in all fields aimed at improving the existing services to mankind, studies of radio propagation over different parts of the world, at different frequencies, are usually carried out from time to time to improve radio communication services. For results of such a study to be meaningful and reliable, observations have to be made for fairly long periods of time in a given climatic zone; and when accumulated, predictions on propagation conditions can then be made when planning radio links within that zone.

Based on results of such studies carried out in more advanced countries - most of which are in the temperate climatic zones - the International Radio Consultative Committee (CCIR) has compiled propagation charts and curves for planning purposes. However, these are naturally only useful in the temperate zones where the measurements were made. Because propagation records are lacking in the tropical zones where most of the developing countries lie, the CCIR has only extrapolated the results of temperate zones into the tropical zones, and recommended that studies be carried out in the tropics to check-out these extrapolations.

The research conducted in this project therefore aims at:

1. Making available radio propagation data in the V.H.F. range for the purpose of checking out the CCIR recommended charts and curves for radio propagation planning in Africa.

2. Making recommendations for improved transmission of FM and Television channels (in the V.H.F. range) in Nigeria - especially with a view to detecting potential interference between existing and planned co-channels before hand, and

3. Designing and constructing a narrow band V.H.F. pre-amplifier (with low noise) capable of amplifying carrier signals at 192 MHz (and bandwidth at least 4 MHz) with sufficient gain, using S-parameters data for the transistors.

Underlying these aims and objectives is also the more subjective inert desire of the student to be exposed to data processing by computer methods on the one hand, and to gain some practical experience in the design and construction of high frequency amplifiers on the other.

With these goals as the background, the television signal from NTV Jos transmitter was monitored and recorded continuously in Zaria for a period of 13 months - July 1979 to July 1980 inclusive. The field strength data collected were analyzed using a CDC Cyber 72 Computer at the Ahmadu Bello University Computer Centre, and some interesting results have been obtained.

The need to actually boost this signal to the delight of Zaria viewers has been pointed out and as a step towards this end a narrow band booster amplifier with specifications as in 3 above has also been designed and constructed.

In the first chapter of this thesis some of the factors underlying propagation of radio frequencies in the V.H.F. and higher ranges have been discussed; and in chapter two those factors relating to propagation beyond the horizon have been expounded, since the Jos - Zaria radio path under study is a transhorizon one. Chapter three has been devoted to the methods and instruments used in collecting data, plus the pre-analysis data handling; while the fourth chapter contains results of the statistical analysis with a brief discussion aimed at interpreting them as well as highlighting some of their possible implications. The theory, design and construction of the pre-amplifier is contained in chapter five, and the concluding remarks are madde in the sixth and last chapter. It has been found convenient to furnish the following as an appendix: (1) the computer programs used in the analyses (appendix A); the data for rainfall figures (appendix B); the data for the NTV Jos daily transmitter power output (appendix C); and the list of components used for constructing the amplifier (appendix D).

CHAPTER ONE

PROPAGATION OF TELEVISION AND FM SIGNALS

Radio waves are generally subject to a variety of factors affecting their propagation. These factors depend on the frequency range and the type of propagation medium involved. Television and FM signals are normally broadcast in the Very High Frequency (V.H.F.) and Ultra High Frequency (U.H.F.) bands which cover, respectively, 30 - 300 MHz and 300 - 3000 MHz. The TV and FM bands are allocated the frequency channels between 50 and 1000 MHz. These frequencies normally propagate as direct, ground or tropospheric waves. Consequently, both the ground and the troposphere considerably affect and actually dictate the propagation modes of the waves.

Although the ionosphere may affect some signals in the V.H.F. band, its effect on TV and FM channels (if any) is too small to justify its discussion here.

1.1 The Earth's Surface

The earth is an imperfectly conducting medium with varying electrical constants which may be determined by the nature of the soil (the soil's ability to absorb and retain moisture appears more important than its chemical composition), the moisture content and temperature, the surface irregularities and the general geological structure of the ground.

Signals propagating as surface waves close to ground may suffer varying amounts of I^2R losses due to induced ground displacement and conduction currents on the one hand, and diffuse reflection on rough ground surfaces on the other. Also a direct wave and a ground-reflected wave reaching a receiver may differ both in amplitude and phase - the former because of losses in reflection and differential absorption in the wave resulting from the path length difference Δr between the two waves, while the phase difference $\Delta \phi$ results from the phase shift θ in reflection and the retardation in phase due to path length difference. The antenna directive gain in the direction of the reflected ray can also affect the amplitude of received signal. The complex reflection coefficient may be expressed as

$$R = |R| e^{-j\theta} \quad .... \quad 1.1$$

and the total phase shift $\Delta \phi$ is

$$\Delta \phi = \theta + \frac{2\pi}{\lambda} \Delta r \quad .... \quad 1.2$$

both of which may result in the fading of the received signal. But for reflection from the earth's surface to be significant the reflecting surface must be sufficiently large to accommodate the region bounded by the first Fresnel zone (see p.8), and since hill tops hardly satisfy this condition reflections in the forward direction from a hilly terrain is generally negligible. However, at frequencies greater than 10 MHz the electrical characteristics are relatively less important compared with the effect of the physical configuration of the earth's surface.

Surface irregularities on land range from vegetation to built-up areas and topography. The effect of these irregularities vary with wavelength (Saxton et al, 1953) (23) as well as height and depth of obstacles and the angle of incidence (Kinase, 1959)(23). Terrain roughness may first increase the expected or median field strength by breaking up the destructive phasing between direct line-of-sight propagation and waves reflected or diffracted by the ground, or by enhancing reception at an angle away from the optical line-of-sight path. Obstacle gain is common in TV and FM broadcasts and generally obtains when the direct path between the transmitter and receiver is non-optical but can be seen from the top of the obstacle (e.g. mountain). Obstacle gain referring to gain relative to calculated field strength over a homogeneous spherical earth involves only diffraction* and standard atmospheric refraction, but if scattering* and super-refraction* are considered as well, the gain may include knife-edge diffraction (see section 2.1) and possible scattering over a mounting ridge as against an equivalent path clear of obstacles (Dickson et al, 1953; Norton et al, 1955; Iwai, 1959; and others)(23).

However, increasing terrain clutter will reduce signals due to shadowing, absorption (including attenuation caused by vegetation) and the scattering and/or defocussing of diffracted waves. Attenuation caused by terrain irregularities increases with the parameter Δh (defined in

---

* See sections 2.1, 2.2.2, and 1.2 respectively.

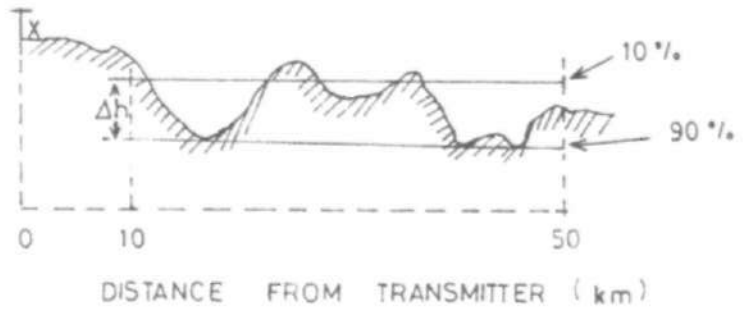


FIG.1: DEFINITION OF THE PARAMETER ΔH
REF. (23), P. 129).

Figure 1) which is a measure of terrain roughness. The effect of Δh increases with frequency, and the mean slope of the terrain could equally be an important factor in ground attenuation.

In order to avoid shadow loss the aerial heights must be chosen so as to obtain the first Fresnel zone clearance defined as

$$H_1 = \left[\frac{\lambda d_1 (d - d_1)}{d}\right]^{\frac{1}{2}} \quad \ldots\ldots 1.3$$

where λ = wavelength

d_1 = distance from transmitter

d = distance between antennas.

Polarization is also a factor influencing ground attenuation. Comparative measurements in the Federal Republic of Germany and elsewhere show that at 190 MHz the field strength over line-of-sight paths is 3 dB lower with vertical polarization as compared with horizontal polarization (this difference increases in shadow regions) and that at higher frequencies both individual values and the difference between them decrease.(23)

1.2 The Troposphere

The troposphere is the main medium of transmission for TV and FM signals. Extending from sea level up to an altitude of about 15 km, it is an inhomogeneous medium characterized by time-varying properties, most of which result

from changes in the water vapour content. Ordinarily the troposphere has a negative temperature gradient with a lapse rate of about $0.55^{o}C$ per 100 m , a pressure lapse rate of about 12 millibars per 100 m , and a decreasing index of refraction with altitude.

The dynamic nature of the troposphere and the consequent localized irregularities give rise to various types of refraction of radio waves ranging from inverse refraction at one extreme to super-refraction at the other. Under critical refraction condition, radio waves propagate parallel to the earth's surface without bending. The vertical gradient of refractive index $\frac{dN}{dh}$ at any height h and the lapse rate of this gradient is mainly determined by the gradients of pressure, temperature and humidity, than the numerical values of these variables, as shown in equation (1.4):

$$\frac{dN}{dh} = 77.6 \left(\frac{1}{T}\frac{dP}{dh} - \frac{dP}{dh} - \left(\frac{P}{T^2} + \frac{9620}{T^3} e\right)\frac{dT}{dh} + \frac{4810}{T^2}\frac{de}{dh}\right) m^{-1} \quad \ldots\ldots 1.4\,(6)$$

where e = humidity

P = pressure

T = temperature

h = height above earth's surface

$N = (n-1) \times 10^{6}$

n = refractive index,

and it can be shown that super refraction occurs when the vertical gradient of refractive index $\frac{dN}{dh}$ is less than $-0.157\,m^{-1}$ (6). Tropospheric inhomogeneities also give rise to multipathing (and the associated fading) which may

be enhanced by possible scattering by these inhomogeneities as well as by reflection from rain streaks or well defined cloud boundaries. Measurements in the U.S.A. (Crawford and Jakes, 1952) (23) have shown that as many as six ray components may exist at a given time. Multipathing in the troposphere also cause limitation of the transmissible bandwidth which becomes narrower (to a degree that depends on the climate) as the distance from the transmitter increases. Duct formation (elevated or ground-based) is also possible in the troposphere under conditions of temperature inversion. Such ducts may propagate waves of frequency greater than 100 MHz to abnormally long distances beyond the horizon.

Generally tropospheric loss increases with frequency. Also TV and FM channels relatively suffer less tropospheric loss than their higher frequency counterparts because the effects of absorption and scattering by precipitation particles, or absorption by atmospheric molecules are either negligible or non-existent in this frequency range.

1.3 Some Characteristics And Potential Use of The V.H.F./ U.H.F. Bands For Television And FM Transmission

The V.H.F. and U.H.F. bands of frequency have outstanding characteristics favourable to television and FM broadcast. Some of these include:

1. Atmospheric noise decreases with increasing operating frequency, and falls below thermal noise level, essentially

putting radio circuits above 100 MHz at par with their wire and cable counterparts. The V.H.F. band is a unique one for which all propagation modes are possible.

2. Propagation is not significantly affected by the ionosphere but takes place largely in the troposphere which is more stable and affected only by meteorological influences such as pressure, temperature, turbulence and stratification of the atmosphere - as previously noted in Section 1.2.

3. Propagation approaches, with increasing frequency, an optical straight line path, making simultaneous transmission of the same frequency between different sites possible, provided none is in the optical line-of-sight of the other.

4. Both the available spectrum and the modulation bandwidth are much wider (about 1000 times) than those of the H.F.

However, relay stations (usually with about 10 kW of power output per link) are necessary because the line-of-sight operation with its limited diffraction around the curved earth limits the propagation range more or less within the horizon - usually about 50 km from the transmitter; although under abnormal atmospheric conditions or specially designed circuits useful signals may be received beyond the horizon.

CHAPTER TWO

PROPAGATION OF TELEVISION SIGNALS BEYOND THE HORIZON

The optical horizon is the visual distance between an observer and the point where his line of vision grazes the earth's surface. However, the radio horizon seen by radio waves is longer because of the effects of atmospheric refraction. For an antenna of height h in metres, the optical horizon r_o and the radio horizon r_R may be expressed respectively as

$$r_o = 3.57 \sqrt{h} \text{ km} \quad \ldots \quad 2.1$$

$$r_R = 4.13 \sqrt{h} \text{ km} \quad \ldots \quad 2.2$$

as shown in Figure 2.

The need to expound the propagation mechanism featuring on transhorizon propagation arises from the fact that the Jos to Zaria transmission under study is essentially a transhorizon link, as can be seen from Figure 3. However, because the Jos transmitter transmits equally in all horizontal directions, propagation terms and techniques relating to directional antennas will, as much as possible, not be discussed.

Propagation of TV/FM signals beyond the horizon may be characterized under two dominant influences - notably the effect of the ground and that of the troposphere.

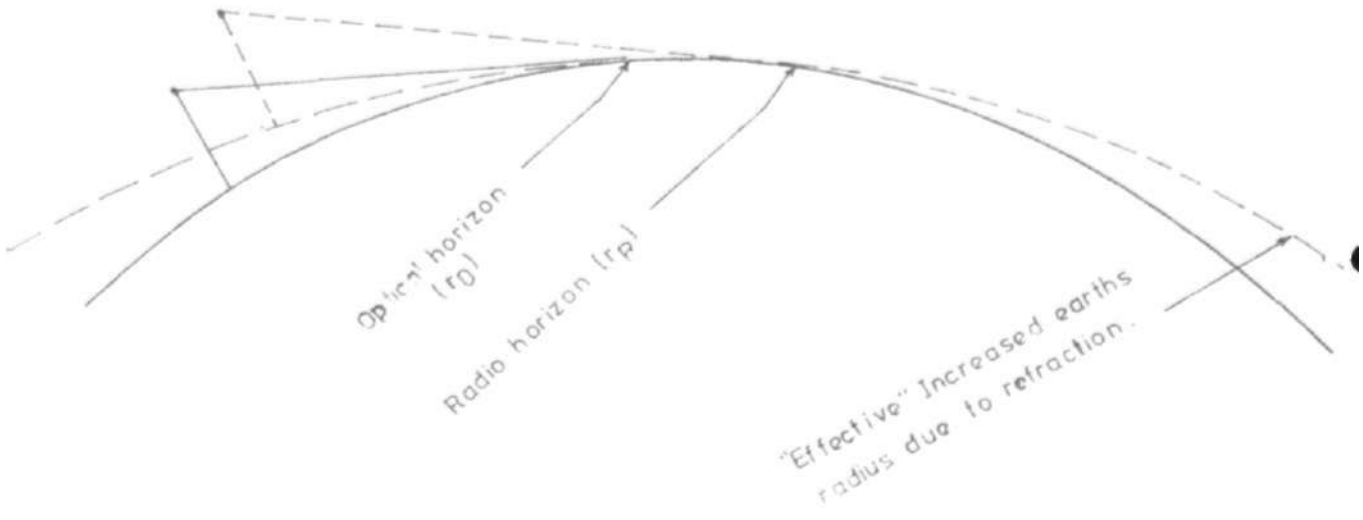


FIG. 2 OPTICAL HORIZON r_O AND RADIO HORIZON r_R

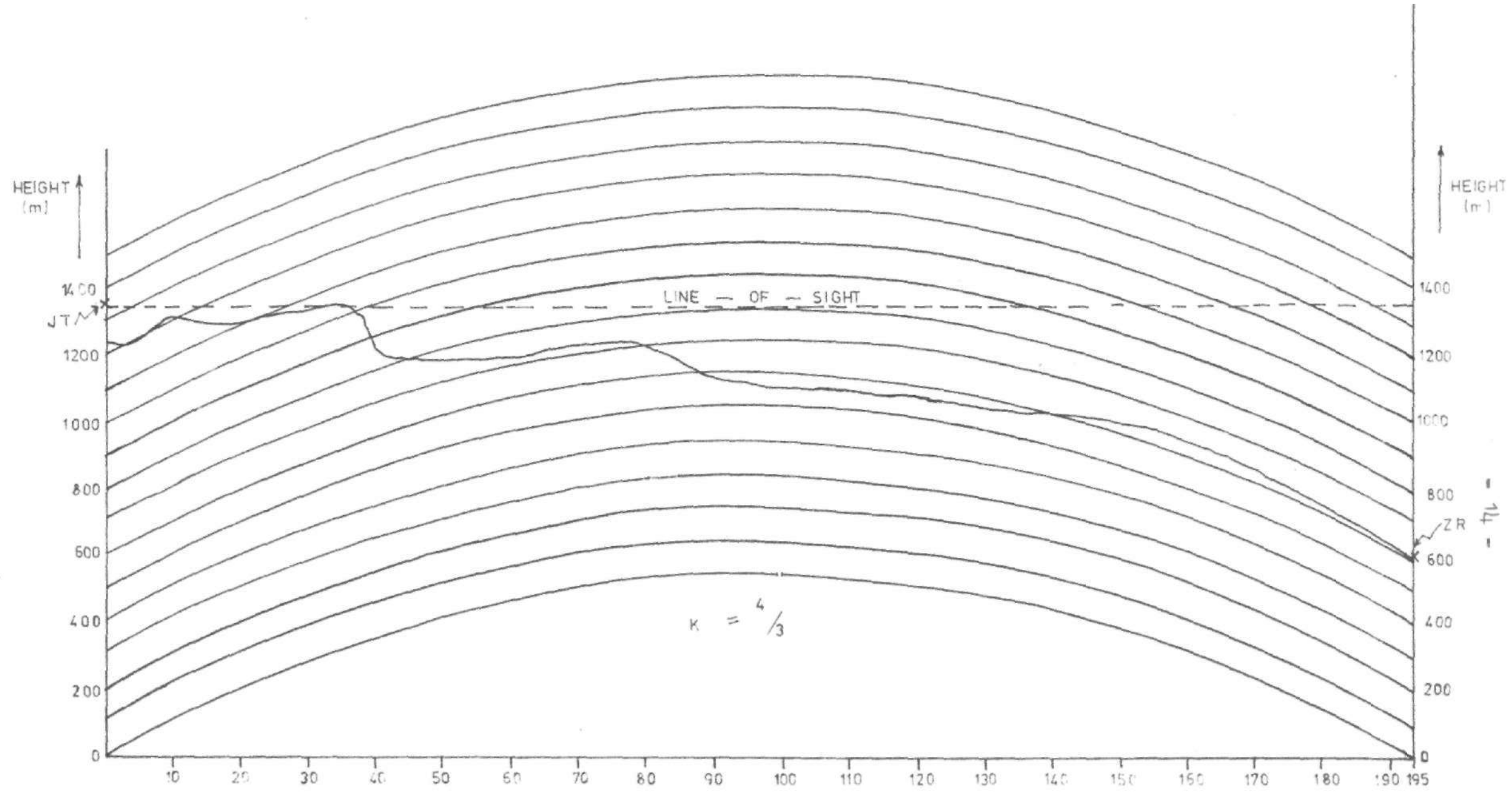


FIG. 3 PROFILE DIAGRAM OF JOS — ZARIA RADIO PATH SHOWING RELATIVE HEIGHTS (ABOVE SEA LEVEL) AND POSITIONS OF THE NTV JOS TRANSMITTER (JT) AND THE ZARIA RECEIVER (ZR).

The effects of these media apart, radio waves propagating in free space are subject to some loss due to divergence or defocussing. The expected free-space field intensity E_o and the free-space system loss L (dB) may be expressed respectively as

$$E_o = \frac{(30\ P_t\ g_t)^{\frac{1}{2}}}{d} \text{ volts per metre} \quad \ldots\ldots \quad 2.3$$

and

$$L = 10 \log \frac{d^2\ \lambda^2}{A_t\ A_r} \text{ dB} \quad \ldots\ldots \quad 2.4$$

where

P_t = transmitted power in watts

g_t = transmitted aerial gain

A_t , A_r = transmitter, receiver effective aperture (For an isotropic transmitting antenna $A_t = 1$)

λ = Propagating wavelength

d = distance (in metres) from the transmitter.

2.1 Effect of Terrain On Transhorizon Propagation

The ground affects the propagation of radio waves in such a way that the received field intensity is ordinarily less than would be expected in free-space. This effect falls into two categories: The effect of a plane earth and the effect of a curved earth.

It can be shown that the effect of a plane earth is to make the received signal to oscillate around the free-space value in a lobe form, as shown in Figure 4 (10),(11). In the Jos - Zaria link under study this effect might reach a maximum around fourty kilometres from Jos (see Figure 3)

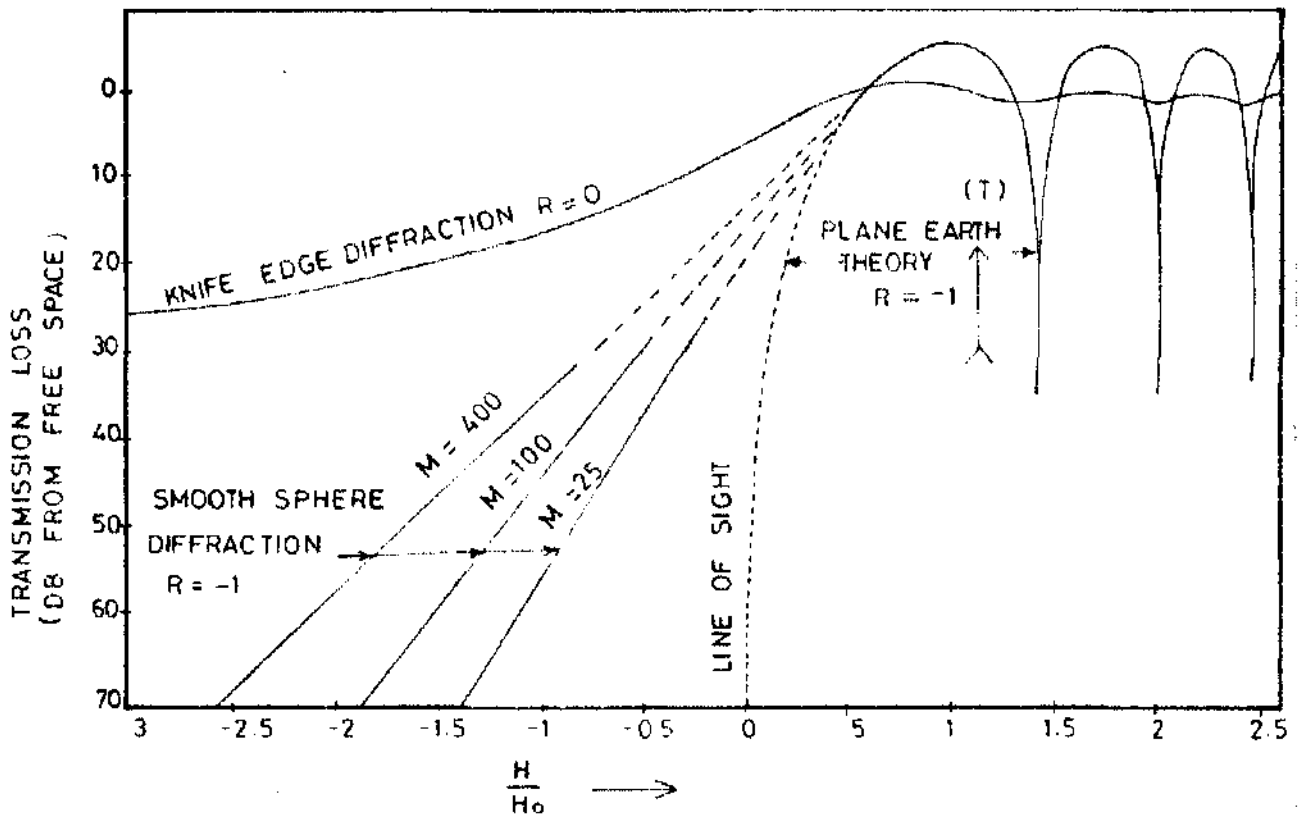


FIG 4 :- COMPARING DIFFRACTION LOSS WITH THE RATIO OF OBSTACLE CLEARANCE H AND THE FIRST FRESNEL ZONE Ho.
REF. (10), (11)

and thereafter has no effect on the remaining transhorizon distance to Zaria, which now features the effects of a curved earth,

Propagation of radio waves to moderate distances beyond the horizon can occur due to diffraction from the earth's curvature. Diffraction is an edge effect that occurs because the phase surface of a propagating wave is not infinite. Propagation in diffraction mode falls between two extremes: Diffraction over a perfectly SMOOTH SPHERICAL earth with uniform atmosphere, and diffraction over a perfectly ABSORBING KNIFE-EDGE. Whereas the former is caused by propagation over a fairly smooth surface with uniform atm sphere, the latter is represented in practice by propagation over hill tops, trees and buildings. The transmission loss resulting from the earth's curving obstruction generally increases both with distance and frequency, and depends to some extent on the antenna height. This loss adds to the free-space and effective plane earth model losses, and approximates to 230 dB at a distance of 182 km from the transmitter horizon and a frequency of 170 MHz.(23)

Knife-edge diffraction (Figure 5(a)) loss depends on the height H of the top of the obstacle above the straight line joining the two ends of the path (H is negative if the height is below this line (Figure 5(b)), the distance d_1, d_2 of the two ends of the path from the obstacle, the angle of diffraction θ in radians, the angles α_1, α_2 between the

top of the obstacle and the straight line joining the ends (α_1 , α_2 are negative if H is negative), and the wavelength λ. The diffraction loss approaches 6 dB at grazing incidence (i.e. $H \longrightarrow 0$), and increases with increasing H. For negative values of H the diffraction loss tends to zero with increasing negative values of H in an oscillatory manner. It is thus necessary for a substantial clearance of the line-of-sight ray over a valley, if an obstacle-free path is desired. Knife-edge diffraction is independent of polarization provided the distances d_1, d_2 (figure 5(a) and (b)) are more than a few wavelengths.

Smooth-sphere diffraction loss (figure 6(b)) depends on the effective radius of curvature R for the terrain feature between the horizons, the distances d_1, d_2 from each terminal to their horizons, the angle of diffraction θ, and the wavelength λ.

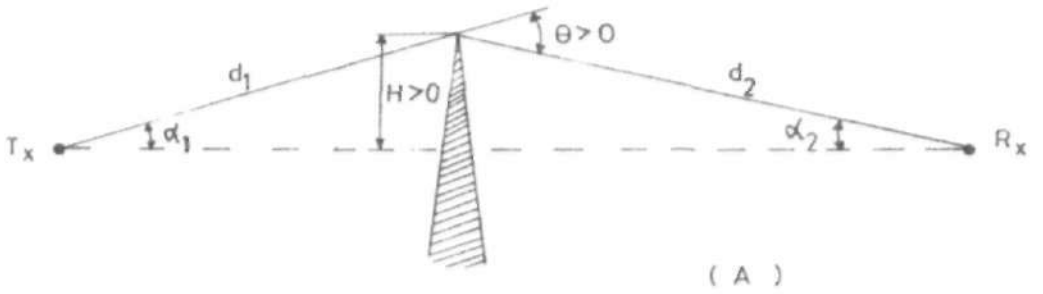
Figure 4 compares losses from these two diffraction modes with the line-of-sight path loss over a plane earth. The losses (ordinate) are in dB from free-space while the absissa is the clearance H measured in terms of first Fresnel zone clearance H_0. The smooth-sphere diffraction is represented by a family of curves with a parameter M which is given by

$$M = \frac{H_1}{K^{\frac{1}{3}}} \left[\frac{1 + (\frac{H_2}{H_1})}{2} \right] \left[\frac{F}{4000} \right]^{\frac{1}{3}} \quad \ldots. \quad 2.5\ (10),(11).$$

H_1, H_2 = antenna heights

F = frequency in MHz

K = earth's radius factor $(\frac{4}{3})$



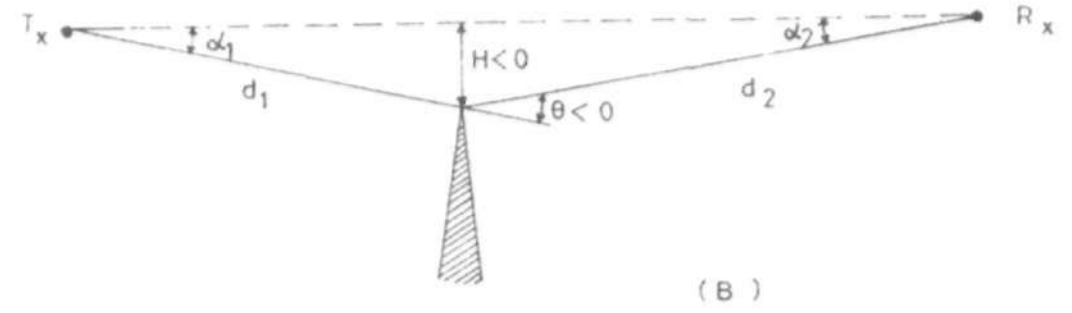


FIG. 5 : KNIFE EDGE DIFFRACTION FOR POSITIVE OBSTACLE HEIGHT (A) AND NEGATIVE OBSTACLE HEIGHT (B

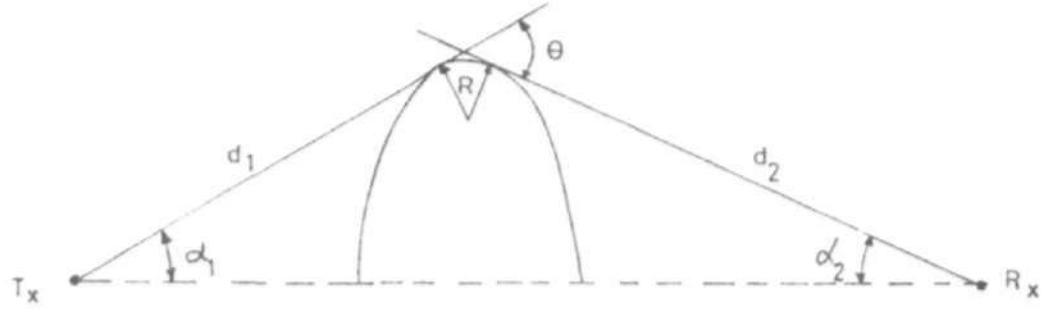


FIG. 6 : SMOOTH – SPHERE DIFFRACTION.

From the figure it can be seen that for positive values of H, attenuation is in lobular form for smooth-sphere diffraction and a bit oscillatory for the knife-edge; and at grazing incidence (H = 0) attenuation tends to infinity. However, with increasing clearance from the obstacle H becomes increasingly negative and attenuation decreases for both types of diffraction (and with increasing values of M in the case of smooth-sphere diffraction). Attenuation due to knife-edge diffraction is much less than that due to smooth-sphere diffraction, and because attenuation due to all other forms of propagation mechanisms featuring in transhorizon paths (except ducting) fall between values for knife-edge and smooth-sphere diffractions, knife-edge diffraction is also associated with the term 'obstacle gain'. Figure 4 also shows how critically an estimate of diffraction loss can depend on the assumed terrain profile. The infinite attenuation at grazing incidence again shows how heavily the loss suffered in the Jos - Zaria path can depend on the earth constants around 40 km from the transmitter (see figure 3).

However, as further illustrated in Figure 7, the effect of diffraction can only be significant at moderate distances beyond the horizon; at distances very far away from the horizon, as Zaria is from Jos transmitter horizon - about 153 km - the tropospheric influence, for which attenuation increases less rapidly with distance, becomes more important.

2.2 Effects Of The Troposphere On Transhorizon Propagation

The troposphere vitally influences transhorizon propagation. Transhorizon waves are usually subject to tropospheric refraction, scattering, reflection, multi-path

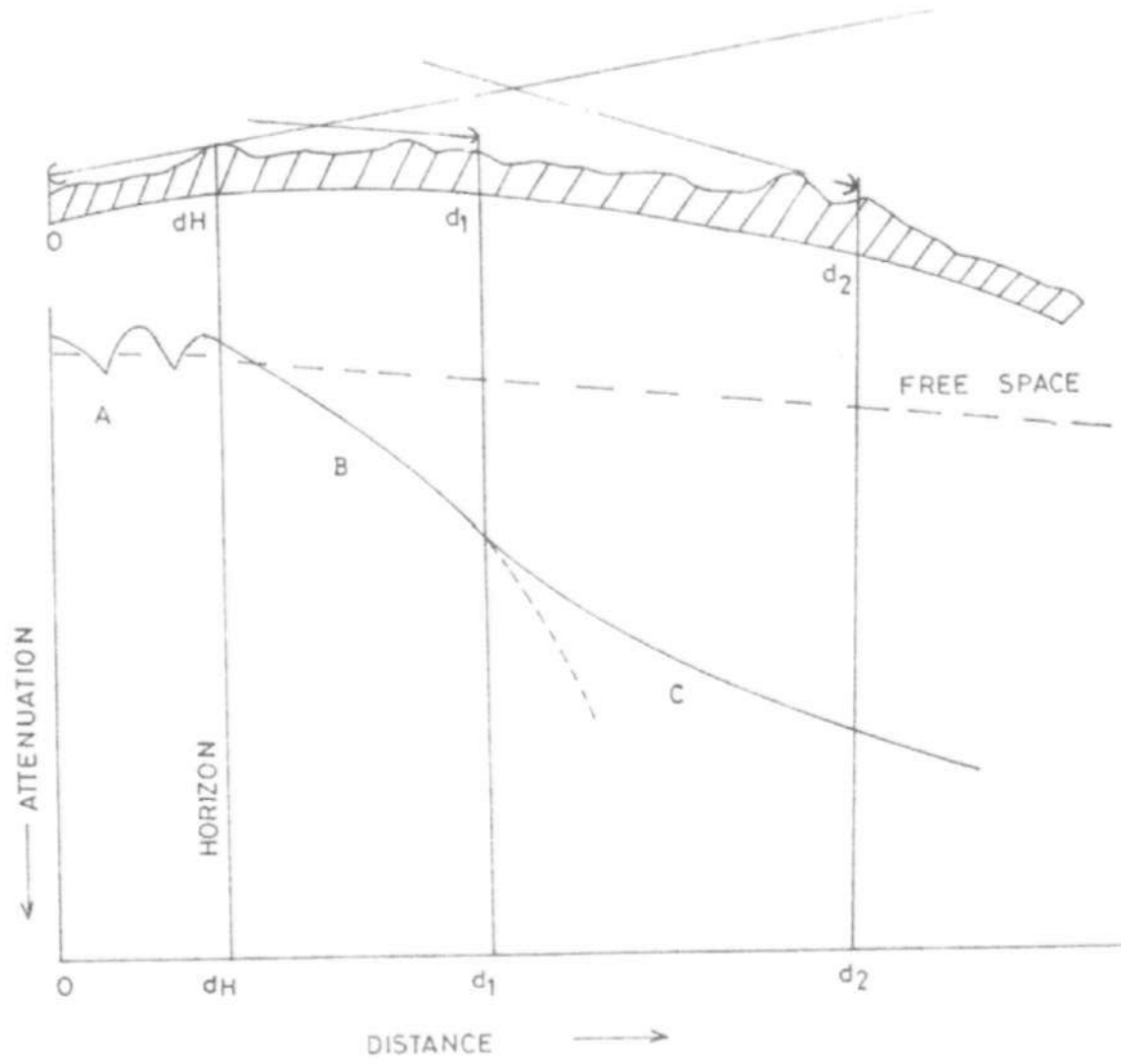


FIG 7. COMPARING THE EFFECTS OF THE GROUND AND THE TROPOSPHERE ON TRANSHORIZON PATH LOSS.

A — LINE OF SIGHT

B — IMMEDIATE VICINITY BEYOND THE HORIZON, EARTHS INFLUENCE PREPONDERANT.

C — FAR AWAY FROM THE HORIZON, INFLUENCE OF THE TROPOSPHERE PREPONDERANT. ATTENUATION INCREASES LESS RAPIDLY WITH DISTANCE.

REF (7)

fading and, occasionally ducting.

2.2.1 Tropospheric Refraction

Tropospheric refraction enhances transhorizon propagation through the apparent increase of the earth's radius (see figure 2) and sometimes ducting. Refraction can extend radio waves to considerably far distances beyond the horizon, and might well be a significant factor in the Jos - Zaria link.

However, propagation by ducting is random and unreliable for commercial TV purposes.

2.2.2 Tropospheric Scattering

Tropospheric scattering featuring on transhorizon paths may take the form of tropospheric-scatter or precipitation-scatter propagation.

Tropospheric-scatter propagation involves scattering from tropospheric inhomogeneities and discontinuities in the refractive index of the air scatter volume seen by both transmitting and receiving antennas (Figure 8). It is characterized by attenuation which increases rapidly with distance in all directions other than the incident direction, being concentrated in the forward direction for wavelengths smaller than the elementary induced eddies. Hence it is often referred to as forward scatter.

Precipitation-scatter is scattering from precipitation particles. Unlike forward scattering, precipitation-scatter re-radiates energy isotropically (to a first approximation), and is the only mechanism giving rise to significant

$\theta = (\theta_o - \theta_1 - \theta_2)$ deg.

$\left(\frac{d - d_1 - d_2}{R}\right)\frac{180}{\pi}$ deg.

R earth's radius.

h_1 h_2=Antenna heights.

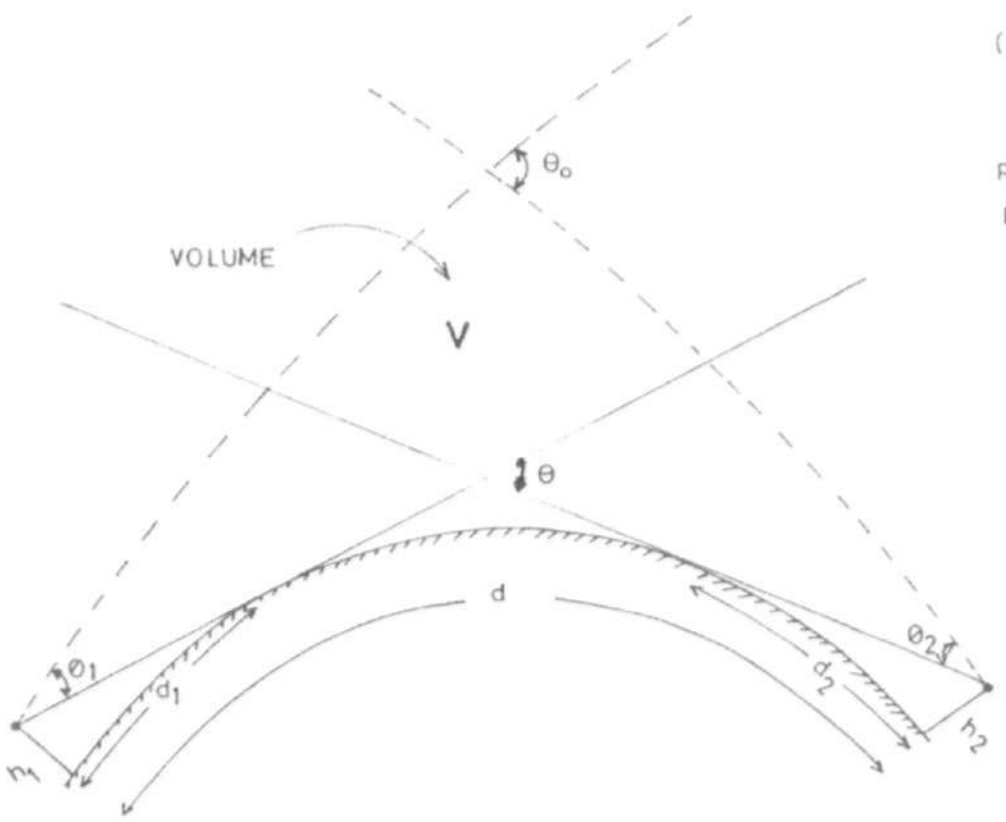


FIG 8. :— SCATTERING VOLUME (V) AND SCATTERING ANGLE (θ)

propagation offa great circle path. The strength of precipitation-scatter power may also be augmented by the rainfall rate.. The scattering cross-section η for rain scatter may be expressed as

$$= \frac{\lambda^5 / K /^2 Z \times 10^{-18}}{4} \ m^{-1} \quad .... \ 2.6 \ (23)$$

where $K = (\varepsilon - 1) / (\varepsilon + 2)$

ε = dielectric constant of water

λ = wavelength (m)

Z = reflectivity factor

Generally, scattered radiation varies with scattering angle θ, and scattering volume V (Figure 8), and theoretical analysis show that the scattering cross-section is inversely proportional to θ^5. The attenuation of scattered radiation is highly correlated with the surface index of refraction and is a function of the sun's position, being less in summer than in winter. (6),(7). Although scattered power decreases less rapidly with frequency (proportional to λ) than reflected power, it is normally associated with a combination of fast and slow fading - the former having a Rayleigh distribution while the latter has a normal distribution.

Whereas forward scattering could play a significant role in the Jos - Zaria transhorizon link during wet and dry seasons, the impact of precipitation-scatter can only be felt during the wet season.

2.2.3 Tropospheric Reflection

Tropospheric reflection is another principal propagation mechanism responsible for the reception of NTV Jos signals in Zaria. It can take the form of diffuse or specular reflection of the waves by atmospheric irregularities, (figure 9).

Specular and partial reflections may occur at the surface of a stable discontinuity (like rain streaks and well defined cloud boundaries) while irregular surfaces of these discontinuities cause diffuse reflection, some of which may satisfy the Rayleigh criterion (Figure 10), specular power decreases more rapidly with frequency (proportional to λ^3) than diffuse power (proportional to λ^2), and only waves with wavelength less than 10 m may be propagated significantly beyond the horizon by specular reflection. Again, the fact that discontinuities in the atmosphere tend to increase in spatial coverage with altitude makes diffuse reflection preponderant at greater distances than specular reflection. So, because the effect of the earth is comparatively negligible in the V.H.F. range and above, at great distances from the horizon, diffuse reflection and scattering constitute the essential elements of transhorizon propagation; while specular reflection which occurs for a smaller percentage of the time is responsible for the high field strengths (with small variations) observed on transhorizon circuits. As with scattering, the fast multipath fluctuations arising from diffuse reflection

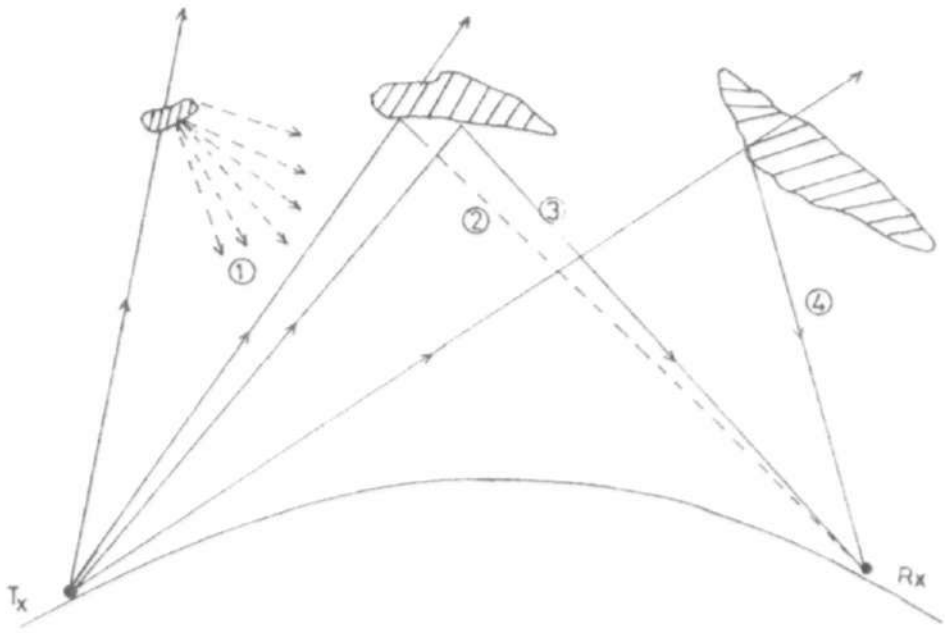


FIG 9 TROPOSPHERIC SCATTERING (1), PARTIAL REFLECTION (2), SPECULAR REFLECTION (3), AND DIFFUSE REFLECTION (4) FROM ATMOSPHERIC INHOMOGENEITIES.

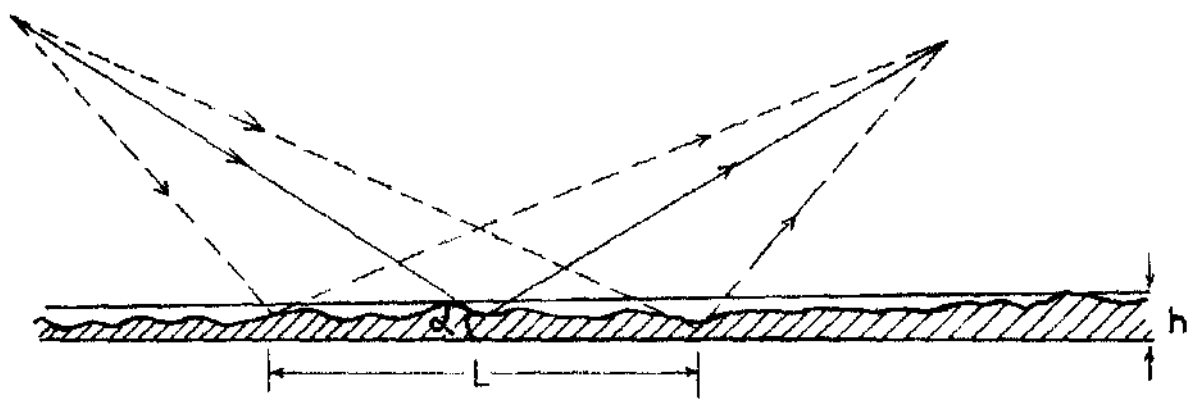


FIGURE 10 THE RAYLEIGH CRITERION : REFLECTION AT AN IRREGULAR SURFACE IS EQUIVALENT TO REFLECTION AT A UNIFORM SURFACE (SPECULAR REFLECTION) IF THE HEIGHT h OF THE IRREGULARITIES IN THE FRESNEL ZONE L IS SUCH THAT $4h \sin \alpha < \lambda$.
REF (7)

approximate to a Rayleigh distribution, but the transmissible bandwidth is greater with reflection than with scattering.

Figure 11 compares theoretically variations in decibel signal level with (a) frequency and (b) distance, for specular and diffuse reflections, and scattering. The figure further reveals that at a given frequency of 200 MHz, the differences between these propagation mechanisms are more pronounced than at a given distance of 200 km - figures which compare with those of the Jos - Zaria link, climatic effects notwithstanding.

Specular reflection has been identified with thunderstorm activities occurring within the radio path by Kühn and Täumer (12) who have observed and studied this mechanism in a temperate zone. Their study which involved probing the tropospheric vertical temperature structure of the zone confirms the existence of strong inversion above the ground, caused by production of cold air masses in the thunderstorm cells; it also reveals inter-alia:

1. that the degree of thunderstorm signal enhancement depends on the intensity of thunderstorm activities within the radio path;

2. that field strength in daytime is mostly low with scattering components, but sudden field strength thunderstorm enhancement (up to 20 or 30 dB above the normal level) may sometimes occur, lasting from about ten minutes to one or two hours;

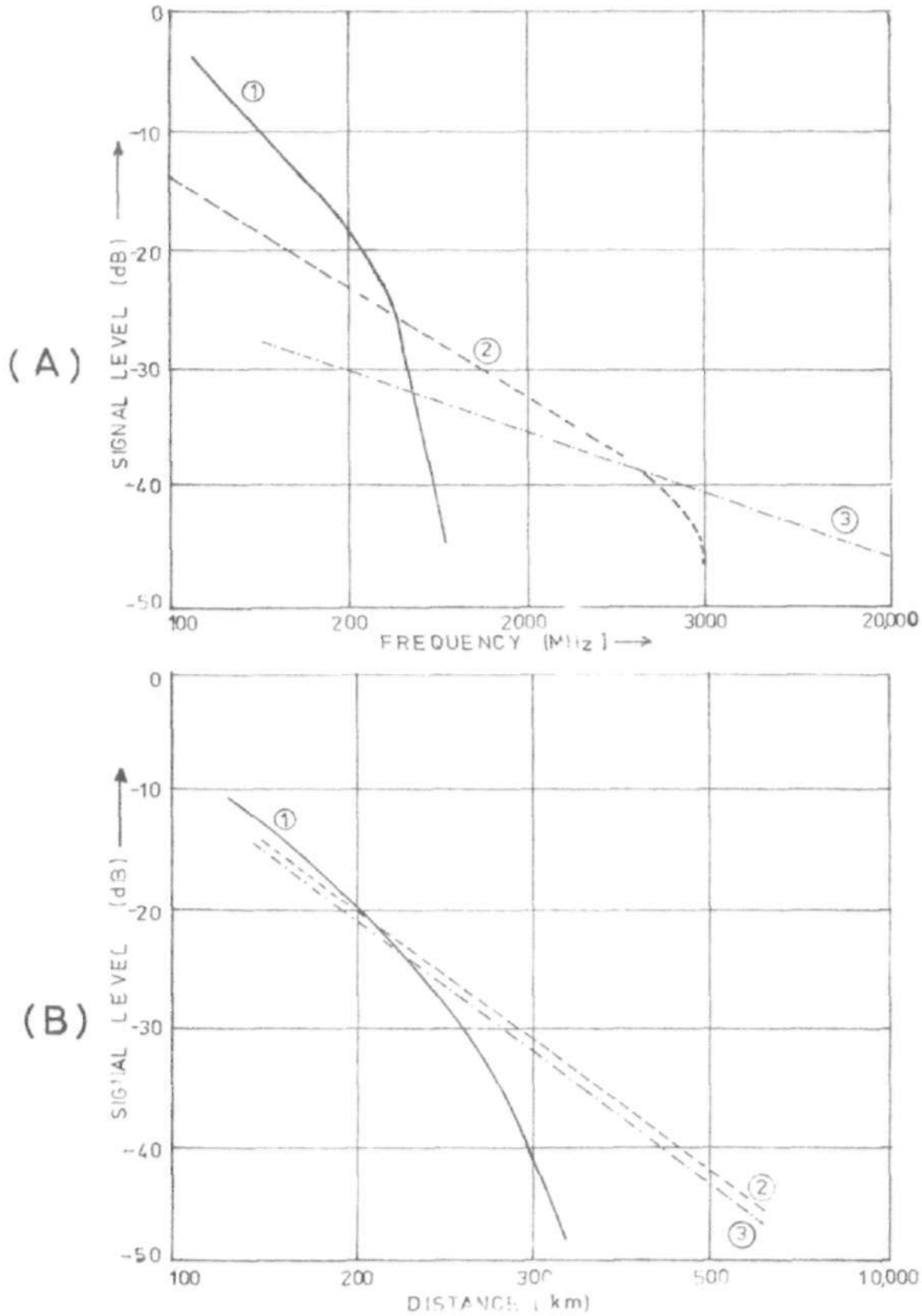


FIG. II THEORETICAL COMPARISON OF VARIATIONS OF SIGNAL LEVEL WITH FREQUENCY (A) AND DISTANCE (B) FOR SPECULAR REFLECTION (1) DIFFUSE REFLECTION(2) AND SCATTERING (3) REF (7).

3. that thunderstorm enhancement of radio signals naturally increases with path length, is frequency dependent - with about 17 dB increase over the normal field strength at 200 MHz on a 125 - 210 km path (in the temperate zone).

The impact of signal enhancement by thunderstorm is expected to be more on the Jos - Zaria radio link (at 192 MHz) than in the temperate zone in view of the relatively less signal attenuation and increased thunderstorm activities in the tropics. Hence this mechanism can be a dominant factor on the Jos - Zaria transhorizon link.

2.2.4 Some Other Factors Relating To Transhorizon Propagation

An appraisal of the factors enhancing or militating against reception of NTV Jos signal at Zaria cannot be completed without assessing possible effects of buildings and trees.

Apart from offering much more back scatter than solid earth, buildings tend to be more transparent to radio waves and this tends to reduce shadow losses caused by buildings; however, the angles of diffraction (see figure 5) over or around buildings are naturally greater than for natural terrain - a factor which tends to increase the loss due to the presence of buildings. The effect of buildings does not vary significantly with frequency in the range 40 - 450 MHz for which losses caused by buildings has been estimated at 25 dB below the corresponding plane earth value, but beyond 450 MHz the loss increases with frequency (11) This effect could be troublesome for the highest U.H.F. TV channels between 470 and 890 MHz, but can only have a

minimal effect on the reception of the 192 MHz NTV Jos signal in Zaria, moreso, when the only two built-up areas in the path (Jos and Zaria) form a negligible percentage of the 193 km path length.

Localized large rapid variations in received field intensity may arise from the standing wave pattern set up by reflections from trees located up to five to ten wavelengths away from the transmitter. Signal attenuation caused by the presence of trees is more with vertical polarization, and could be as much as 70 dB/km at 200 MHz for horizontal polarization (23). In the frequency range of 300 MHz and above trees thick enough to block vision approximate to a solid obstruction of the same overall size, thus affecting more adversely the higher U.H.F. TV channels. Vegetation can constitute a significant attenuation factor on the Jos - Zaria transhorizon link, especially around the Jos transmitter horizon (about 40 km from Jos), and during the wet season when trees are in full leaves.

Lastly, it is worth mentioning that echo effects also complement the limitation of the transmissible bandwidth by multipath effects characterizing transhorizon links; deep fast fades due to reflection from a frontal object like an aircraft have been observed during field strength measurements for this research, Zaria being an aviation training centre. Such variations have been identified with Doppler effect.(7)

CHAPTER THREE

DATA COLLECTION AND COMPILATION

3.1 Data Collection

The field strength of the Nigerian Television (NTV) Jos transmission was monitored continuously in Zaria (at a distance of about 200 km) over a period of thirteen months - July 1979 to July 1980*. Except for the few occasions of either transmitter failure at Jos or receiver instrument failure at Zaria during the period, this exercise was otherwise steady and uninterrupted.

3.1.1 Instruments Used For Field Strength Measurements

The receiving antenna used was a broadband log periodic type, covering the frequency range of 80 - 1300 MHz; it was placed at a height of 5 m above the ground and located in a position away from buildings and other obstacles. The antenna was coupled through a down lead of 50 ohm characteristic impedance to a Rhodes and Schwarz V.H.F. - U.H.F. Field Strength Meter of the ESU type with RF plug-in unit 1 which covers 25 - 230 MHz frequency range (see figure 12).

This instrument is reliable for accurate field strength measurements and functions in effect as a highly selective voltmeter of 60 kHz bandwidth, and with a logarithmic response

---

* All field strength recordings were made by Dr. E.B. Ojeba.

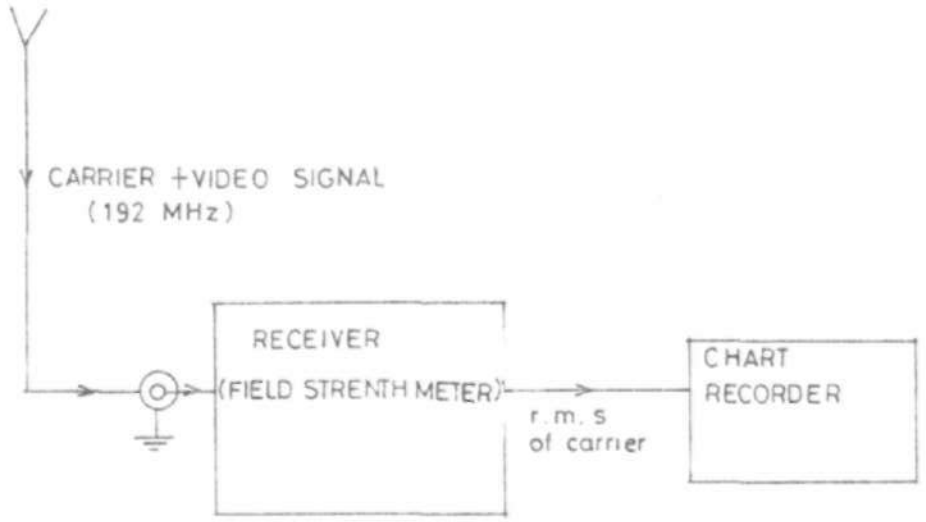


FIG. 12: BLOCK DIAGRAM OF THE FIELD STRENGTH MEASURING INSTRUMENT SET-UP.

covering a dynamic range from 20 to 60 dB. The instrument also has built-in precision oscillators (for amplitude and frequency self-calibrations) as well as a provision for monitoring the field strengths of video - modulated RF signals to give outputs whose amplitude depends only on that of the carrier, and the d.c. output of the diode detector in the receiver was fed into the recorder to drive the pen.

3.1.2 Recording of Field Strength

The instrument reading was the r.m.s. value of the carrier signal which is independent of the picture and sound signals; an analogue representation of this field strength in dB above 1 microvolt per metre was plotted as the ordinate against time as abscissa on a Hewlett Packard strip chart recorder of type 7155B. The chart speed used corresponds to 2.5 minutes per centimetre; this gave sufficient details of the field strength variations with time without consuming too much chart paper.

Measurements were carried out on the video carrier of 192.25 MHz which was the frequency of transmission of NTV Jos during the period of measurements.

Observations showed that the field strength hardly ever exceeded 50 dB above 1 uV/m. Accordingly the instrument was calibrated so that the upper limit of the voltage axis of the chart paper corresponds to this maximum vertical deflection of the pen, while the instrument noise level was made to correspond to the minimum level line. This calibration

was checked routinely so as to ensure that the instrument reading always corresponded to the true value of the input voltage (i.e. received signal).

Throughout the period of measurement field strength readings were recorded continuously from 5.00 pm to 11.30 pm which covers the normal transmission time of NTV Jos. The time and date of commencement of recording was always noted on the chart paper as well as the few occasions of transmission breakdown (which was usually short-lived) or instrument failure in Zaria, usually caused by sticking of the pen on the chart paper or power problems. This ensured post-recording identification of the charts.

Typical recordings for the wet and dry seasons are shown in Figures 13(a), (b) and (c).

3.1.3 Data Transcription From Analogue to Digital Form

For the purpose of computer analysis it was necessary to transcribe the analogue representation of field strengths into discrete quantities. To do this a decibel scale was constructed on a transparent plastic sheet such that when this is placed over the analogue plot the decibel levels of field strengths at different times can be read off, (see figure 14).

Signal levels in decibel were painfully read every 75 seconds at intervals of ·5 cm along the abscissa - i.e. the median level for each interval*. The 1.25 minutely medians were considered sufficiently close to allow a fairly accurate digitization of the analogue plots without excessive

---

* The contribution of some Part III students in this direction is gratefully acknowledged.

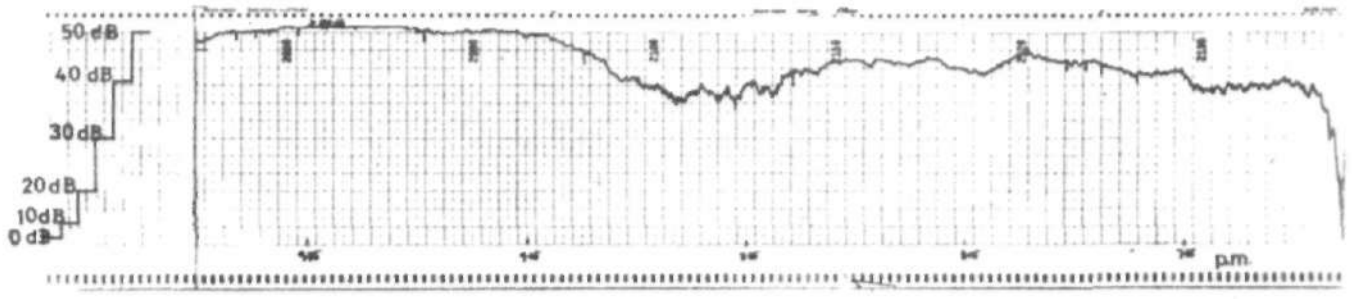


Fig. 13(A) Recordings of signal variations on 13th Oct. 1979. Very high level signal with little variations, typical of thunderstorm enhancement mode of propagation.

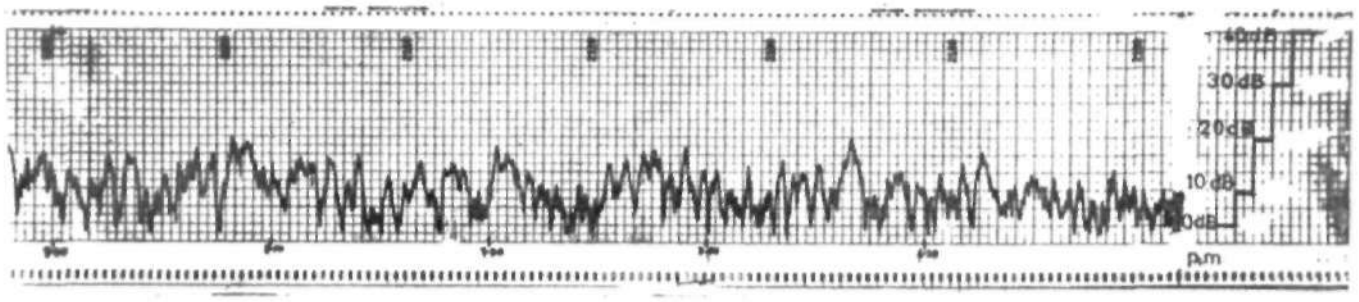


Fig. 13(B) Recordings of signal variations on 11th Feb. 1980. Moderate signal level with variations, typical of diffusion reflection mode propagation.

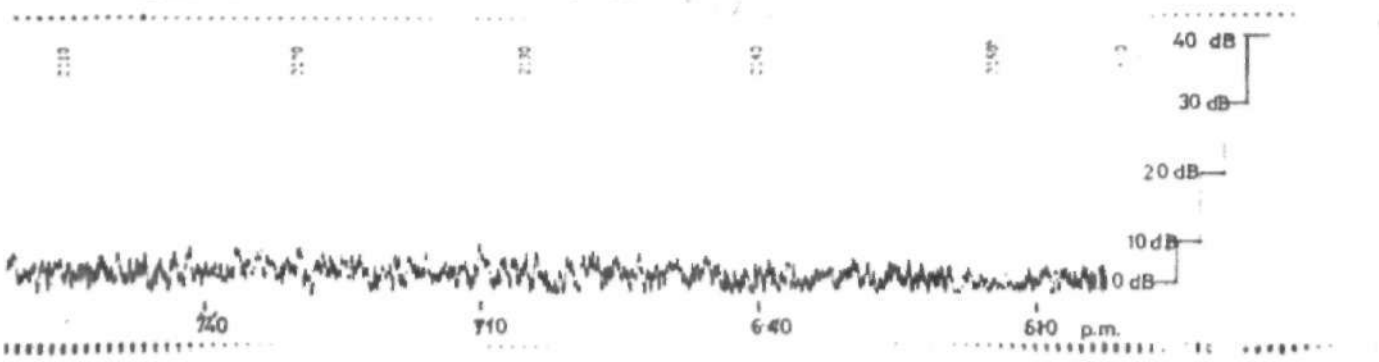


Fig. 13(C) Recordings of signal variations on 14th March 1980. Very weak and rapidly varying signal, typical of turbulent scattering.

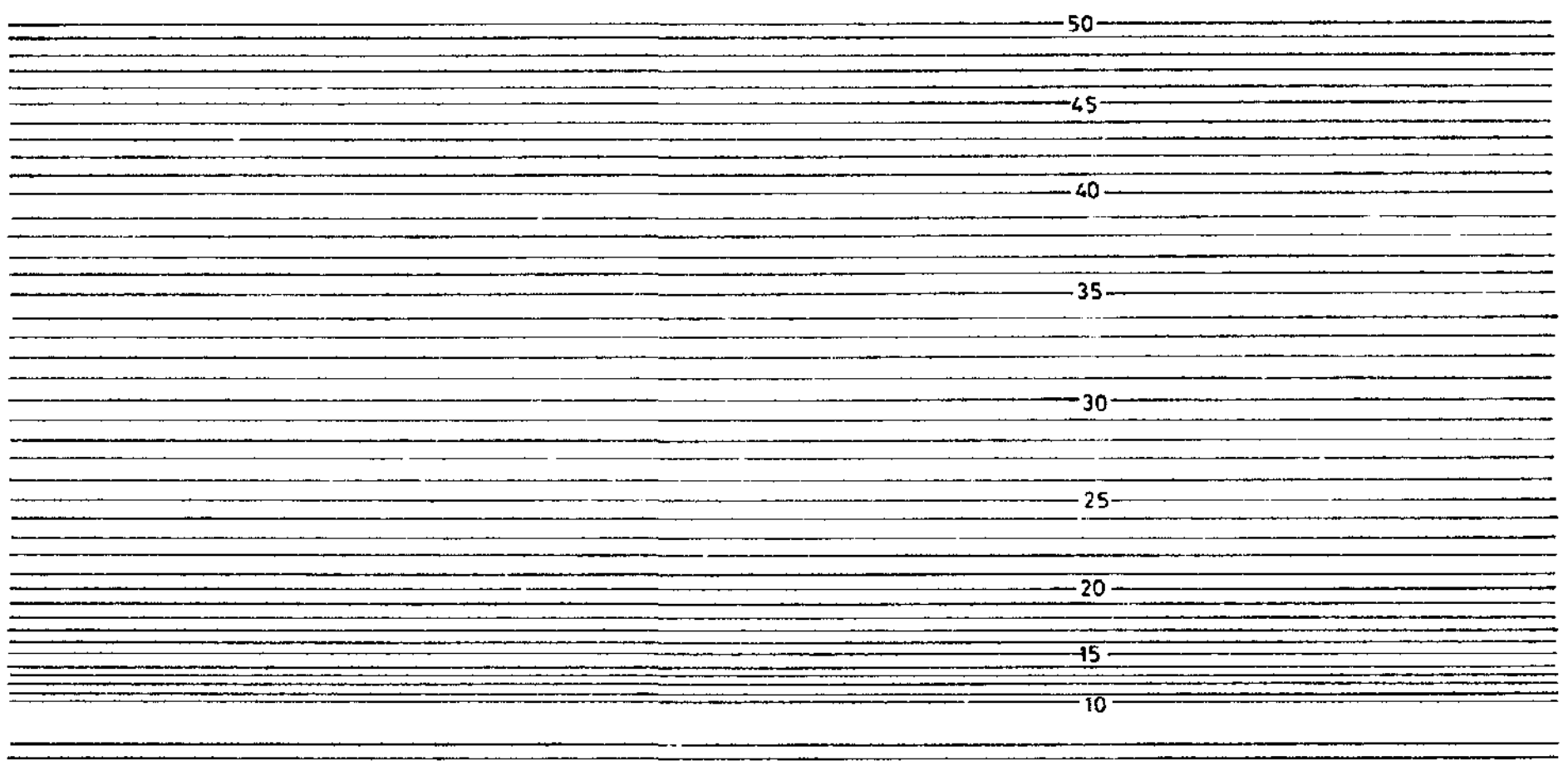


FIG. 14. — THE DB SCALE.
(CAN BE ADJUSTED FOR HIGH OR LOW SIGNAL LEVELS)

waste of time and energy on redundant digits. The digitized readings thus obtained were then tabulated in a matrix form that reflects the time, day, and month of the year the analogue equivalent was plotted.

Each matrix of readings contains data for a particular month of a given year, with the columns corresponding to days while the rows correspond to the time the analogue equivalent was recorded. Hence the matrix elements may be defined as

$$a_{i,j} \quad , \qquad i = 312, \qquad j = 31.$$

Readings which fell below - 9 dB were transcribed as - 10 dB to ensure that all readings below the instrument noise level were clamped down still after the addition of the antenna factor (see section 3.2.2.). Also the cause of unavailability of reading (if known) was always stated in the appropriate space of the table.

3.1.4 Rainfall And Transmitter Power Data

The rainfall data used in this study were recorded during the period of measurement (by the Department of Meteorological Service, Lagos) from 6.00 p.m. of a given day to 6.00 a.m. of the next day in both Zaria and Jos. On days when only a trace of rainfall was observed, the reading is taken as 0 mm .

The record of daily power transmission from NTV Jos shows that a minimum of 6 kW and a maximum of 10 kW were transmitted during the period of measurement, and that 7.5 kW was transmitted most often.

The rainfall and transmitter power records are contained in appendix B and C respectively.

3.2 Data Compilation Into The Computer

Each matrix of digitized data was then stored in a separate file in the computer; a fourteenth file was created for the data of the daily transmitted power from Jos. However, in order that the computer can handle the data, it was necessary to compile them in a suitable uniform format. It was also vitally necessary to standardize all data so that each reading was matched against a uniform and specific power level from Jos transmitter.

3.2.1 The Computer Input Format

For convenience, three spaces were allotted to each matrix element in the computer, with a blank between adjacent readings. Each matrix element of Section 3.1.3 was therefore multiplied by ten before it was stored in the system; thus a one-digit reading X was stored as bX0 where b stands for a blank space, while a two-digit reading XY was entered as XY0. To conform with this three spaces per reading format, - 10 was stored as - 90 instead of - 100. The effect of multiplying each element by ten was annulled by later dividing each reading of the result by ten. Codes 970, 980 and 990 were used to identify absence of reading caused by receiver instrument failure, power failure and absence caused by unknown factors, respectively. It

was also found convenient to bring up some data files to 31 columns by filling the appropriate columns with the 990 code.

The same input format was also used for entering the data for daily transmitted power from NTV Jos, except that out of the three spaces allotted to each element the decimal point now takes one. The highest reading of 10 kW was stored as 10. All readings were entered to the first place of decimal and the multiplication by ten does not apply here. Before running each program this file was edited and its contents replaced with the data for the appropriate month.

3.2.2 Data Standardization

The field strength data as now stored in the computer are not yet in a form suitable for analysis. This is partly because the transmitter power output from Jos varied from day to day as mentioned in section 3.1.4. It was therefore necessary to standardize all recorded field strength readings against a nominal value of transmitted power so that as much as possible the results of analyses will be based only on propagation conditions. The nominal value chosen for this purpose was 7.5 kW since this value was most frequently transmitted.

To do this a computer program was developed (see appendix A.1) which compares the power transmitted each day with 7.5 kW and adds or subtracts the appropriate correction factor (in decibel) from all the readings of the day - depending

on whether a lower or higher power (respectively) was transmitted on that day. On days when the transmitted power was same as the 7.5 kW nominal value all readings remain unchanged.

Another factor necessitating pre-analysis data standardization was the need to add a total of 12.9 dB due to the antenna correction factor K, and the small signal attenuation caused by the extra coupling coaxial cable mentioned in Section 3.1.1. The latter was determined from measurements while the former was supplied along with the instrument. This 12.9 dB loss must therefore be added to all readings so as to bring them as much as possible to what the field strength at Zaria actually was at the time of measurement.

Since each element of matrix was multiplied by ten, then 12.9 was added as 129 by the same program. Each element $a_{i,j}$ was therefore first modified to

$$X_{i,j} = 1_{i,j} - 10 \log_{10} \left(\frac{a_{i,j}}{7.5} \right), \; j \leq 31 \quad .... \quad 3.1$$

and then to

$$A_{i,j} = X_{i,j} + 129, \quad j \leq 31 \quad .... \quad 3.2$$

Data standardization could be a cumbersome exercise, but serves as an effective check on the strict adherence to the input format (for well over 9000 data readings of each month), since the program would not run if there existed any slight shift from this format, until the error is removed. However, once the program runs successfully with

any file, the data therein becomes standardized and thus suitable for analysis.

CHAPTER FOUR

THE ANALYSIS OF FIELD STRENGTH DATA COLLECTED JULY 1979 - JULY 1980

The statistical analysis chosen in this study is based on median values of signal level. The median of a given set of data is that value of the variates which occupies the middle position when all the variates are arranged in the order of their magnitudes. A median value is more informative than the mean in analysis of time-varying variates, such as signal levels - where it represents the level exceeded during a half of the reception time. It is thus more representative of the value expected most of the time than the mean. Besides, it is a factual value existing as one of the variates, whereas it is possible to have none of the variates having the actual value of the mean.

The median values evaluated in this study include :

1. Hourly median from 5 p.m. to 11.30 p.m. for all the months,
2. Daily median for all the days of each month,
3. Monthly median for each of the thirteen months, and
4. Seasonal and annual medians.

Based on these median values a number of other statistical analyses have been applied to further elucidate the signal behaviour. Attempts have also been made to

correlate this behaviour with the available rainfall data recorded in Jos (T_x) and Zaria (R_x) during the period of measurement, besides explaining it on the basis of established propagation theories.

The data to be analysed have already been stored in the computer system as described in Chapter 3. Computer programs were then written and also stored in the computer either to re-arrange the data in the computer memory cells in a form suitable for the application of a given statistical operation or to actually apply this operation.

4.1 Hourly Median of Signal Level

Evaluation of the hourly median of signal levels for each of the thirteen months was made using the computer programs given in appendix A.3 and A.4.

The resulting numerical values obtained (in decibel relative to 1 μV/m) are shown in Table 4.1(A), and the graphical plots of these values as ordinate with time (Hours) as abscissa are shown in Figures 15(a) - (m). From these observations a number of observations can be made:

1. There is a general tendency for the hourly medians to rise from 5 p.m. (when programme transmission begins) to about 10 p.m.; between 10 p.m. and about mid-night (when transmission shuts down) the rise rate either decreases sharply or there is altogether a fall in the median level. Thus the lowest median values occur around 5 p.m., while signal level is usually high

TABLE 4:1 (A)

HOURLY MEDIAN OF SIGNAL LEVEL IN dB Above 1 μV/m

Time (p.m.)	JULY 1979	AUG. 1979	SEPT.1979	OCT. 1979	NOV. 1979	DEC. 1979	JAN. 1980	FEB. 1980	MAR. 1980	APR. 1980	MAY 1980	JUNE 1980	JULY 1980
5.00 - 6.00	23.5	24.2	*	24.4	15.9	17.2	14.8	16.4	14.3	15.6	24.2	23.3	22.7
6.00 - 7.00	26.1	28.4	29.5	27.1	19.8	18.5	17.2	16.7	15.9	15.1	24.5	25.2	24.7
7.00 - 8.00	29.1	29.3	30.1	30.7	23.7	22.4	19.2	18.8	17.8	15.7	27.8	27.3	28.8
8.00 - 9.00	31.5	33.0	33.0	33.9	27.3	25.4	22.0	20.7	19.7	17.8	32.6	29.7	30.9
9.00 - 10.00	33.1	32.1	37.8	34.8	28.8	27.6	24.2	23.5	20.8	20.9	34.3	31.2	33.8
10.00 - 11.00	33.4	33.0	40.5	38.1	32.0	20.6	26.2	24.9	23.1	23.1	37.6	33.8	34.9
11.00 - 11.30	35.3	29.7	35.2	52.7	35.0	29.8	24.7	25.5	23.9	23.8	35.3	37.0	36.1

* Missing Data

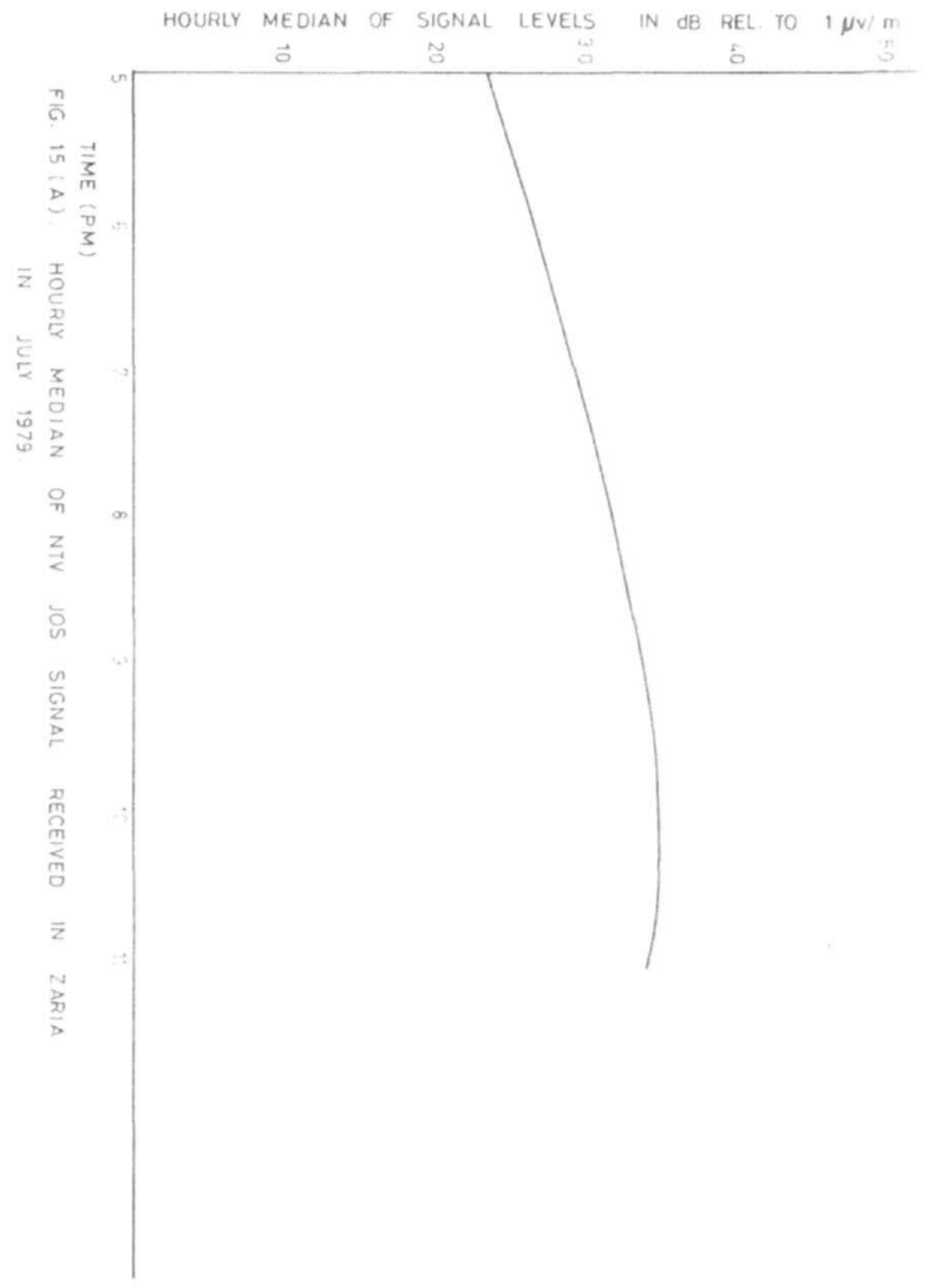


FIG. 15 (A) : HOURLY MEDIAN OF NTV JOS SIGNAL RECEIVED IN ZARIA IN JULY 1979.

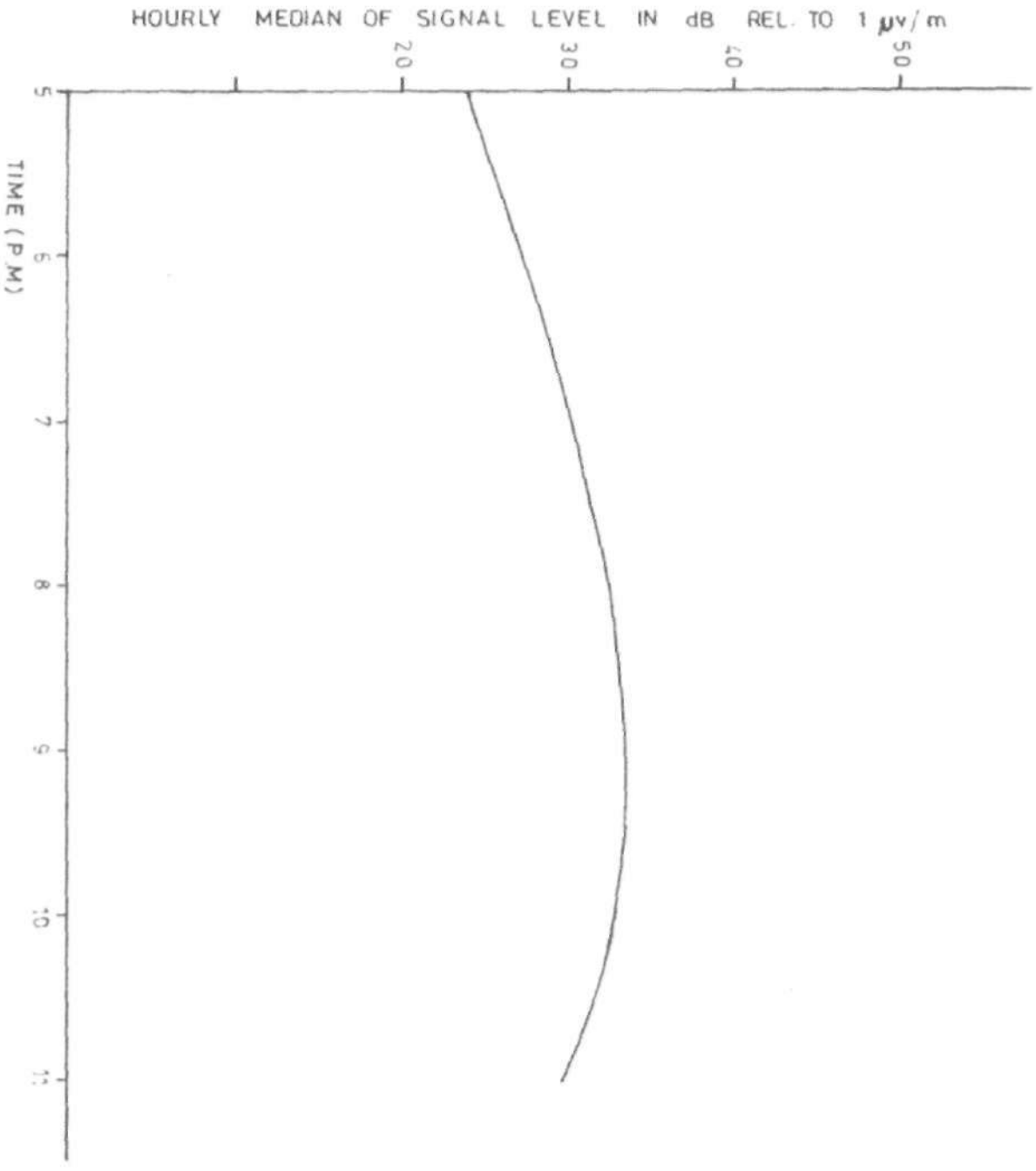


FIG.15 (B). HOURLY MEDIAN OF NTV JOS SIGNAL LEVELS RECEIVED IN ZARIA IN AUGUST 1979.

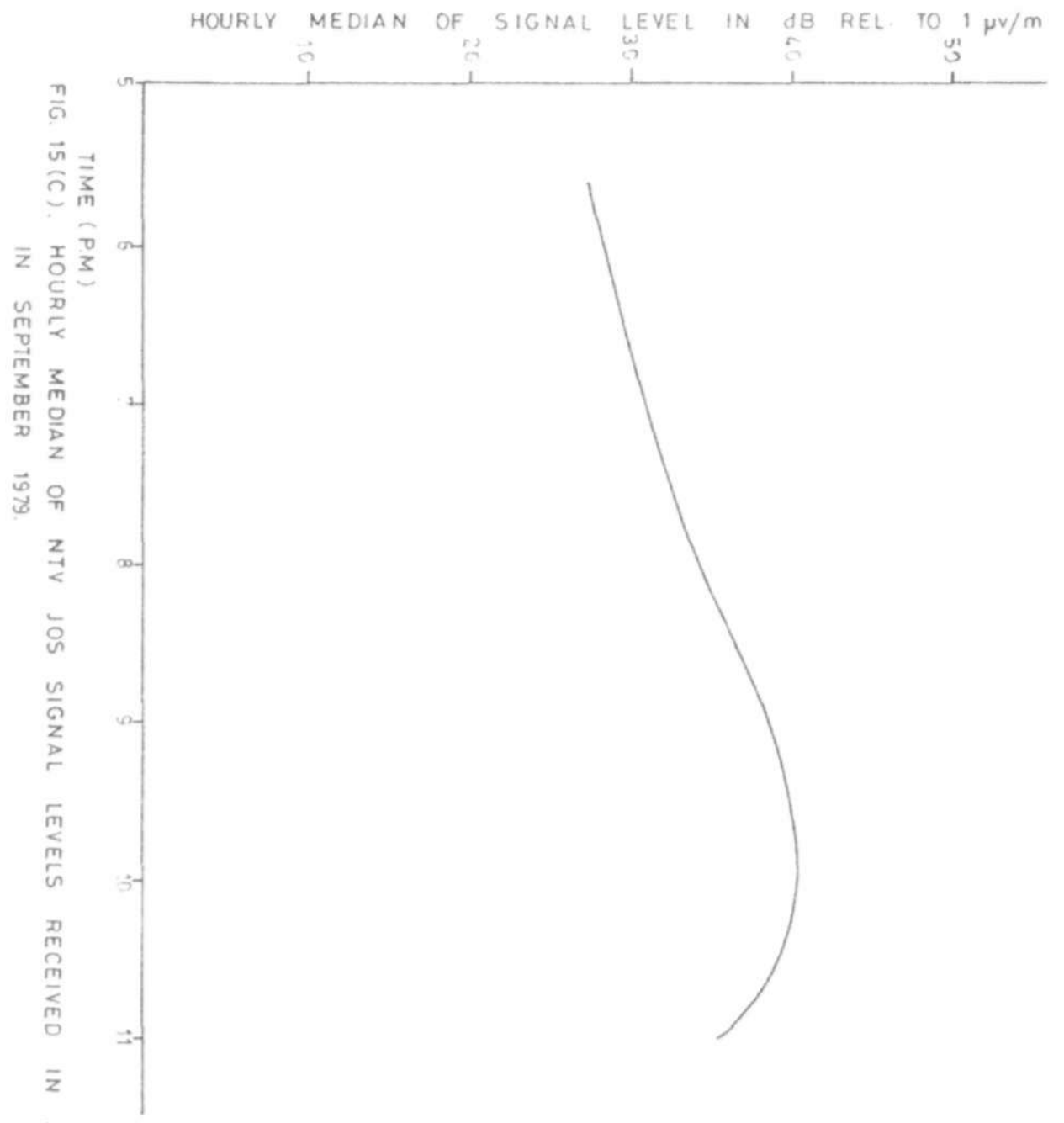


FIG. 15(C). HOURLY MEDIAN OF NTV JOS SIGNAL LEVELS RECEIVED IN ZARIA IN SEPTEMBER 1979.

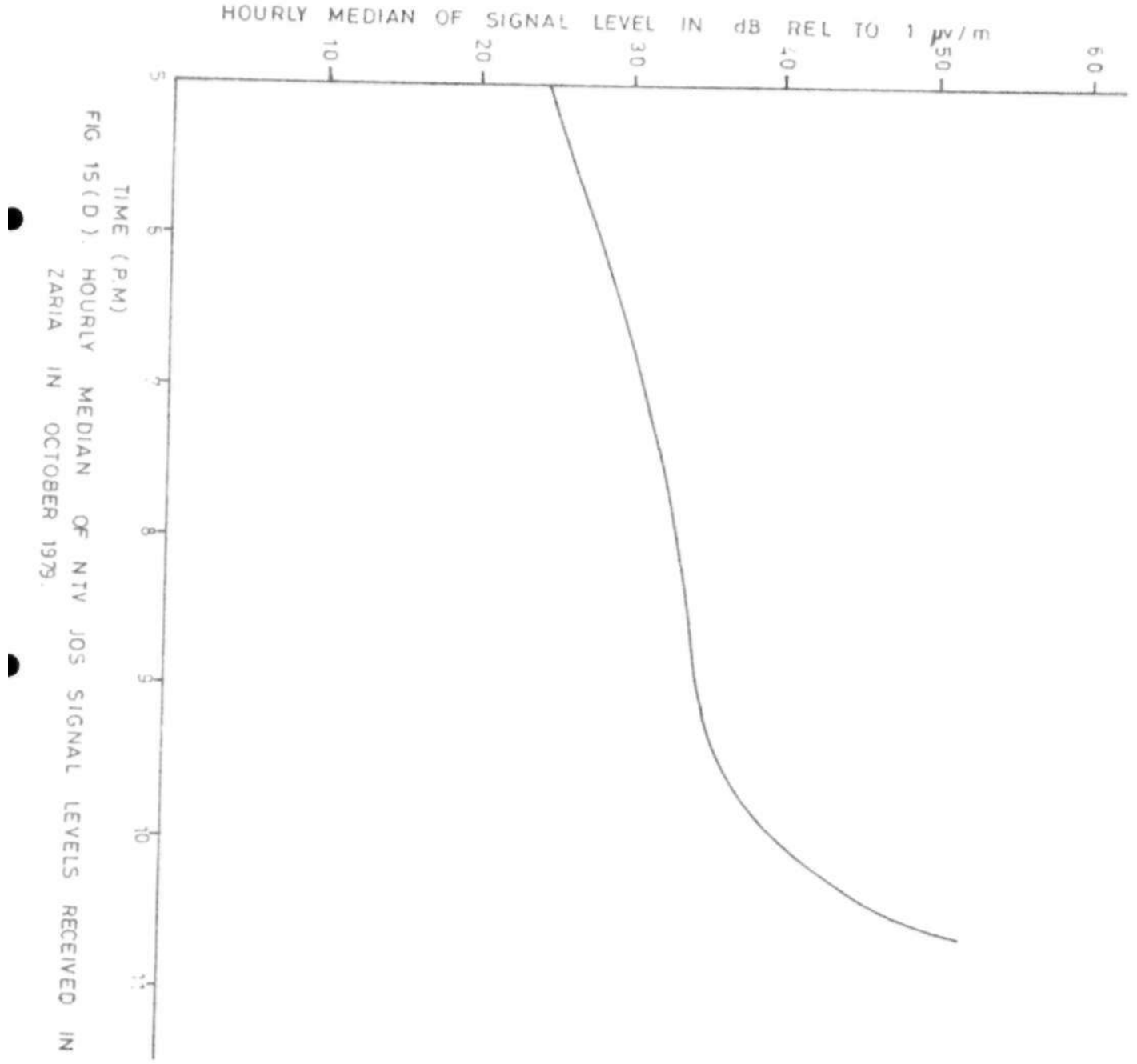


FIG 15 (D). HOURLY MEDIAN OF NTV JOS SIGNAL LEVELS RECEIVED IN ZARIA IN OCTOBER 1979.

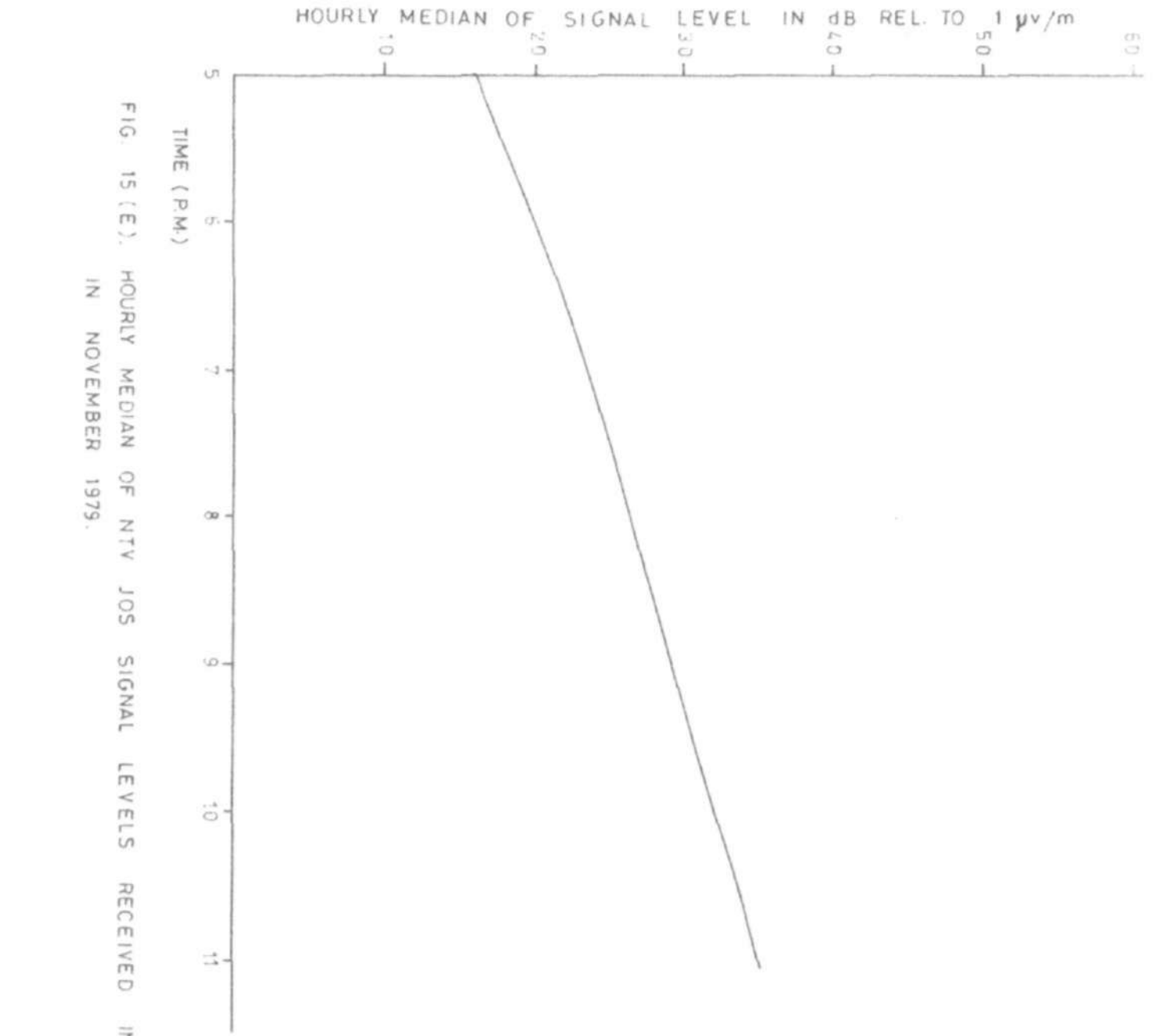


FIG. 15 (E). HOURLY MEDIAN OF NTV JOS SIGNAL LEVELS RECEIVED IN ZARIA IN NOVEMBER 1979.

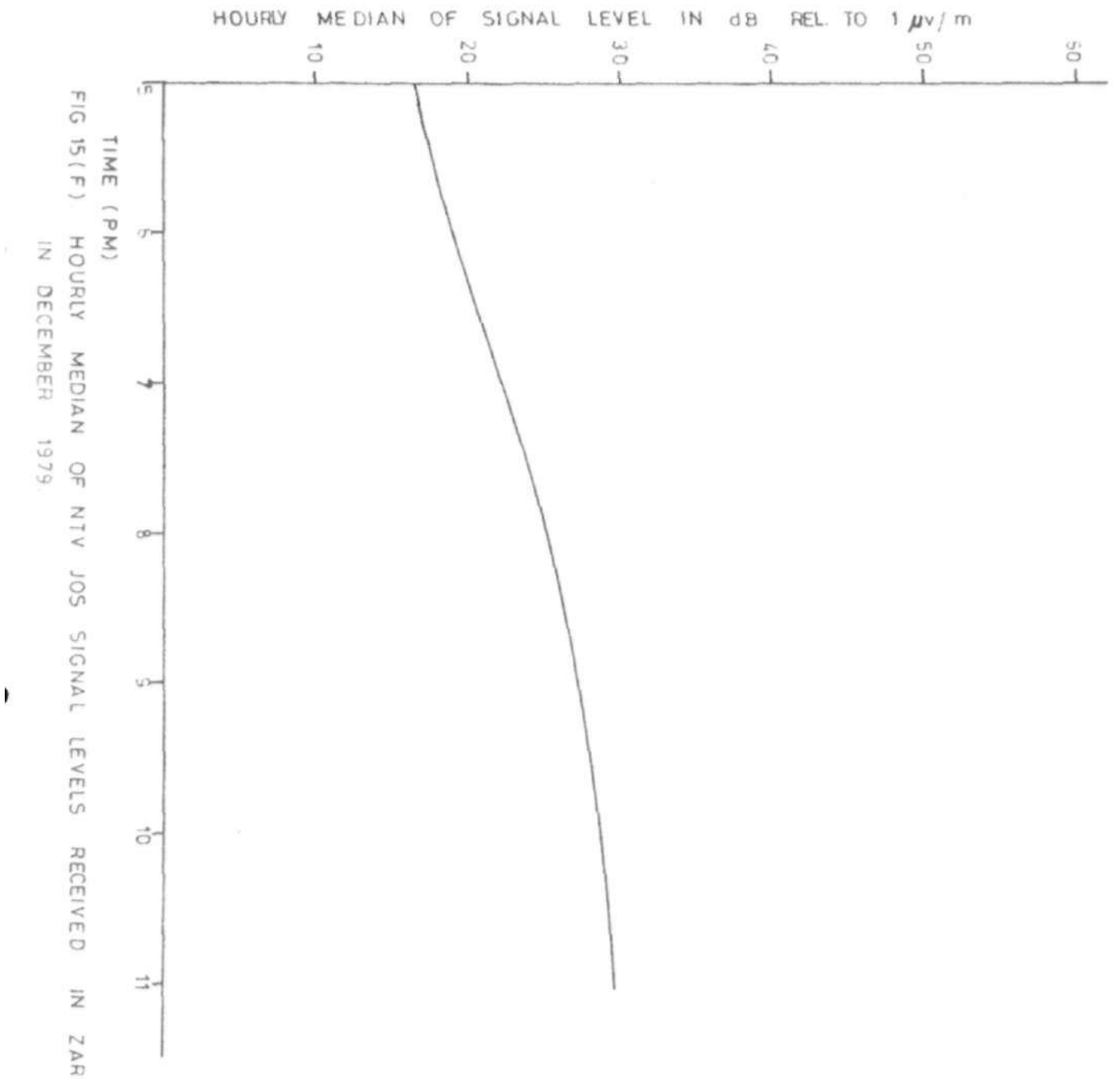


FIG 15(F) HOURLY MEDIAN OF NTV JOS SIGNAL LEVELS RECEIVED IN ZARIA IN DECEMBER 1979

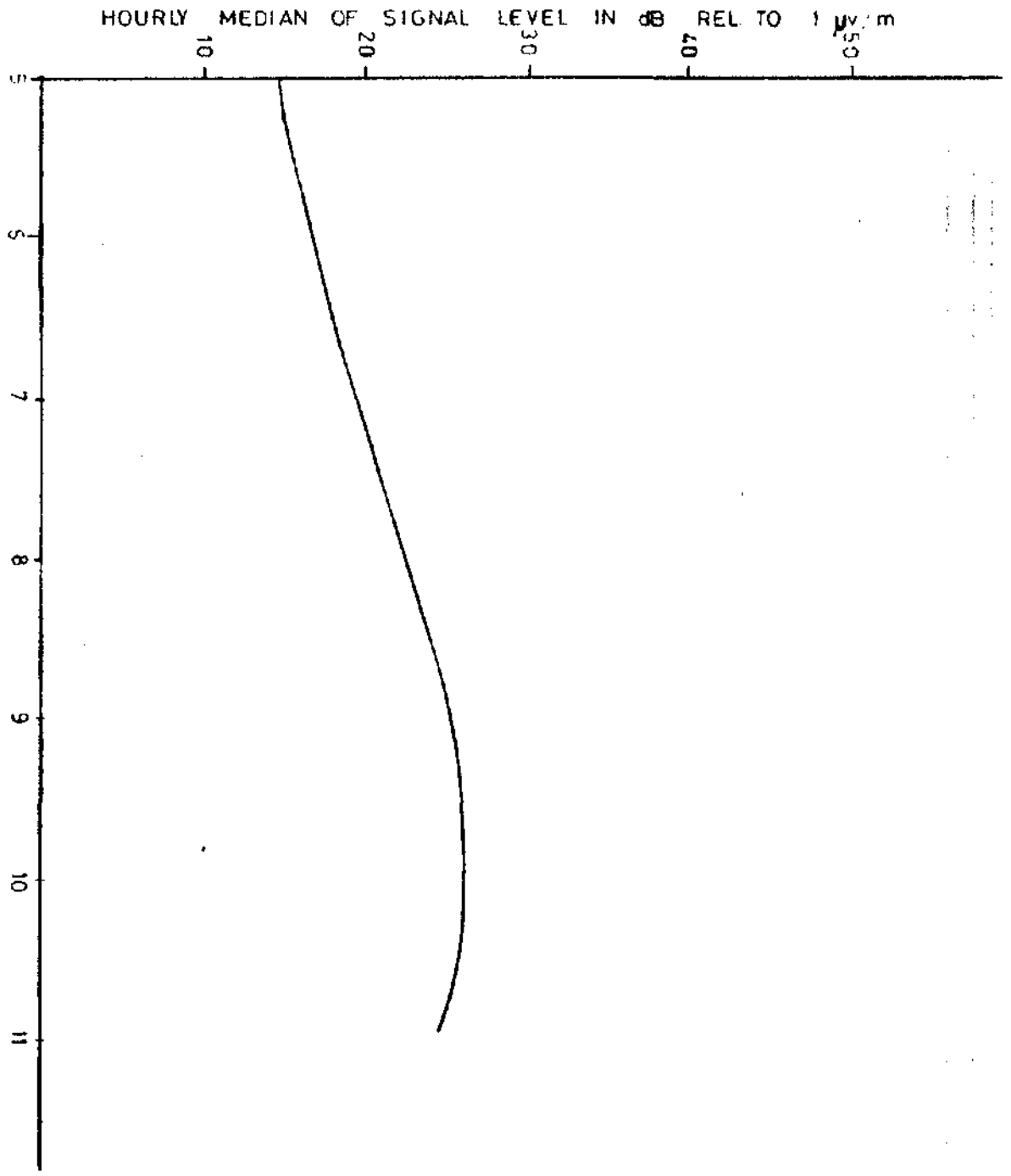


FIG. 15(G). HOURLY MEDIAN OF NTV JOS SIGNAL LEVELS RECEIVED IN ZARIA IN JANUARY 1980.

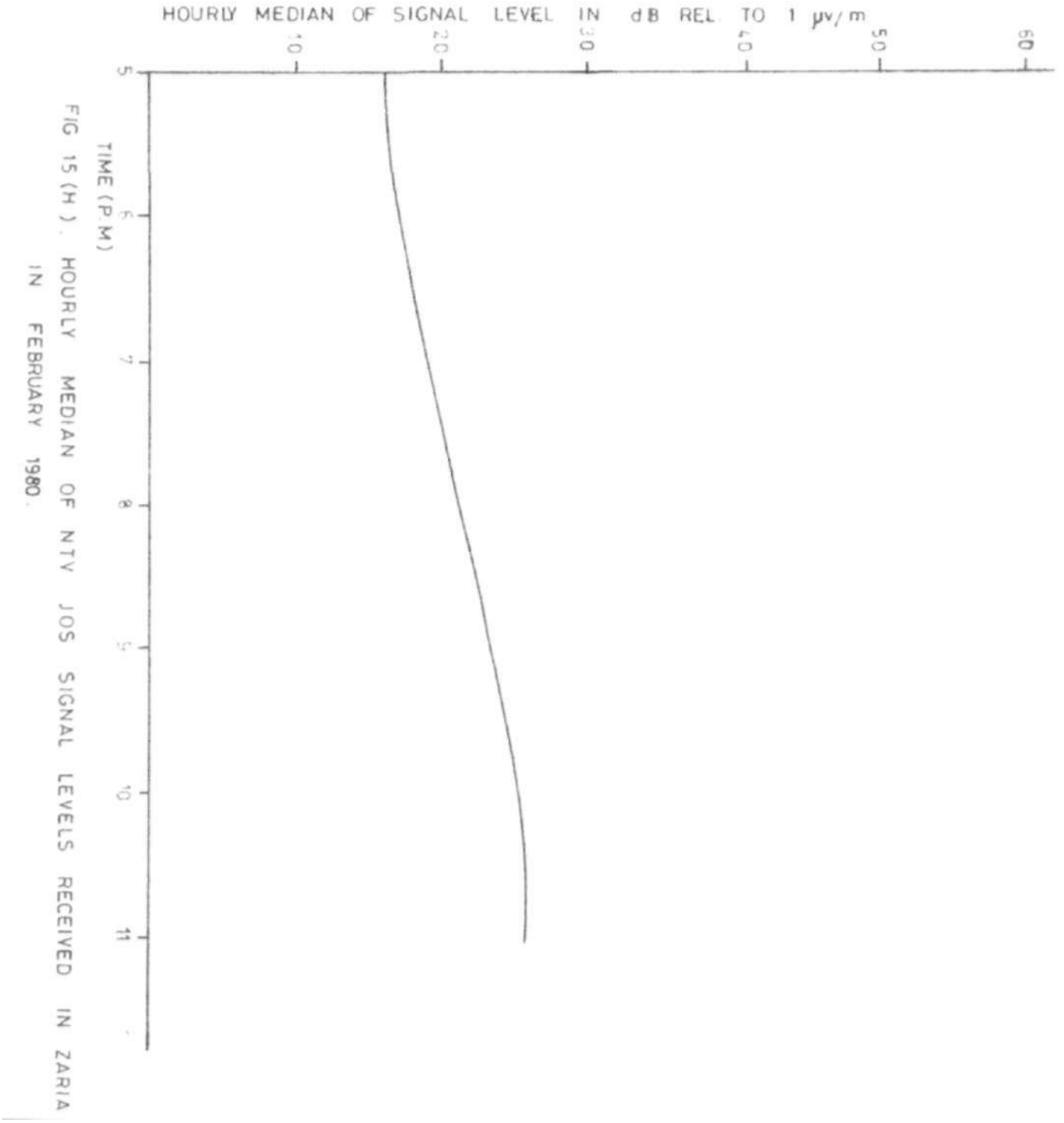


FIG 15 (H). HOURLY MEDIAN OF NTV JOS SIGNAL LEVELS RECEIVED IN ZARIA IN FEBRUARY 1980.

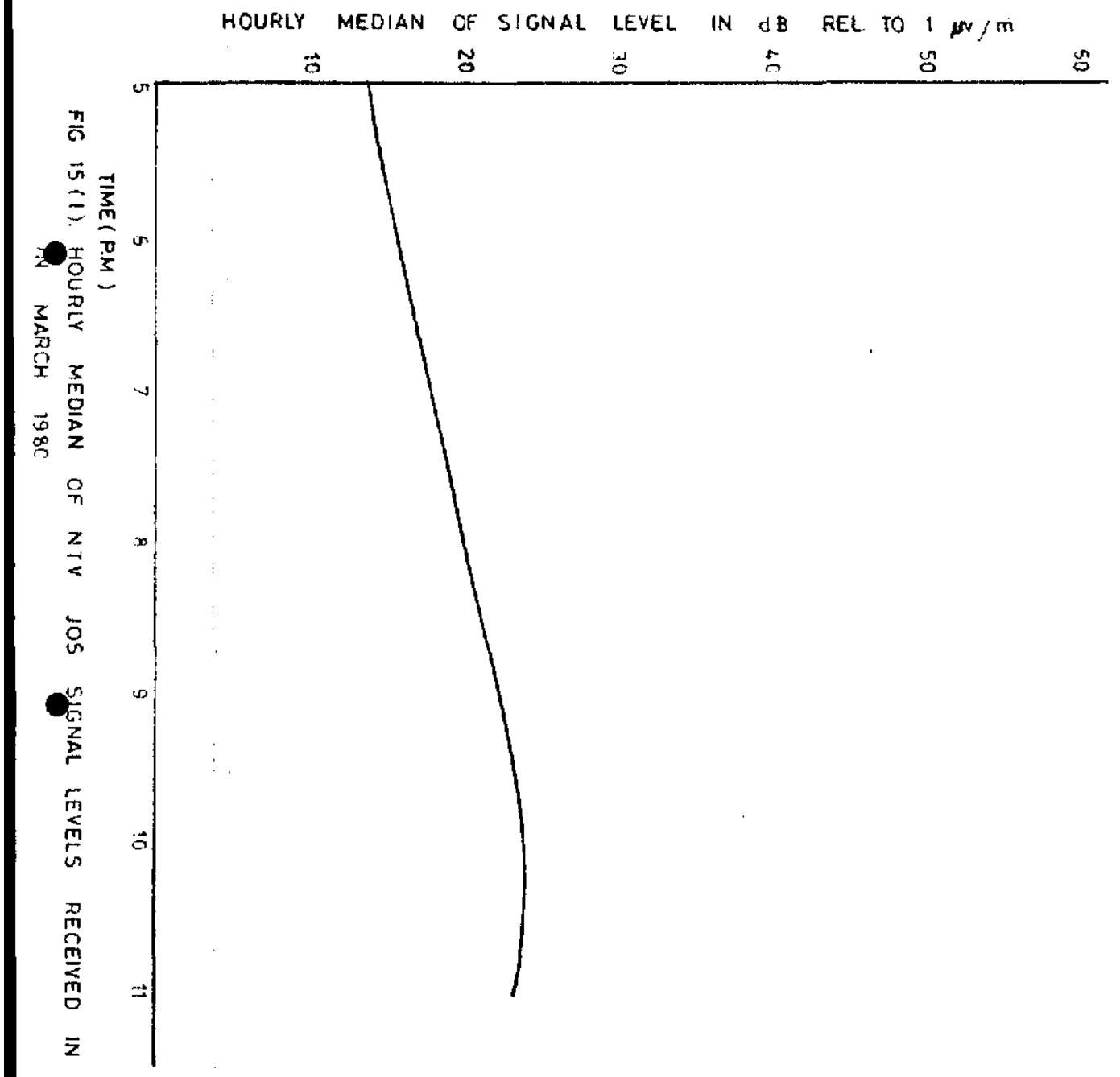


FIG 15 (i). HOURLY MEDIAN OF NTV JOS SIGNAL LEVELS RECEIVED IN ZARIA IN MARCH 1980

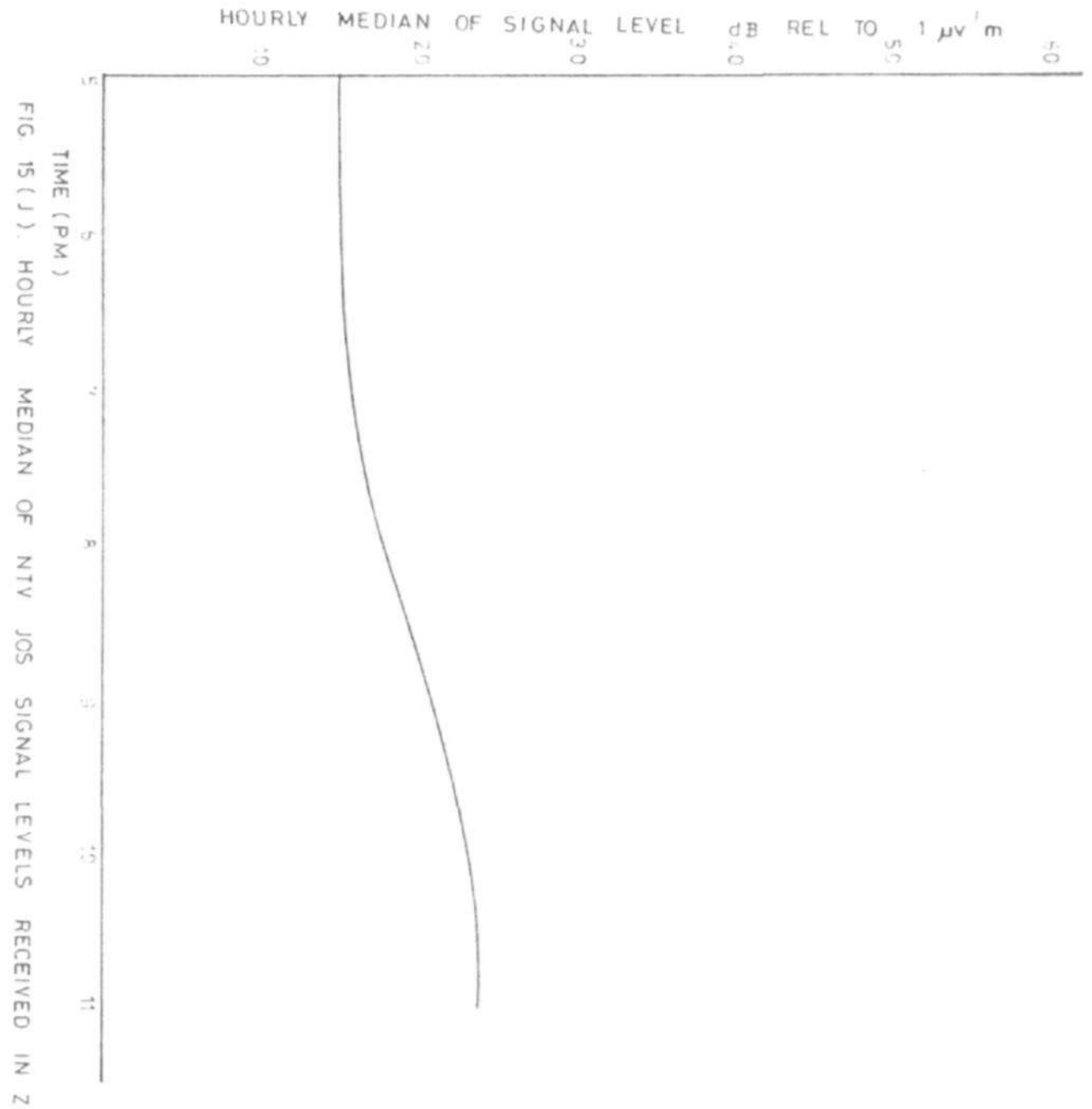


FIG. 15 (J). HOURLY MEDIAN OF NTV JOS SIGNAL LEVELS RECEIVED IN ZARIA IN APRIL 1980

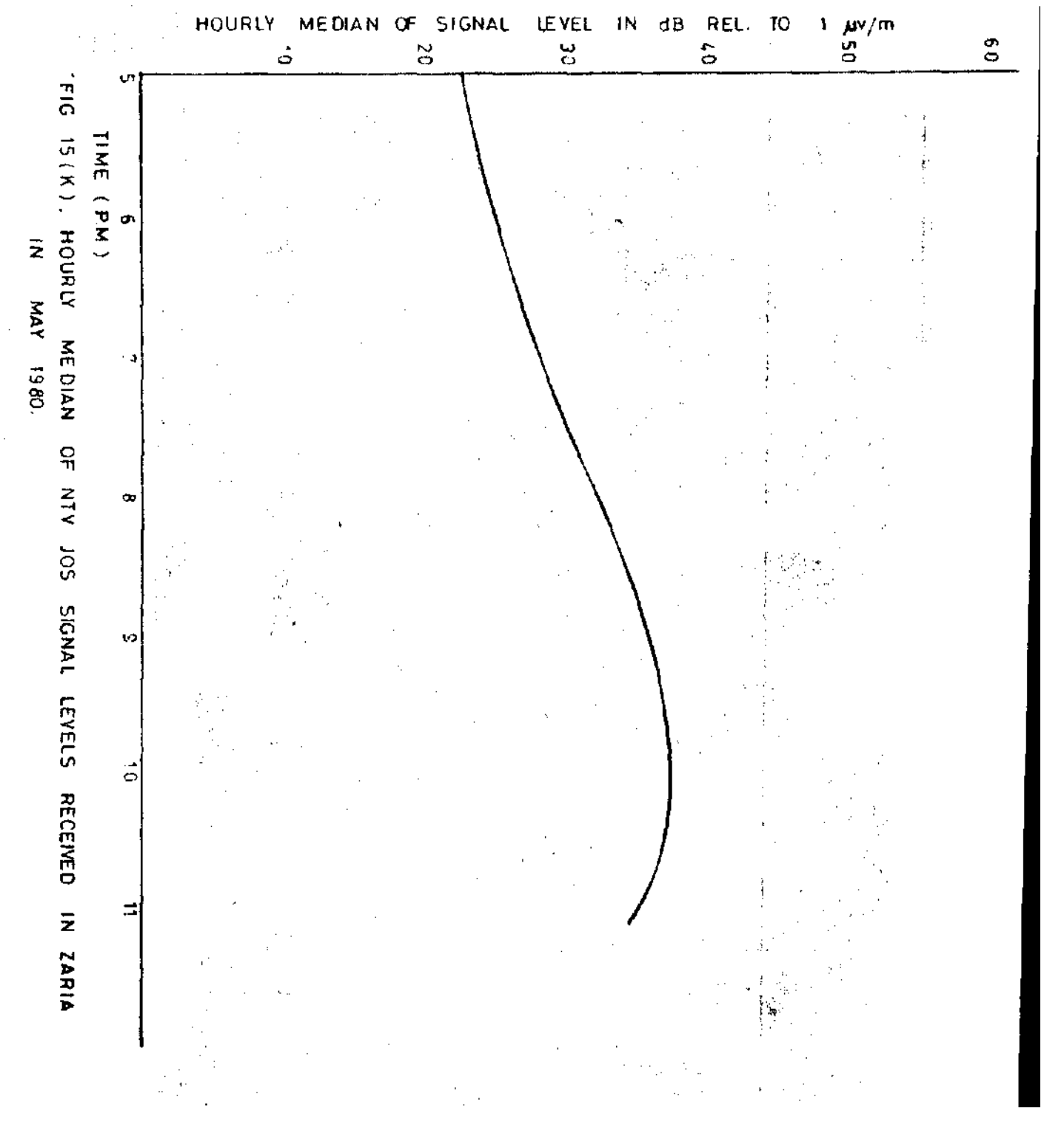


FIG 15(K). HOURLY MEDIAN OF NTV JOS SIGNAL LEVELS RECEIVED IN ZARIA IN MAY 1980.

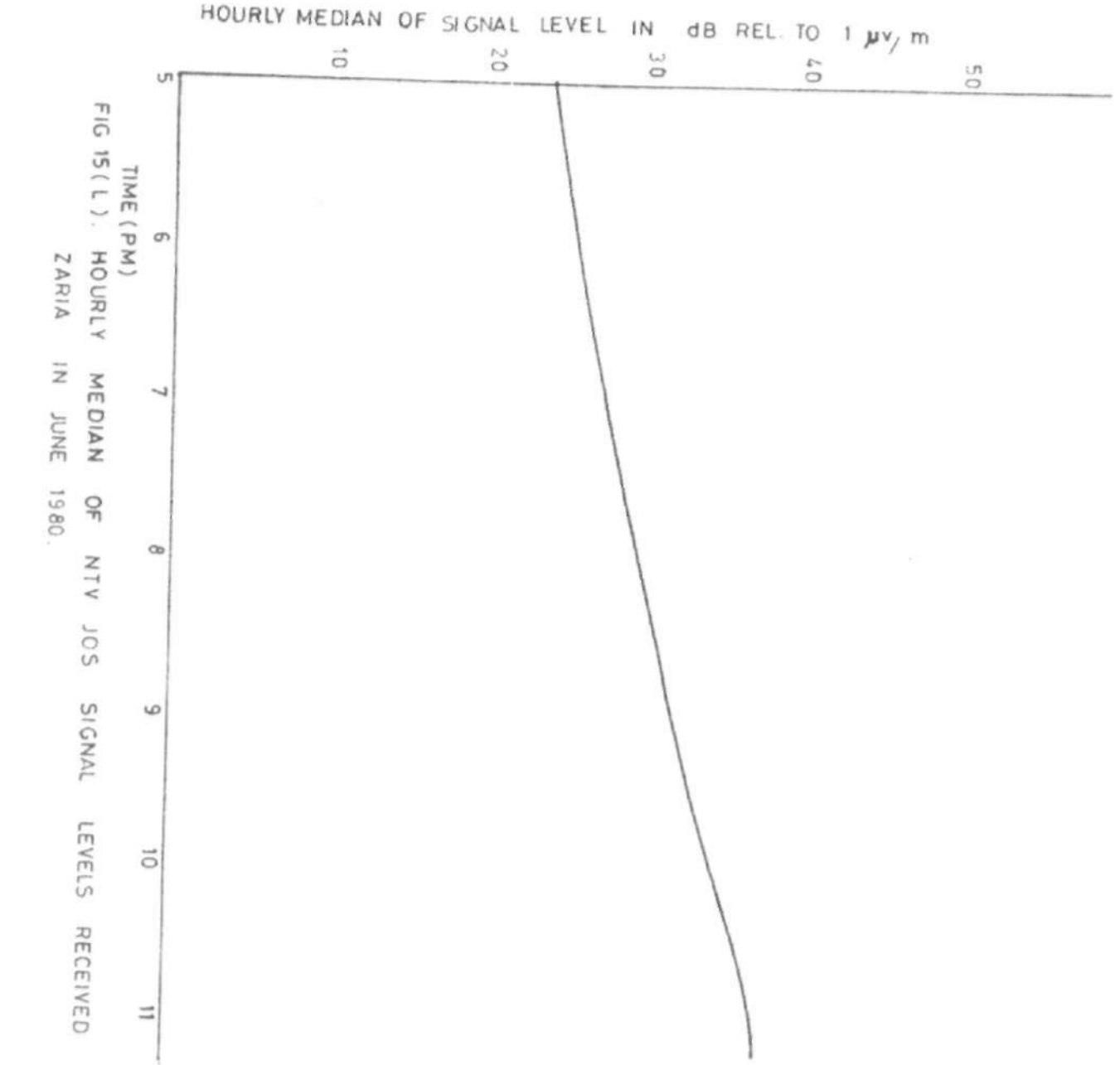


FIG 15(L). HOURLY MEDIAN OF NTV JOS SIGNAL LEVELS RECEIVED IN ZARIA IN JUNE 1980.

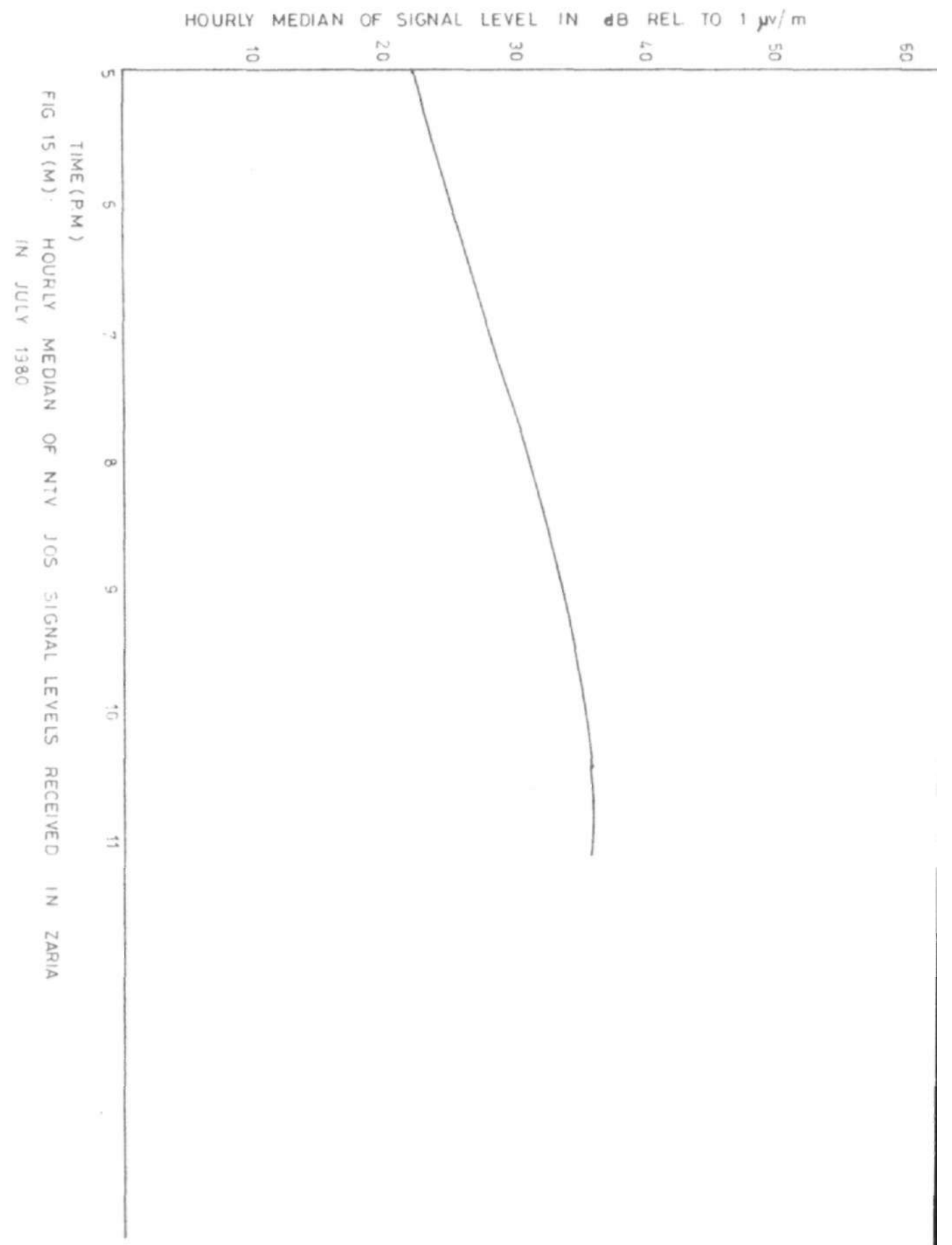


FIG 15 (M): HOURLY MEDIAN OF NTV JOS SIGNAL LEVELS RECEIVED IN ZARIA IN JULY 1980

between 8 p.m. and 11 p.m. Peak values occur between 10 and 11 p.m. The "towards-midnight - fall" trend was violated only once (in October 1979), while the steepest fall around this time was recorded between August and September 1979.

2. The rise rate tended to be higher between July and December (greater or equal to 2 dB/hr) and lower in the months of January to June (less than 2 dB/hr) except in May 1980 when there was a slight increase above this figure. The rise rate is more or less linear between 5 and 7 p.m., but may increase or decrease between 7 and 8 p.m. As can be seen from figure 16 the highest initial rise rate was 3.9 dB/hr, recorded in November 1979 (although this quickly fell to 2.7 dB/hr after 7 p.m.), while the least value of 0.9 dB/hr was recorded in April 1980. The mean rise rate was 2.1 dB/hr in the dry season and 3.0 dB/hr in the wet season. The apparent radical rise from September to November 1979 would be less if the unreliable September reading is ignored.

3. In order to gain some insight into the relationship (if any) between the median value in a given hour of a given month, to the median values in the same hour of the other months, the computed hourly median values have been plotted as ordinate with the months as abscissa (figure 17). To correlate the observed trend with rainfall, a plot of mean monthly rainfall in Jos and Zaria has also been superimposed on the

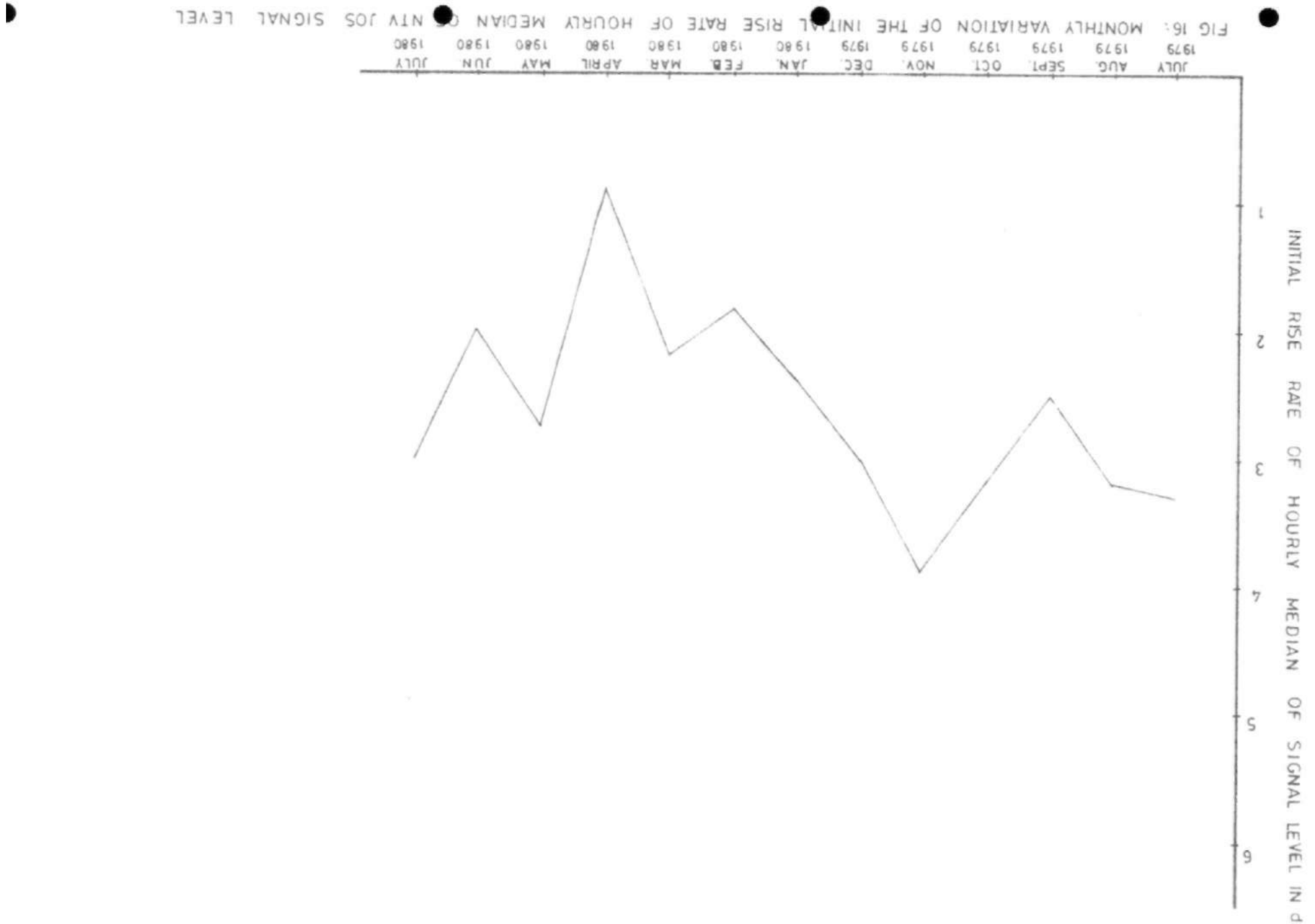

INITIAL RISE RATE OF HOURLY MEDIAN OF SIGNAL LEVEL IN dB PER HR
1
2
3
4
5
6
JULY 1979
AUG. 1979
SEPT. 1979
OCT. 1979
NOV. 1979
DEC. 1979
JAN. 1980
FEB. 1980
MAR. 1980
APRIL 1980
MAY 1980
JUN 1980
JULY 1980
MONTHLY VARIATION OF THE INITIAL RISE RATE OF HOURLY MEDIAN OF NTV JOS SIGNAL LEVEL

FIG 16:

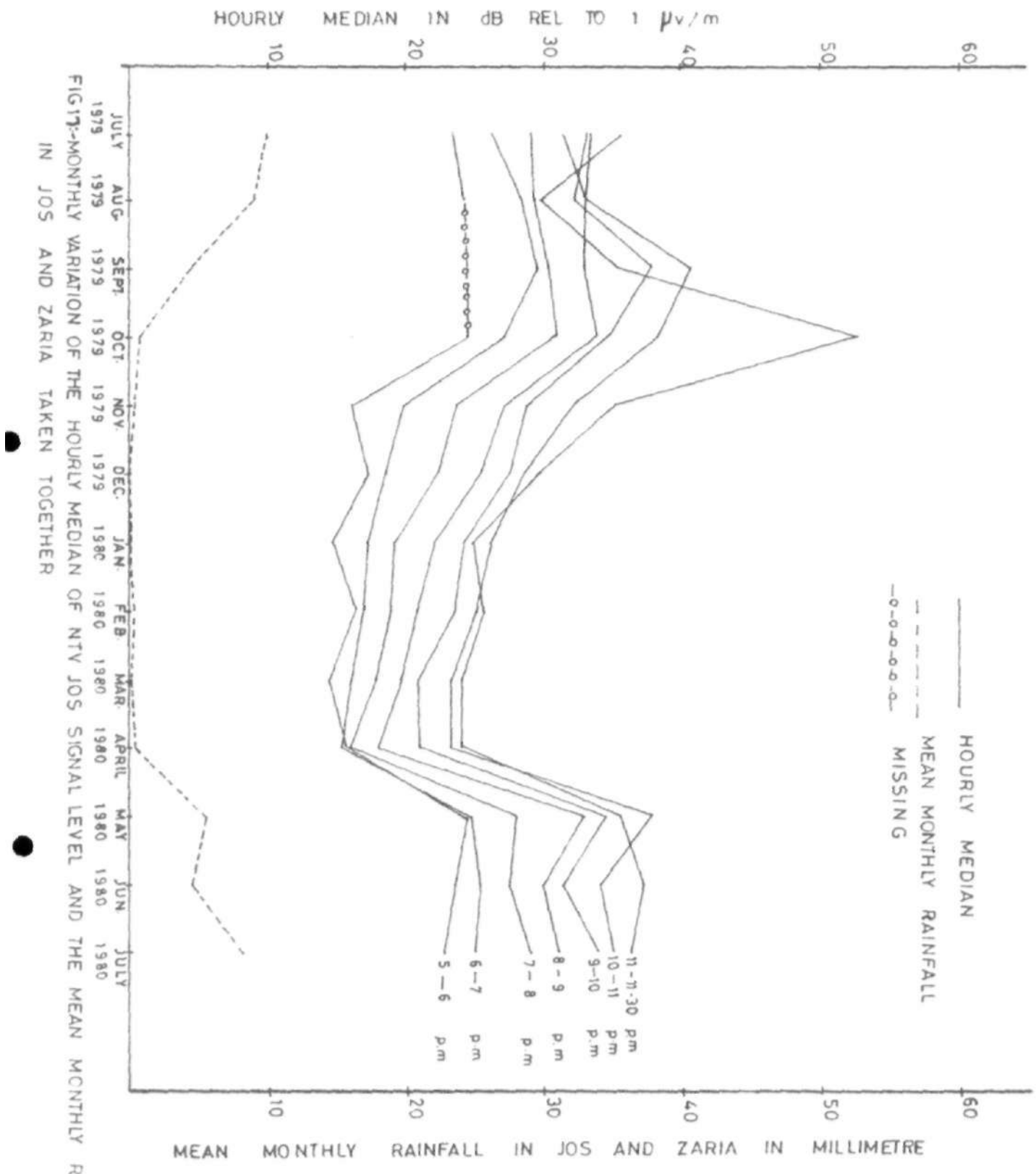


FIG 17:-MONTHLY VARIATION OF THE HOURLY MEDIAN OF NTV JOS SIGNAL LEVEL AND THE MEAN MONTHLY RAINFALL IN JOS AND ZARIA TAKEN TOGETHER

same figure. In this and subsequent combination of graphs, field strength medians are shown in solid lines while rainfall figures are plotted in hatched lines. A combination of hatched line and circles is used where readings are unavailable. Both figures are plotted as ordinate on the same scale. The rainfall figure used (ordinate) was derived by taking the arithmetic mean of the monthly means of rainfall (in millimetre) for Jos and Zaria, as shown in Table 4.2.

In addition to the observations in 1 above, these graphs further reveal that:

(a) hourly median levels are generally high from the month of May to October, with highest levels in September*; a sharp fall in median signal level occurs from October to November, and thereafter a more gradual fall prevails, up to the month of April after which signal level begins to rise again;

(b) this trend agrees considerably with that of the mean monthly rainfall in Jos and Zaria.

4. To expose any trend(s) in the variation of the hourly medians, the figures of Table 4.1(A) were subjected to further statistical analysis for which the arithmetic mean of all the median values in each hour ($\bar{X}$), the mean deviation ($(X - \bar{X}) / N$, $N \leqslant 13$), and the standard deviation

---

* Data for this month are scanty, and thus may not be completely reliable.

$\left((X - \bar{X})^2/N \right)^{\frac{1}{2}}$, $N \leqslant 13$) were evaluated (see table 4.1(B)).

The result of this analysis shows that:

(a) the standard deviation from the mean of the median values in each hour increases from 5 p.m. towards midnight, and

(b) the mean deviation in the 10 - 11 p.m. time interval is positive, indicating that most of the median values in this hour usually are above the mean.

The increasing value of the mean ($\bar{X}$) towards midnight agrees with the observation 1 above, and as indicated then, this trend is violated if the figure of the last hour in October 1979 is considered. It is also of interest to note that without this abnormal seventh hour rise in October 1979, the standard deviation in this hour would be less than that of the sixth hour and the mean deviation positive, although much less than that of the sixth hour.

Some possible implications of these observations are discussed in Section 4.5 below.

4.2 Daily Median Of Signal Level

The median of all the signal levels in each of the 397 days of field strength measurement was computed, using the computer program of appendix A.2. The numerical results obtained are shown in Table 4.3 in decibel relative to 1 uV/m. Graphs of these values are plotted with the rainfall

TABLE 4.1(B)

HOURLY MEDIAN IN dB uV/m(x), MEAN OF HOURLY MEDIAN(x), MEAN DEVIATION AND STANDARD DEVIATION

MONTH	5 - 6 p.m.			6 - 7 p.m.			7 - 8 p.m.			8 - 9 p.m.			
	x	$x-\bar{x}$	$(x-\bar{x})^2$	x	$x-\bar{x}$	$(x-\bar{x})^2$	x	$x-\bar{x}$	$(x-\bar{x})^2$	x	$x-\bar{x}$	$(x-\bar{x})^2$	
July 1979	23.5	3.79	14.36	26.1	3.9	15.15	29.10	4.40	19.36	31.50	4.00	16.00	33
August 1979	24.2	4.49	20.16	28.4	6.2	38.34	29.30	4.60	21.16	33.00	5.50	30.25	32
Sept.1979	-	-	-	29.5	7.3	53.17	30.10	5.40	29.16	33.00	5.50	30.25	37
Oct. 1979	24.4	4.69	22.00	27.1	4.9	23.93	30.70	6.00	36.00	33.90	6.40	40.96	34
Nov. 1979	15.9	3.81	14.52	19.8	2.4	5.80	23.70	1.00	1.00	27.30	0.20	0.04	28
Dec. 1979	17.2	2.51	6.30	18.5	3.7	13.75	22.40	2.30	5.29	25.40	2.10	4.41	27
Jan. 1980	14.8	4.91	24.11	17.2	5.0	0.25	19.20	5.50	34.75	22.00	5.50	30.75	24
Feb. 1980	16.4	3.31	10.96	16.7	5.5	30.3	18.80	5.90	34.81	20.70	6.80	46.24	23.
Mar. 1980	14.3	5.41	29.27	15.9	6.3	39.8	17.80	6.90	47.61	19.70	7.80	60.84	20.
Apr. 1980	15.6	4.11	16.89	15.1	7.1	50.5	15.70	9.00	81.00	19.80	9.70	94.09	20.
May. 1980	24.2	4.49	20.16	24.5	2.3	5.25	27.80	3.10	6.76	32.60	5.10	26.01	34.
Jun. 1980	23.3	3.59	12.89	25.2	3	8.95	27.30	2.60	6.76	29.70	2.20	4.84	31.
July 1980	22.7	2.99	8.94	24.7	2.49	6.21	28.80	4.10	16.81	30.90	3.40	11.56	33.
MEAN ($\bar{x}$)	19.71			22.21			24.70			27.5			
MEAN DEV.	- .000017			- .000023			- .030769			-			
VARIANCE	16.71			24.33			26.06			30.44			
STD. DEV.	4.09			4.93			5.10			5.52			

* Without the abnormal October 1979 figure, these values would be 30.94, .000

TABLE 4.2

MEAN* DAILY RAINFALL (IN mm) IN JOS AND ZARIA

DAY	JULY 1979	AUG. 1979	SEPT. 1979	OCT. 1979	NOV. 1979	DEC. 1979	JAN. 1980	FEB. 1980	MAR. 1980	APRIL 1980	MAY 1980	JUN. 1980	JUL. 1980
1	0.0	2.0	11.9	5.8	0.0	0.0	0.0	0.0	0.0	0.0	33.7	10.8	24.2
2	0.0	7.7	8.8	0.0	0.0	0.0	0.0	0.0	0.0	0.0	0.5	0.0	2.9
3	17.8	2.8	20.4	1.9	0.0	0.0	0.0	0.0	0.0	0.0	6.2	2.2	0.5
4	19.1	18.0	1.0	0.0	14.6	0.0	0.0	0.0	0.0	0.0	0.0	0.0	3.8
5	4.0	3.8	0.0	6.6	0.0	0.0	0.0	0.0	0.0	0.0	10.7	4.2	5.9
6	9.3	0.6	4.0	0.0	0.0	0.0	0.0	0.0	0.0	0.0	18.0	0.0	0.8
7	37.7	9.7	0.1	6.1	0.0	0.0	0.0	0.0	0.0	0.0	0.0	0.0	2.0
8	6.6	0.0	9.7	0.0	0.0	0.0	0.0	0.0	0.0	0.0	12.2	5.7	23.1
9	5.2	0.2	5.2	0.0	0.0	0.0	0.0	0.0	0.0	0.0	0.0	0.0	0.0
10	4.0	6.0	0.0	0.0	0.0	0.0	0.0	0.0	0.0	1.0	0.0	0.0	0.0
11	25.7	14.8	1.0	0.0	0.0	0.0	0.0	0.0	0.0	0.0	0.0	32.8	31.3
12.	11.4	4.0	1.2	3.4	0.0	0.0	0.0	0.0	0.0	0.0	0.0	0.0	6.9
13	0.0	16.2	0.0	0.0	0.0	0.0	0.0	0.0	0.0	0.0	0.0	14.6	0.0
14	9.1	7.8	0.0	0.0	0.0	0.0	0.0	0.0	0.0	0.0	0.0	0.0	0.0
15	0.a	0.0	9.7	0.0	0.0	0.0	0.0	0.0	0.0	0.0	9.4	0.0	0.5
16	23.4	27.2	3.6	0.0	0.0	0.0	0.0	0.0	0.0	0.0	12.3	1.0	24.8
17	25.4	17.9	0.8	0.0	0.0	0.0	0.0	0.0	0.0	0.0	0.0	2.5	2.2
18	5.1	16.4	0.0	0.0	0.0	0.0	0.0	0.0	0.0	0.0	5.0	32.6	5.1
19	5.0	0.0	0.0	0.0	0.0	0.0	0.0	0.0	0.0	0.0	12.2	1.8	23.2
20	0.0	33.2	1.3	0.0	0.0	0.0	0.0	0.0	0.0	0.8	1.3	5.0	9.7
21	8.9	5.0	11.6	0.0	0.0	0.0	0.0	0.0	0.0	0.0	11.3	1.7	0.0
22	8.5	7.8	8.4	0.0	0.0	0.0	0.0	0.0	0.4	0.0	0.0	5.7	21.4
23.	0.0	0.0	5.6	0.0	0.0	0.0	0.0	0.0	1.8	0.0	6.2	0.0	4.7
24	15.1	19.1	7.6	0.0	0.0	0.0	0.0	0.0	0.0	1.4	0.0	18.1	0.0
25	1.3	16.3	1.0	0.0	0.0	0.0	0.0	0.0	5.0	0.0	6.2	0.0	9.7
26	7.5	0.0	16.3	0.0	0.0	0.0	0.0	0.0	0.0	0.0	1.5	0.0	4.0
27	8.6	30.9	0.1	0.0	0.0	0.0	0.0	9.1	0.0	0.0	6.7	0.0	1.9
28	5.1	3.8	0.0	0.0	0.0	0.0	0.0	0.0	0.0	12.6	3.8	0.0	2.7
29	0.7	6.9	6.0	0.0	0.0	0.0	0.0	0.0	0.0	0.0	0.0	0.0	5.2
30	25.1	5.0	1.8	0.0	0.0	0.0	0.0	0.0	0.0	0.0	9.8	0.6	10.8
31	24.6	3.1	-	0.0	-	0.0	0.0	-	0.0	-	2.6	-	2.5

* Derived from the Arithmetic Mean of the Daily Mean Rainfall in Jos and Daily Mean Rainfall in Zaria.

TABLE 4.1

DAILY MEDIAN OF SIGNAL LEVEL IN dB ABOVE 1 μV/m

MONTH	DAILY MEDIAN																													
Jul. 1979	30.2	21.4	22.1	23.0	30.5	22.0	31.5	29.3	32.0	*	25.9	39.0	31.4	56.7	*	39.7	33.3	38.9	26.1	35.9	34.7	33.6	31.4	30.3	45.4	19.1	27.8	22.6	44.9	22.2	17.9
Aug. 1979	33.2	32.8	23.0	44.3	33.3	25.2	22.7	32.3	29.9	26.9	29.8	12.1	25.2	32.7	35.9	27.5	36.9	22.2	24.2	40.9	23.2	26.6	17.0	44.4	26.2	23.9	*	*	*	24.6	26.5
Sept.1979	*	*	*	30.3	31.9	30.9	23.2	60.9	*	31.5	42.1	41.0	*	*	*	*	*	*	*	*	*	*	*	*	*	*	*	*	*	*	-
Oct. 1979	*	*	33.1	21.9	21.5	*	*	40.0	32.9	32.2	33.6	37.1	56.2	36.5	29.2	30.9	30.9	*	33.2	30.3			*	23.5	32.1	36.3	33.4	31.2	78.2	25.1	46.8
Nov. 1979	33.8	32.5	*	31.6	32.7	48.4	*	30.0	27.0	*	27.9	27.3	25.0	29.0	23.8	23.0	*	21.0	19.0	24.4	15.6	23.0	25.8	*	28.7	25.1	25.0	23.7	20.4	29.1	-
Dec. 1979	28.0	27.7	29.0	27.4	27.3	36.3	29.0	33.2	19.8	29.0	26.6	26.0	22.4	15.3	21.2	*	28.7	13.3	25.6	24.1	24.0	*	*	14.3	16.9	31.3	27.1	33.5	35.7	*	26.0
Jan. 1980	21.2	*	*	*	*	*	25.6	24.9	21.0	26.5	22.0	24.5	20.6	23.2	21.9	21.6	20.1	25.8	18.3	18.2	18.8	20.8	21.9	29.2	16.8	21.8	19.2	28.9	28.5	*	20.7
Feb. 1980	*	*	26.0	23.6	27.2	26.9	19.1	*	20.1	21.8	25.1	23.1	21.6	20.4	21.2	18.8	25.0	20.2	18.7	*	19.0	*	*	18.9	15.6	19.6	16.3	17.4	22.0	-	-
Mar. 1980	23.7	20.7	20.1	18.5	18.5	17.2	27.4	19.4	19.9	15.3	16.1	18.1	17.2	17.7	15.3	20.5	16.0	21.9	24.7	16.9	24.3	45.0	33.4	21.4	21.7	*	21.6	19.5	16.7	19.7	15.9
Apr. 1980	18.7	15.1	13.0	13.5	16.7	15.3	18.8	21.1	*	29.3	20.1	17.0	16.2	16.7	14.4	*	*	*	*	*	*	*	*	*	30.9	21.5	20.6	23.2	18.2	*	-
May. 1980	*	*	24.1	26.6	26.0	25.1	12.8	26.4	24.3	27.2	46.3	*	25.2	15.9	27.0	42.9	34.2	36.7	26.1	44.1	20.6	24.3	32.3	*	*	*	27.2	29.1	27.0	*	44.8
June 1980	27.2	32.7	43.2	27.9	35.8	33.2	26.4	48.0	36.2	23.3	45.7	25.7	27.0	35.9	26.1	26.7	42.0	47.9	32.8	25.9	18.5	22.9	28.9	38.7	29.7	26.4	23.0	27.4	27.7	23.0	-
July 1980	29.7	30.6	30.9	37.8	39.1	28.8	26.9	25.0	*	28.0	*	*	*	*	*	*	*	*	*	*	*	*	*	*	*	*	*	*	*	*	*
DAY	1	2	3	4	5	6	7	8	9	10	11	12	13	14	15	16	17	18	19	20	21	22	23	24	25	26	27	28	29	30	31

* Missing Data

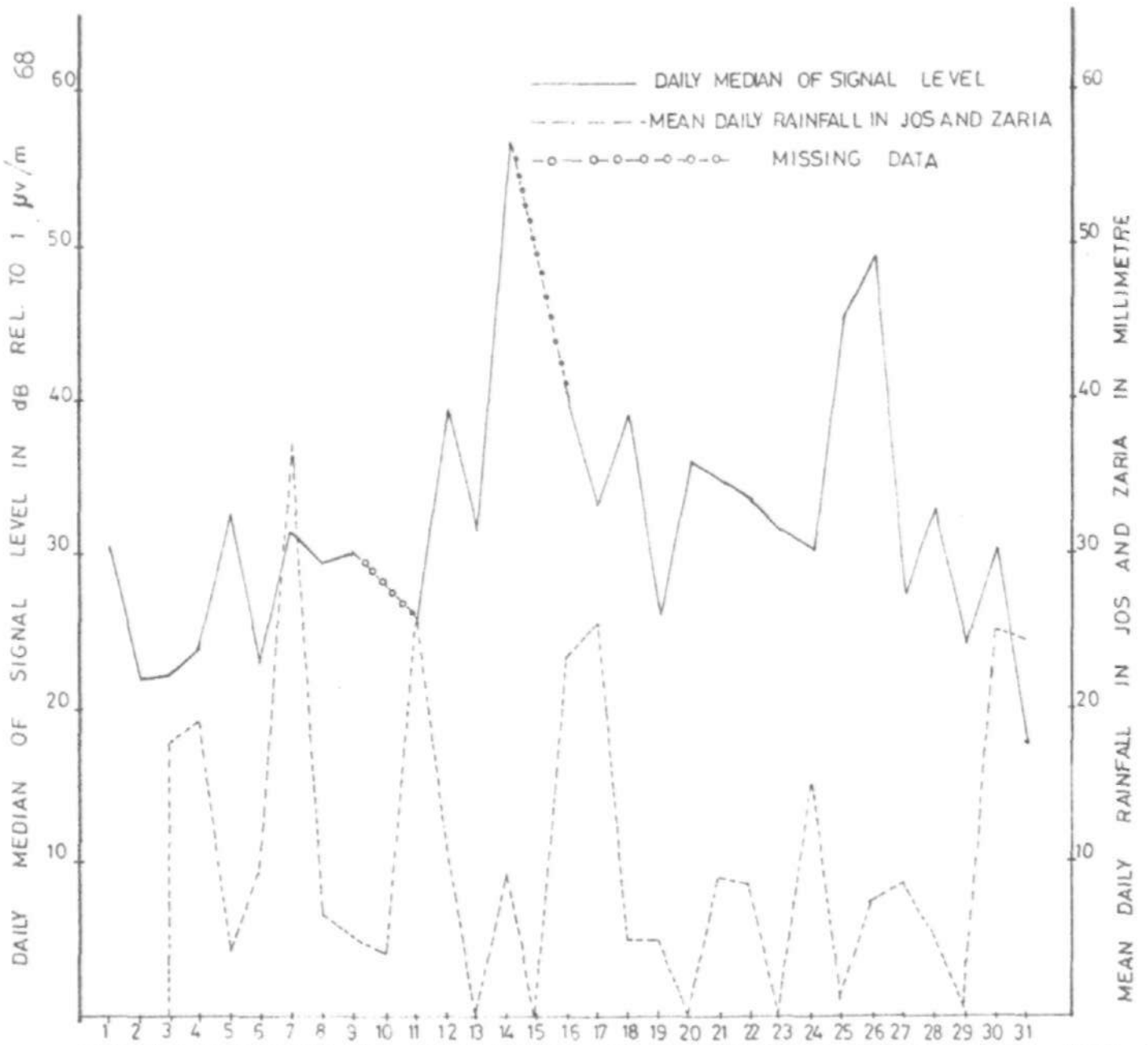


FIG 18(A). COMPARING THE DAILY MEDIAN OF NTV JOS SIGNAL LEVEL IN ZARIA WITH DAILY MEAN RAINFALL IN JOS AND ZARIA (TAKEN TOGETHER) IN THE MONTH OF JULY 1979

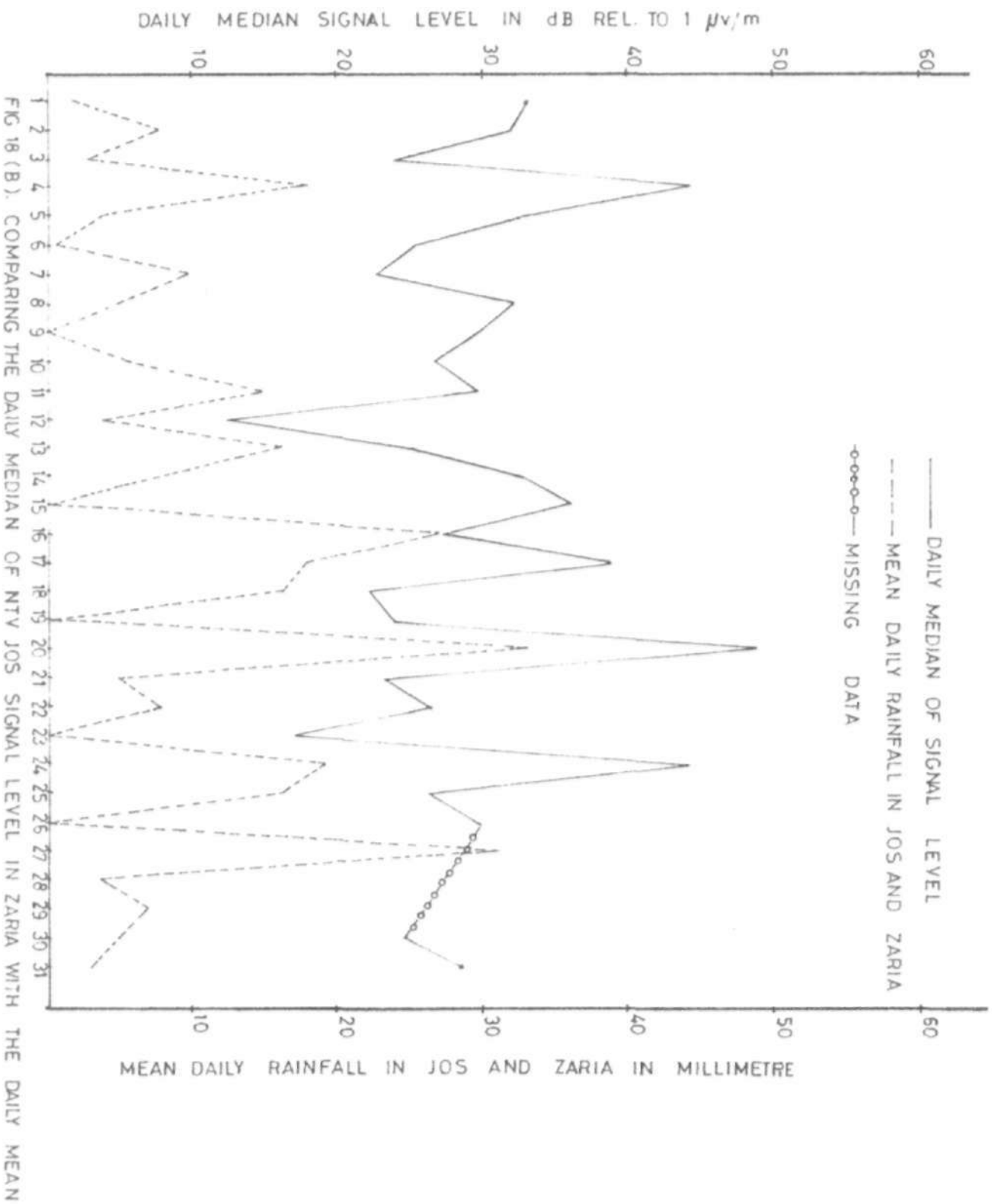


FIG 18 (B). COMPARING THE DAILY MEDIAN OF NTV JOS SIGNAL LEVEL IN ZARIA WITH THE DAILY MEAN RAINFALL IN JOS AND ZARIA (TAKEN TOGETHER) IN THE MONTH OF AUGUST 1979.

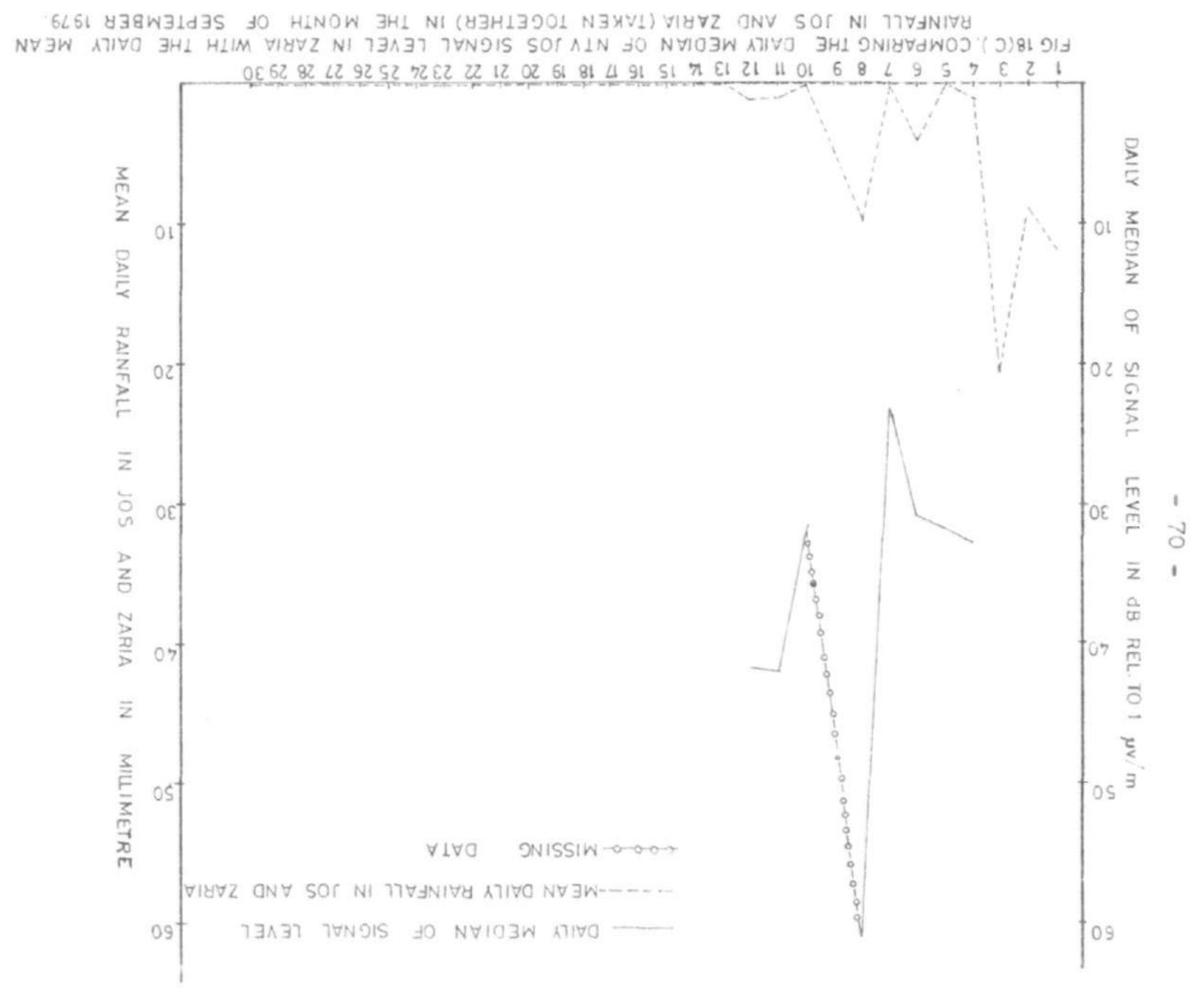


FIG 18(C). COMPARING THE DAILY MEDIAN OF NTV JOS SIGNAL LEVEL IN ZARIA WITH THE DAILY MEAN RAINFALL IN JOS AND ZARIA (TAKEN TOGETHER) IN THE MONTH OF SEPTEMBER 1979.

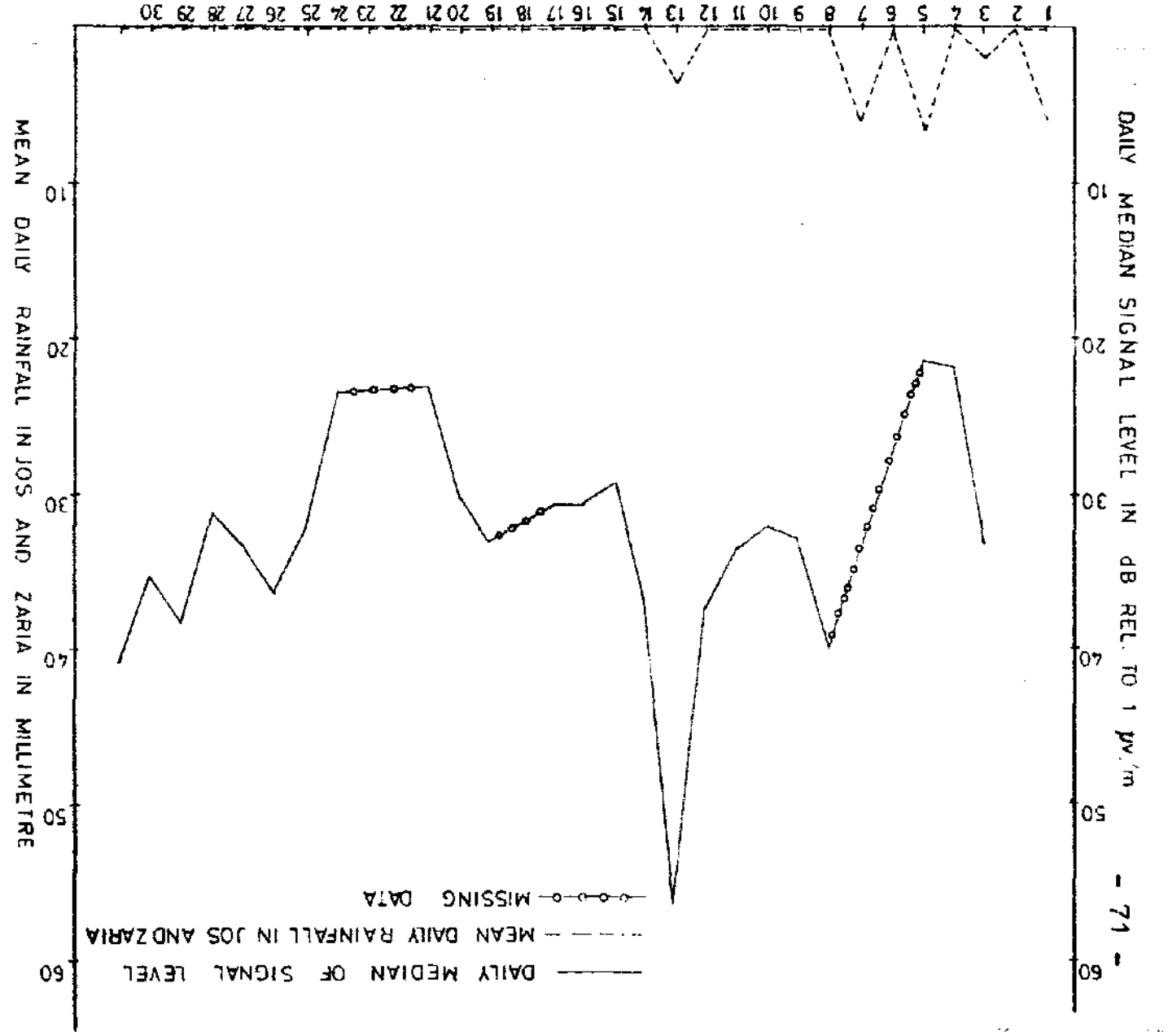


FIG 18(D): COMPARING THE DAILY MEDIAN OF NTV JOS SIGNAL LEVEL IN ZARIA WITH THE DAILY MEAN RAINFALL IN JOS AND ZARIA (TAKEN TOGETHER) IN THE MONTH OF OCTOBER 1979.

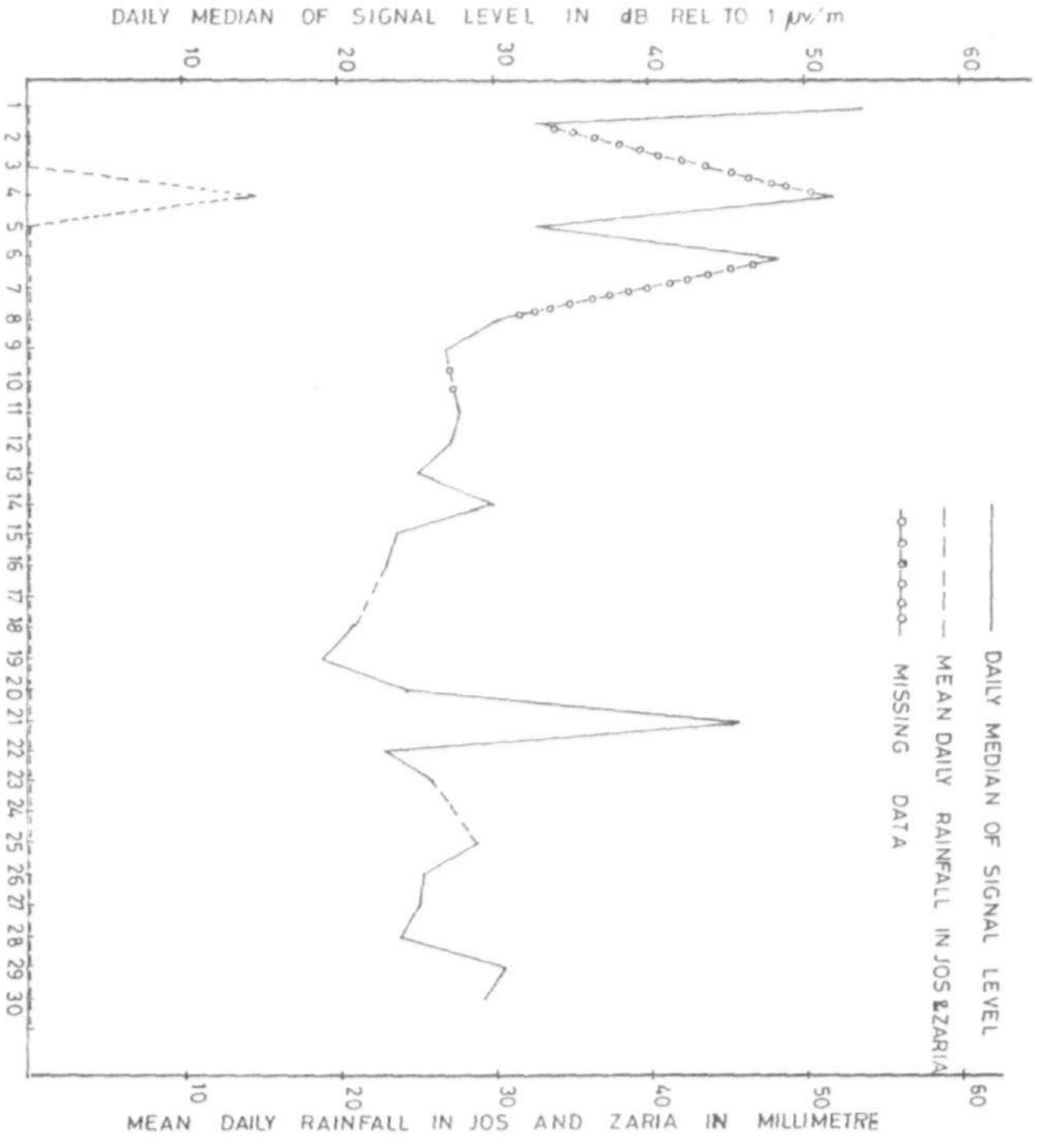


FIG 18(E) COMPARING THE DAILY MEDIAN OF N TV JOS SIGNAL LEVEL IN ZARIA WITH THE DAILY MEAN RAINFALL IN JOS AND ZARIA (TAKEN TOGETHER) IN THE MONTH OF NOVEMBER 1979.



FIG 18(G). COMPARING THE DAILY MEDIAN OF NTV JOS SIGNAL LEVEL IN ZARIA WITH THE DAILY MEAN RAINFALL IN JOS AND ZARIA (TAKEN TOGETHER) IN THE MONTH OF JANUARY 1980

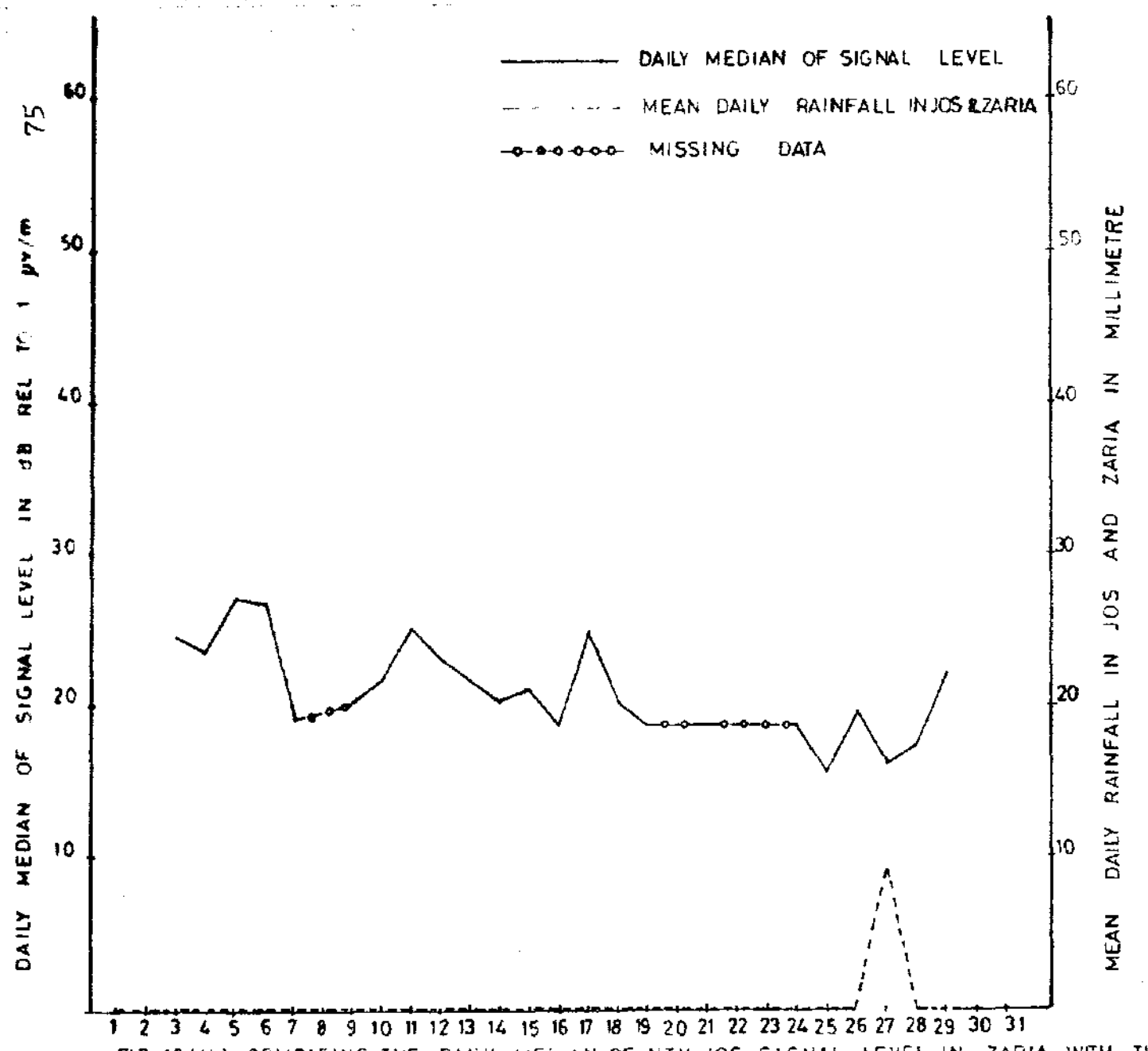


FIG 18(H) COMPARING THE DAILY MEDIAN OF NTV JOS SIGNAL LEVEL IN ZARIA WITH THE DAILY MEAN RAINFALL IN JOS AND ZARIA (TAKEN TOGETHER) IN THE MONTH OF FEBRUARY 1980.

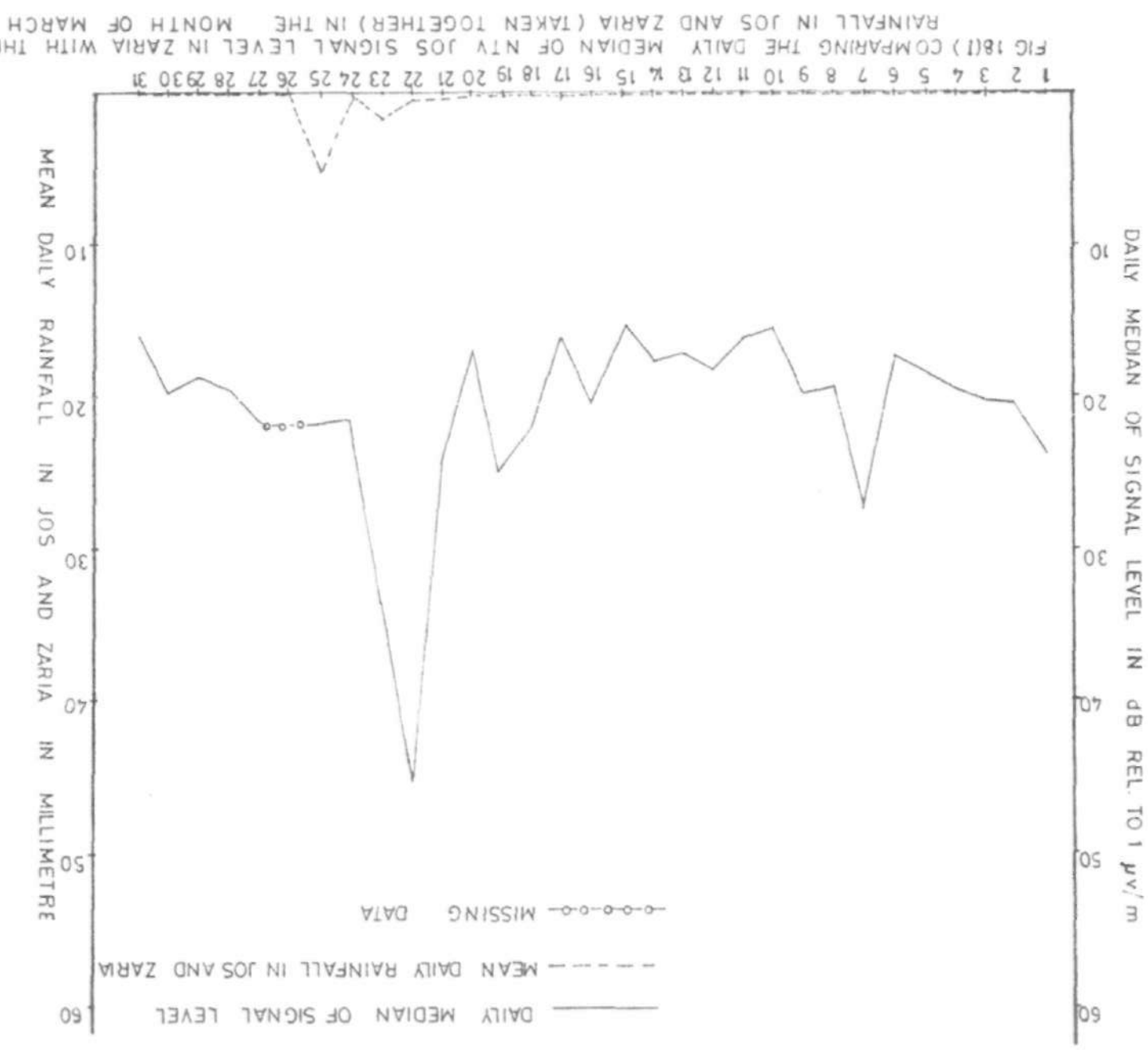


FIG 18(I) COMPARING THE DAILY MEDIAN OF NTV JOS SIGNAL LEVEL IN ZARIA WITH THE DAILY MEAN RAINFALL IN JOS AND ZARIA (TAKEN TOGETHER) IN THE MONTH OF MARCH 1980

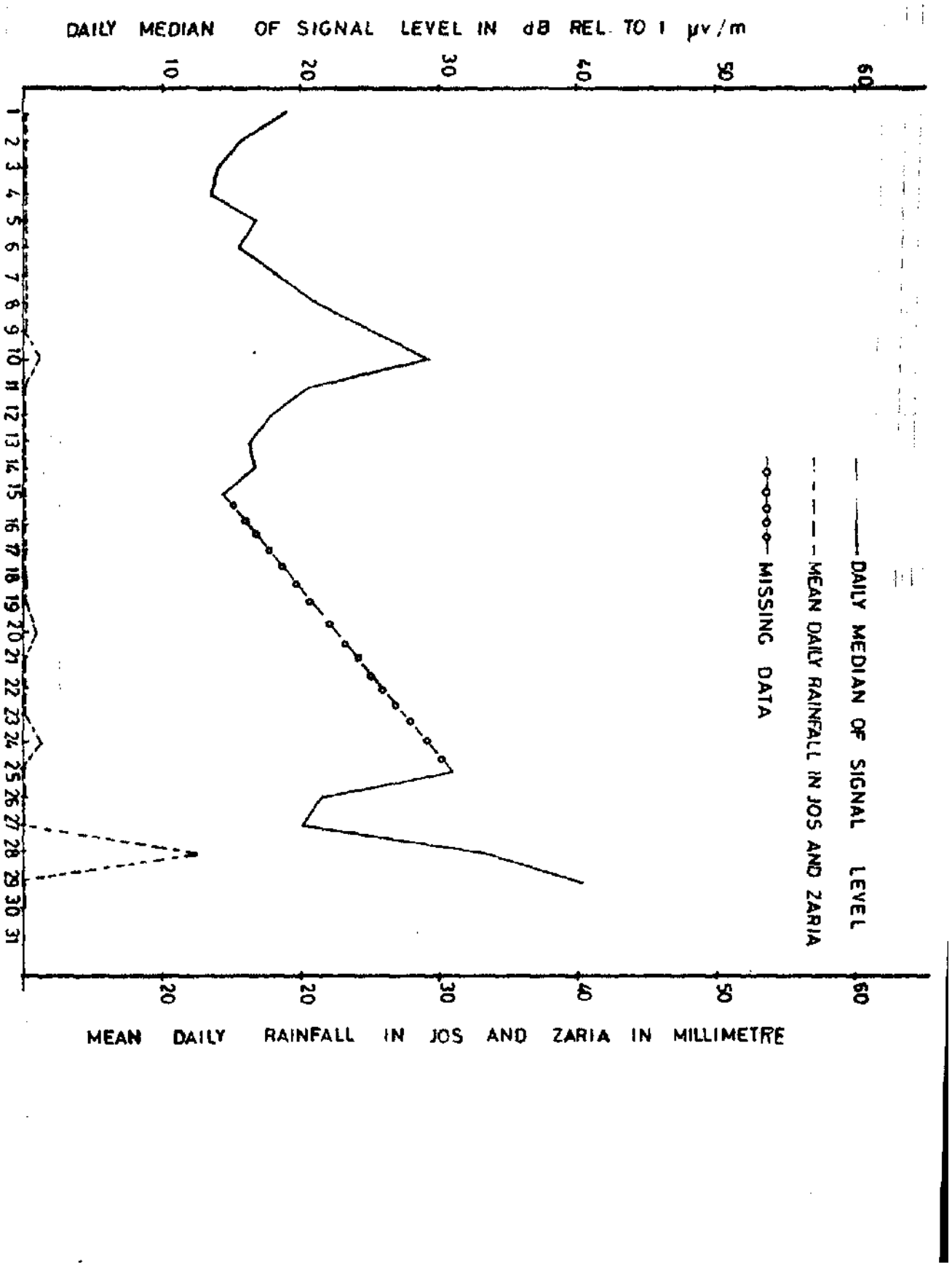


FIG 18(J). COMPARING THE DAILY MEDIAN OF NTV JOS SIGNAL LEVEL IN ZARIA WITH THE DAILY MEAN RAINFALL IN JOS AND ZARIA (TAKEN TOGETHER) IN THE MONTH OF APRIL 1980.

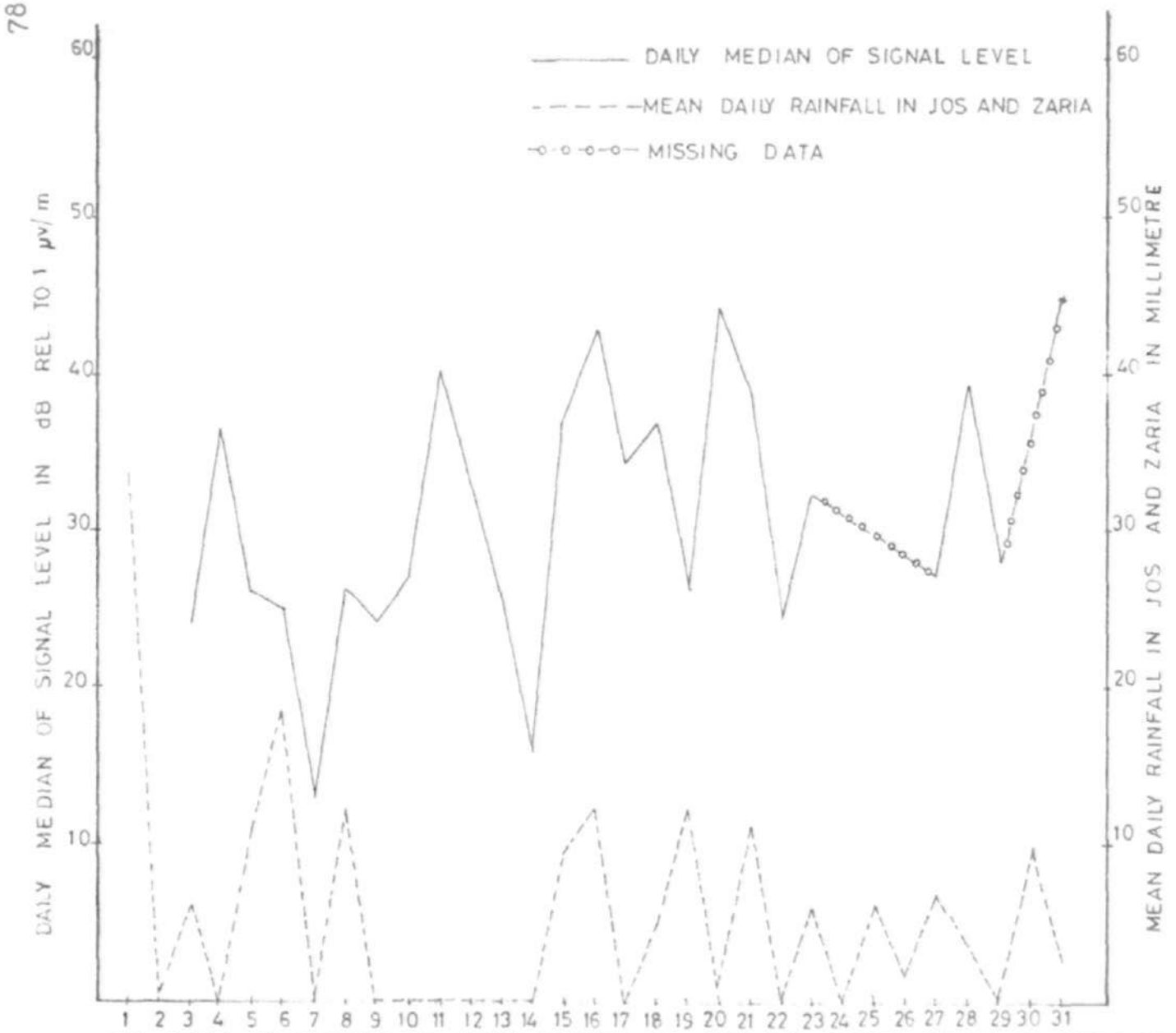


FIG 18(K). COMPARING THE DAILY MEDIAN OF NTV JOS SIGNAL LEVEL IN ZARIA WITH THE DAILY MEAN RAINFALL IN JOS AND ZARIA (TAKEN TOGETHER) IN THE MONTH OF MAY 1980

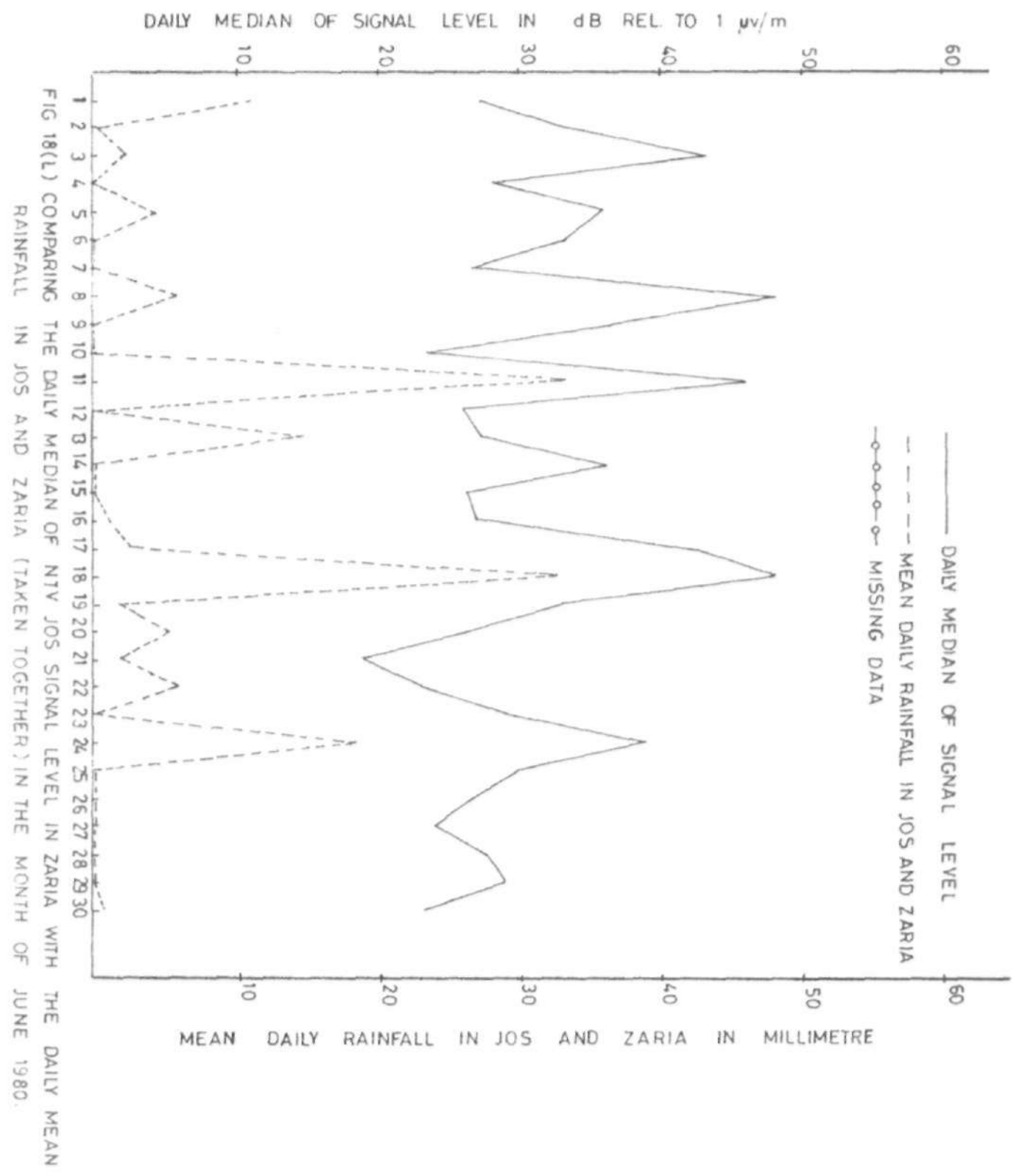


FIG 18(L) COMPARING THE DAILY MEDIAN OF NTV JOS SIGNAL LEVEL IN ZARIA WITH THE DAILY MEAN RAINFALL IN JOS AND ZARIA (TAKEN TOGETHER) IN THE MONTH OF JUNE 1980.

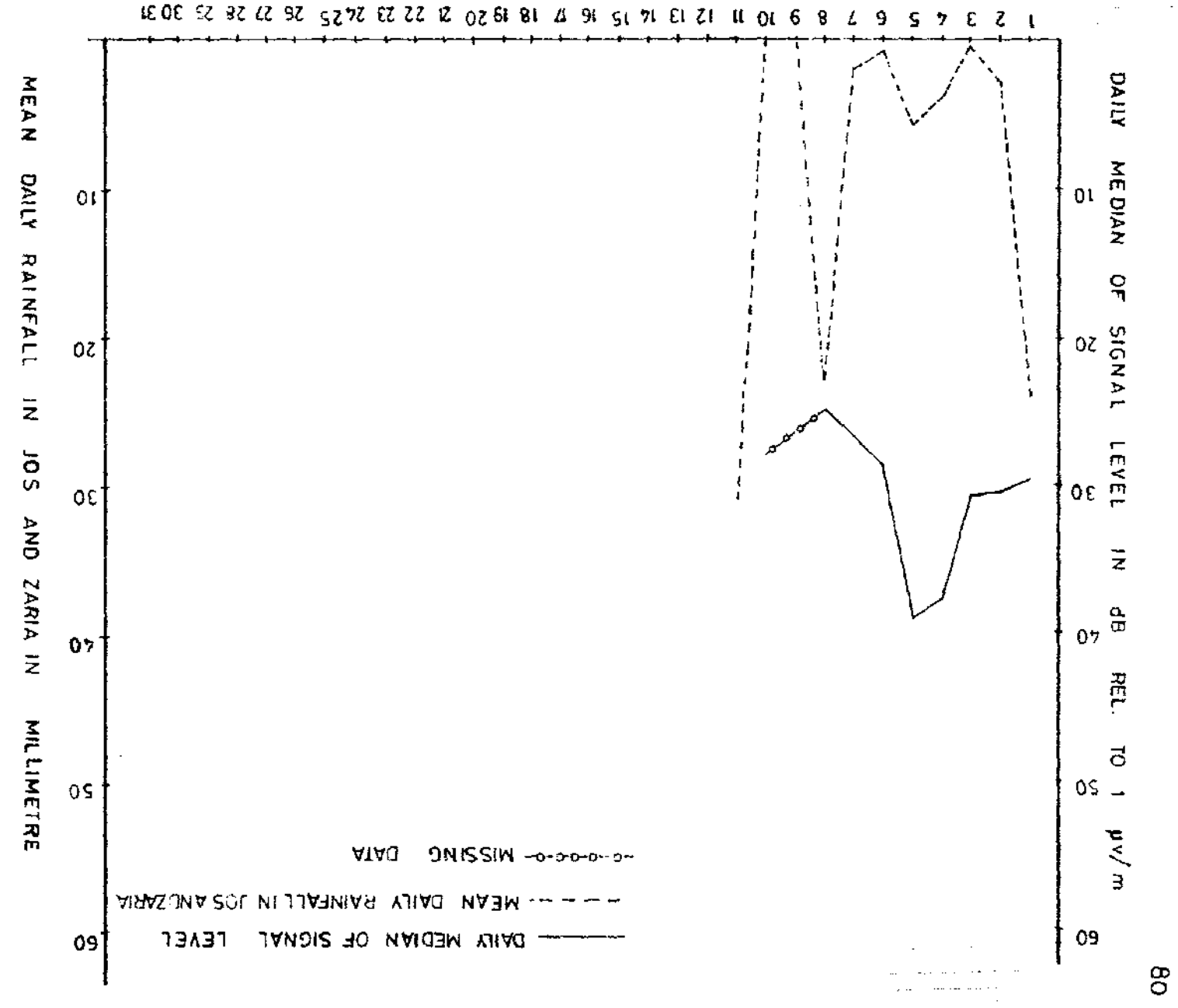


FIG 18 (M) COMPARING THE DAILY MEDIAN OF NTV JOS SIGNAL LEVEL IN ZARIA WITH THE DAILY MEAN RAINFALL IN JOS AND ZARIA (TAKEN TOGETHER) IN THE MONTH OF JULY 1980

figures (in millimetre) as ordinate and the days of the month as abscissa (figures 18(A) - (M)). Deductions from these graphs include:

1. The daily median of signal levels are higher in the rainy season months (May - October) than in the dry season (November - April).

2. There is a degree of correlation between the daily median and the mean daily rainfall figures, as typified in the months of March, April and June 1980 (figures 18 (I), (J), and (L). Correlation is, however, not a hundred per cent as there exist cases of either one day shift between peak values, (or troughs) or altogether complete absence of correlation. Typical examples of these features can be seen between April 27th - 29th 1980, July 17th - 18th 1979, August 6th - 10th 1979 and November 20th - 22nd 1979 (figures 18 (J), (A), (B), (E) respectively. Correlation also becomes less obvious in the months of heavy rains like July and August 1979 (figures 18 (A) and (B) respectively).

3. There is a greater degree of variation of daily median in the wet season than in the dry season. (Compare graphs for February 1980, typical dry season month, and May 1980, typical rainy season month in figures 18(H) and (K) respectively).

4.3 Monthly Median Of Signal Level

The median of all the signal levels in each month was computed using the computer programs of appendix A.5 and A.6. The numerical results obtained are shown in Table 4.4 in decibel relative to 1 μV/m. These are compared graphically with the mean monthly rainfall (in millimetre) in Zaria and Jos together which was derived as explained in Section 4.1 (table 4.5), and then with the mean monthly rainfall in Zaria and Jos separately (figure 19(a), (b) and (c) respectively).

Two trends are discernible from these plots:

1. The monthly median and the mean monthly rainfall show a high correlation tendency.
2. Correlation is improved if the median signal levels are compared with rainfall in both Zaria and Jos taken together, than when they are compared with rainfall in either of these towns separately - as can be seen from the lack of correlation from July to September 1979 (figure 19(B)) and from May to June 1980 (figure 19(C)) for the isolated cases. Correlation is lacking, however, in all three cases between August and September 1979.

4.4 Cumulative Distribution of Signal Levels

Computation was also made of the cumulative distribution of the 1.25 minutely median of signal levels taken on a monthly basis, then seasonal basis and also for the whole period of measurement. The numerical results obtained are shown in table 4.6, and the graphical plots are shown in

TABLE 4.4

MEAN MONTHLY RAINFALL (IN mm) IN JOS AND ZARIA
AND MONTHLY MEDIAN OF SIGNAL LEVEL (IN dB Above 1 μVm)

MONTH	Mean Rainfall In Jos (mm)	Mean Rainfall in Zaria (mm)	Mean Rainfall in Jos And Zaria (mm)	Median of Signal Level (dB)
Jul. 1979	8.2	11.7	10.0	31.2
Aug. 1979	9.9	8.4	9.2	28.2
Sep. 1979	5.2	3.9	4.6	34.5
Oct. 1979	0.5	1.1	0.8	32.8
Nov. 1979	0.2	.8	0.5	26.9
Dec. 1979	0.0	0.0	0.0	25.6
Jan. 1980	0.0	0.0	0.0	22.0
Feb. 1980	0.6	0.0	0.3	20.8
Mar. 1980	0.4	0.0	0.2	19.8
Apr. 1980	0.4	0.7	0.5	18.5
May. 1980	7.7	3.3	5.5	31.0
June 1980	5.5	3.7	4.6	29.7
July 1980	7.7	8.7	8.2	30.9

TABLE 4.5.

MEAN JOS - ZARIA MONTHLY RAINFALL

Month	Mean Monthly Rainfall (mm)		
	Zaria	Jos	Jos - Zaria
Jul. 1979	11.7	8.2	10
Aug. 1979	8.4	10.0	9.2
Sep. 1979	3.9	5.2	4.6
Oct. 1979	1.1	.5	.8
Nov. 1979	.8	.2	.5
Dec. 1979	0	0	0
Jan. 1980	0	0	0
Feb. 1980	0	.6	.3
Mar. 1980	0	.5	.2
Apr. 1980	.7	.4	.5
May. 1980	3.3	7.7	5.5
Jun. 1980	3.7	5.5	4.6
Jul. 1980	8.7	7.7	8.2

TABLE 4.6

CUMULATIVE DISTRIBUTION OF THE 1.25 MINUTELY MEDIANS OF SIGNAL LEVEL

SIGNAL LEVEL IN dB μV/m	CUMULATIVE FREQUENCY IN THE MONTH OF																							
	JULY 1979	AUG. 1979	SEPT. 1979	OCT. 1979	NOV. 1979	DEC. 1979	JAN. 1980	FEB. 1980	MAR. 1980	APR. 1980	MAY 1980	JUNE 1980	JULY 1980	DRY SEASON	WET SEASON	JULY 1979 TO JULY 1980								
63	.4	.2	.3	.4	.2	0	0	0	.4	.2	.6	.8	.2	.1	.1	.1								
62	.8	.2	.3	.4	.2	0	0	0	.4	.2	.6	.8	.2	.1	.1	.1								
61	1.0	.2	.3	.4	.2	0	0	0	.4	.2	.6	.8	.2	.1	.1	.1								
60	1.3	.2	.3	.4	.2	0	0	0	.4	.2	.6	.8	.2	.1	.1	.1								
59	1.3	.2	.3	.4	.2	0	0	0	.4	.2	.6	.8	.2	.1	.1	.1								
58	1.3	.2	.3	.4	.2	0	0	0	.4	.2	.6	.8	.2	.1	.1	.1								
57	1.6	.2	.3	.4	.2	0	0	0	.4	.2	.6	.8	.2	.1	.1	.1								
56	1.6	.2	.3	.4	.2	0	0	0	.4	.2	.6	.8	.2	.1	.1	.1								
55	1.6	.2	.3	.4	.2	0	0	0	.4	.2	.6	.8	.2	.1	.1	.1								
54	1.6	.2	.3	.4	.2	0	0	0	.4	.2	.6	.8	.2	.1	.1	.1								
53	1.9	.2	.3	.4	.2	0	0	0	.4	.2	.6	.8	.2	.1	.1	.1								
52	2.1	.2	.3	.4	.2	0	0	0	.4	.2	.6	.8	.2	.1	.1	.1								
51	2.4	.2	.3	.4	.2	0	0	0	.4	.2	.6	.8	.2	.1	.1	.1								
50	2.7	.2	.3	.4	.2	0	0	0	.4	.2	.6	.8	.2	.1	.1	.1								
49	3.0	.2	.3	.4	.2	0	0	0	.4	.2	.6	.8	.2	.1	.1	.1								
48	3.3	.2	.3	.4	.2	0	0	0	.4	.2	.6	.8	.2	.1	.1	.1								
47	3.8	.2	.3	.4	.2	0	0	0	.4	.2	.6	.8	.2	.1	.1	.1								
46	4.2	.2	.3	.4	.2	0	0	0	.4	.2	.6	.8	.2	.1	.1	.1								
45	4.7	.2	.3	.4	.2	0	0	0	.4	.2	.6	.8	.2	.1	.1	.1								
44	5.2	.2	.3	.4	.2	0	0	0	.4	.2	.6	.8	.2	.1	.1	.1								
43	6.0	.2	.3	.4	.2	0	0	0	.4	.2	.6	.8	.2	.1	.1	.1								
42	7.0	.2	.3	.4	.2	0	0	0	.4	.2	.6	.8	.2	.1	.1	.1								
41	7.8	.2	.3	.4	.2	0	0	0	.4	.2	.6	.8	.2	.1	.1	.1								
40	8.7	.2	.3	.4	.2	0	0	0	.4	.2	.6	.8	.2	.1	.1	.1								
39	9.8	.2	.3	.4	.2	0	0	0	.4	.2	.6	.8	.2	.1	.1	.1								
38	11.2	.2	.3	.4	.2	0	0	0	.4	.2	.6	.8	.2	.1	.1	.1								
37	12.8	.2	.3	.4	.2	0	0	0	.4	.2	.6	.8	.2	.1	.1	.1								
36	14.2	.2	.3	.4	.2	0	0	0	.4	.2	.6	.8	.2	.1	.1	.1								
35	15.8	.2	.3	.4	.2	0	0	0	.4	.2	.6	.8	.2	.1	.1	.1								
34	18.0	.2	.3	.4	.2	0	0	0	.4	.2	.6	.8	.2	.1	.1	.1								
33	20.1	.2	.3	.4	.2	0	0	0	.4	.2	.6	.8	.2	.1	.1	.1								
32	22.7	.2	.3	.4	.2	0	0	0	.4	.2	.6	.8	.2	.1	.1	.1								
31	25.8	.2	.3	.4	.2	0	0	0	.4	.2	.6	.8	.2	.1	.1	.1								
30	29.2	.2	.3	.4	.2	0	0	0	.4	.2	.6	.8	.2	.1	.1	.1								
29	32.8	.2	.3	.4	.2	0	0	0	.4	.2	.6	.8	.2	.1	.1	.1								
28	35.7	.2	.3	.4	.2	0	0	0	.4	.2	.6	.8	.2	.1	.1	.1								
27	39.4	.2	.3	.4	.2	0	0	0	.4	.2	.6	.8	.2	.1	.1	.1								
26	44.4	.2	.3	.4	.2	0	0	0	.4	.2	.6	.8	.2	.1	.1	.1								
25	48.0	.2	.3	.4	.2	0	0	0	.4	.2	.6	.8	.2	.1	.1	.1								
24	52.7	.2	.3	.4	.2	0	0	0	.4	.2	.6	.8	.2	.1	.1	.1								
23	56.9	.2	.3	.4	.2	0	0	0	.4	.2	.6	.8	.2	.1	.1	.1								
22	60.6	.2	.3	.4	.2	0	0	0	.4	.2	.6	.8	.2	.1	.1	.1								
21	64.3	.2	.3	.4	.2	0	0	0	.4	.2	.6	.8	.2	.1	.1	.1								
20	68.0	.2	.3	.4	.2	0	0	0	.4	.2	.6	.8	.2	.1	.1	.1								
19	71.3	.2	.3	.4	.2	0	0	0	.4	.2	.6	.8	.2	.1	.1	.1								
18	74.0	.2	.3	.4	.2	0	0	0	.4	.2	.6	.8	.2	.1	.1	.1								
17	76.6	.2	.3	.4	.2	0	0	0	.4	.2	.6	.8	.2	.1	.1	.1								
16	78.9	.2	.3	.4	.2	0	0	0	.4	.2	.6	.8	.2	.1	.1	.1								
15	80.9	.2	.3	.4	.2	0	0	0	.4	.2	.6	.8	.2	.1	.1	.1								
14	82.7	.2	.3	.4	.2	0	0	0	.4	.2	.6	.8	.2	.1	.1	.1								
13	84.3	.2	.3	.4	.2	0	0	0	.4	.2	.6	.8	.2	.1	.1	.1								
12	85.7	.2	.3	.4	.2	0	0	0	.4	.2	.6	.8	.2	.1	.1	.1								
11	87.0	.2	.3	.4	.2	0	0	0	.4	.2	.6	.8	.2	.1	.1	.1								
10	88.0	.2	.3	.4	.2	0	0	0	.4	.2	.6	.8	.2	.1	.1	.1								
9	89.0	.2	.3	.4	.2	0	0	0	.4	.2	.6	.8	.2	.1	.1	.1								
8	89.8	.2	.3	.4	.2	0	0	0	.4	.2	.6	.8	.2	.1	.1	.1								
7	90.5	.2	.3	.4	.2	0	0	0	.4	.2	.6	.8	.2	.1	.1	.1								
6	91.1	.2	.3	.4	.2	0	0	0	.4	.2	.6	.8	.2	.1	.1	.1								
5	91.6	.2	.3	.4	.2	0	0	0	.4	.2	.6	.8	.2	.1	.1	.1								
4	92.1	.2	.3	.4	.2	0	0	0	.4	.2	.6	.8	.2	.1	.1	.1								
3	92.6	.2	.3	.4	.2	0	0	0	.4	.2	.6	.8	.2	.1	.1	.1								
2	93.0	.2	.3	.4	.2	0	0	0	.4	.2	.6	.8	.2	.1	.1	.1								
1	93.5	.2	.3	.4	.2	0	0	0	.4	.2	.6	.8	.2	.1	.1	.1								
0	93.9	.2	.3	.4	.2	0	0	0	.4	.2	.6	.8	.2	.1	.1	.1								

* Data Scanty

Table 4.6 Contd.

SIGNAL LEVEL IN dB µV/m	JULY 1979	AUG. 1979	SEPT. 1979	OCT. 1979	NOV. 1979	DEC. 1979	JAN. 1980	FEB. 1980	MAR. 1980	APR. 1980	MAY
36	33.0	24.5	47.0	39.5	18.9	7.1	1.1	.5	4.0	11.2	37.
35	37.0	27.0	50.1	43.1	21.0	9.0	1.8	1.0	4.7	12.8	39.
34	41.3	30.0	53.4	46.9	23.2	11.7	3.0	2.0	5.6	14.2	42
33	45.7	33.3	56.5	50.7	26.6	15.1	4.2	3.5	6.7	16.4	46
32	49.5	37.0	60.5	54.5	30.1	19.2	5.8	5.0	7.8	17.9	49
31	53.0	40.6	63.8	58.7	34.0	23.2	7.8	6.8	9.0	19.6	57
30	57.4	44.2	68.5	63.0	38.5	28.0	11.0	8.9	10.5	20.7	55
29	61.6	48.9	72.2	67.2	43.5	33.3	14.3	11.9	11.6	22.2	59
28	66.3	54.0	76.0	71.9	48.8	39.7	18.6	15.9	13.3	23.6	63
27	71.2	58.9	79.3	75.6	54.5	45.7	24.5	20.4	16.0	25.0	68
26	74.7	63.4	81.7	78.9	59.7	50.6	29.8	24.5	18.8	26.5	72
25	77.8	67.2	84.1	81.8	64.3	55.4	35.9	29.9	23.0	28.2	76
24	81.4	71.5	87.9	84.7	69.7	60.1	41.6	35.1	26.9	29.8	79
23	85.6	77.1	91.7	88.7	75.7	65.0	48.0	40.4	31.4	32.1	83
22	88.2	80.6	93.0	91.7	79.7	67.1	54.6	46.2	37.2	35.0	87
21	89.2	81.4	93.8	92.6	80.8	70.7	61.5	52.8	44.6	38.7	90
20	90.1	82.7	94.3	93.7	84.3	73.7	67.4	59.3	50.9	44.7	93
19	91.1	83.2	95.4	94.5	85.6	75.4	72.8	65.5	57.0	50.5	94
18	94.6	89.4	96.9	96.4	87.8	79.6	77.2	71.1	63.1	56.1	95
17	96.1	91.1	97.4	97.7	91.0	82.3	82.4	78.7	71.1	63.8	96
16	96.8	91.6	98.0	98.1	93.0	85.4	87.3	84.3	78.6	67.4	97
15	97.2	92.4	98.6	99.3	95.7	89.6	90.3	88.8	84.2	78.5	97
14	97.5	93.1	98.6	99.4	96.9	91.3	93.4	92.5	89.6	86.0	97
13	99.3	94.6	100	100	98.5	97.4	98.9	96.8	97.0	95.2	99
12	100	100			100	100	100	100	100	100	10

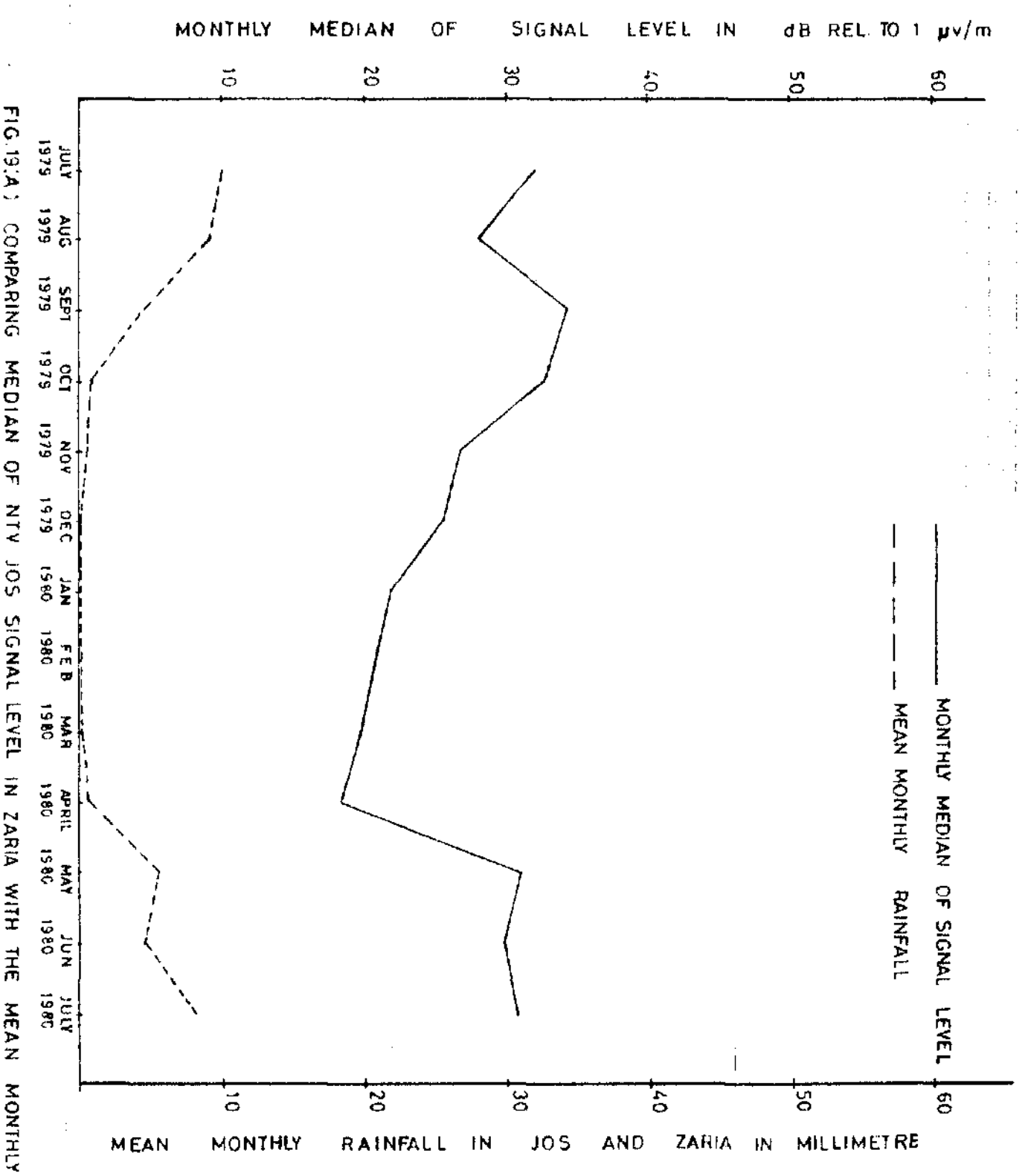


FIG. 19(A) COMPARING MEDIAN OF NTV JOS SIGNAL LEVEL IN ZARIA WITH THE MEAN MONTHLY RAINFALL IN JOS AND ZARIA TAKEN TOGETHER

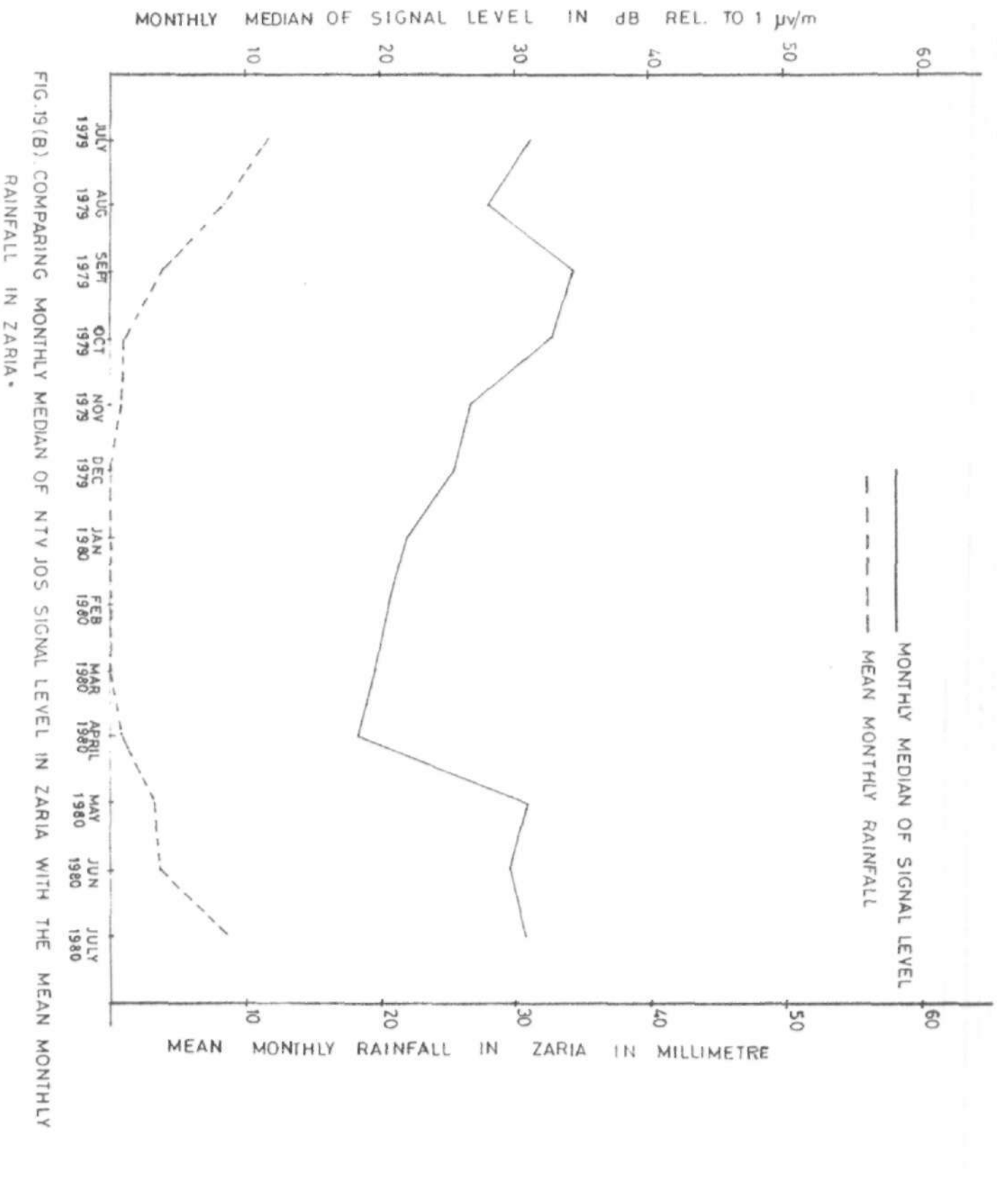


FIG. 19(B) COMPARING MONTHLY MEDIAN OF NTV JOS SIGNAL LEVEL IN ZARIA WITH THE MEAN MONTHLY RAINFALL IN ZARIA.

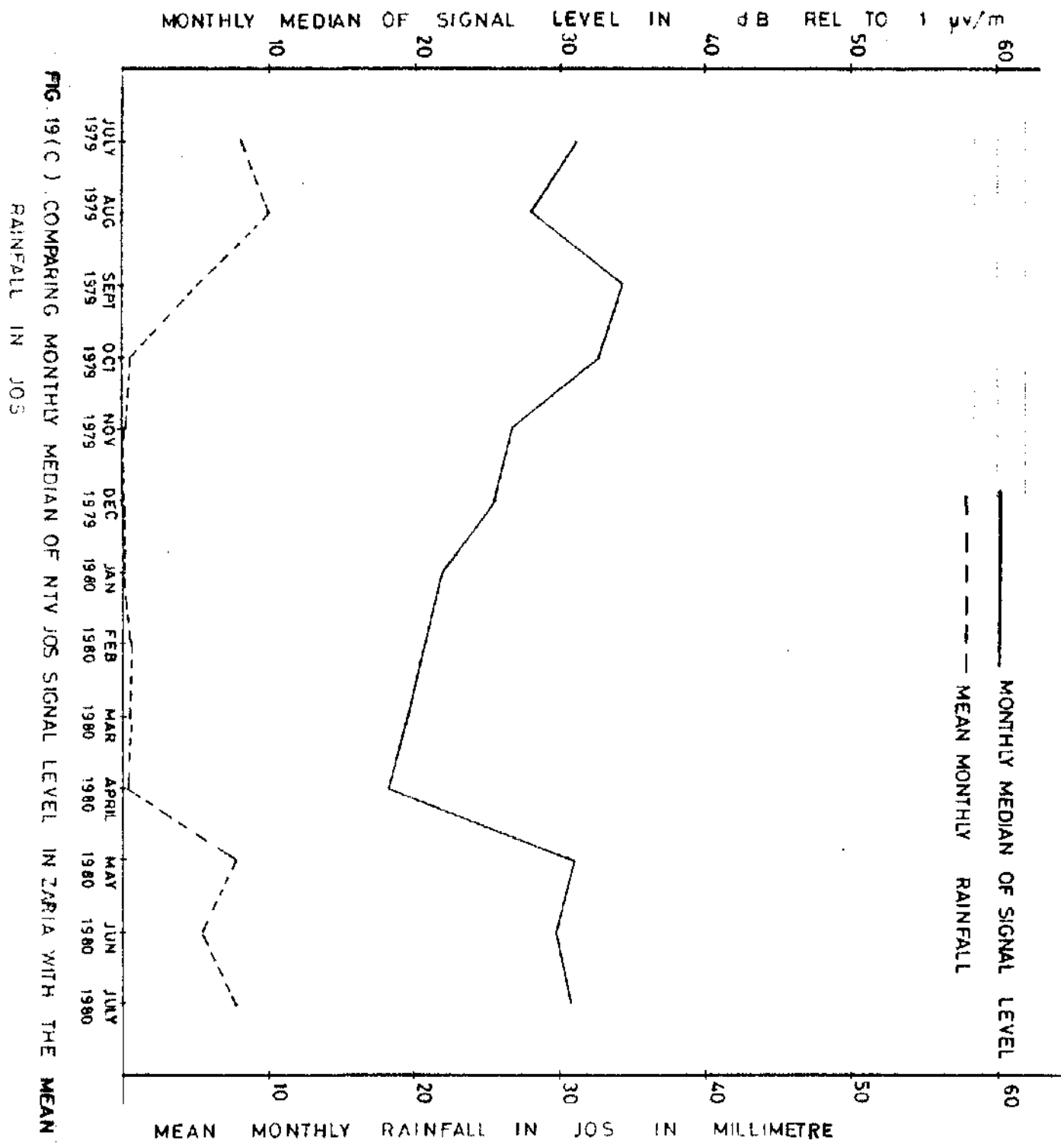


FIG. 19(C) COMPARING MONTHLY MEDIAN OF NTV JOS SIGNAL LEVEL IN ZARIA WITH THE MEAN MONTHLY RAINFALL IN JOS

figures 20 (A) - (P). These distributions are compared in Table 4.7. The numerical values are then subjected to further statistical analyses with a view to exposing any trends concerning the mean variation of the signal levels about the monthly medians.

Table 4.7 shows that the August 1979 distribution has the highest range (59.0 dB) while February 1980 has the least (32.0 dB); it also reveals that the weakest signals were received in February 1980 while the strongest signals were received in September 1979 - although the September figures could be erroneous in view of the inadequacy of data in this month.

To estimate the degree of variation of the signal levels about the monthly medians the ratio of the semi-interquartile range to the whole range has also been evaluated for each month, as a measure of scatter. This analysis shows that the 1.25 minutely median values are closer to the monthly median in the dry season months, than in the wet season; and that the worst month from scattering point of view was May 1980 while March 1980 was the best. Thus the relatively high median signal levels obtained in the wet season are fraught with greater variations about the monthly medians, than in the dry season when median signal levels are lower but more steady. A similar observation has been made in Section 4.2 above.

TABLE 4.7

CUMULATIVE DISTRIBUTION OF MEDIAN SIGNAL LEVELS
In dB Rel. To 1 μV/m

MONTH	% OF MEDIAN SIGNAL LEVEL ABOVE						RANGE (dB)	SEMI-INTER-QUARTILE RANGE	MEASURE OF SCATTER*
	60 dB	50 dB	40 dB	30 dB	20 dB	10 dB			
JUL. 1979	1.1	6.0	20.0	57.4	92.3	99.6	56.0	6.7	.12
AUG. 1979	.4	3.6	16.5	42.0	84.0	97.2	59.0	8.3	.14
SEP. 1979	7.5	3.8	35.0	68.0	95.0	100	50.5	8.4	.17
OCT. 1979	2.2	7.8	25.0	64.5	94.0	100	51.0	6.5	.13
NOV. 1979	2.2	8.0	13.8	38.6	84.6	100	51.3	5.5	.11
DEC. 1979	0	.2	3.0	30.0	74.0	98.0	44.8	4.6	.10
JAN. 1980	0	0	.2	10.0	67.0	98.3	33.2	4.3	.13
FEB. 1980	0	0	0	9.0	59.0	97.8	32.0	4.5	.14
MAR. 1980	0	.6	2.6	10.4	57.0	97.6	48.0	4.4	.09
APR. 1980	0	.5	6.8	19.8	43.5	94.3	50.0	8.6	.17
MAY. 1980	0	3.4	26.5	56.4	92.0	99.6	46.0	8.7	.19.
JUN. 1980	0	4.7	20.3	52.0	88.4	100	45.5	7.5	.16
JUL. 1980**	0	0	10.0	50.0	88.0	100	39.0	6.0	.15

* MEASURE OF SCATTER = $\frac{\text{SEMI-INTER QUARTILE RANGE}}{\text{RANGE}}$

** DATA Scanty.

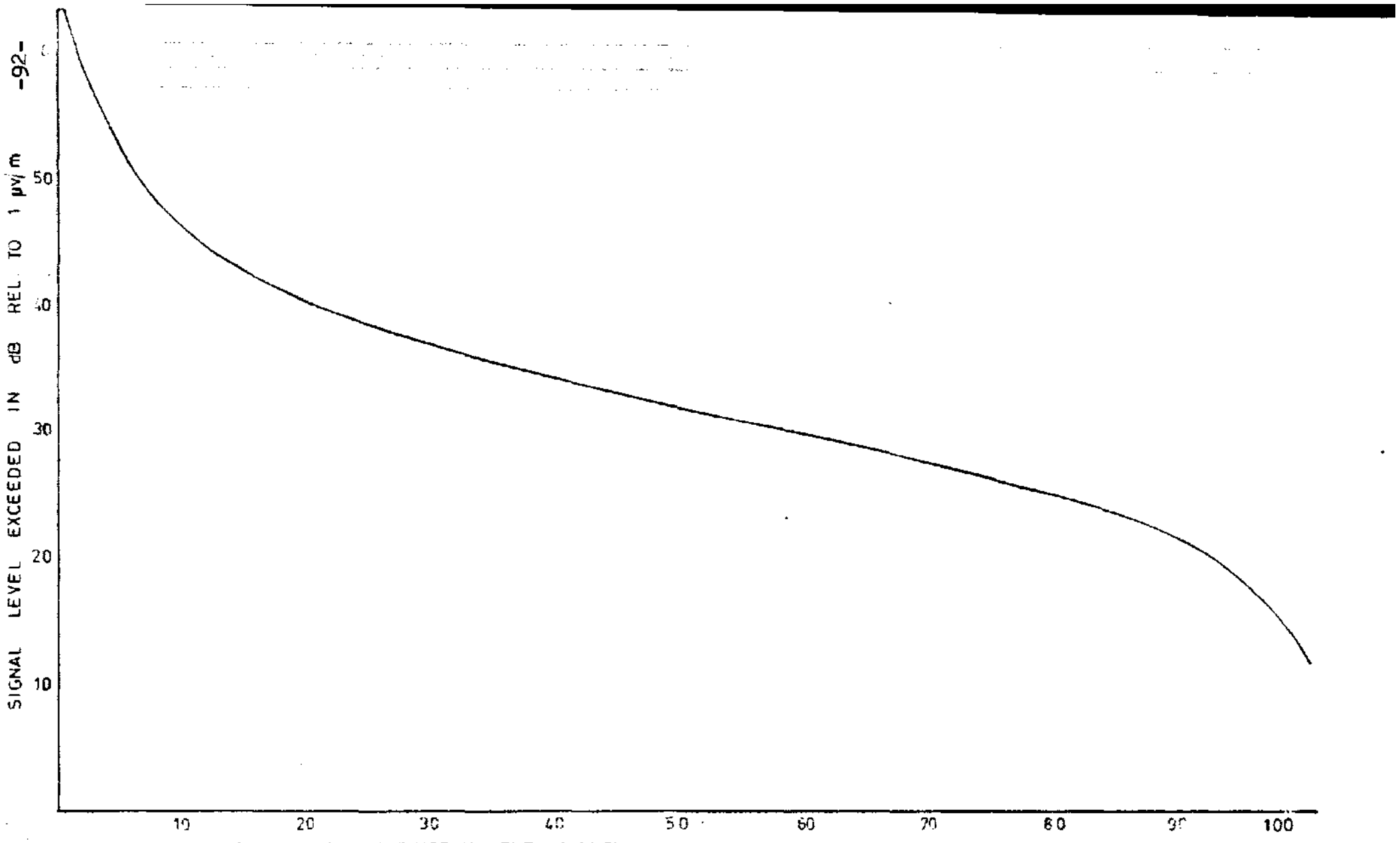


FIG 20(A) CUMULATIVE DISTRIBUTION OF 1.25 MINUTELY MEDIAN OF NTV JOS SIGNAL RECEIVED IN ZARIA IN JULY 1979.

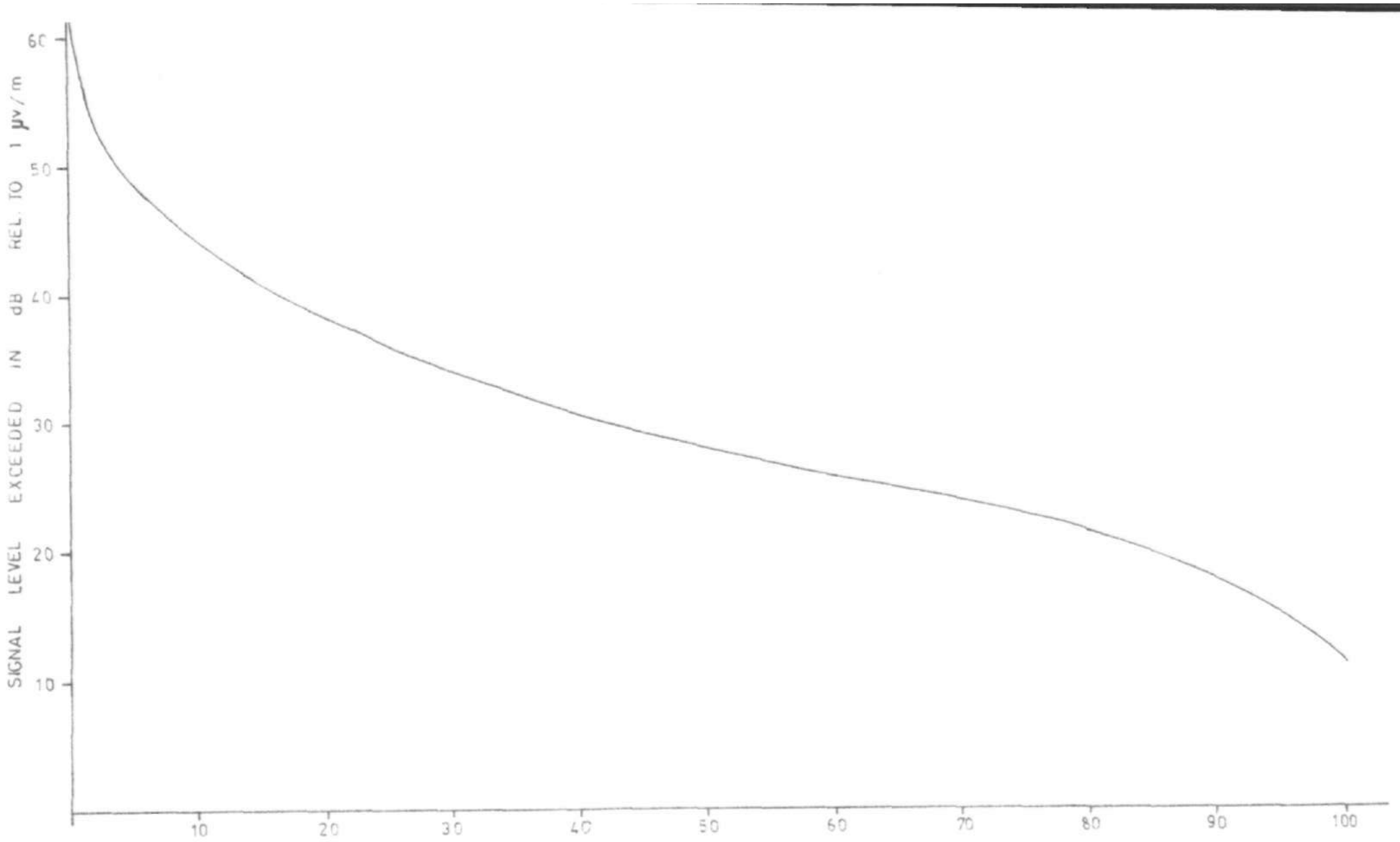


FIG 20(B). CUMULATIVE DISTRIBUTION OF 1.25 MINUTELY MEDIAN OF NTV JOS SIGNAL RECEIVED IN ZARIA IN AUGUST 1979.

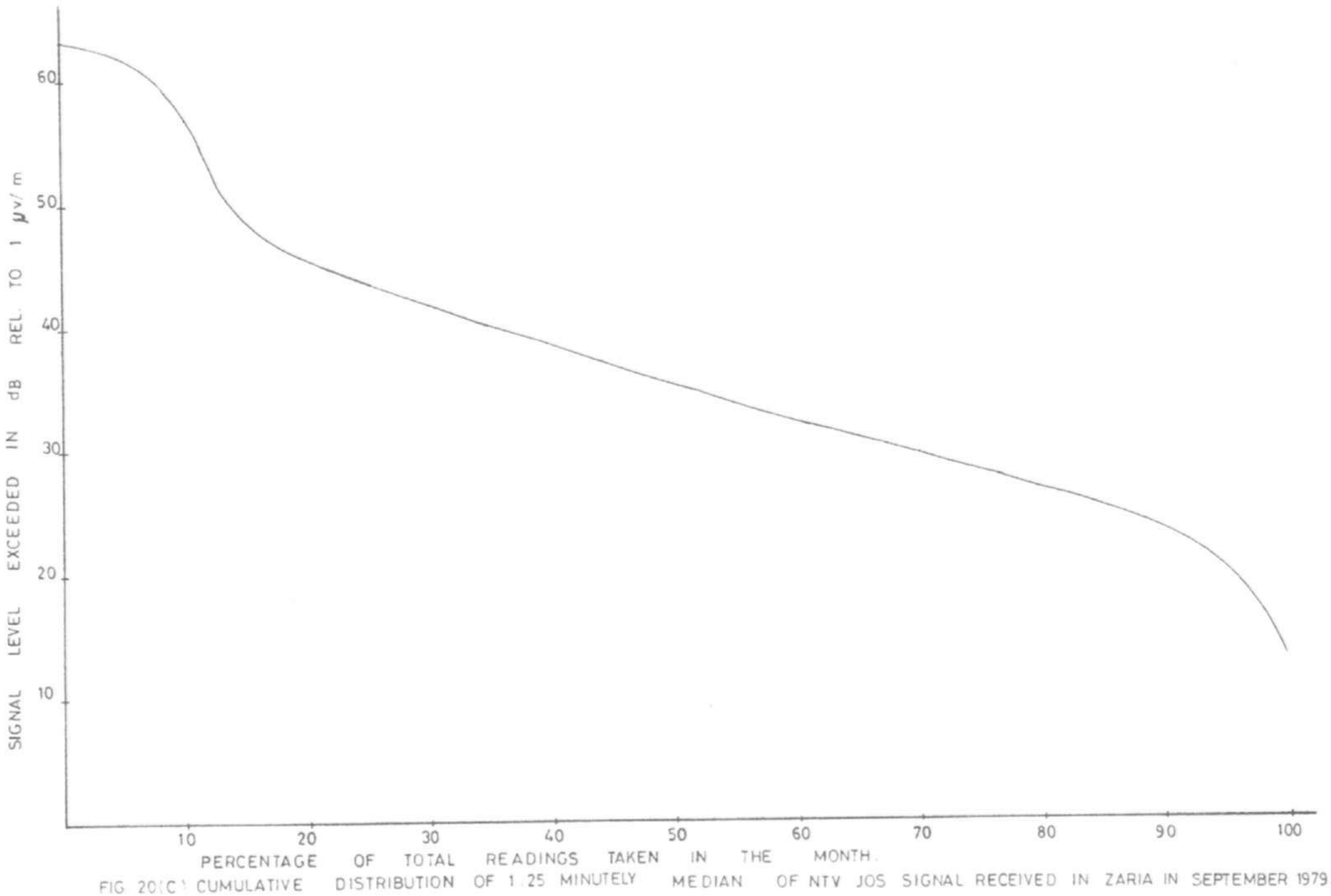


FIG. 20(C) CUMULATIVE DISTRIBUTION OF 1.25 MINUTELY MEDIAN OF NTV JOS SIGNAL RECEIVED IN ZARIA IN SEPTEMBER 1979.

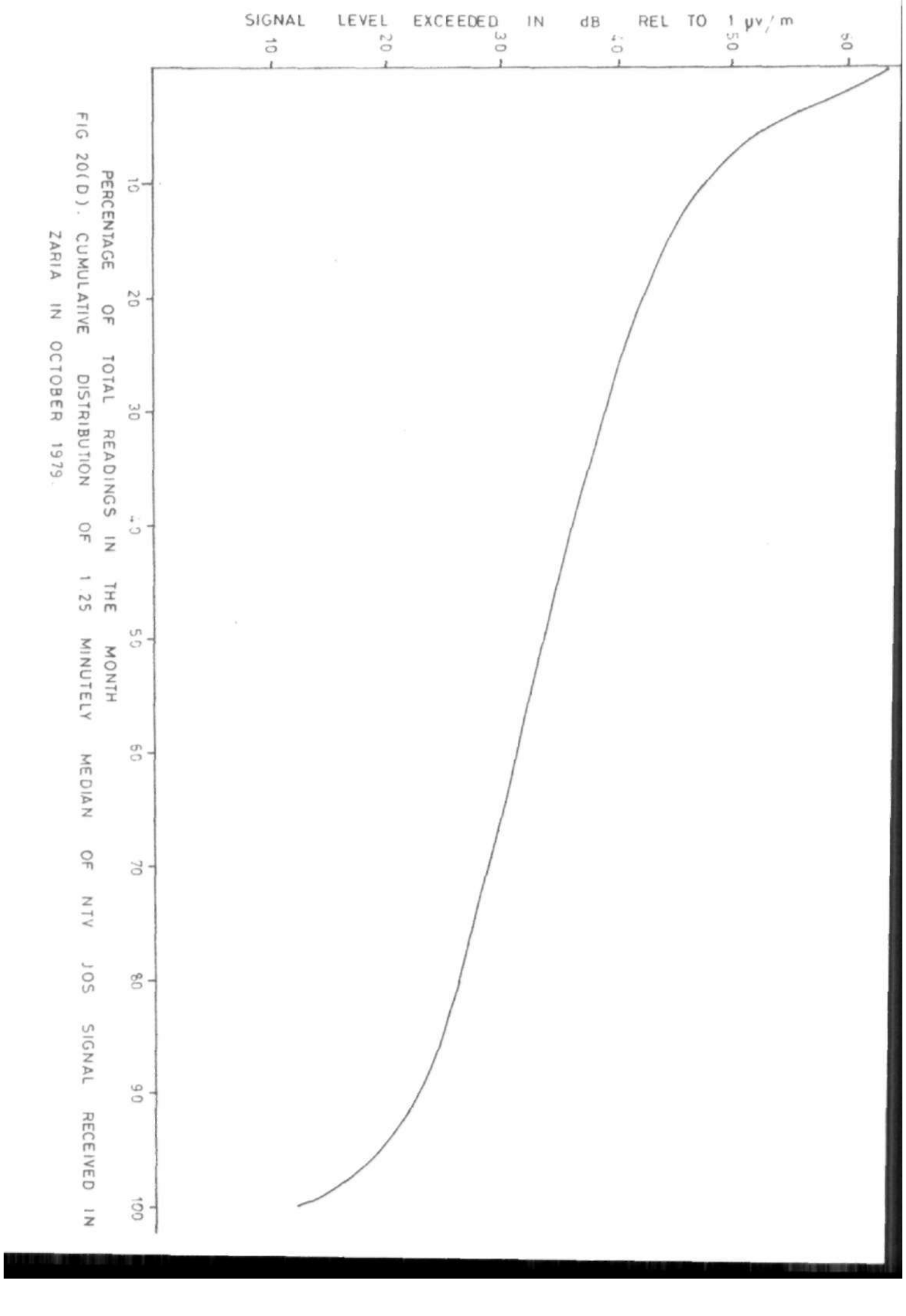


FIG 20(D). CUMULATIVE DISTRIBUTION OF 1.25 MINUTELY MEDIAN OF NTV JOS SIGNAL RECEIVED IN ZARIA IN OCTOBER 1979.

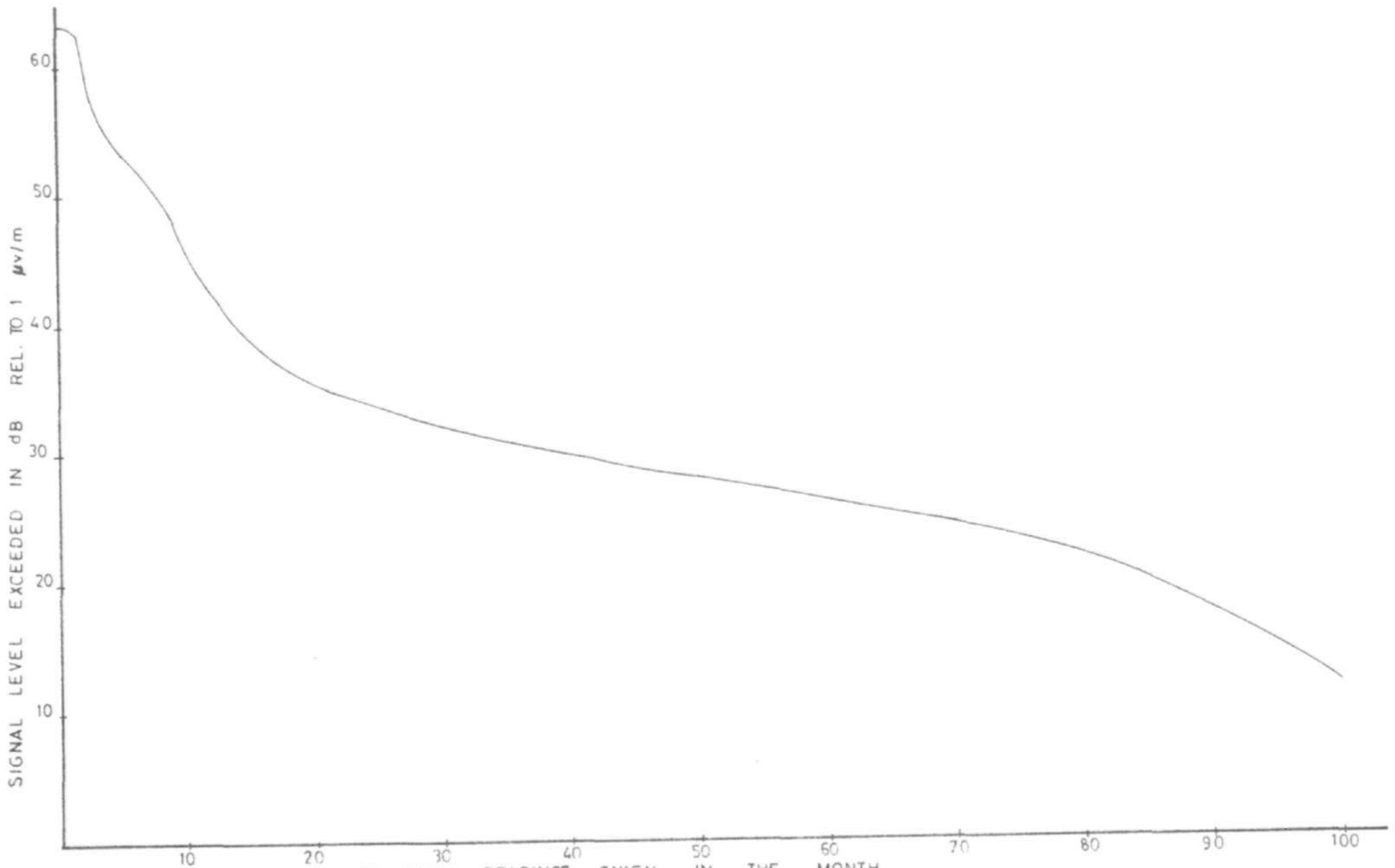


FIG 20(E) CUMULATIVE DISTRIBUTION OF 1.25 MINUTELY MEDIAN OF NTV JOS SIGNAL RECEIVED IN ZARIA IN NOVEMBER 1979.

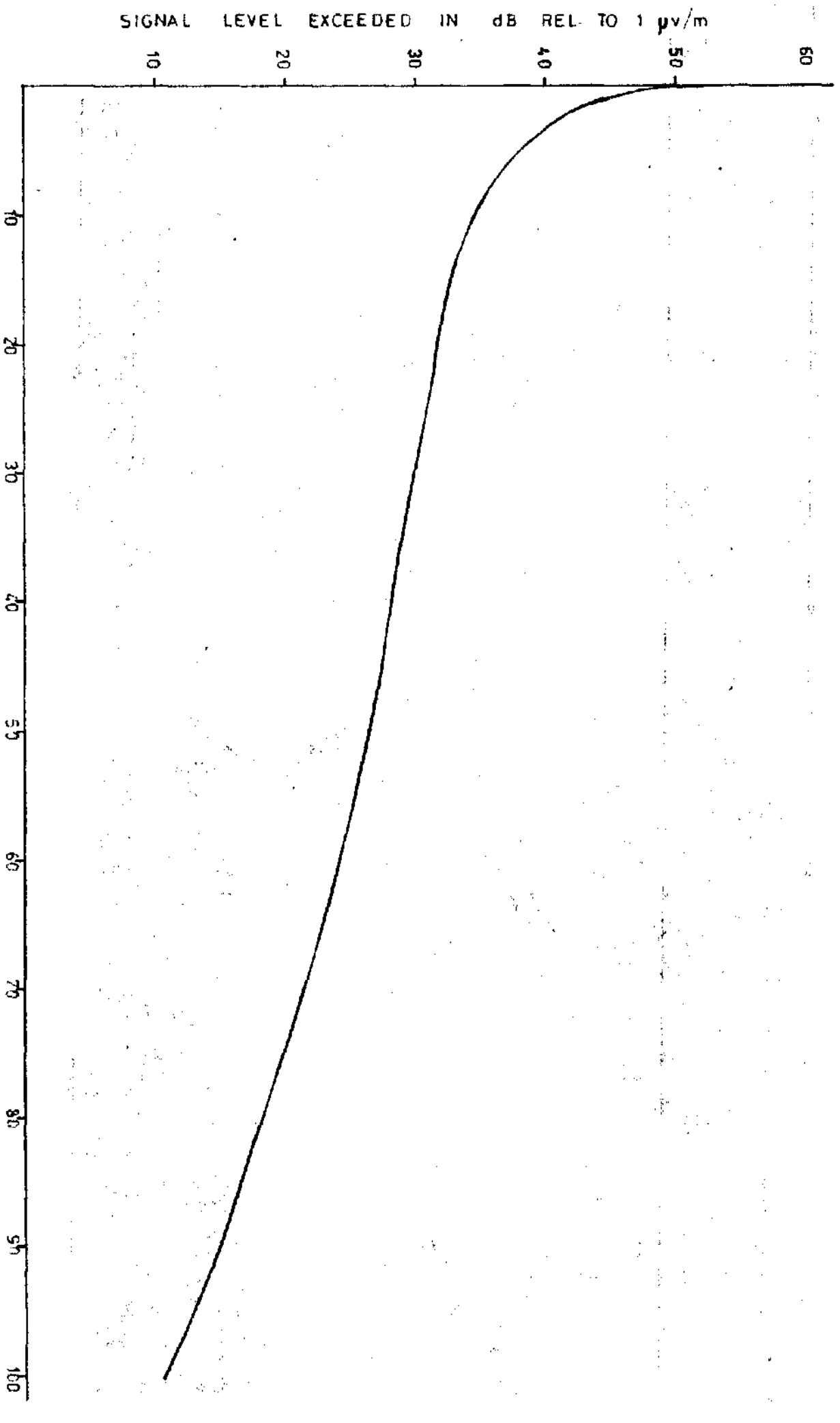


FIG 20(F). CUMULATIVE DISTRIBUTION OF 1.25 MINUTELY MEDIAN OF NTV JOS SIGNAL RECEIVED IN ZARIA IN DECEMBER 1979.

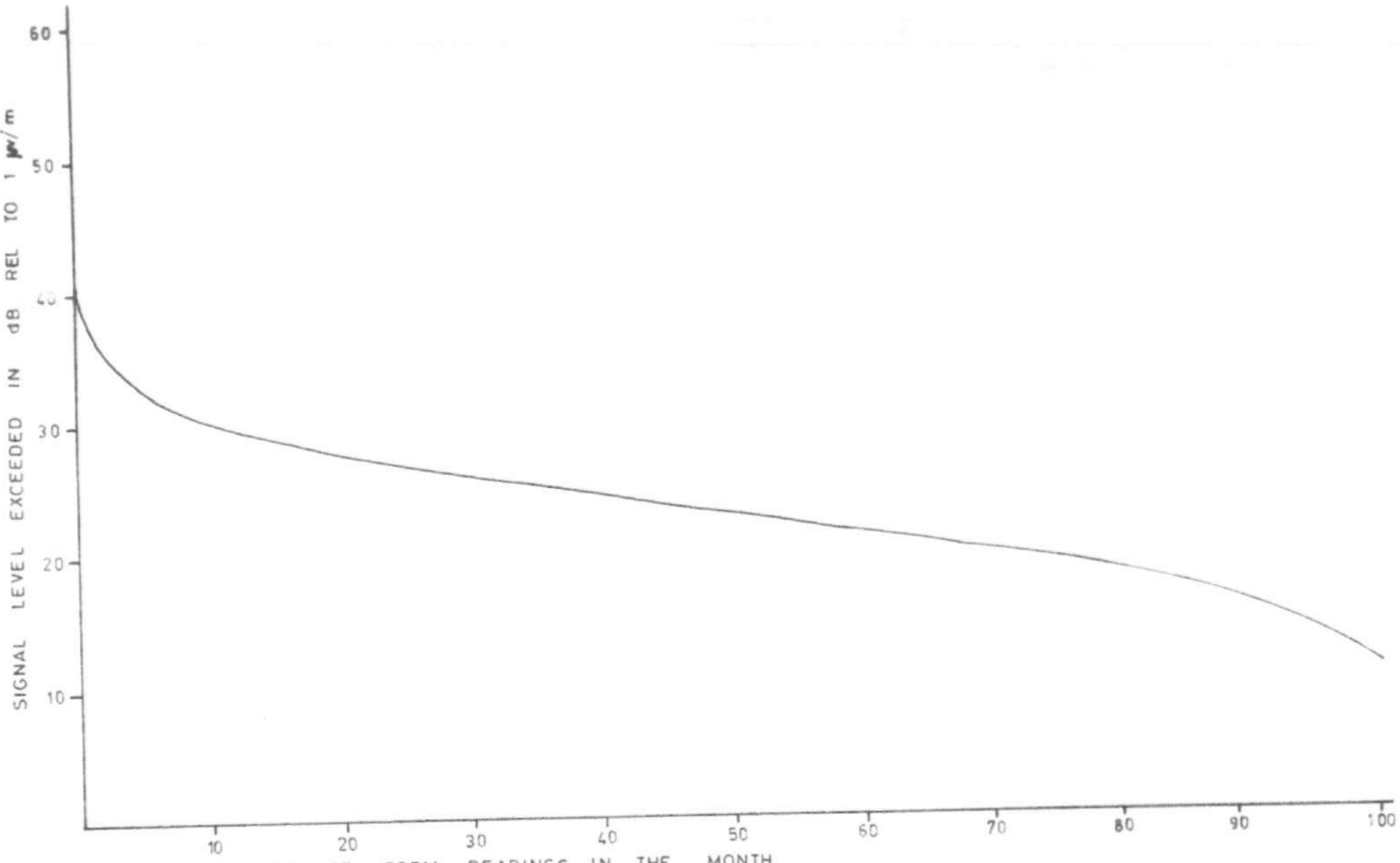


FIG 20(G). CUMULATIVE DISTRIBUTION OF 1.25 MINUTELY MEDIAN OF NTV JOS SIGNAL RECEIVED IN ZARIA IN JANUARY 1980.

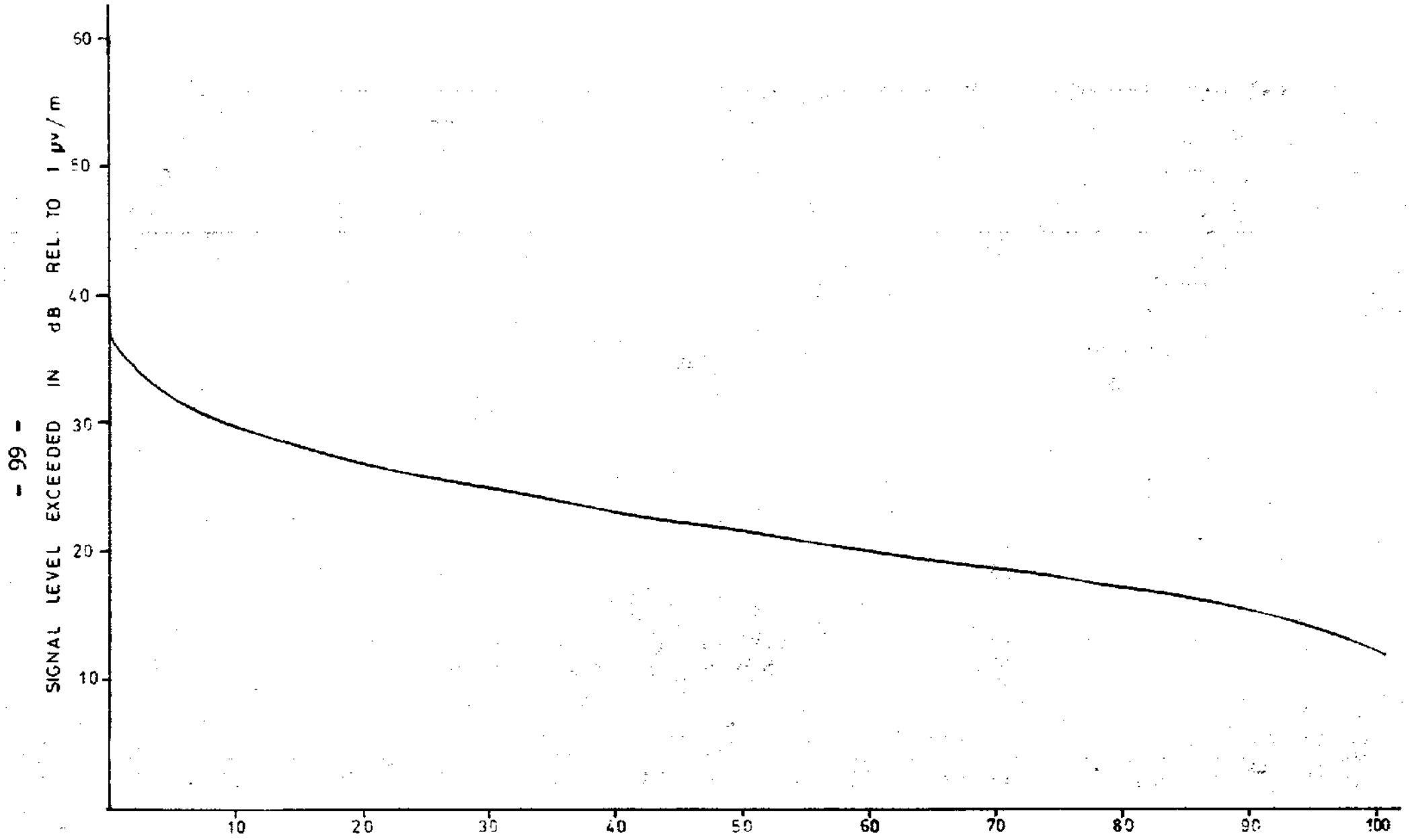


FIG 20(H) CUMULATIVE DISTRIBUTION OF 1.25 MINUTELY MEDIAN OF NTV JOS SIGNAL RECEIVED IN ZARIA IN FEBRUARY 1980.

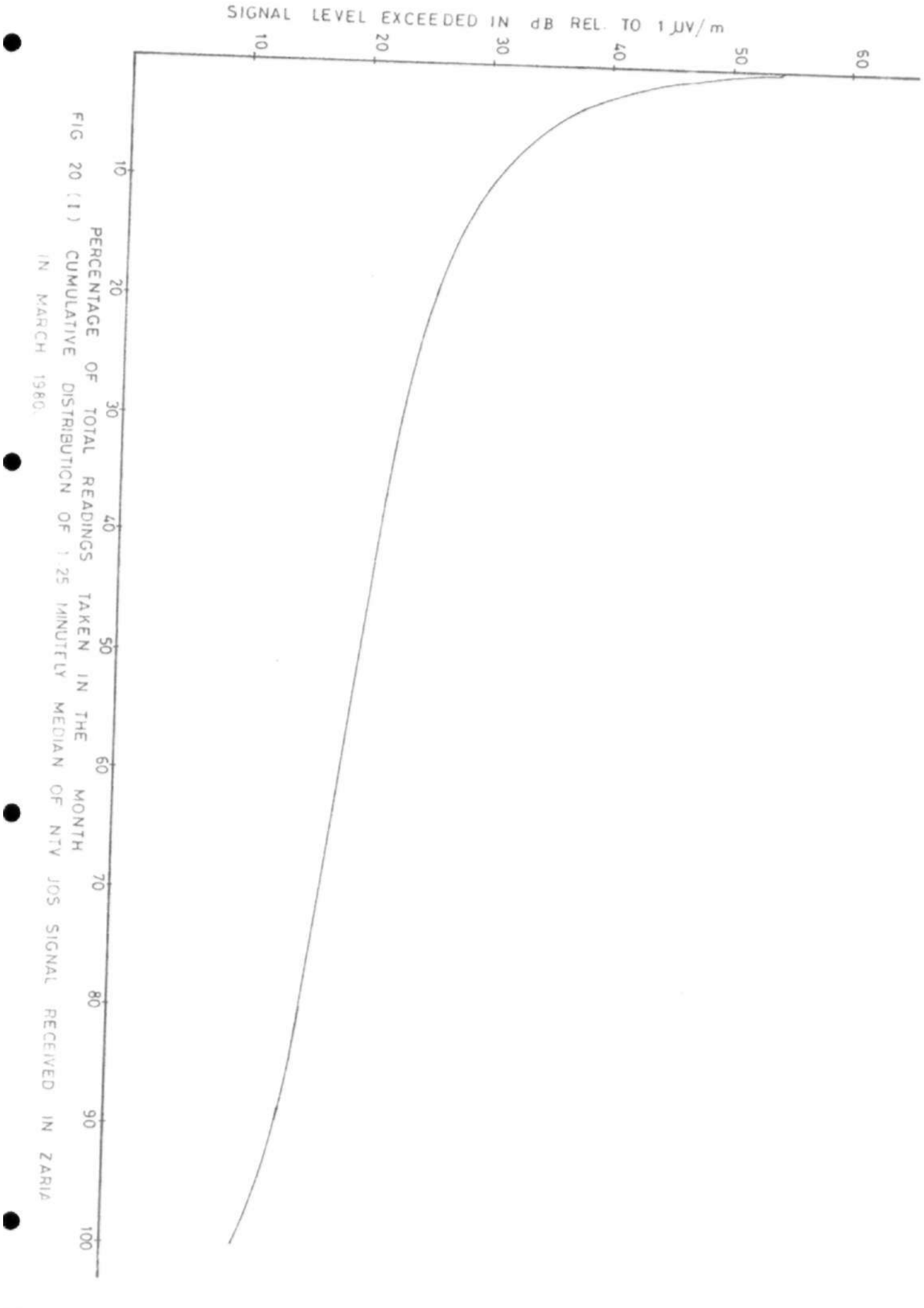


FIG 20 (I) CUMULATIVE DISTRIBUTION OF 1.25 MINUTELY MEDIAN OF NTV JOS SIGNAL RECEIVED IN ZARIA IN MARCH 1980.

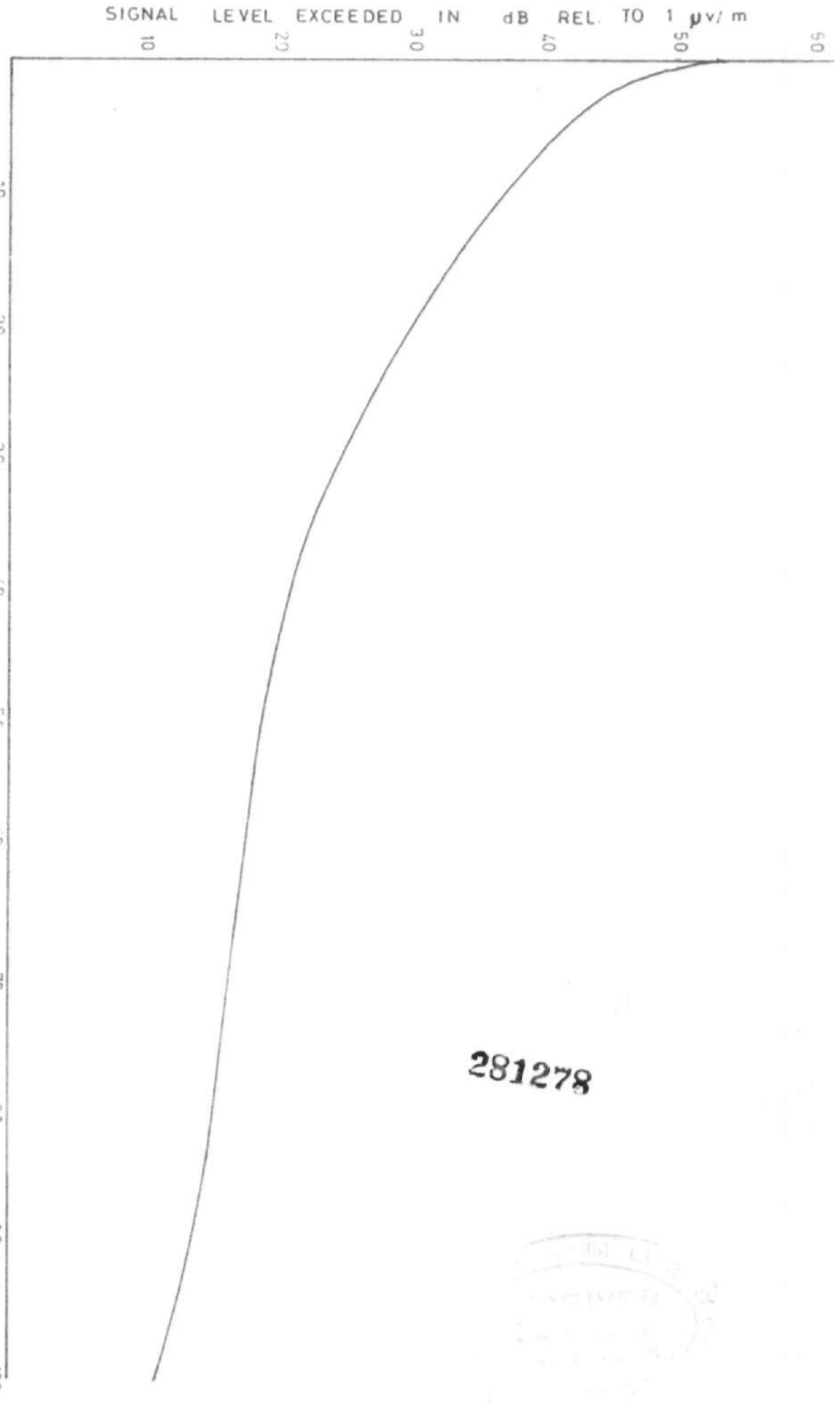


FIG 20(J). CUMULATIVE DISTRIBUTION OF 1.25 MINUTELY MEDIAN OF NTV JOS SIGNAL RECEIVED IN ZARIA IN APRIL 1980.

281278

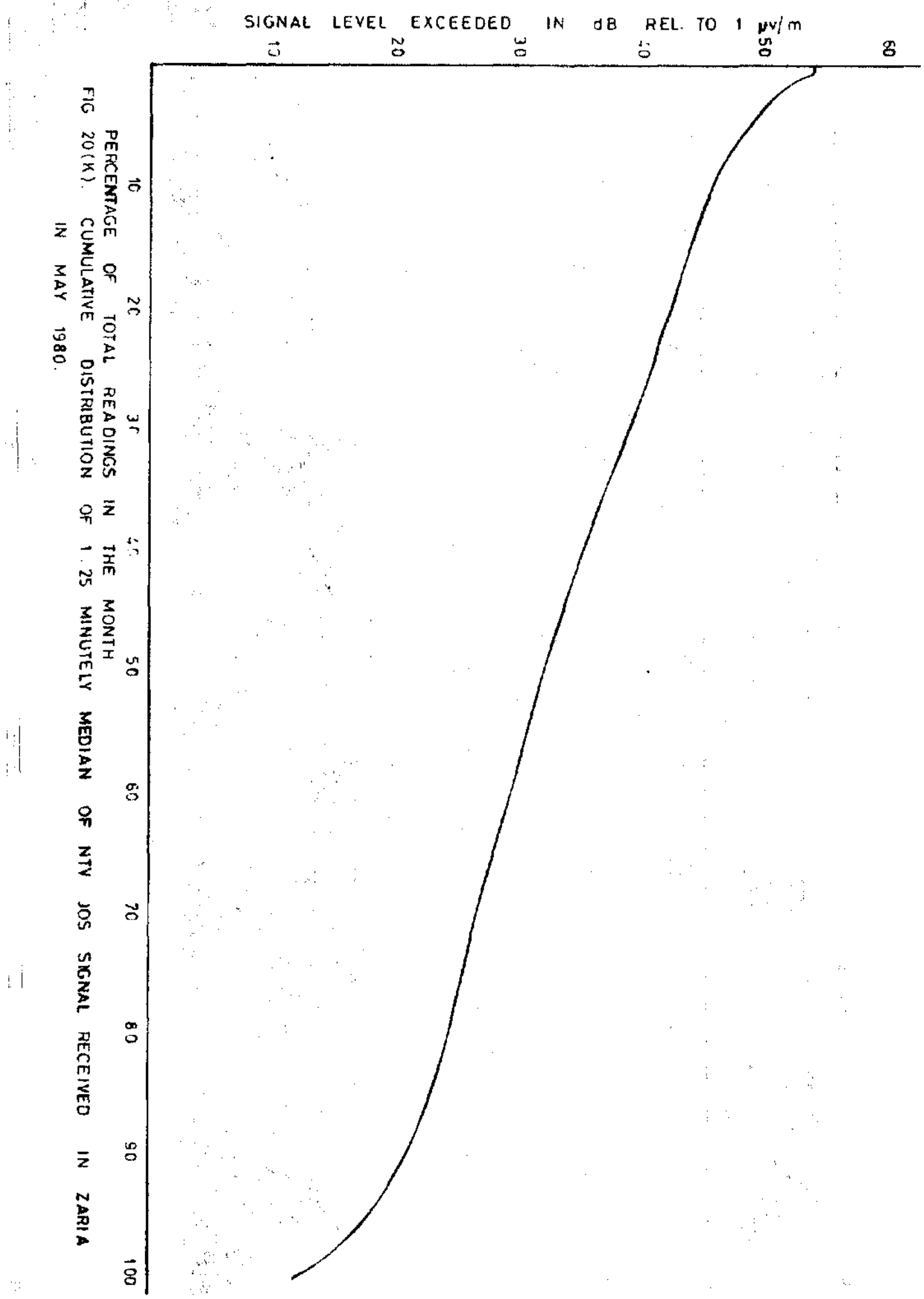


FIG 20(K). CUMULATIVE DISTRIBUTION OF 1.25 MINUTELY MEDIAN OF NTV JOS SIGNAL RECEIVED IN ZARIA IN MAY 1980.

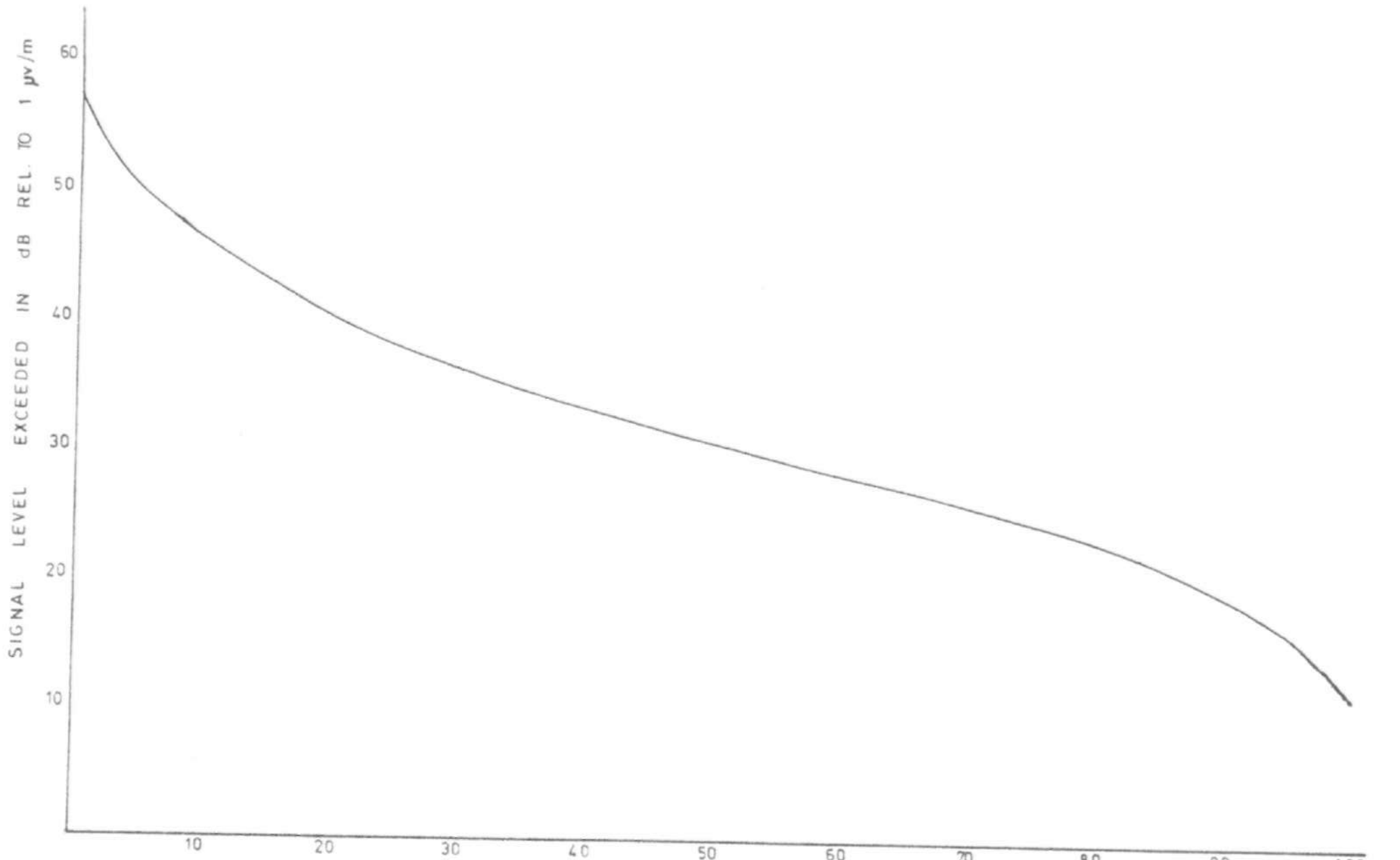


FIG 20(L). CUMULATIVE DISTRIBUTION OF 1.25 MINUTELY MEDIAN OF NTV JOS SIGNAL RECEIVED IN ZARIA IN JUNE 1980

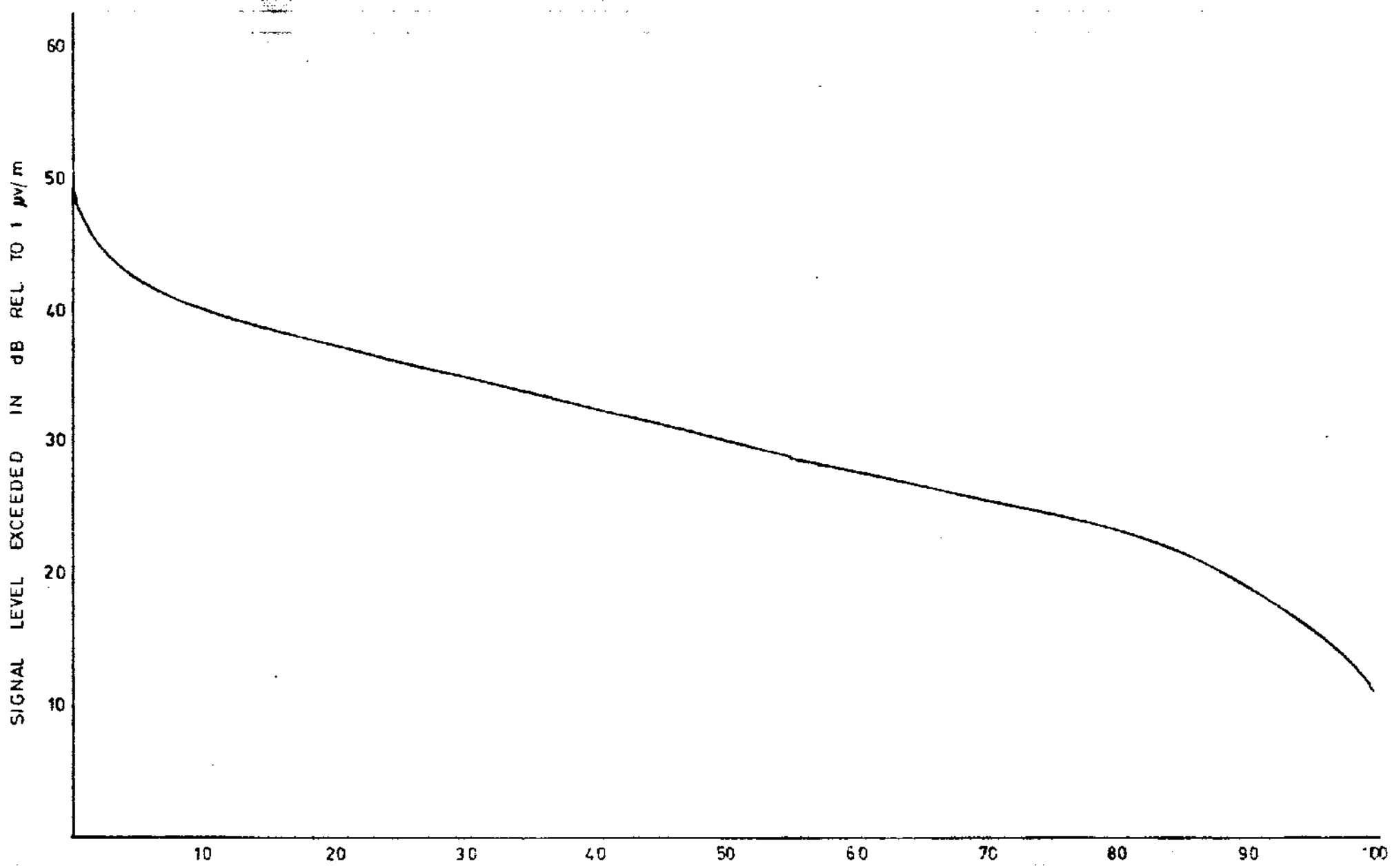


FIG 20(M). CUMULATIVE DISTRIBUTION OF 1.25 MINUTELY MEDIAN OF NTV JOS SIGNAL RECEIVED IN ZARIA IN JULY 1980.

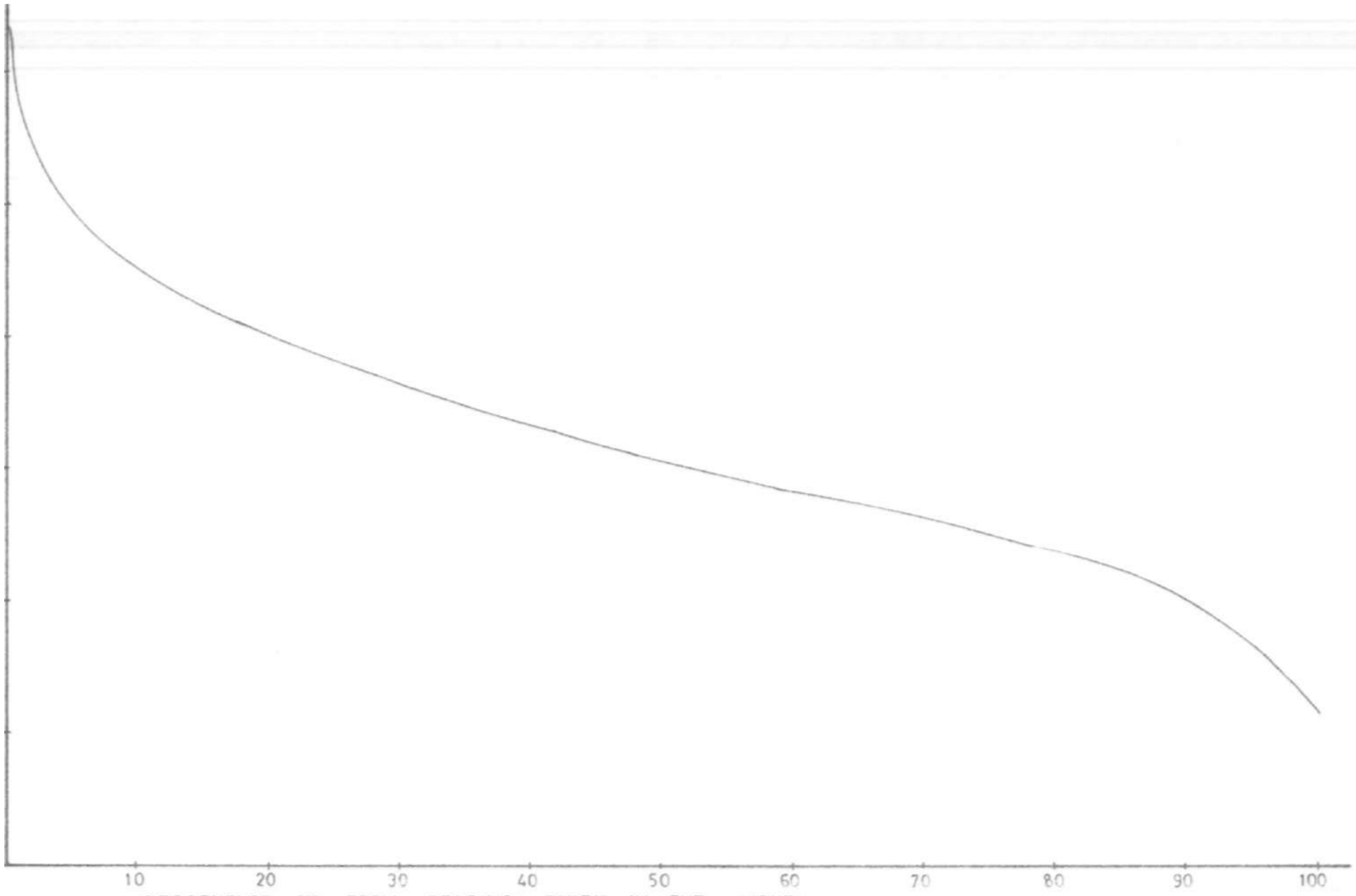


FIG. 20(N): CUMULATIVE DISTRIBUTION OF 1.25 MINUTELY MEDIAN OF NTV JOS SIGNAL RECEIVED IN ZARIA DURING THE RAINY SEASON MONTHS OF JULY 1979 — SEPTEMBER 1979 AND MAY 1980 — JULY 1980

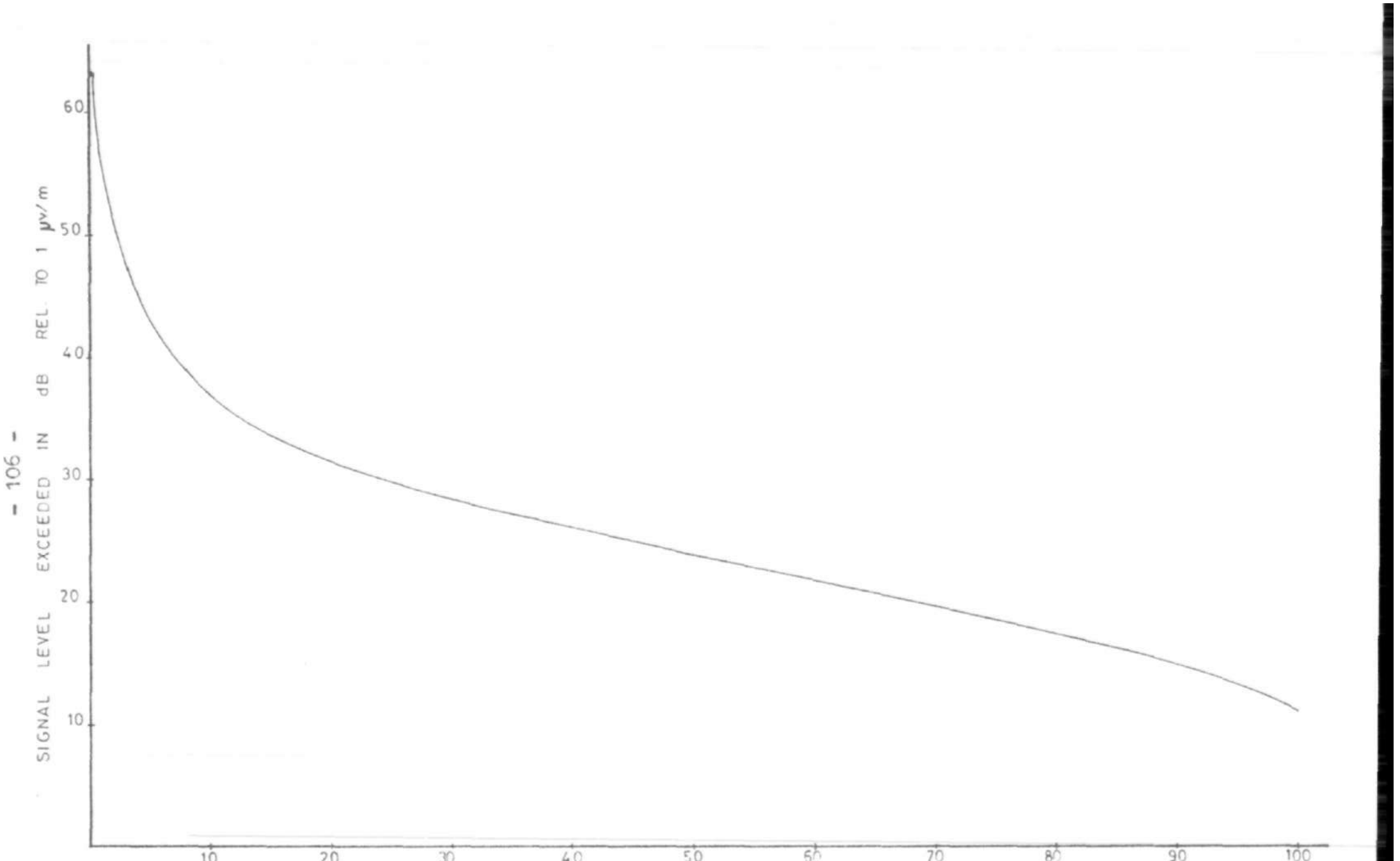


FIG. 20(Q) CUMULATIVE DISTRIBUTION OF 1.25 MINUTELY MEDIAN OF NTV JOS SIGNAL RECEIVED IN ZARIA DURING THE DRY SEASON MONTHS OF OCTOBER 1979 — APRIL 1980.

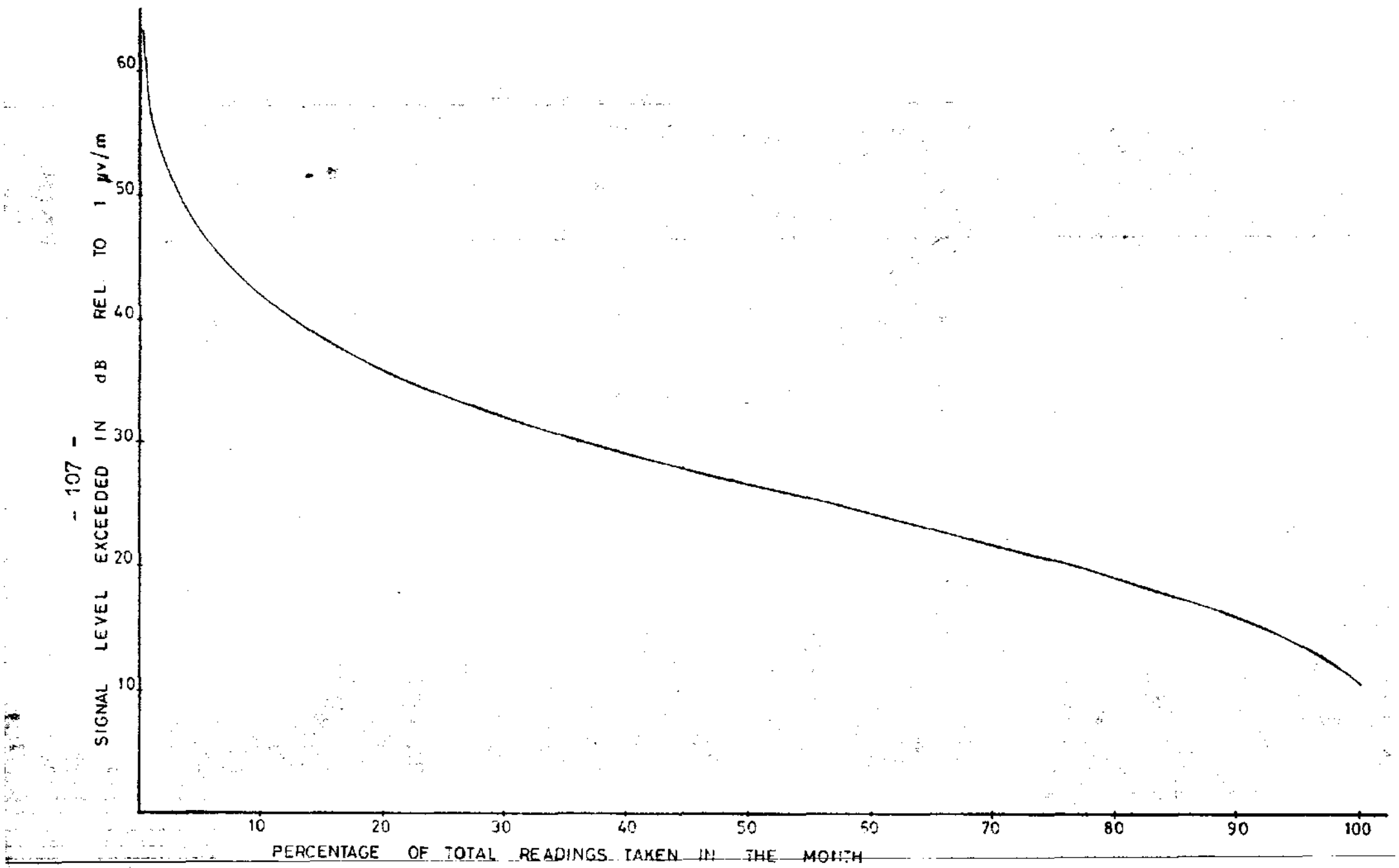


FIG. 20(P). CUMULATIVE DISTRIBUTION OF 1.25 MINUTELY MEDIAN OF NTV JOS SIGNAL RECEIVED IN ZARIA IN ONE YEAR (JULY 1979 — JULY 1980)

To characterize the fading associated with the reception of the transhorizon signals, the percentage of time for which a specified decibel level (relative to a seasonal or annual median) was exceeded was also computed (see table 4.8). The resulting graphical plots given in figure 21 show that the variation of the 1.25 minutely medians about the wet season median (30.5 dB μV/m), dry season median (23.8 dB μV/m) and annual median (26.5 dB μV/m) approaches a log-normal probability law, especially in the wet season.

4.5 Some Implications Of The Computed Results

The rise of signal level from 5 p.m. towards 10-11 p.m. may be attributed to the fact that during the day the predominant propagation mechanisms on the link are scattering and diffuse reflection both of which are favoured by instability and turbulence in the atmosphere. However, with reduced solar activity towards night, these give way (in preponderance) to specular reflection, known to be favoured by stability of the atmosphere with stratification and cloud formation, and to be responsible for higher signal levels obtained on transhorizon links, as already indicated in chapter two. The "towards-midnight-dip" in signal level might be connected with increased turbulence due to other meteorological factors like changes in the gradients of pressure and temperature caused by the increasing impact of thermal radiation from the earth's surface and hence change in the refractive index gradient as mentioned in Section 1.1. above.

TABLE 4.8

PROBABILITY DISTRIBUTION OF THE 1.25 MINUTELY MEDIANS

Signal level in dB rel. to Annual Median	10	5	0	- 5	- 10	- 15	- 20	- 25	- 30
Percentage of time level was exceeded	18.4	32	50	71	88	98.5	99.5	100	100
Signal level in dB rel. to Wet Season Median	10	5	0	- 5	10	- 15	- 20	- 25	- 30
Percentage of Time level was exceeded	19	32.5	50	72	89.5	95.6	98.5	99.6	100
Signal level in dB rel. to Season median	10	5	0	- 5	- 10	- 15	- 20	- 25	- 30
Percentage of time level was exceeded	15	28.5	50	73	95	99.4	100	-	-

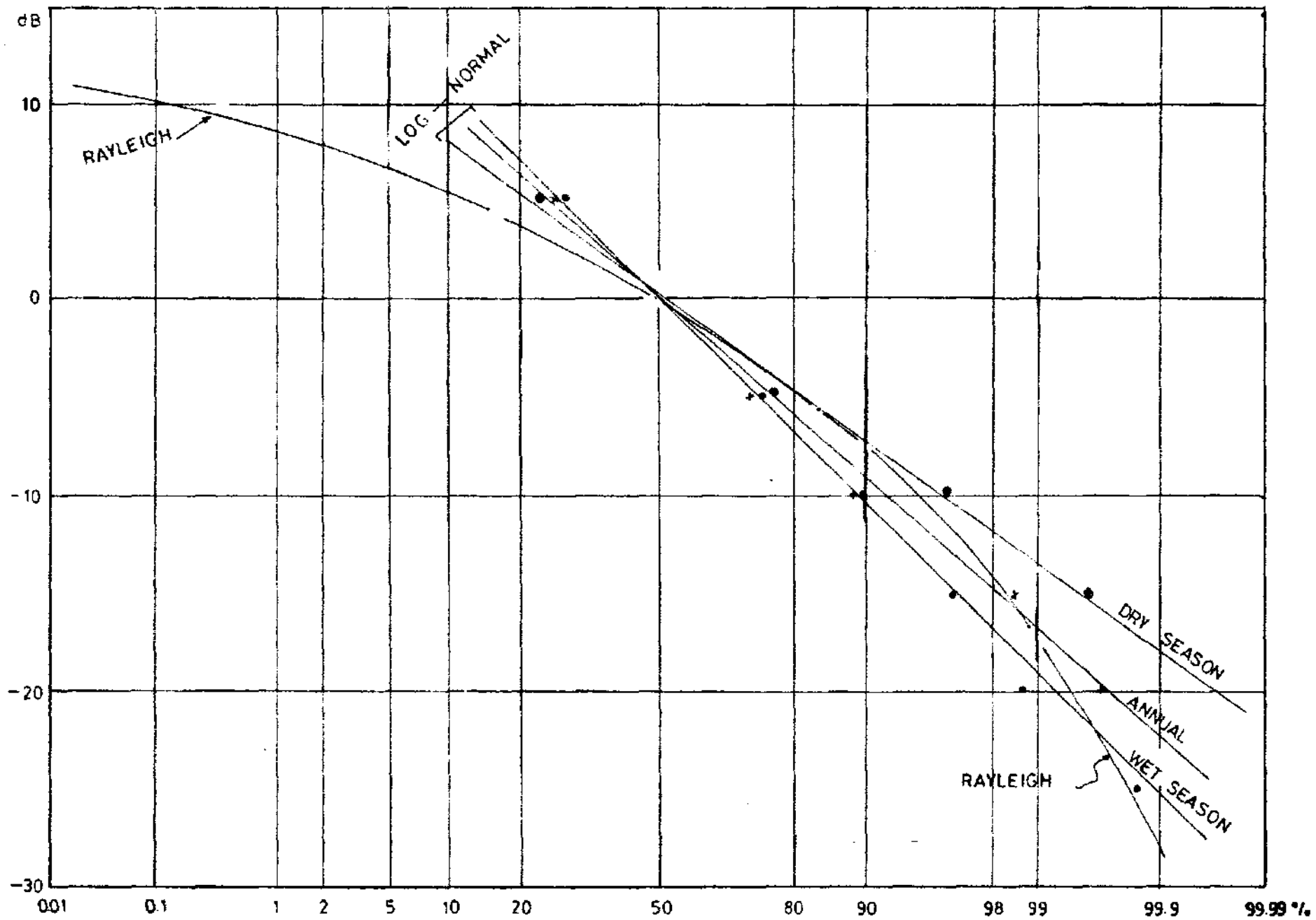


FIG 21 : THE PROBABILITY DISTRIBUTION OF THE 1.25 MINUTELY MEDIAN OF NTV JOS SIGNALS RECEIVED IN ZARIA APPROACHES A LOG-NORMAL DISTRIBUTION LAW.

Terrestrial radiation is characterized by long wave length. The atmosphere is about 95% opaque to this long wave radiation, carbon dioxide and water vapour being good absorbers. The high concentration of these gases above cloud tops cause greater loss of heat at a cloud top than at the base. This relative radiative base warming and top cooling of clouds of appreciable thickness has a net warming effect on the cloud and can radically change the temperature lapse rate in cloud parcels within a short time. This phenomenon is also responsible for the evening thunderstorms due to destabilization*. The tendency for signal level to decrease towards midnight can, however, be violated as was the case in October 1979 (see figures 13(A), 17(D)). This is further discussed in a later paragraph.

The increase in signal level in the wet season (summer) relative to the dry season values is in accordance with already established radio propagation trend, which is discussed in chapter two. Mean monthly signal attenuation is known to follow closely the changes in the refractive index gradient and tests conducted in the temperate climate have shown that an improvement in this correlation may be realized when attenuation is compared with a combination of refractive index gradient and atmospheric stability as the radiometeorological parameter (7). Similar effects might be expected on the Jos - Zaria radio path, its location in a tropical climate notwithstanding.

---

* (27), (29)

The increase field strength in the wet season, may however, be largely attributed to thunderstorm activities (see chapter two) during this period. And as suggested earlier, this effect is expected to be more pronounced in the tropics than in the temperate climate. A study of thunderstorm in the U.S.A. (see (27) pp. 71 - 72) has shown that within a thunderstorm cell temperatures are everywhere slightly cooler than the environment; that considerable amounts of water are encountered in the storm; and that the maximum updrafts and turbulence were found in the upper levels of the cloud (with the cells capable of reaching a height of 60,000 ft.) such that starting from the lower part of the cell, turbulence progressively becomes less severe and finally disappears. These features can readily be associated with temperature inversion, change in dielectric constant and relative stability of the part of the troposphere involved - all of which are favourable to strong specular reflection, (see (28) pp. 24 - 46). Hence the increased specular reflection observed during thunderstorms. Thus with the effect of the thunderstorm cells at the background correlation between median signal levels and mean rainfall figures can be better appreciated if the following points are noted:

1. Formation of thunderstorm cells does not necessarily occur under rain conditions, but rather when the atmosphere holds sufficient moisture , as exemplified by cases of trace rainfall which (as indicated in Section 3.1.4) were regarded as 0 mm.

2. Rainfall figures considered were only from Zaria and Jos, whereas rainfall in any other part of the 200 km

stretch radio link path could equally have affected transmission, and

3. Rainfall figure for a particular day was measured from 6 p.m. of that day to 6 a.m. of the following day. Hence rains which fell in the afternoon and did not extend beyond 6 p.m. would not be recorded but may have substantial effect on the evening signal transmission; on the other hand, rains which fell after twelve midnight would be recorded but have no effect on transmission which occurred between 5 and 11.30 p.m. Correlation may, thus, not be ruled out when there is a one day shift between peak values (or troughs) of median signal level and rainfall figures.

During the dry season months when signal levels are relatively lower, other transhorizon propagation mechanisms predominate. These are mainly tropospheric scattering and diffuse reflection (see figures 9, 11 and 13). The diffraction mode makes the least contribution, but its effect on this path can nevertheless not be ignored - the theoretical boundary between diffraction and tropospheric effects being between 100 and 200 km, depending on frequency (7). Thus diffraction is a major attenuation factor on the transhorizon path (see figures 4, 5, 6 and 7).

Some possible implications of the relatively high level of NTV Jos signal in Zaria, especially during the wet season, can be appraised from two view points: Useful transhorizon signals and interference problems.

4.5.1 Useful Transhorizon Signal

One aspect of television broadcasting which viewers in Nigeria are yet to enjoy is multichannel service. As a result viewers in Zaria are usually delighted when they pick NTV Jos signal on their receiver sets, be it of poor quality (usually without sound) or for brief time durations. There is thus a strong desire that this signal reaching Zaria is actually boosted by conventional means such as increasing the transmitted power or the antenna directive gain of the receiver.

The efforts required in this direction will no doubt be considerably reduced by the natural transhorizon radio propagation mechanisms featuring on the Jos - Zaria radio path which ensures that the field strength in Zaria exceed 26.5 dB (relative to 1 μV/m) during 50% of the reception time, especially in the wet season when the thunderstorm signal enhancement phenomenon can increase the field strength up to 40 - 63 dB μV/m for over 25% of the reception time (see table 4.7). However, such strong signals reaching Zaria and its surroundings from the Jos transmitter will be useful only if no other co-channel signals reach the area from another transmitter located elsewhere, otherwise there would be serious interference problem.

4.5.2 Interference Problems

Figure 22 is part of map of Nigeria showing coverage areas (nominally 50 km from the transmitter) of the television stations planned and already established in the North Central

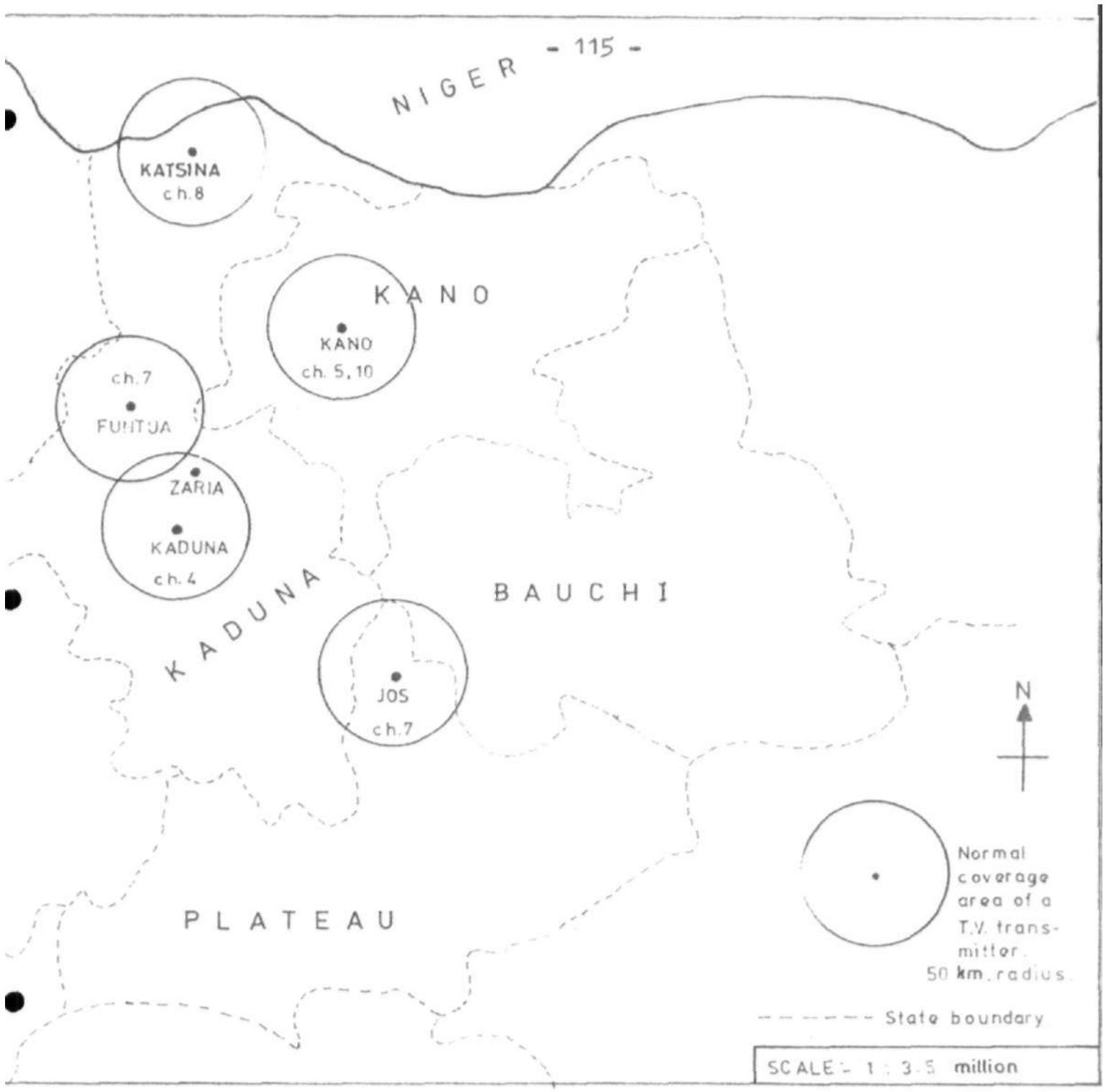


FIG. 22: COVERAGE AREAS OF PLANNED AND EXISTING TELEVISION STATIONS IN THE NORTH CENTRAL PART OF NIGERIA.

areas of Nigeria. The relative positions of Funtua and Zaria indicate that part of the coverage area of the Funtua transmitter (channel 7) would be exposed to adverse interference from the co-channel NTV Jos transmitter (channel 7), especially in the wet season.

For protection against interference, the International Radio Consultative Committee (CCIR) recommended a ratio of 45 dB between wanted and unwanted signals where there is no special control on the nominal frequency difference between the carriers for 1% to 10% of the time (22). This condition is rather severe and used only for planning purposes. In practice, interference becomes perceptible only after the ratio is 10 - 20 dB above the planning level. In band III to which both Jos and the proposed Funtua channels belong, the minimum level to which protection is sought is 55 dB μV/m. Taking an expected field strength in Zaria from Funtua to be, say, 56 dB μV/m, this would then mean keeping the NTV Jos signal level below 31 dB μV/m in Zaria. But as can be seen from the cumulative distribution graphs of figures 20 (A) - (P), this was violated for 7% of the total reception time in a typical dry season month of February 1980, and for 65% of the time in September 1979. On the average this violation was for 22% of the time in dry season, a little over 48.5% in wet season, and for 33% of the whole period of measurement. These figures are sufficiently high to mar a smooth entertainment of viewers of the proposed channel 7 from Funtua. Moreso, if the more

severe 45 dB protection ratio recommended by the CCIR were used, the NTV Jos signal level would then have to be kept below 11 dB μV/m in Zaria, and this would be violated for 99 - 100% of the reception time in both seasons and for the whole period of measurement (see figures 20 (N), (O) and (P)).

Lastly, the fact that the distribution of median values taken in as small interval of time as 1.25 minutes approaches a log-normal distribution law is a confirmation of the preponderance of specular reflection on the Jos - Zaria radio path; otherwise a preponderance of diffuse reflection and/or scattering should have been manifested through a distribution which tends to Rayleigh distribution law (as discussed in chapter two). In the wet season specular reflection is very much augmented by the formation of thunderstorm cells, which effects signal enhancement to such extent that signal level can remain high and almost steady for over two hours (see figure 13 (A)), thus completely overshadowing effects of scattering and diffuse reflection which is characterized by fast rapid fading, as shown in figures 13 (B) and (C). These figures further reveal that the lowest signal levels were received in the dry season, and largely due to scattering. This again explains the greater deviation of the dry season probability distribution curve from the normal distribution, than the curves for the wet season or for the whole period of measurement (figure 21). The relatively diminished role of

tropospheric scattering on the Jos - Zaria transhorizon radio path agrees with information contained in figure 11 (A) at 200 MHz and 11(B) at 200 km. Also the high level of harmattan dust which fill the lower troposphere during a greater part of the dry season in this part of Nigeria can possibly affect the signals through a change in the dielectric constant of the troposphere.

CHAPTER FIVE

THE DESIGN AND CONSTRUCTION OF A V.H.F. PRE-AMPLIFIER USING S - PARAMETERS

5.1 Introduction

The normal useful range for television varies from 50 - 83 kilometres, and for F.M. sound broadcasting from 83 - 133 kilometres, depending on the nature of the terrain, absorption by nearby structures, local interference, and the antenna heights. Outside these ranges the signals would be weak and may be unreliable. Some improvement in reception in the fringe zones and beyond can be obtained by the use of high-gain directional receiving aerials and/or a pre-amplifier.

Such a pre-amplifier can considerably boost the weak signals prior to their reaching the receiving TV sets; and in the case of very weak signals as in this project, it is necessary that the pre-amplifier be as close as possible to the receiving antenna to check further degradation of the signal to noise ratio in the antenna-receiver coupling cable prior to amplification.

This part of the project therefore, aims at designing and constructing a pre-amplifier which can boost the reception of NTV Jos signals at a frequency of 192 MHz in Zaria which is at a distance of about 200 km from the Jos transmitter. Obviously a prime requirement of such an amplifier should be the realization of a reasonably high gain, especially as the bandwidth can be very narrow (provided it is not less than 6 MHz), and more importantly to keep the noise figure as low as possible.

5.2 Transistor S - Parameters

The performance of a transistor may be characterized by h, y or z parameters. However, transistor characterization at high frequencies ($\geq$ 100 MHz) is usually difficult using these parameters, and often the data is either incomplete or in an inconvenient form; moreso, these data cannot be measured accurately at high frequencies. However, the development of scattering or S - parameters has made it possible to accurately characterize the high frequency performance of transistors. Also the S - parameters can be readily converted to the y (hence h or z) equivalent.

Under the S - parameter method a transistor is represented as a two-port network whose terminal behaviour is defined by four S - parameters - S_{11}, S_{12}, S_{21} and S_{22}.

To appreciate the meaning of S - parameters, consider a two-port network (figure 23). The normalized incident and reflected waves at port i may be defined respectively as

$$a_i = \frac{V_i + I_i Z_o}{2\sqrt{Z_o}} \quad \ldots \quad 5.1$$

and

$$b_i = \frac{V_i - I_i Z_o}{2\sqrt{Z_o}} \quad \ldots \quad 5.2$$

where V_i is the voltage at port i, Z_o is the characteristic impedance of the two-port measuring system, and I_i is current at port i.

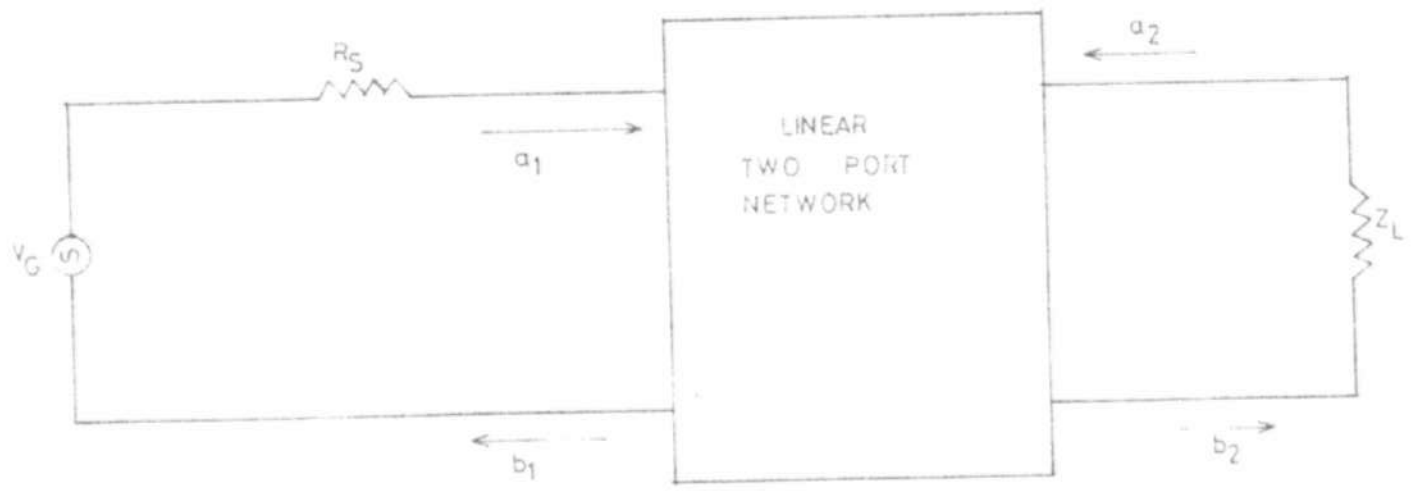


FIG. 23 COMPLEX INCIDENT AND REFLECTED WAVES OF A LINEAR TWO PORT NETWORK

The effect of waves (a_i) entering the system from other ports on the waves (b_i) leaving a given port may be expressed in a matrix form viz:-

$$[B] = [S][A] \quad \ldots\ 5.3$$

where $[S]$ is a square matrix whose elements are the coefficients of the independent variables a_i;

$[A]$ and $[B]$ are column matrices whose elements are respectively the independent and dependent variables.

For a two-port system equation 5.3 becomes, on expansion

$$\begin{bmatrix} b_1 \\ b_2 \end{bmatrix} = \begin{bmatrix} s_{11} & s_{12} \\ s_{21} & s_{22} \end{bmatrix} \begin{bmatrix} a_1 \\ a_2 \end{bmatrix} \quad \ldots\ 5.4$$

From equation 5.4 it can be seen that

$$b_1 = s_{11}\, a_1 + s_{12}\, a_2 \quad \ldots\ 5.5$$

$$b_2 = s_{21}\, a_1 + s_{22}\, a_2 \quad \ldots\ 5.6$$

The solution to these equations in terms of the S-parameters are

$$s_{11} = \frac{b_1}{a_1} \quad \ldots\ 5.7$$

$$s_{21} \quad \frac{b_2}{a_1}$$

and

$$s_{12} = \frac{b_1}{a_2}$$

$$s_{22} = \frac{b_2}{a_2} \quad \ldots\ 5.8$$

Equation 5.7 implies that no wave is reflected from the load Z_L; hence to satisfy this solution $Z_L = Z_o$ is a necessary and sufficient condition. Also equation 5.8 implies that there must be no wave from the source; and to satisfy this $V_s = 0$ and $Z_s = Z_o$ are sufficient conditions.

The S-parameters may therefore be defined as follows:

$S_{11} = \frac{b_1}{a_1}$ $a_2 = 0$ — $\frac{\text{voltage wave reflected from Port 1}}{\text{voltage wave incident on Port 1}}$

Input reflection coefficient (with the output port terminated in Z_o)

$S_{22} = \frac{b_2}{a_2}$ $a_1 = 0$ — $\frac{\text{voltage wave reflected from Port 2}}{\text{voltage wave incident on Port 2}}$

output reflection coefficient (with the input port terminated in Z_o)

$S_{21} = \frac{b_2}{a_1}$ $a_2 = 0$ — $\frac{\text{voltage wave leaving Port 2}}{\text{voltage wave incident on Port 1}}$

Forward transmission coefficient (with the output port terminated in Z_o)

$S_{12} = \frac{b_1}{a_2}$ $a_1 = 0$ — $\frac{\text{voltage wave leaving Port 1}}{\text{voltage wave incident on Port 2}}$

Reverse transmission coefficient (with input port terminated in Z_o)

From the definitions of S_{11} and S_{22}, and the expressions of equations 5.1 and 5.2, it can be shown that,

$$S_{11} = \frac{Z_{in} - Z_o}{Z_{in} + Z_o} \qquad \ldots\ldots \quad 5.9$$

and

$$S_{22} = \frac{Z_{out} - Z_o}{Z_{out} + Z_o} \qquad \ldots\ldots \quad 5.10$$

where

Z_{in} is the input impedance of the network when the output port is terminated in Z_o, and Z_{out} is the output impedance when the input is terminated in Z_o.

Being reflection coefficients, S_{11} and S_{22} can be represented on Smith Chart (see figure 30). Also from their definitions, it is seen that

$$S_{21} = \left[\frac{\text{Power leaving Port 2}}{\text{Power entering Port 1}}\right]^{\frac{1}{2}} \qquad \ldots\ldots \quad 5.11$$

and

$$S_{12} = \left[\frac{\text{Power leaving Port 1}}{\text{Power entering Port 2}}\right]^{\frac{1}{2}} \qquad \ldots\ldots \quad 5.12$$

so that

$|S_{21}|^2$ = Forward gain

and

$|S_{12}|^2$ = Reverse gain

} when the network is terminated in Z_o at either ports.

The above definitions of the various S-parameters have been based on the condition that the load and source impedances (Z_L and Z_s) are each equal to the characteristic impedance Z_o of the system. When any of these impedances

is not equal to Z_o the expressions for the input and output reflection coefficients become modified thus:

$$S'_{11} = S_{11} + \frac{S_{21}\, S_{12}\, \Gamma_L}{1 - S_{22}\, \Gamma_L} \qquad \ldots\ldots \qquad 5.13$$

and

$$S'_{22} = S_{22} + \frac{S_{21}\, S_{12}\, \Gamma_s}{1 - S_{11}\, \Gamma_s} \qquad \ldots\ldots \qquad 5.14$$

where $\Gamma_L = \dfrac{Z_L - Z_o}{Z_L + Z_o}$,

$$\Gamma_s = \frac{Z_s - Z_o}{Z_s + Z_o}$$

It can be seen from these expressions that if $Z_L = Z_o$ and $Z_s = Z_o$, then $S'_{11} = S_{11}$ and $S'_{22} = S_{22}$. Also from equations 5.9 and 5.10 the input and output impedance may therefore be expressed respectively as:

$$Z_{in} = Z_o \left(\frac{1 + S'_{11}}{1 - S'_{11}} \right) \qquad \ldots\ldots \qquad 5.15$$

$$Z_{out} = Z_o \left(\frac{1 + S'_{22}}{1 - S'_{22}} \right) \qquad \ldots\ldots \qquad 5.16$$

The magnitude of the product $S_{21}\, S_{12}$ is a measure of stability and the input/output isolation of the network. For an active device the S-parameters depend on the d.c. bias conditions and the frequency of operation; for a passive two-port network $S_{12} = S_{21}$.

Other transistor parameters may also be expressed in terms of S-parameters. The transducer power gain (G_T) which is the ratio of power absorbed by the load over that available from the generator is

$$G_T = \frac{|S_{21}|^2 [1 - |\Gamma_s|^2][1 - |\Gamma_L|^2]}{|(1 - S_{11}\Gamma_s)(1 - S_{22}\Gamma_L) - S_{21}S_{12}\Gamma_L\Gamma_s|^2} \quad \ldots\ldots 5.17$$

Usually the smaller the magnitude of the reverse transfer coefficient the better the transistor performance. When S_{12} is sufficiently small it can be regarded as zero, and the resultant unilateral transducer power gain is

$$G_{TU} = \frac{|S_{21}|^2 (1 - |\Gamma_s|^2)(1 - |\Gamma_L|^2)}{(1 - S_{11}|\Gamma_s|^2)(1 - S_{22}|\Gamma_L|^2)} \quad \ldots\ldots 5.18$$

The assumption that $S_{12} = 0$ is valid if

$$\frac{1}{(1+U)^2} < \frac{G_T}{G_{TU}} < \frac{1}{(1-U)^2} ,$$

where U is the unilateral figure of merit defined as

$$U = \frac{|S_{11}S_{12}S_{21}S_{22}|}{(1 - |S_{11}|^2)(1 - |S_{22}|^2)} \quad \ldots\ldots (5.19$$

Rewriting equation 5.18 as

$$G_{TU} = |S_{21}|^2 \cdot \frac{(1 - |\Gamma_s|^2)}{|1 - S_{11}\Gamma_s|^2} \cdot \frac{(1 - |\Gamma_L|^2)}{|1 - S_{22}\Gamma_L|^2} \quad \ldots\ldots 5.20$$

It can be seen that the first term depends on the transistor only while the second and third terms depend in addition on the input and output matching respectively. Hence with appropriate matching networks the S - parameters can be manipulated to effect optimum gain, and the maximum transducer power gain may be obtained if $\Gamma_s = S^*_{11}$ and $\Gamma_L = S^*_{22}$, so that

$$G_{TU\ max.} = |S_{21}|^2 \cdot \frac{1}{1 - |S_{11}|^2} \cdot \frac{1}{1 - |S_{22}|^2} \quad \ldots\ldots 5.21$$

Another important device consideration which can be elucidated by S - parameters is stability. A device may oscillate if either S_{11} or S_{22}, or both are greater than unity — a negative resistance condition, since the reflected wave becomes greater than the incident wave. A device is unconditionally stable if S_{11} and S_{22} are each smaller than unity on the one hand, and the inherent stability factor K is greater than unity and positive on the other. K may be expressed as

$$K = \frac{1 + |\Delta|^2 - |S_{11}|^2 - |S_{22}|^2}{2|S_{21}\ S_{12}|}$$

where $\Delta = S_{11}\ S_{22} - S_{12}\ S_{21}$

5.3 The Design Theory

5.3.1. Stability Factor And Stability Circles

The stability factor K takes a unique position in the theory of this design. If the stability factor is not

greater than unity and positive, the circuit is potentially unstable and may oscillate. It is possible to plot stability circles on the input and output planes, such that on each plane the stability circle separates the stable region from the potentially unstable region. For cases where the stability circle does not enclose the origin of the Smith Chart the area of the circle defines the unstable region while the stable region lies outside the circle; however, if the stability circle encloses the origin of the Smith Chart the area of the circle defines the stable region while the region outside defines the potentially unstable region (see figure 24).

The stability circle may be defined by the centre and radius given by the expressions 5.23 - 5.26 below:

On the input plane: the centre of the stability circle is

$$r_{s_1} = \frac{C_1^*}{|S_{11}|^2 - |\Delta|^2} \qquad \ldots\ldots \qquad 5.23$$

where $C_1 = S_{11} - \Delta S_{22}^*$ (Δ as earlier defined)

and

the radius of the stability circle is

$$R_{s_1} = \frac{|S_{12}\, S_{21}|}{|S_{11}|^2 - |\Delta|^2}$$

Similarly, on the output plane:

$$r_{s2} = \frac{C_2^*}{|S_{22}|^2 - |\Delta|^2}$$

where $C_2 = S_{22} - \Delta S_{11}^*$,

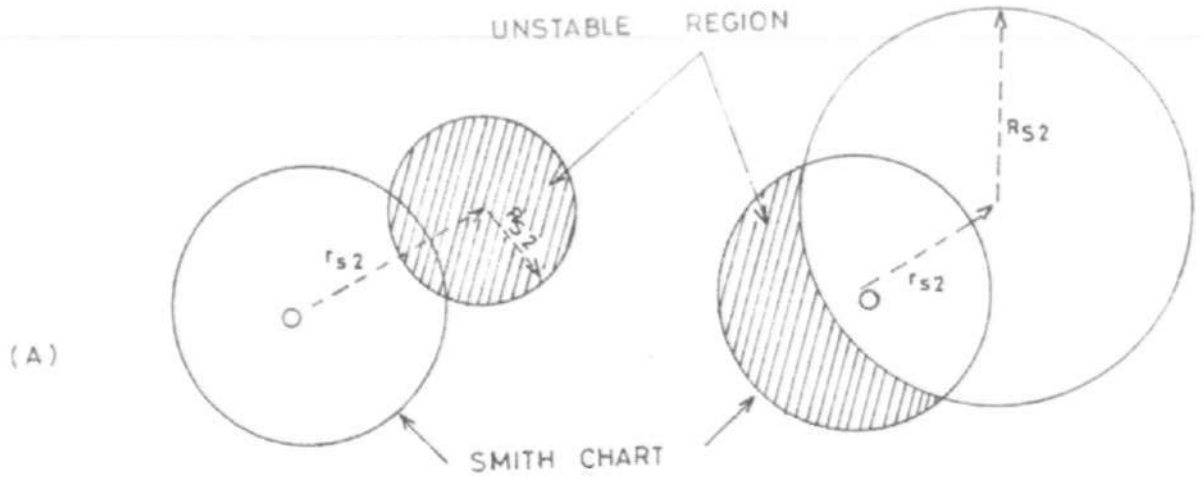


FIG. 2.4. STABILITY CIRCLES ON THE OUTPUT PLANE

(A) S_{11}, S_{22} LESS THAN 1, $K<1$; CONDITIONALLY STABLE.

(B) S_{11}, S_{22} NOT LESS THAN 1, $K<1$; CONDITIONALLY STABLE

and

$$R_{s2} = \frac{|S_{12}\, S_{21}|}{|S_{22}|^2 - |\Delta|^2} \qquad \ldots\ldots \qquad 5.26$$

With the stability circles plotted, stable operation is assured as long as no load is picked within the unstable region.

The maximum power gain obtainable from a transistor may be expressed as

$$G_{max} = \left|\frac{S_{21}}{S_{12}}\right| \cdot \left| K + \sqrt{K^2 - 1} \right| \qquad \ldots\ldots \quad 5.27$$

(+ sign is used if B_1 of equation 5.21 is negative, else the - sign is used).

However, the gain of a potentially unstable device tends to infinity and the above expression cannot apply to such cases.

To obtain any desired gain a constant gain circle can be plotted such that any load picked on the circle would give the desired gain. The centre and radius of a constant gain circle are respectively given by

$$r_{02} = \left[\frac{G}{1 + D_2\, G}\right] C_2^* \qquad \ldots\ldots \qquad 5.28$$

and

$$R_{02} = \frac{(1 - 2K\,|S_{12}\, S_{21}|\, G + |S_{12}\, S_{21}|^2\, G^2)^{\frac{1}{2}}}{1 + D_2\, G}$$

where

$$D_2 = \left|S_{22}\right|^2 - \left|\Delta\right|^2$$

$$G = \frac{G_P}{G_o}$$

G_p = numeric value of the desired total amplifier gain.

$$G_o = \left|S_{21}\right|^2$$

The value of the generator impedance that simultaneously matches the input load may be computed from

$$R_{ms} = \left[\frac{S_{11} - R_{ML}\Delta}{1 - R_{ML} S_{22}}\right]^* \qquad \text{---- 5.30}$$

where

R_{ms} = the reflection coefficient of the required source impedance.

R_{ML} = the reflection coefficient of the load picked.

If the R_{ms} obtained from equation 5.30 lies within the stable region of the input stability circle a stable operation is assured, otherwise another load (still on the appropriate gain circle and within the stable region as determined by the output stability circle) must be chosen and equation 5.30 re-evaluated.

R_{MS} and R_{ML} are plotted on the Smith Chart and the actual values of the optimum source and load impedances can be read from the Smith Chart co-ordinates as Z_s and Z_L respectively. A lossless matching network can be inserted

between the transistor and the source so as to match the source impedance to Z_s. Similarly another matching network must be inserted at the output port to match the output impedance to the actual load.

When the value of the stability factor K is greater than unity and positive the device is unconditionally stable, and will not oscillate under any load conditions. Under this condition it is possible to realize the maximum gain of the device and expression 5.27 becomes valid; what is needed is only to compute the values of R_{MS} and R_{ML} that will conjugately match the input and output ports respectively. These values may be thus computed:

$$R_{MS} = C_1^* \left[\frac{B_1 \pm \sqrt{B_1^2 - 4\,|C_1|^2}}{2\,C_1{}^2} \right] \quad .... \quad 5.31$$

where

$$B_1 = 1 + |S_{11}|^2 - |S_{22}|^2 - |\Delta|^2$$

(other parameters are as previously defined)

and

$$R_{ML} = C_2^* \left[\frac{B_2 \pm \sqrt{B_2^2 - 4\,|C_2|^2}}{2\,C_2{}^2} \right] \quad .... \quad 5.32$$

where

$$B_2 = 1 + |S_{22}|^2 - |S_{11}|^2 - |\Delta|^2$$

(other parameters as previously defined).

In expressions5.31 and 5.32 the positive sign (+) is used infront of the radical if the value of the corresponding B is negative, and the negative sign (-) is used if B is positive. In each case the computed reflection coefficient should be less than unity in magnitude.

When K > 1 but the device is conditionally stable (figure 24 (B)) or when the device is unconditionally stable (figure 25) but a power gain other than G_{max} is desired, constant gain circles must be constructed and the design process follows that previously described for K < 1 ; in all cases lossless transformation networks must be used to match the input port to the generator impedance and the output port to the load impedance - as illustrated in figure 25 below.

5.3.2 Graphical Method of Impedance Matching

The need often arises in circuit design to transform one impedance value into another for the purpose of obtaining either maximum power transfer or zero reflection coefficient, or both. For obtaining maximum power transfer the load impedance must be transformed to the complex conjugate of the source impedance (i.e. $Z_L = Z_s^*$), while for minimum reflection coefficient Z_L must be transformed to the characteristic impedance of the line (i.e. $Z_L = Z_o$). In an ideal system it is aimed at obtaining both maximum power transfer and eliminating reflections, else the power in the load would be reduced from the maximum available power by the ratio $1 - \rho^2$

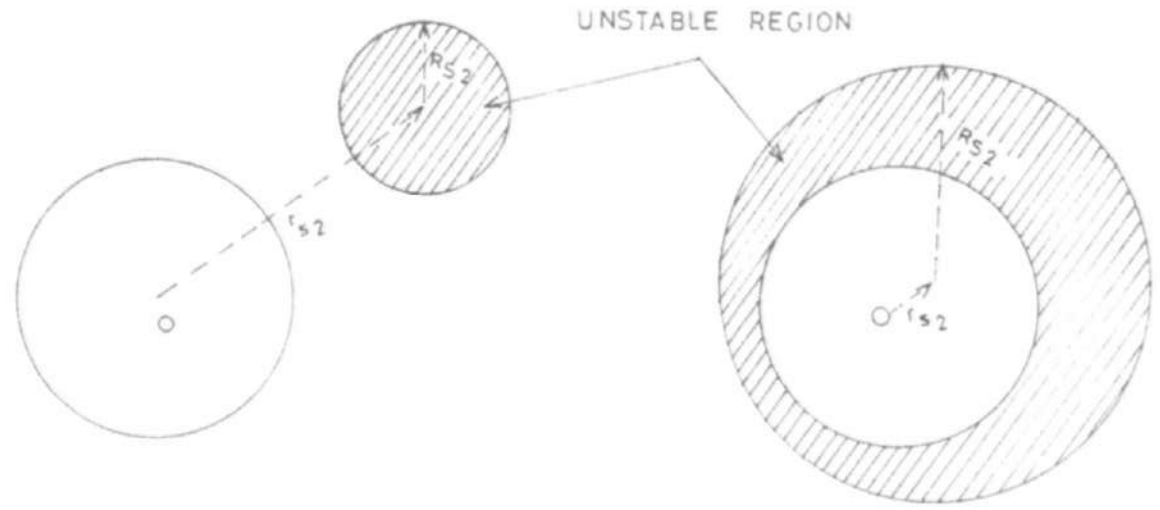


FIG. 25. S_{11}, S_{22} LESS THAN 1, K> 1; UNCONDITIONALLY STABLE.

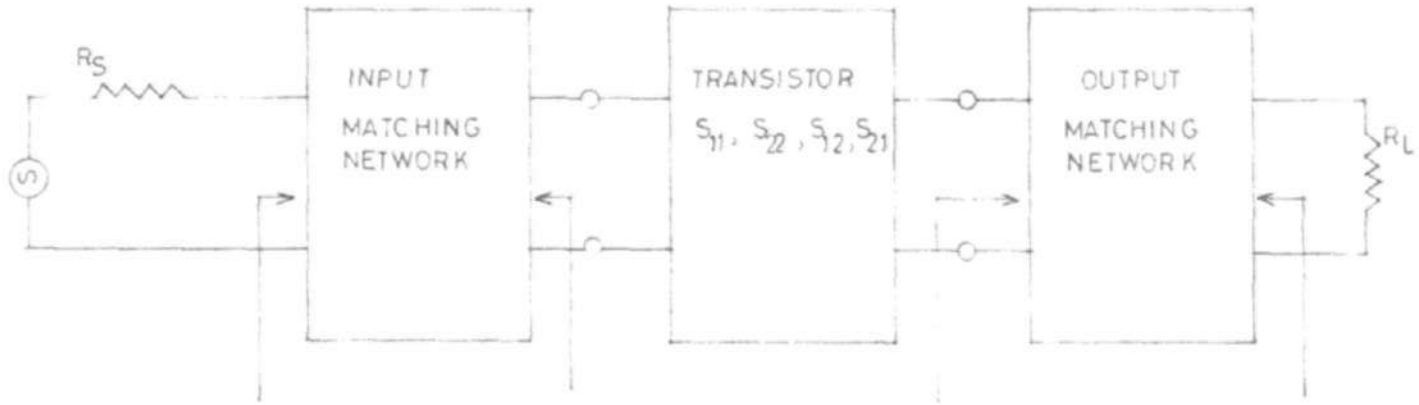


FIG. 26. TWO PORT DEVICE INPUT AND OUTPUT MATCHING NETWORK.

where $\rho = \frac{Z_L - Z_o}{Z_L - Z_o}$ is the reflection coefficient.

To realize this ideal, two conditions must be met:

1. The source is loaded by the complex conjugate of its internal impedance, and
2. The line is terminated in its characteristic impedance, as shown in figure 27.

Impedance transformation can be effected by various methods ranging from use of Smith's Chart to pattern combinations of resistances. However, the graphical method described here has been found very handy in the present amplifier design, and thus worthy of expounding. It involves designing lossless matching networks with lumped elements whose reactance values are determined from an impedance - admittance chart. It can be used to match Real to Real, Real to Complex or Complex to Complex impedances. Any rectangular impedance co-ordinate system with positive real parts can be transformed into an orthogonal admittance co-ordinate system with positive real conductance values such that any impedance $Z = R + jX$ in the former is transformed to a corresponding admittance value $Y = G + jB$ in the latter. Consequently any impedance $Z = R + jX$ may be obtained from the reciprocal of its transformed admittance value thus:

$$Z = \frac{1}{Y} = \frac{1}{G + jB}, \text{ or vice versa.}$$

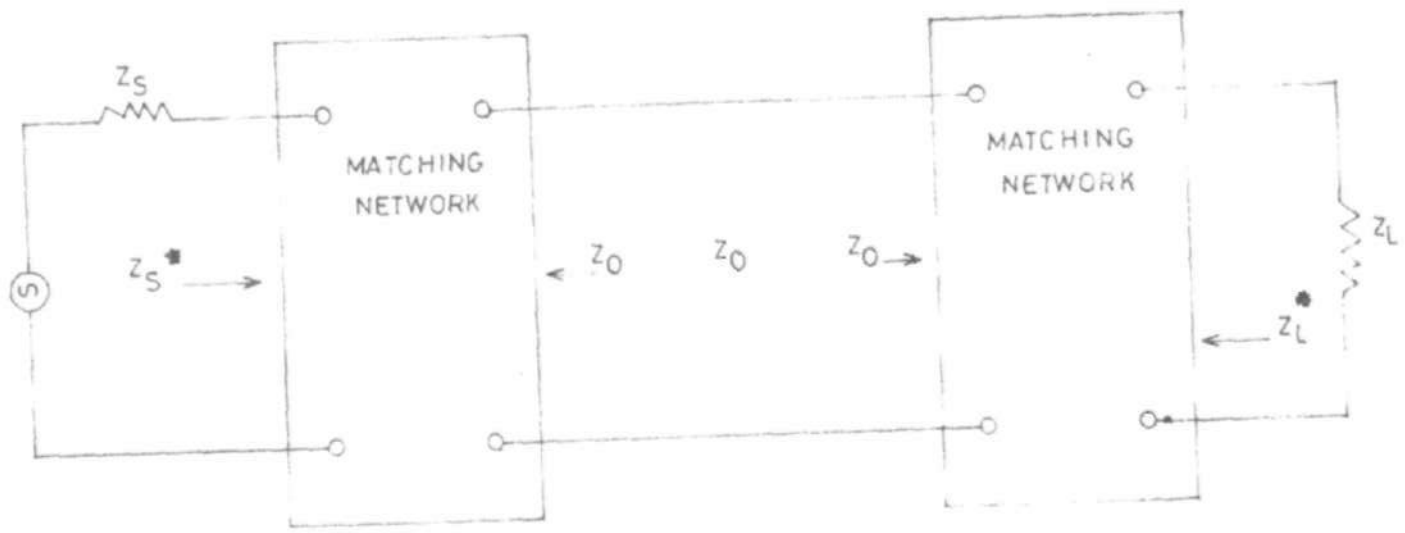


FIG. 27. IMPEDANCE MATCHING FOR MAXIMUM POWER TRANSFER AND ZERO REFLECTION COEFFICIENT.

This may be more easily appreciated from a superimposition of the two co-ordinate systems (figure 28).

In making a transformation the dual chart of figure 28 is used; the first step in such a transformation is to choose a convenient scale that would contain the conductance circle(s)* which must be drawn as large as possible for more accurate results. Having drawn the required conductance circles, matching is completed by moving from one impedance point A (see figure 29) on the appropriate conductance circle vertically up or down to the other conductance circle (at B), and then moving along this circle until the appropriate load point C is reached. Susceptance arcs are then drawn to pass through points A, B and C and tangent at point O*. An upward vertical movement from point A implies addition of a series inductance to the load represented by point A, while a downward vertical movement implies addition of a series capacitance; also a clockwise movement on a conductance circle implies addition of a shunt capacitance while anti-clockwise movement implies addition of shunt inductance to the load represented by point B.

The amount of series reactance required is equal to the value of the rectangular co-ordinate value at B minus the value at A , i.e.

$X_C = X_B - X_A$; and the amount shunt reactance required is similarly given as

$X_L = \frac{1}{B_T}$, where $B_T = B_C - B_B$

---

* This does not apply to any point on the conductance axis.

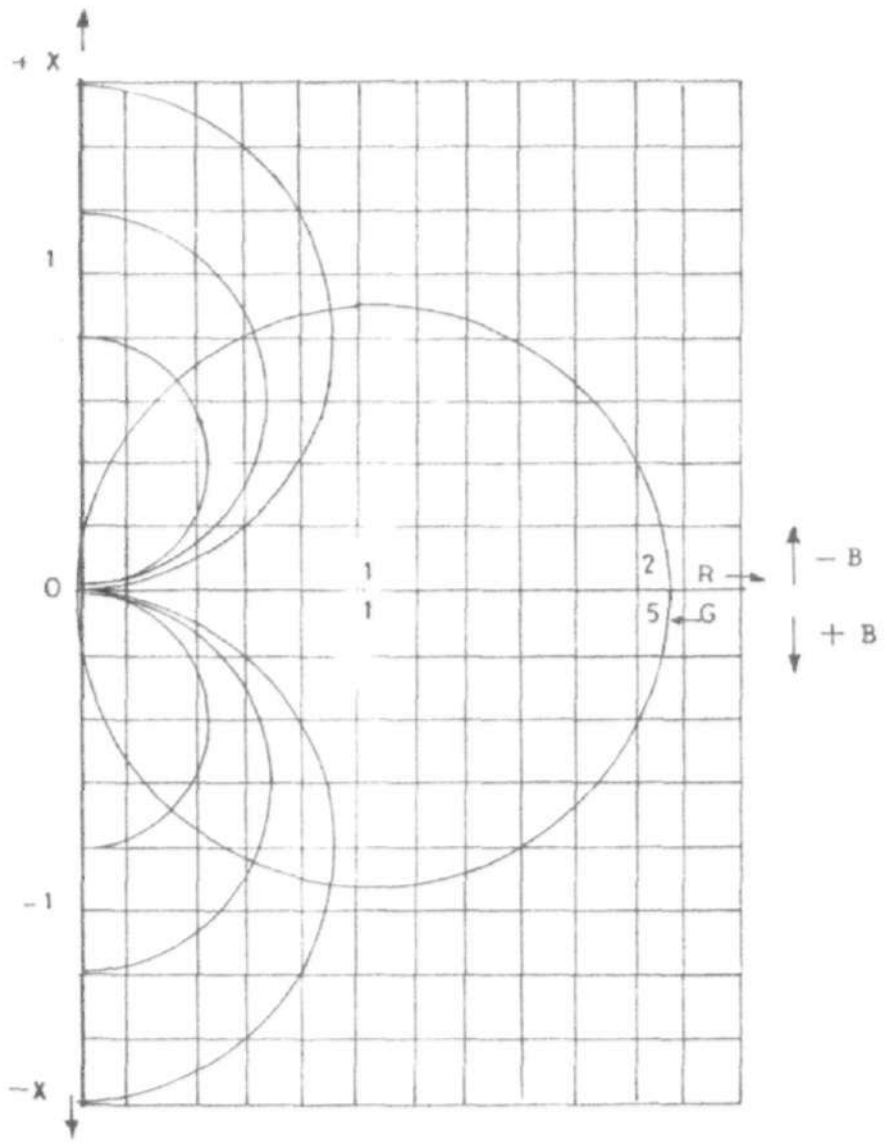


FIG. 28 . A SUPERIMPOSITION OF THE RECTANGULAR AND ORTHOGONAL IMPEDANCE CO ORDINATE SYSTEMS

These are illustrated in figure 29.

The series equivalent impedance ($Z = R + jX$) of any point on the chart is easily determined by reading the rectangular co-ordinate values of R and X; the value of the susceptance of the point may, however, be given by

$$B = \left(\frac{X_p}{S}\right)^{-1} \quad \ldots\ldots \quad 5.33$$

where

X_p = reactance of the parallel equivalent impedance $Z_p = R_p + jX_p$,

S = the scale factor used in preparing the chart.

Also,

$$X_p = R_p \left(\frac{S}{X_s}\right) \quad \ldots\ldots \quad 5.34$$

and

$$R_p = \frac{R_s^2 + X_s^2}{R_s} \quad \ldots\ldots \quad 5.35$$

R_s, X_s = real, imaginary parts of the series equivalent impedance $Z = R + jX$.

X_p is also given by the rectangular co-ordinate value of the point where the B arc cuts the reactance axis.

With the required series and shunt reactances determined, it is necessary to verify that a combination of these reactances and the series equivalent of the impedance being transformed yields the desired transformation.

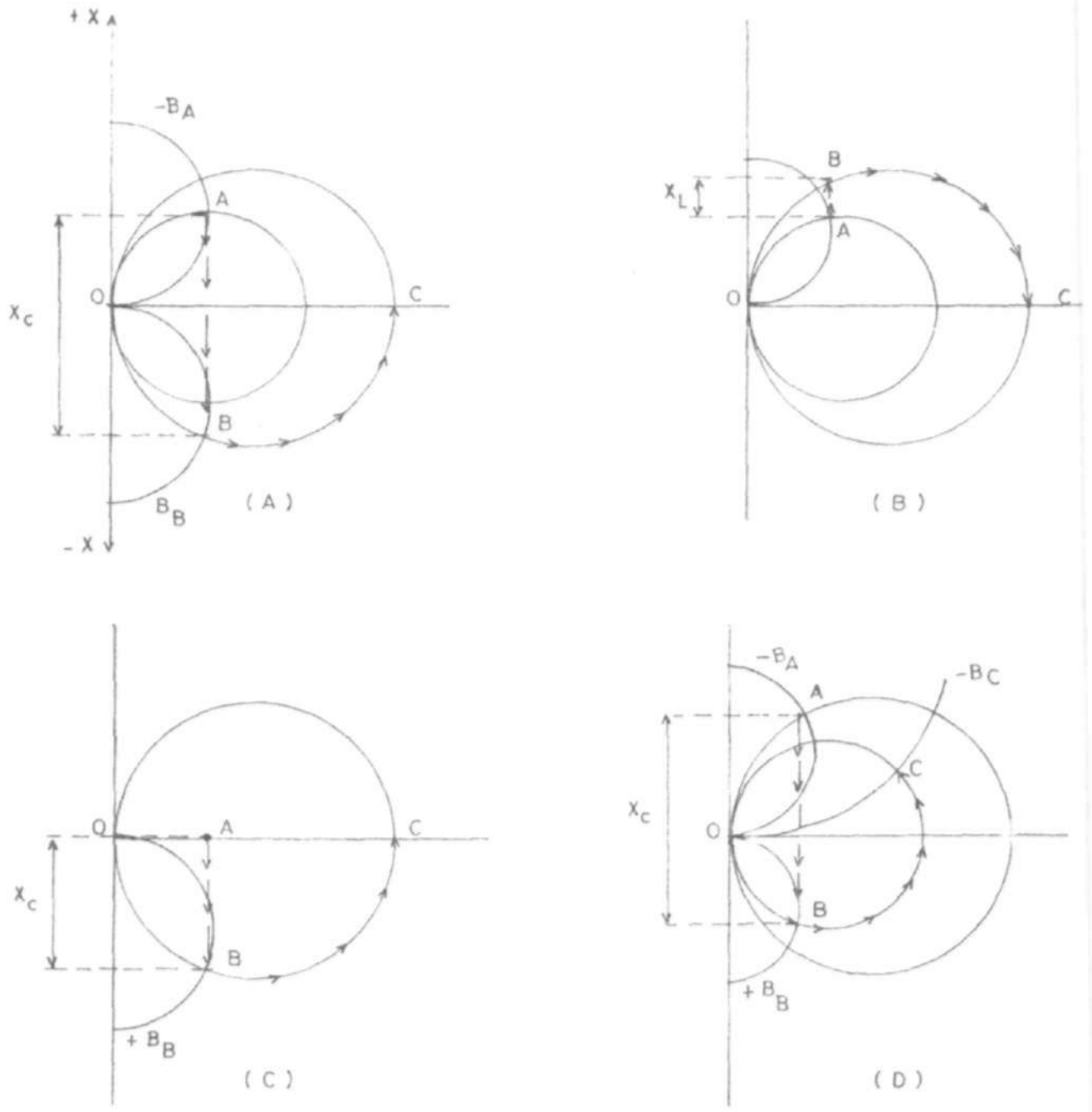


FIG 29. SOME ILLUSTRATIVE APPROACHES TO IMPEDANCE TRANSFORMATION :—

(a) COMPLEX IMPEDANCE TO REAL IMPEDANCE
(b) COMPLEX IMPEDANCE TO REAL IMPEDANCE
(c) REAL IMPEDANCE TO REAL IMPEDANCE
(d) COMPLEX IMPEDANCE TO COMPLEX IMPEDANCE

The corresponding values of capacitance and inductance are then given respectively as:

$$C = \frac{1}{2 \times \pi \times f \times X_o} \quad \ldots \quad 5.36$$

and

$$L = \frac{X_L}{2 \times \pi \times f} \quad \ldots \quad 5.37$$

where f = frequency in hertz.

5.4 The Design

The transistor used in the design was MA 42001 - 509. It was chosen because of its low noise figure, large dynamic range and availability.

The S - parameter characteristics used were given at a frequency of 200 MHz and a d.c. bias of I_c = 20 mA, V_{cc} = 10 V, and under the common-emitter configuration. These are as shown below* :

$$S_{11} = .381 \angle -142.6^\circ$$

$$S_{12} = .041 \angle 60.3^\circ$$

$$S_{21} = 3.057 \angle 92.8^\circ$$

$$S_{22} = .481 \angle -24.5^\circ$$

Now, following the design procedure earlier described, the a.c. circuit of the second stage may be designed as follows:

$$\Delta = S_{11} S_{22} - S_{12} S_{21}$$

$$= .18326 \angle -167.1^\circ - .33034 \angle 153.1^\circ$$

---

* Other relevant transistor parameters are given in table 5.1.

$$= .11596 - j.19037$$

$$= .22291 \angle -58.7^\circ,$$

$$C_1 = S_{11} - \Delta S_{22}^*$$

$$.381 \angle -142.6^\circ - (.22291 \angle -58.7^\circ)(.481 \angle 24.5^\circ)$$

$$= -.3914 - j\ 1712$$

$$= .4272 \angle -156.4^\circ,$$

$$C_2 = S_{22} - \Delta S_{11}^*$$

$$= .481 \angle -24.5^\circ - (.2229 \angle -58.7^\circ)(.381 \angle 142.6^\circ$$

$$= .4287 - j\ .2839$$

$$= .5142 \angle -33.5^\circ ,$$

$$B_1 = 1 + |S_{11}|^2 - |S_{22}|^2 - |\Delta|^2$$

$$= 1 + .381^2 - .481^2 - .2229^2$$

$$= .8641$$

$$B_2 = 1 + |S_{22}|^2 - |S_{11}|^2 - |\Delta|^2$$

$$= 1 + .481^2 - .381^2 - .2229^2$$

$$= 1.0365,$$

and

$$D_2 = |S_{22}|^2 - |\Delta|^2$$

$$= .481^2 - .2229^2$$

$$= .1817$$

Also the stability factor is given from expression 22 as

$$K = \frac{1 + |\Delta|^2 - |S_{11}|^2 - |S_{22}|^2}{2\ S_{12}\ S_{21}}$$

$$= \frac{1 + .0497 - .1452 - .2314}{2 \times .3303}$$

$$= 1.0189$$

i.e. $K > 1$, which implies that the transistor is unconditionally stable under the bias conditions and frequency since S_{11} and S_{22} are also less than 1, (see figure 28). The maximum gain is

$$G_{MAX} = \frac{|S_{21}|}{|S_{12}|} \left| K - \sqrt{K^2 - 1} \right|$$

$$= \frac{8.057}{.041} \times \left| 1.0189 - \sqrt{1.0189^2 - 1} \right|$$

$$= 161.84$$

$$= 22 \text{ dB.}$$

The reflection coefficient of the generator impedance required to conjugately match the input of the transistor is

$$R_{MS} = C_1^* \left[\frac{B_1 - \sqrt{B_1^2 - 4\,|C_1|^2}}{2\,|C_1|^2} \right]$$

$$= .4272 \angle 156.4^\circ \left[\frac{.8641 - \sqrt{.8641^2 - 4 \times .4272^2}}{2 \times 4272^2} \right]$$

$$= .8603 \angle 156.4^\circ$$

The reflection coefficient of the load impedance required to conjugately match the output of the transistor is

$$R_{ML} = C_2^* \left[\frac{B_2 - \sqrt{B_2 - 4\,|C_2|^2}}{2|C_2|^2} \right]$$

$$= .5142 \angle 33.5^\circ \left[\frac{1.0365 - \sqrt{1.0365^2 - 4 \times .5142^2}}{2 \times .5142^2} \right]$$

$$= .8821 \angle 33.5^\circ$$

On the Smith Chart used unit radius = 8.5 cm, so the source and load reflection coefficients are represented as

R_{MS} = 7.3 cm $\angle 156.4^\circ$ and

R_{ML} = 7.5 cm $\angle 33.5^\circ$ (see figure 30).

5.4.1 The Output Matching Network Of The Second Stage*

Since a 75 ohm load was expected, the R_{ML} must be transformed to 75 $\pm$ jZ ohms or 13.3 $\pm$ jb mS. To do this, the R_{ML} is first converted to its parallel equivalent by adding -180° to its argument.**

i.e. $R_{ML\,1} = 0.8821 \angle (33.5^\circ - 180^\circ)$

$= 0.8821 \angle -146.5^\circ$.

The required parallel admittance is then given by

$$Y_L = \left[\frac{1 + R_{ML\,1}}{1 - R_{ML\,1}} \right] Y_o$$

where Y_o = 13.3 mS.

---

* Sections 5.4.1 - 5.4.4. refer to figure 27

** See ref. (8).

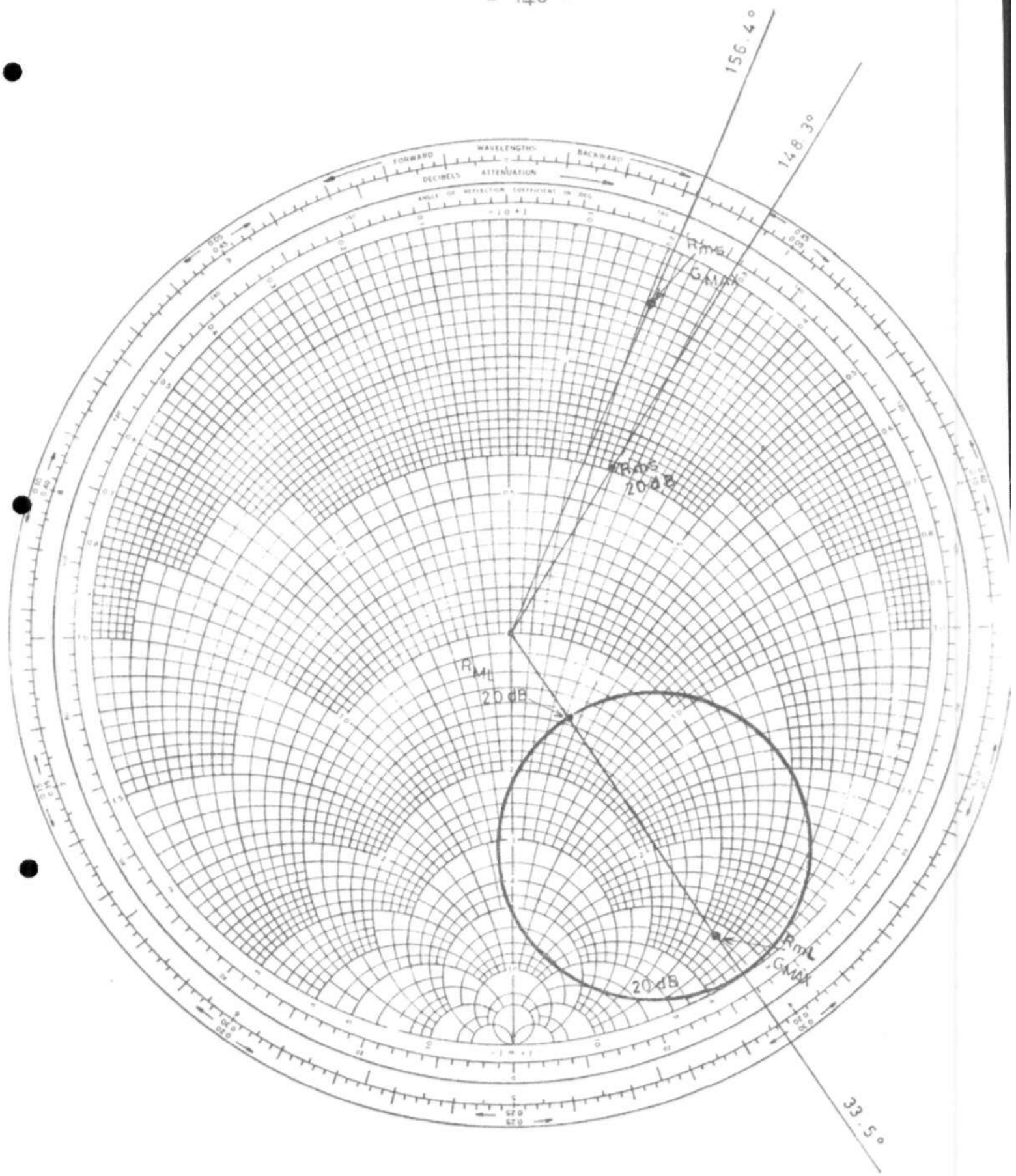


FIG 30 — DETERMINING R_{ms}, R_{mL} AND THE 20 dB GAIN CIRCLE ON A SMITH CHART

$$\text{i.e.} \quad Y_L = \left[\frac{1 + .8821 \angle -146.5^\circ}{1 - .8821 \angle -146.5^\circ} \right] 13.3 \text{ mS}$$

$$= 4.0994 \angle -77.2^\circ \text{ mS}$$

$$= .9106 - j\ 3.9970 \text{ mS}$$

Converting this parallel admittance to impedance yields

$$Z_L = (1098.2 + j\ 250.2) \text{ ohms.}$$

The values of the lumped elements to effect this transformation are given by

$$X_c = \sqrt{(R_p - R_s) R_s}, \quad R_p = R_e (Z_L)$$

$$R_s = 75 \text{ ohms}$$

$$= \sqrt{(1098.2 - 75)\ 75}, \quad X_c \text{ capacitive reactance}$$

$$= 277.02 \text{ ohms}$$

$$\therefore \quad C_2 = \frac{1}{2\pi f X_c}$$

$$= \frac{1}{2\pi \times 200 \times 10^6 \times 277.02}$$

$$= 2.87 \text{ pF},$$

$$X_{L1} = \frac{R_s^2 + X_c^2}{X_c}, \qquad X_L = \text{inductive reactance}$$

$$= \frac{75^2 + 277.02^2}{277.0^2}$$

$$= 297.3 \text{ ohms},$$

So that the total inductive reactance is

$$X_{LT} = \frac{X_{L1} \cdot X_L}{X_{L1} + X_L}, \quad X_L = \text{Imaginary part of } Z_L$$

$$= \frac{297.3 \times 250.2}{297.3 + 250.2}$$

$$= 135.87 \text{ ohms}$$

$$\therefore \quad L_2 = \frac{X_{LT}}{2\pi f}$$

$$= \frac{135.87}{2\pi \times 200 \times 10^6}$$

$$= .108 \ \mu H$$

5.4.2 The Input Matching Network Of The Second Stage

The R_{MS} must be converted to its parallel equivalent so as to match it to the output impedance of the first stage. First, we add -180° to its argument to get

$$R_{MS_1} = .8603 \angle (156.4^\circ - 180^\circ),$$

$$= .8603 \angle -23.6^\circ,$$

so that the parallel admittance is

$$Y_s = \left[\frac{1 + R_{MS_1}}{1 - R_{MS_1}}\right] Y_o, \quad Y_o = 13.3 \text{ mS}$$

$$= \left[\frac{1 + .8603 \angle -23.6^\circ}{1 + .8603 \angle -23.6^\circ}\right] 13.3 \text{ mS}$$

$$= 59.99 \angle -69.4^{\circ} \text{ mS}$$

$$= 21.156 - j\ 56.136 \text{ mS}$$

and the parallel impedance is

$$Z_s = 47.267 + j\ 17.81 \text{ ohms}$$

This completes the a.c. circuit design of the second stage which is shown in figure 31.

The first stage is designed for a gain of 20 dB using the same S-parameters. The design is as follows:

$$G_p = 100 \quad \text{(i.e. numeric value of 20 dB)}$$

$$G_o = |S_{21}|^2$$

$$= 8.057^2$$

$$= 64.9153$$

$$\therefore \quad G = \frac{G_p}{G_o}$$

$$= \frac{100}{64.9153}$$

$$= 1.5405$$

The centre of the 20 dB gain circle is

$$r_{02} = \left[\frac{G}{1 + D_2\ G}\right] C_2^*$$

$$= \frac{1.5405}{1 + .1817 \times 1.5405} \times .5142 \angle 33.52^{\circ}$$

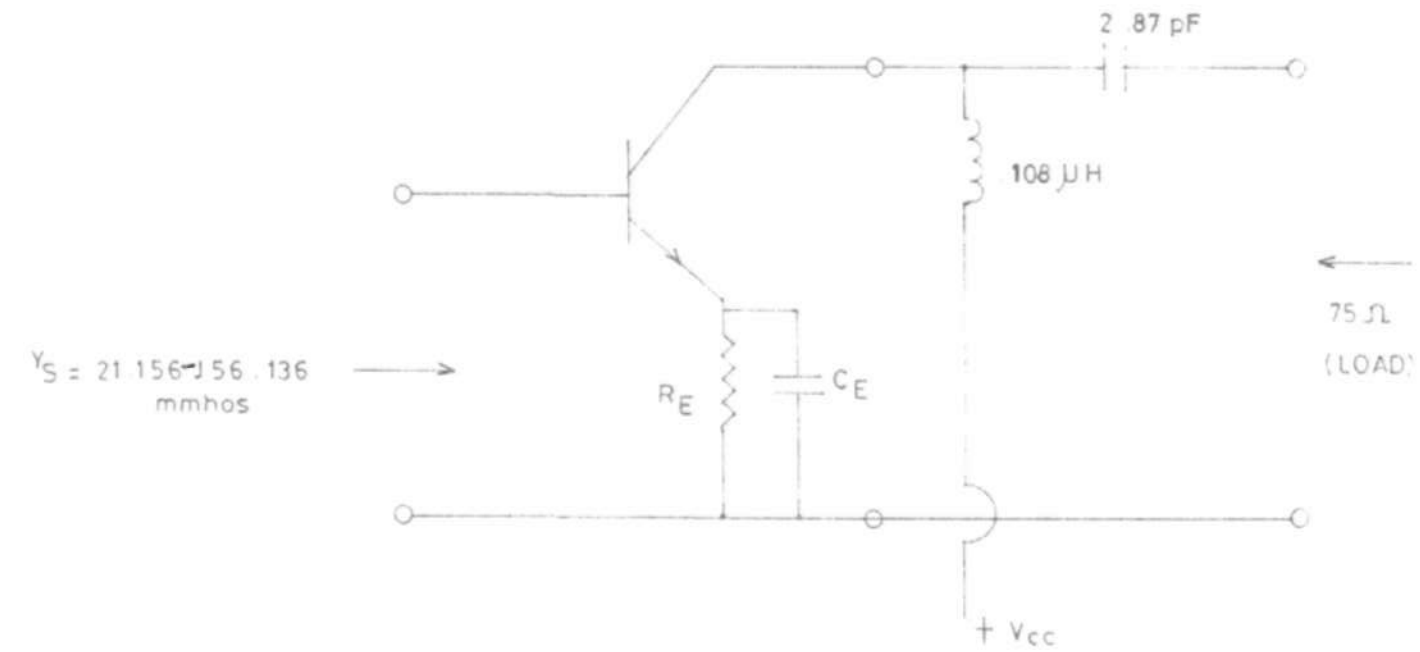


FIG 31 (A). A.C. CIRCUIT OF SECOND STAGE SHOWING THE OUTPUT MATCHING NETWORK

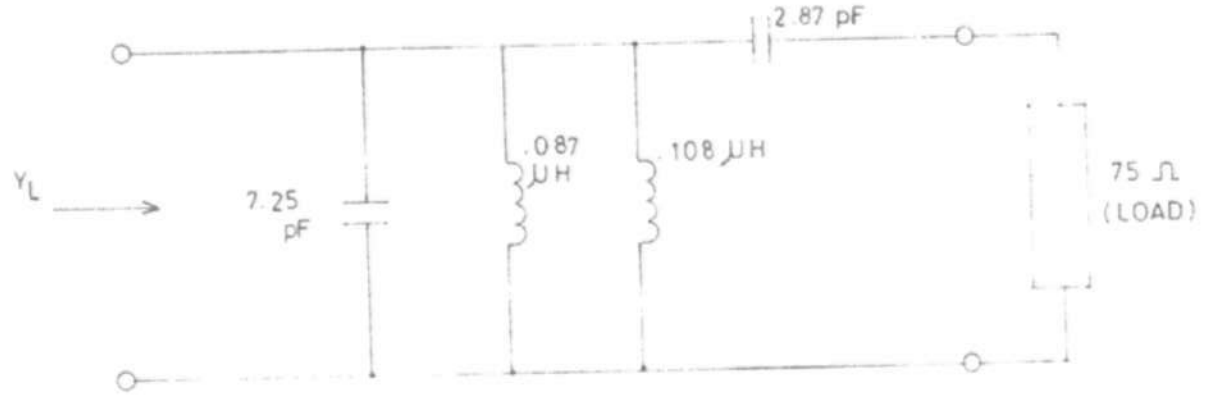


FIG. 31(B). OUTPUT NETWORK OF SECOND STAGE WITH TURING COMPONENTS.

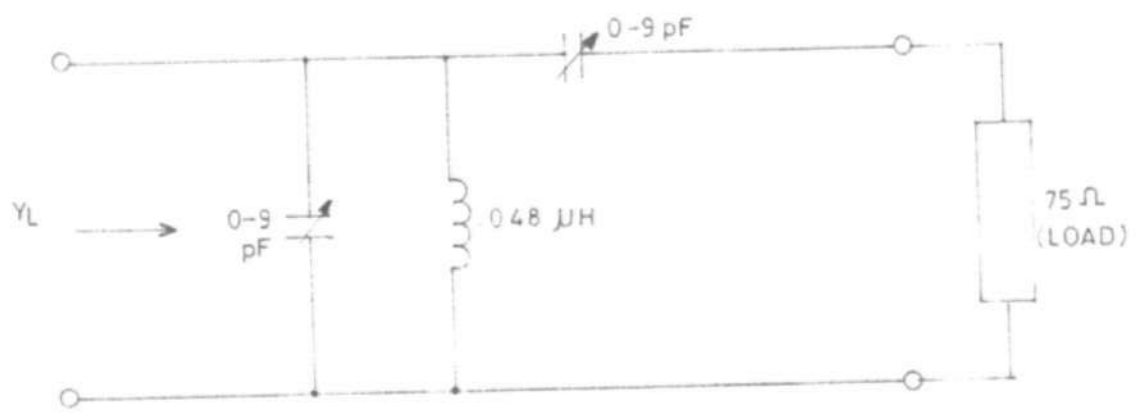


FIG 31(C) FINAL OUTPUT CIRCUIT FOR SECOND STAGE.

$$= \frac{1.5405}{1.2799} \times .5142 \angle 33.52^{\circ}$$

$$= 1.2036 \times .5142 \angle 33.52^{\circ}$$

$$= .6189 \angle 33.52^{\circ}$$

(i.e. 5.3 cm $\angle 33.5^{\circ}$ on the Smith Chart used)

The radius of the gain circle is

$$R_{02} = \frac{(1 - 2K|S_{12}\,S_{21}|\,G + |S_{12}\,S_{21}|^2\,G^2)}{1 + D_2\,G}$$

$$= \frac{(1 - 2 \times 1.0189 \times .33034 \times 1.5405 + .33034^2 \times 1.5405^2)^{\frac{1}{2}}}{1 + .1817 \times 1.5405}$$

$$= \frac{(1 - 1.0370 + .2589)^{\frac{1}{2}}}{1.2799}$$

$$= .3681$$

i.e. 3.13 cm on the Smith Chart used (see figure 30)

The R_{ML} chosen on the gain circle is

$R_{ML} = .2506 \angle 33.5^{\circ}$ i.e. 2.13 cm $\angle 33.5^{\circ}$ on the Smith Chart (figure 30), because this gives a suitable value of the source reflection coefficient.

The source reflection coefficient required with the chosen load is

$$R_{MS} = \left[\frac{S_{11} - R_{ML}\Delta}{1 - R_{ML}\,S_{22}}\right]^*$$

$$= \left[\frac{.381 \angle -142.6^\circ - .2506 \times .2229 \angle (33.5^\circ - 58.65^\circ)}{1 - .2506 \times .481 \angle (33.5^\circ - 24.5^\circ)} \right]^*$$

$$= \left[\frac{(-.3027 - j.2314) - (.0506 - j.0237)}{1 - (.1191 + j.0188)} \right]^*$$

$$= \left[\frac{.4098 \angle -149.55^\circ}{.8812 \angle -1.23^\circ} \right]^*$$

$$= .465 \angle -148.32^\circ$$

5.4.3 The Input Matching Of The First Stage:

The optimum input impedance of the stage is calculated as in the previous case, thus* :

$$R_{MS_1} = .465 \angle (148.3 - 180^\circ)$$

$$= .465 \angle -31.7^\circ$$

$$\therefore Y_s = \left[\frac{1 + R_{MS_1}}{1 - R_{MS_1}} \right] Y_o, \quad Y_o = 13.33$$

$$= \left[\frac{1 + .465 \angle -31.7^\circ}{1 - .465 \angle -31.7^\circ} \right] 13.3 \text{ mS}$$

$$= \left[\frac{1 + (.3956 - j.2443)}{1 - (.3956 - j.2443)} \right] 13.3 \text{ mS}$$

$$= \left[\frac{1.4169 \angle -9.93^\circ}{.6519 \angle 22^\circ} \right] 13.3 \text{ mS}$$

$$= 28.97 \angle -31^\circ$$

---

* See p.148

$= 24.83 - j\ 14.92$ mS , and

the parallel equivalent of this input impedance is

40.27 + j 67.02 ohms.

This impedance will be in parallel with the equivalent parallel resistance of 300 Ω , at the base*, for d.c. bias; so that the effective input impedance is modified to 30.2 + j 67 ohms, and this must be transformed to the source impedance of $75 \pm jX$ (where X is negligibly small) for maximum power transfer between the source and the first stage.

From the transformation chart of figure 32 the required series and shunt reactances to effect the transformation are

$$X_{C_1} = 50 \text{ ohms} \quad \text{(for the capacitive reactance)}$$

and

$$X_{L_1} = 57.0 \text{ ohms (for the inductive reactance)}$$

The corresponding values for the lumped components are thus given as

$$C = \frac{1}{2\pi \times 200 \times 10^6 \times 50.6}$$

$$= 15.7 \text{ pF},$$

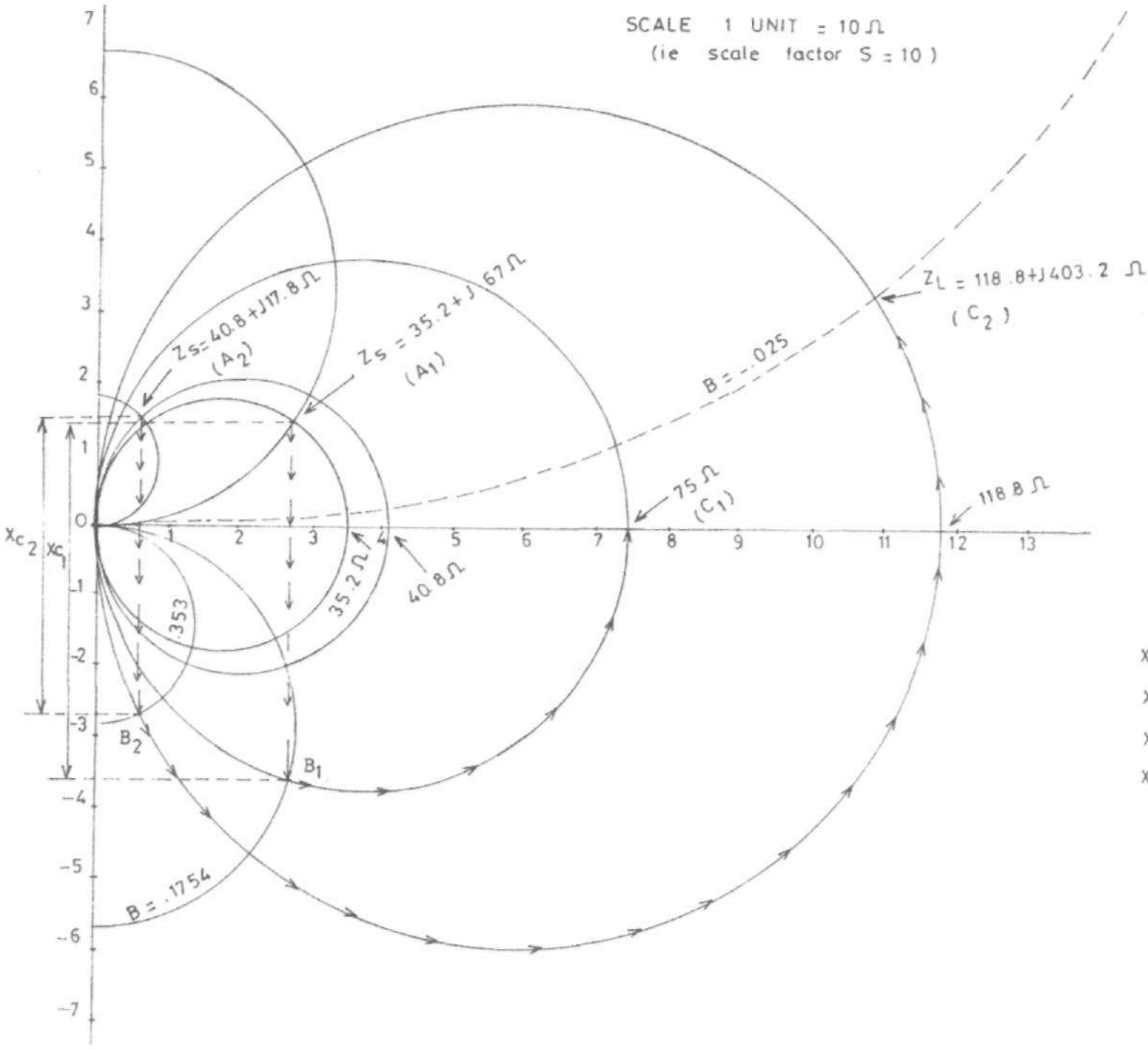
and

$$L = \frac{57.0}{2\pi \times 200 \times 10^6}$$

$$= .045 \ \mu\text{H}, \quad \text{as shown in figure 32 (a) .}$$

---

* See Section 5.5, p.162



X_{C_2} = 41.6 Ω

X_{L_2} = 26.5 Ω

X_{C_1} = (-36)-(14.6) = -50.6 Ω

$X_{L_1} = \frac{10}{(.1754 - 0)} = 57$ Ω

FIG. 32 GRAPHICAL IMPEDANCE MATCHING BETWEEN SOURCE AND INPUT OF FIRST STAGE (A_1--C_1) AND THE INTER-STAGE COUPLING (A_2-C_2)

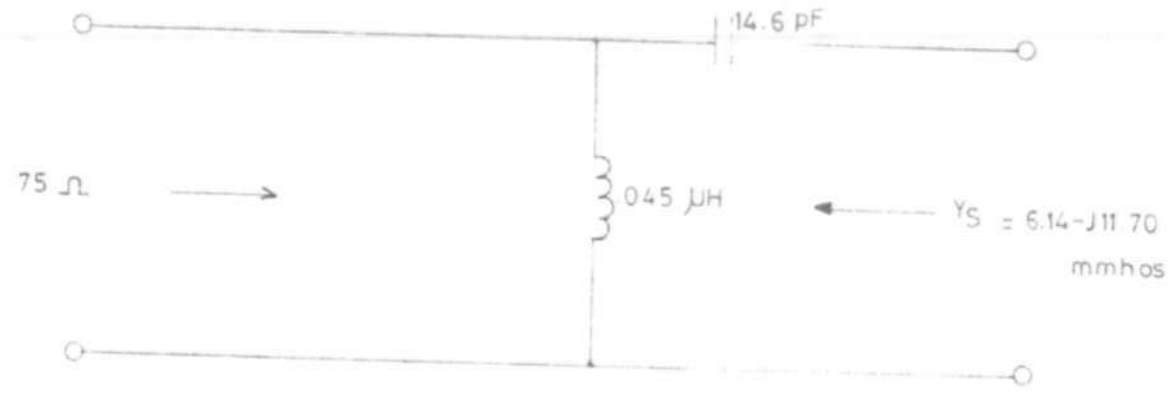


FIG. 33 (A). MATCHING NETWORK FOR INPUT OF FIRST STAGE.

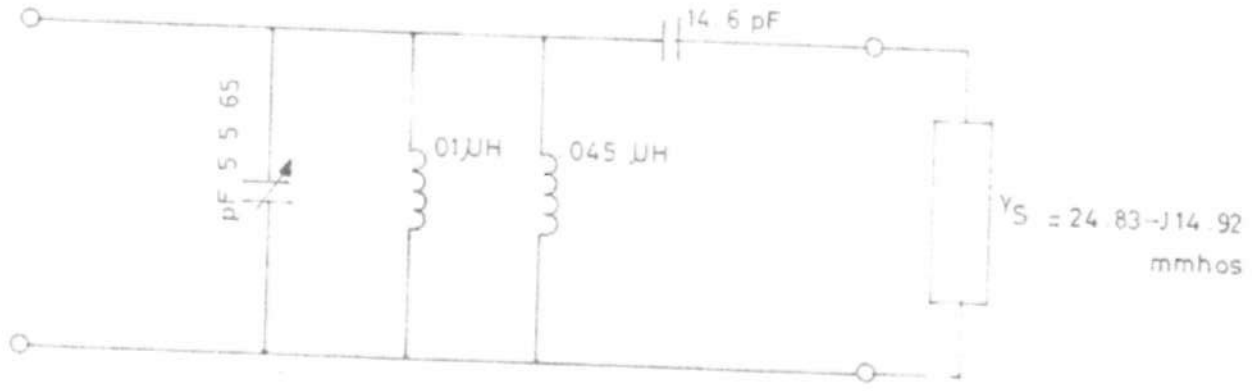


FIG. 33 (B). FIRST STAGE INPUT WITH 192 MHz FILTER.

5.4.4 The Inter-stage Coupling Network

The optimum output impedance must be transformed to its parallel equivalent, thus*

$$R_{ML} = .2506 \angle 33.5^\circ$$

$$R_{ML_1} = .2506 \angle (33.5 - 180)^\circ$$

$$= .2506 \angle -146.5^\circ$$

The parallel admittance is therefore

$$Y_L = \left[\frac{1 + .2506 \angle -146.5^\circ}{1 - .2506 \angle -146.5^\circ} \right] 13.3 \text{ mS}$$

$$= \left[\frac{1 + (.2089 - j.1383}{1 - (-.2089 - j.1383)} \right] 13.3 \text{ mS}$$

$$= \left[\frac{.7911 - j.1383}{1.2089 + .1383} \right] 13.3 \text{ mS}$$

$$= 8.778 \angle -16.4^\circ$$

$$= 8.419 - j\ 2.484 \text{ mS}$$

$$Z_L = 118.8 + j\ 403.2) \text{ ohms}$$

Coupling the first stage to the second demands that this output impedance (of the first stage) be matched with the input impedance of the second stage**. Again the input impedance of the second stage is modified by the 300 ohm effective shunt resistance at the base for d.c.

---

* See section 5.4.1

** See section 5.4.2

bias (see section 5.5); so that the effective input resistance of second stage is (40.8 + j 17.8) ohms. This impedance must then be transformed to (118.8 + j 403.3) ohms. From the transformation chart of figure 32 it is seen that the required reactances are

$$X_{C_2} = 41.6 \text{ ohms} \quad \text{and} \quad X_{L_2} = 26.5 \text{ ohms}.$$

The values of the lumped components are therefore

$$C = \frac{1}{2\pi \times 200 \times 10^6 \times 41.6}$$

$$= 19.0 \text{ pF}, \quad \text{and}$$

$$L = \frac{26.5}{2\pi \times 200 \times 10^6}$$

$$= .021 \ \mu\text{H}, \quad \text{as shown in figure 34.}$$

5.4.5 Tuning The Output And Input Networks

The output network of the second stage is tuned to resonate at 200 MHz centre frequency (see section 5.4.1). If a fractional bandwidth of 0.1 is chosen - i.e. 20 MHz, the output loaded Q should be

$$Q_L = \frac{200}{20}$$

$$= 10$$

But $Q_L = R'_p \ W C$ 5.33

where $W = 2\pi f$,

C = required parallel capacitance

R'_p = total effective parallel equivalent resistance

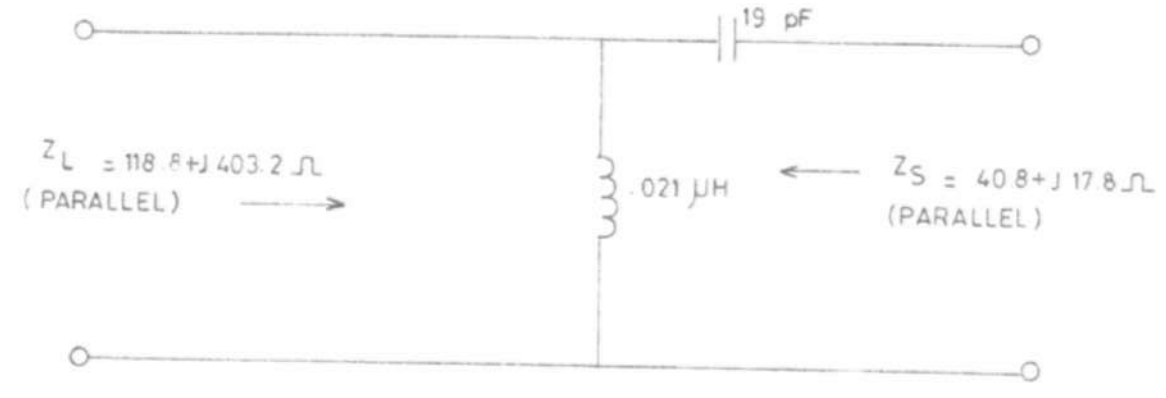


FIG. 34. THEORETICAL DESIGN OF INTER-STAGE COUPLING NETWORK.

of loaded tank circuit, as opposed to R_p which is the parallel equivalent resistance of the unloaded tank on its own.

Therefore,

$$10 = 1098.2 \times 2\pi \times 200 \times 10^6 \times C$$

$$C = \frac{10}{1098.2 \times 400 \times \pi \times 10^6}$$

$$= 7.25 \text{ pF}$$

The inductance required to resonate with this capacitance is given by

$$L = \frac{1}{W^2 C}$$

$$= \frac{1}{(400\pi \times 10^6)^2 \times 7.25 \times 10^{-12}}$$

$$= \frac{1}{16\pi^2 \times 10^{16} \times 7.25 \times 10^{-12}}$$

$$= .0873 \ \mu H$$

The output network of the second stage is then as shown in figure 31(B).

The two parallel inductances in figure 31 (B) may be combined into an equivalent L_T, thus

$$L_T = \left(\frac{.0873 \times .108}{.0873 + .108}\right) \mu H$$

$$= .0483 \ \mu H$$

Accordingly, the output circuit is modified as shown in figure 31 (C), with the 7.25 pF capacitor replaced with a variable type for fine tuning and to take care of any effects of the .108 μH inductor on the tuning of the tank circuit. The 2.87 pF capacitor is also replaced with a variable capacitor to allow for impedance matching **fine** adjustments.

5.4.6 Input Filter For First Stage

A filter circuit may also be inserted at the input circuit of the first stage so that frequencies other than the required 200 MHz are, as much as possible, rejected; and choosing a convenient inductance as .01 μH, the capacitor required for resonance at 200 MHz is 63 pF, A variable capacitor with range 5.5 - 65 pF makes it possible to shift the centre frequency to other close values like 192 MHz which is the actual frequency of NTV Jos signals for which the amplifier is designed. For the purpose of construction convenience the two parallel inductors have not been combined in one, as in the output circuit of second stage in figure 31 (C). The modified input network for first stage is shown in figure 33 (B).

5.5 The D.C. Bias

For stability of the operating point, the transistors must be properly biased. Each transistor has been biased to ensure the conditions under which the S-parameters were determined, i.e. I_C = 20 mA, and V_{CE} = 10 V.

Let potential drop across the emitter be 3V. The value of the emitter resistor would therefore be

$$R_E = \frac{3}{20 \times 10^{-3}} \quad , \quad \text{since} \quad I_c \simeq I_E$$

$$= 150 \text{ ohms}$$

To ensure stability the condition

$$R_B < (\beta_o + 1) \ R_E / 10 \quad \text{must be satisfied.}$$

Where R_B is the equivalent resistance between the base and to a.c. ground (as seen by signal towards the base) due to the presence of R_{B_1} and R_{B_2} in figure 35.

Since the minimum current gain (β_o) under the bias conditions is 20 (see table 5.1) the above inequality becomes

$$R_B \quad (20 + 1) \times \frac{150}{10} \quad \text{ohms}$$

$$21 \times \frac{150}{10} \quad \text{ohms}$$

$$315 \quad \text{ohms}$$

Choose $R_B = 300$ ohms

The voltage across R_B may be given by

$$V_T = V_{BE} + R_E + (\beta_o + 1) R_E \ \frac{I_c}{\beta_o}$$

$$= .7 + 300 + 21 \times 150 \ \frac{20 \times 10^{-3}}{20}$$

$$= 4.15 \text{ volts.}$$

TABLE 5.1

SOME OF THE TRANSISTOR DATA *

PARAMETER	CONDITION OF MEASUREMENT	VALUE
Noise Figure	V_{CE} = 10V, I_c = mA, 200 MHz	$\leq$ 2 dB
Gain, $\left\|S_{21E}\right\|^2$ (G)	V_{CE} = 10V, I_c = 20 mt, $100 \leq f \leq 450$ MHz	$12.5 \leq G \leq 25$ dB
Power Output (P_{out}) at 1 dB compression point	V_{CE} = 10V, I_c = 20 mt, $R_G = R_L$ = 50 ohms	$+ 5.2 \leq P_{out} \leq + 5.4$ dB
Power Dissipation (P_D)	Case Temp. $T_c \leq 25^\circ C$ $25 \leq T \leq 200^\circ C$	P_D = 450 mW P_D = 250 mW per $100^\circ C$
Maximum V_{CBO}	----	20 V
Maximum V_{EBO}	----	3 V
Maximum I_c	----	125 mA
Maximum Junction Temp.	----	$200^\circ C$
Maximum Lead Temp.	Soldering time $\leq$ 10 seconds	$250^\circ C$
I_{CBO}	V_{CB} = 10 V	10 nA
h_{FE}	V_{CE} = 10 V, I_c = 5 mA	Minimum = 20 Maximum = 300
Output Capacitence	V_{CB} = 15 V.	1.3 pF

* See also section 5.4

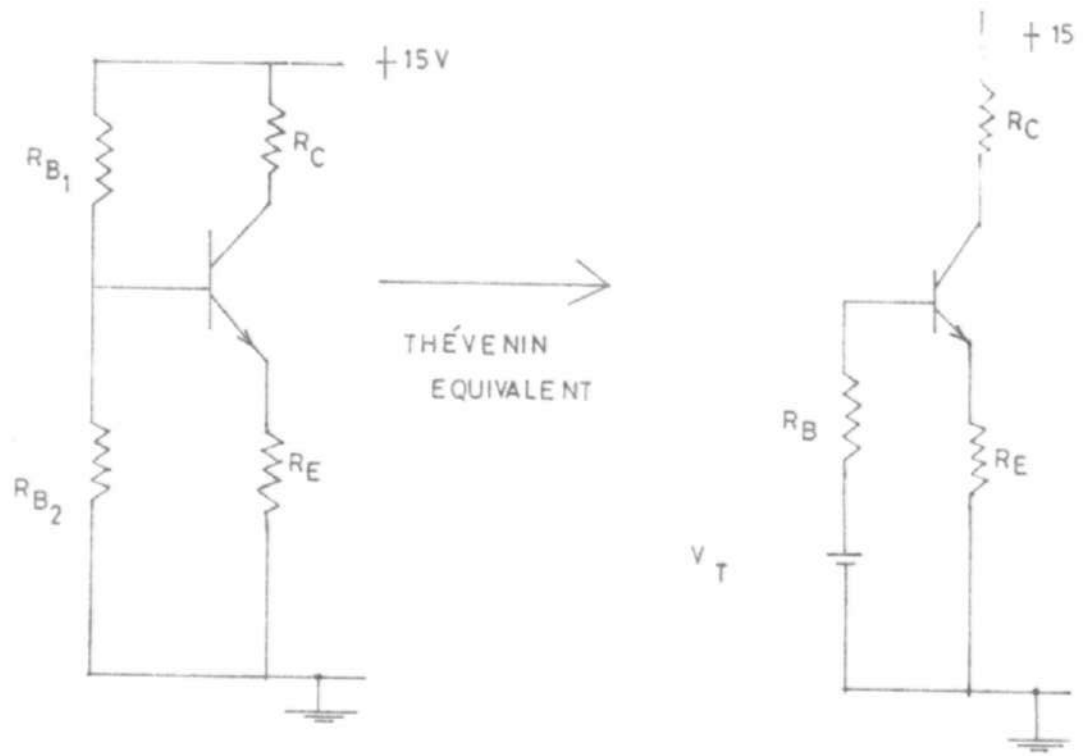


FIG. 35. THE D.C. CIRCUIT AND IT'S THÉVENIN EQUIVALENT.

The value of R_{B_1} can be determined from

$$R_{B_1} = \frac{V_{cc}\, R_B}{V_T}$$

$$= \frac{15 \times 300}{4.15}, \quad \text{for } V_{cc} = +15\,V.$$

$$= 1.08 \text{ K ohms},$$

Also,

$$R_{B2} = \frac{R_B \times R_{B_1}}{R_{B_1} - R_B}$$

$$= \frac{300 \times 1084.34}{1084.34 - 300}$$

$$= 414.75 \text{ ohms}$$

If the supply voltage is $V_{cc} = 15\,V$, the voltage drop across R_c would be

$$V_{RC} = V_{cc} - V_{CE} - V_{RE}$$

$$= 15 - 10 - 3$$

$$= 2 \text{ volts.}$$

$$\therefore R_c = \frac{2}{20 \times 10^{-3}}$$

$$= 100 \text{ ohms}$$

Using standard values, the resistors would then be

R_E = 150 ohms

R_C = 100 ohms

R_{B_1} = 1100 ohms

R_{B_2} = 430 ohms

(see appendix D.1)

The emitter by-pass capacitance may be determined from

$$C_E = \frac{10}{2\pi \times 200 \times 10^6 \times 150}$$

$$= 53 \text{ pF.}$$

Thus the a.c. circuit of the amplifier is as shown in figure 36; the additional 1000 pF capacitors serve as d.c. block, emitter by-pass or to prevent signal entering the power supply. The complete amplifier circuit will therefore be as shown in figure 37.

5.6 The Construction

The physical realization of figure 36 as a working circuit was compounded by the challenges due to the high frequency of operation (200 MHz). These include radiative losses and radiative coupling between close circuit parts which become increasingly important at high frequencies - hence the need for shielding some parts from others. Capacitances are usually of small values in the pico farad range, and inductances are in fractions of a micro henry. This makes self-capacitance and self-inductance of components important,

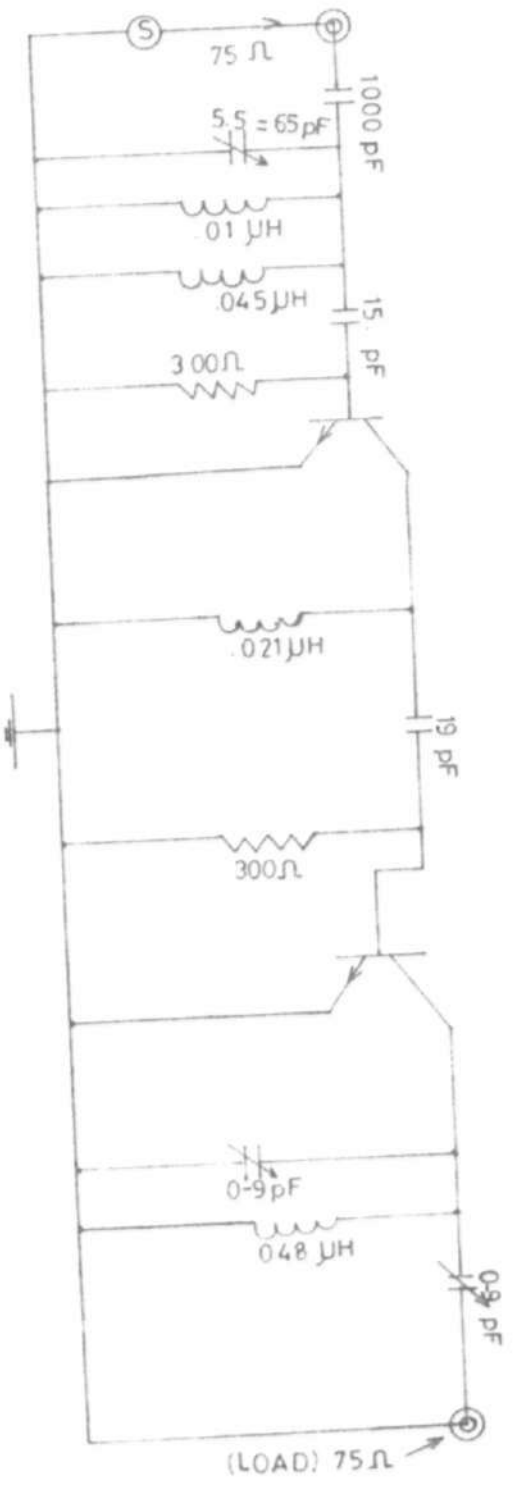


FIG. 36 THE A.C. EQUIVALENT CIRCUIT

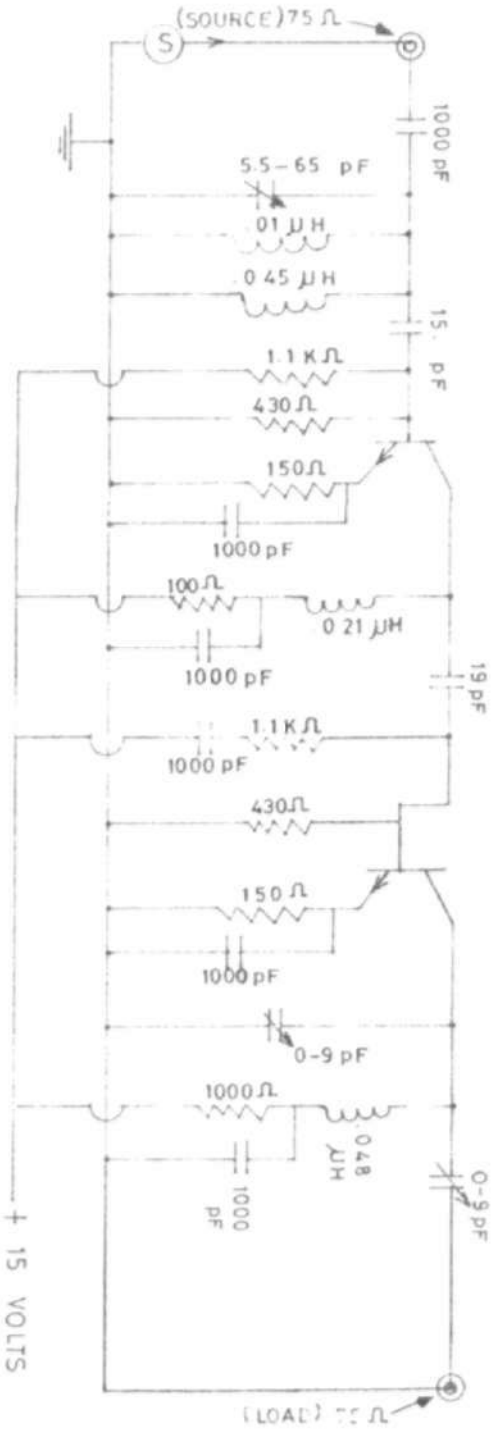


FIG 37. THE COMPLETE COAXIAL CABLE. CIRCUIT. BOTH INPUT AND OUTPUT ARE IN

and a circuit board can introduce as much as 3 pF on its own into the circuit. Because of these and other effects, special attention is given to both the choice of components and the manner in which these are connected up, so as to obtain improved amplifier performance.

5.6.1 Designing V.H.F. Inductors

Inductors are components often used in a.c. circuits to provide a required inductive reactance or a high a.c. impedance d.c. path in a circuit.

Designing inductors for use as a reactance source (as is the case with the present circuit) becomes increasingly difficult at higher frequencies since the reactance is proportional to frequency ($X_L = 2\pi f L$, L = inductance). The designer is therefore faced with the problems of dealing with smaller physical sizes of inductors at higher frequencies - and at V.H.F. and above, a strip of conductor can constitute an inductor, having inductance per unit length as in transmission lines.

The inductance of an inductor may be given by

$$L = \frac{r^2 n^2}{9r + 10h} \text{ micro henries} \quad \ldots \quad 5.34\ (1)$$

where

r = radius of coil

n = number of turns of coil

h = length of coil.

However, in the present exercise, designs based on equation 5.34 proved unsatisfactory, so that direct measurements of L and Q_u were made after winding a large set of inductors of different shapes and sizes. Table 5.2 shows a list of inductors wound as 34 trial examples under this arrangement. The instruments used for measuring the inductances were a Marconi Oscillator type TF 1247 covering a range of 20 - 300 MHz, and a Marconi Circuit Magnification Meter type TF 1247 A . These were coupled through a TM 5725 connector provided by the manufacturers of the instruments for this purpose. From the table (5.2), two points, apart from those obvious from equation 5.34 are discernible:

1. L decreases with increase in standard wire gauge (S.W.G.),
2. Q_u increases with the amount of coil material - i.e. increase in number of turns, diameter or length.

Both of these properties were exploited to design coils used in this circuit with minimum number of turns ($n \leq 2$) so as to reduce I^2R losses, winding capacitance (and associated power losses) as well as radiation losses and interference due to inductive coupling,
Also hysterises losses and eddy current losses due to iron were checked by leaving the inductors completely air-cored.

At the operating frequency range choice of coil configuration is also dictated by the requirement that

TABLE 5.2

SOME TRIAL INDUCTORS AND THEIR SPECIFICATIONS

S.W.G.	INDUCTANCE (uH)	Q_u	EXTERNAL DIAMETER (mm)	No. of TURNS	EXTENSION (mm)
23	.015	75	4.5	$\frac{2}{5}$	-
"	.021	120	9.2	$\frac{2}{5}$	-
"	.029	155	3.0	$1\frac{2}{5}$	10.9
"	.036	130	2.8	$1\frac{2}{5}$	1.8
20	.012	100	10.0	3/5	4.0
"	.013	76	3.7	$\frac{2}{5}$	
"	.014	100	5.9	3/5	
"	.019	140	10.0	$\frac{3}{4}$	
"	.023	160	4.0	$1\frac{1}{2}$	10.0
"	.030	120	3.5	$2\frac{1}{2}$	9.5
"	.032	150	3.5	$3\frac{1}{2}$	7.1
"	.032	160	9.2	3/5	11.5
"	.039	135	3.4	$4\frac{1}{2}$	7.7
"	.051	75	9.0	1.0	3.8
"	.051	100	9.4	2.0	5.5
"	.063	170	9.4	$1\frac{1}{2}$	10.0
"	.067	190	10.0	$1\frac{1}{2}$	10.0
16	.012	80	8.8	3/5	-
"	.012	110	5.9	$\frac{1}{2}$	1.3
"	.012	140	10.7	$\frac{1}{2}$	2.3
"	.015	140	10.6	$\frac{1}{2}$	-
"	.015	125	10.9	$\frac{3}{4}$	-
"	.015	150	6.7	1	5.7
"	.017	120	11.4	1	-
"	.018	140	6.5	1	7.0
"	.022	160	12.5	1	5.0
"	.024	160	9.2	1	7.5
"	.025	170	9.0	1	14.2
"	.028	160	9.4	1	6.4
"	.029	220	6.5	1	12.5
"	.033	210	9.0	$1\frac{1}{2}$	3.1
"	.036	245	22.1	$\frac{3}{4}$	-
"	.056	200	17.0	1	11.5
"	.058	230	11.1	2	13.3

the coil fits into the circuit board with no (or negligible lengths of) additional connecting leads, as these constitute inductors themselves in the V.H.F. range (and above) as already indicated in Section 5.6. This poses some challenge because the smaller the inductor size the more the effect of any additional leads on its inductance, and yet the greater the need for such extra leads to physically connect the inductor to the circuit. The alternative of trimming the ends of the inductor to make it fit into the openings on the circuit board has been used here since the effect of this is more on the Q_u than on the inductance of the coil (see 1 and 2 above).

5.6.2 Choice of Components and Assemblage

The other components used were chosen with preference to small-sized ones with satisfactory power and voltage ratings. It was found that the amplifier performed best with ceramic capacitors, so all capacitors, except the variable ones, were ceramic. A list of the components and their specifications is given in Appendix D.

Components were connected on a perforated stripless board. The use of veroboard with parallel copper strips was avoided because such arrangement would amount to parallel transmission lines (at the high frequency of operation) with the attendant power losses and unwanted resonances due to inductance and capacitance per unit length of the copper strips. The amplifier was housed in an alluminium box of dimension 10.8 cm x 6.3 cm x 2.8 cm. (see Plate I).

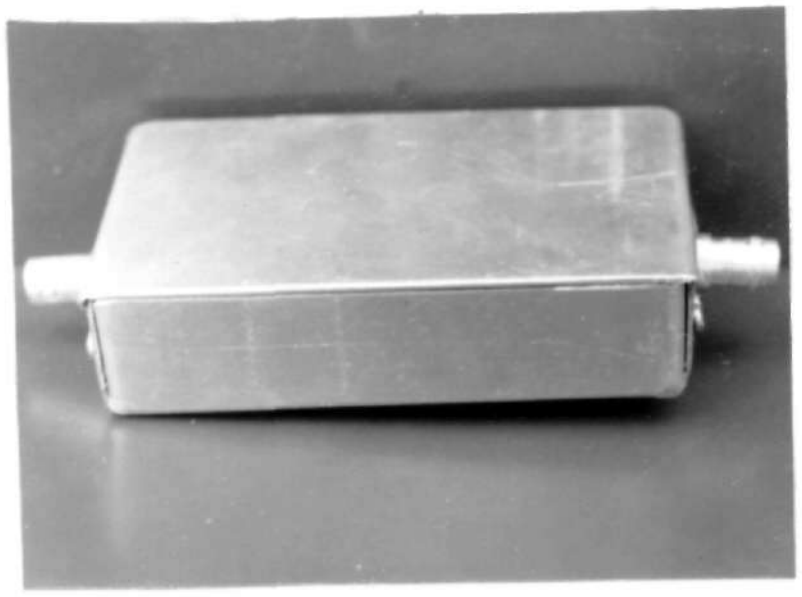


Plate I (A): Amplifier External View

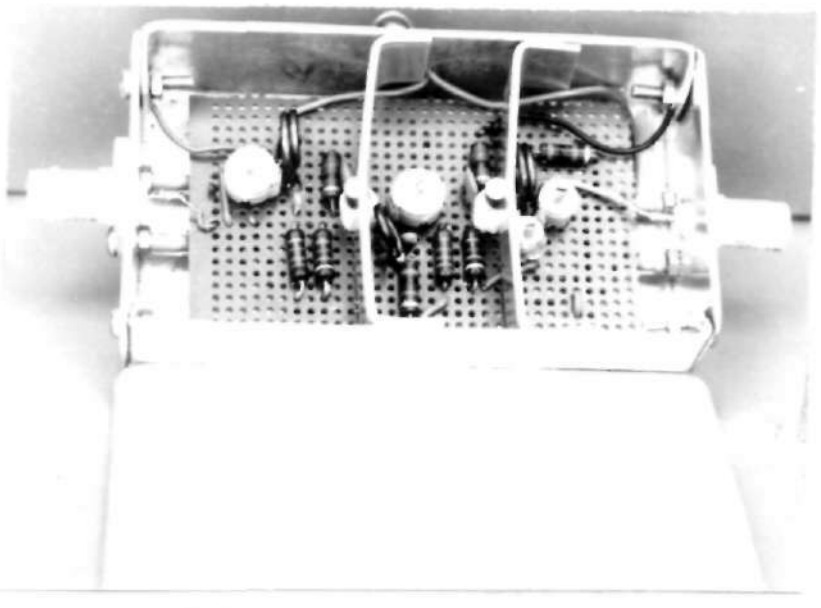


Plate I (B): Amplifier Internal View

In the box, each transistor was mounted on a socket, and the input/output sections were shielded with alluminium plates to minimize radiation losses and any interference from inductive coupling. Also each transistor casing was earthed through the appropriate transistor lead.

5.7 Testing The Amplifier

The amplifier was tested with the following equipment:

1. A Hewlett Packard D.C. Power Supply. type hp 6101 A (Serial Number: 1137 A 01211); with a voltage range of 0 - 24 V .

2. A Hewlett Packard Oscilloscope, type hp 1740 A ; (Serial Number: 1616A, 01980) with a sweep range of 0 - 100 MHz, and an input impedance of 50.

3. A Marconi AM/FM Signal Generator, type TF 2015, (Serial Number: 116908/021) with a frequency range of 10 - 520 MHz; it also has provision for internal modulation, attenuation and varying the modulation depth.

4. Hewlett Packard Crystal Detector, Model 423A (NEG). (Serial Number: 17455 B).

5. A Multitester.

5.7.1 The D.C. Measurements

The multitester was used to monitor current drains and voltage drops across the individual circuit elements.

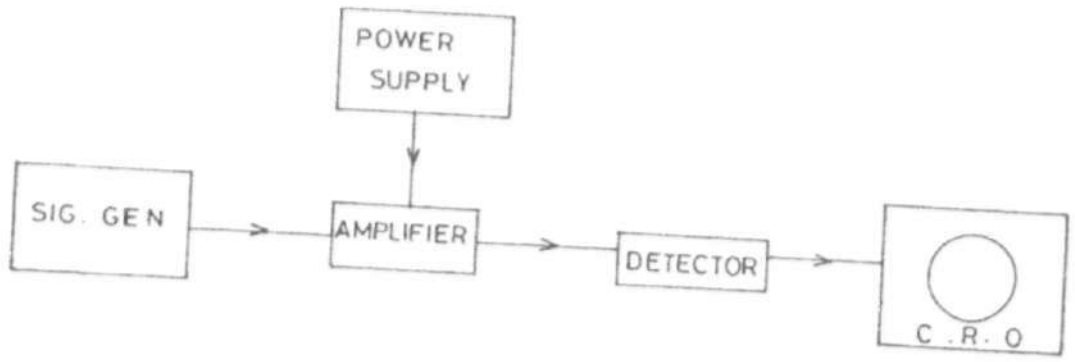


FIG. 38. BLOCK DIAGRAM OF TEST EQUIPMENT SET-UP.

Results of these measurements show that the amplifier turns on around 4 V and reaches maximum output around 12V. Hence, although the design supply voltage is 15 V, voltages over and above 12V may be redundant as well as encourage junction breakdown in the transistors. However, at a supply of 15V, all measured current drain and voltage drops are either exactly the same or very close to their design values. The test-instrument set-up is illustrated in figure 38.

The amplifier can therefore be supplied by a 12 volts d.c. source rather than 15volts.

5.7.2 Frequency Response

The frequency response of the amplifier was initially measured in three stages. The first set of measurements were made without the input tank in the circuit; and then after the input filter has been duely inserted in the circuit. Still with the filter in the circuit a third set of measurements were made to test the transient response.

Since the frequency range of the oscilloscope used does not go beyond 100 MHz, the method of measurement adapted was to modulate the signal generated at the desired frequency by the signal generator (with the generator's internal modulator) and feed the modulated signal into the amplifier. The amplified modulated signal is then fed into the crystal detector; from which only the modulating signal

comes out as the output. This amplified output is then fed into the oscilloscope for measurement (see fig. 38). The initial unamplified input to the amplifier is then measured by coupling the signal generator output directly to the oscilloscope through the crystal detector. All the measurements were made with a constant power output level (< 1 m W) and modulation depth ($< 80\%$) from the generator at intervals of 5 MHz of frequency. The effect of transient response was tested by repeating the measurements starting with the 192 MHz and after the amplifier has been left for long to cool down. In all three cases attempt was made to tune the amplifier to 192 MHz instead of the 200 MHz on which the design was originally based, before the measurements were made.

The numerical results of the measurements are contained in table 5.3 , while the graphical plots are shown in figure 39. The graph of the first set of measurements (without the input tank circuit) can be seen to have two peaks - a low frequency peak at 155 MHz and a higher frequency peak at 198 MHz - suggesting phase shifts at these frequencies. Between these peaks the minimum gain is 18.7 dB and occurs at 170 MHz. The maximum gain of 25 dB occurs at the high frequency peak which extends between 196 MHz and 200 MHz. The second response curve (with the input filter inserted) shows that the insertion of the input filter circuit eliminates the low frequency peak and has an increase in gain of 2.4 - 8.4 dB between 160 and 195 MHz respectively, with a corresponding

TABLE 5.3

AMPLIFIER FREQUENCY RESPONSE

Frequency (MHz)	Voltage Gain (dB)		
	Without i/p Filter Circuit	With i/p Filter Circuit	
		Normal Response	Transient Response
140	5.1	-	-
145	16.2	5.3	3.0
150	19.5	12.5	9.5
155	20.1	18.5	14.6
160	19.5	21.8	18.0
165	18.8	22.9	21.0
170	18.8	23.8	22.0
175	19.5	24.5	23.5
180	20.1	26.0	26.0
185	21.5	27.8	28.6
190	23.0	30.7	32.2
195	24.7	33.3	35.0
196	24.9	33.0	37.0
197	24.9	33.0	37.0
198	24.9	32.2	34.5
200	24.9	28.2	31.0
205	22.7	18.5	27.0
210	21.0	9.5	7.5
215	19.5	0	-
220	17.2	-	-
225	15.0	-	-
230	13.2	-	-
255	11.0	-	-

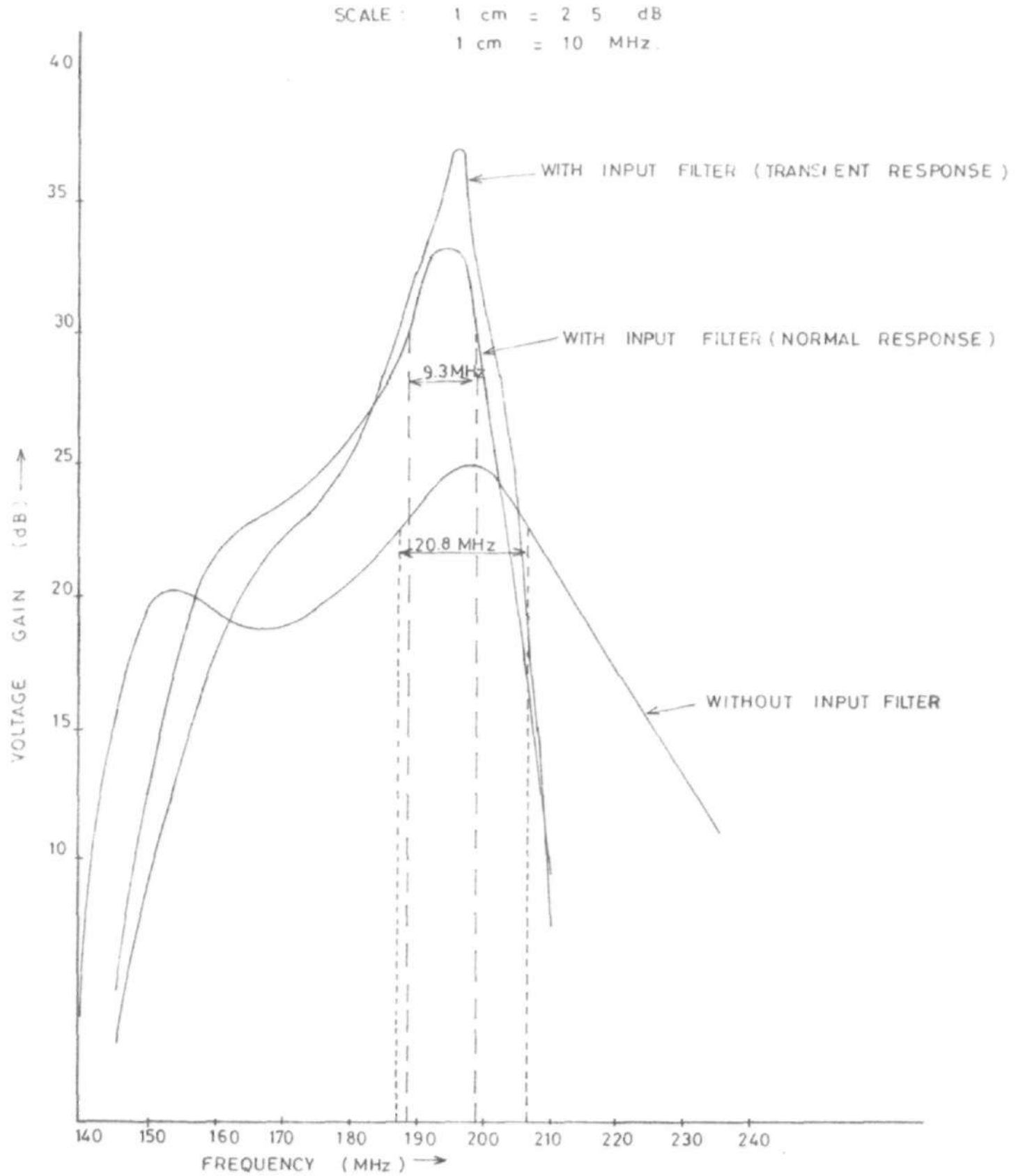


FIG. 39. AMPLIFIER FREQUENCY RESPONSE.

reduction of bandwith. The resonant frequency is 195 MHz, with a gain of 33.3 dB. The third graph shows that the effect of transient overshoot can cause as much as 3.7 dB overshoot above the 33.3 dB peak gain. Also the fact that the amplifier turns on at about 4V d.c. bias (with a gain of up to 25 dB) and reaches a maximum gain at 12V is evidence of good dynamic range.

5.7.3 Stability And Other Performance Consideration

The amplifier is highly stable and this agrees with the design prediction that the amplifier would be unconditionally stable, given that the stability factor K is greater than 1, and S_{11}, S_{22} are both less than 1.

The peaking around the resonant frequency of 195 MHz has a bandwidth of 9.3 MHz which is more than 7.75 MHz required for the video sideband signals. However, on a carrier frequency of 192 MHz the expected gain will go down to 29.5 dB to accommodate this bandwidth. Also the corresponding peak on the curve without input filter circuit has a bandwidth of 20.8 MHz which compares well with the design value of 20 MHz. The overall amplifier noise level is sufficiently low (as guaranteed by the transistor specifications). This was roughly estimated by amplifying the lowest signal level possible from the source (with an extra 10 dB attenuation) for which there was no noticeable distortions of the amplifier output displayed on the oscilloscope.

Although a total gain of 42 dB was theoretically designed for the maximum realizeable gain so far is 33.3 dB.

The apparent loss of 7.7 dB was initially attributed to the 50/75 ohm impedance mismatch which featured in the test equipment connections due to the 50 ohm input/output terminals of these equipments. Also the frequency response suggests existence of some negative feedback paths and such negative feedback also reduces the gain. The fact that screening could not have been so perfectly done that radiative losses are completely eliminated is also appreciated. However, poor choice of the emitter by-pass capacitors proved to be largely responsible. This was discovered when one of the fragile 1000pF miniature ceramic capacitors used got damaged and was inevitably replaced with another 100 pF ceramic type. Because of the large improvement observed the other emitter capacitor was similarly replaced. The frequency response was re-tested, and with careful adjustment of the variable capacitors a gain of over 40 dB was realized at 192 MHz. The numerical values of this improved frequency response and the graphical plot are respectively shown in table 5.4 and figure 40.

TABLE 5.4

Numerical Results Of Frequency Response Measurements With Improved Gain

Frequency (MHz)	Voltage Gain	
	Numeric	Decibel
240	1.6	4.0
235	2.5	7.9
230	3.6	11.1
225	4.6	13.3
220	5.6	14.6
215	8.0	18.1
210	12.0	21.6
205	20.0	26.0
200	43.0	32.7
198	68.0	36.7
196	92.0	39.3
194	106.0	40.5
192	104.0	40.3
190	76.0	37.6
185	38.0	31.6
180	28.0	28.9
175	26.0	28.3
170	26.0	28.3
165	34.0	30.1
160	44.0	32.9
155	44.0	32.9
150	36.0	31.1
145	38.0	31.6
140	40.0	32.0
135	14.4	23.2
130	12.4	21.9
125	2	6.0

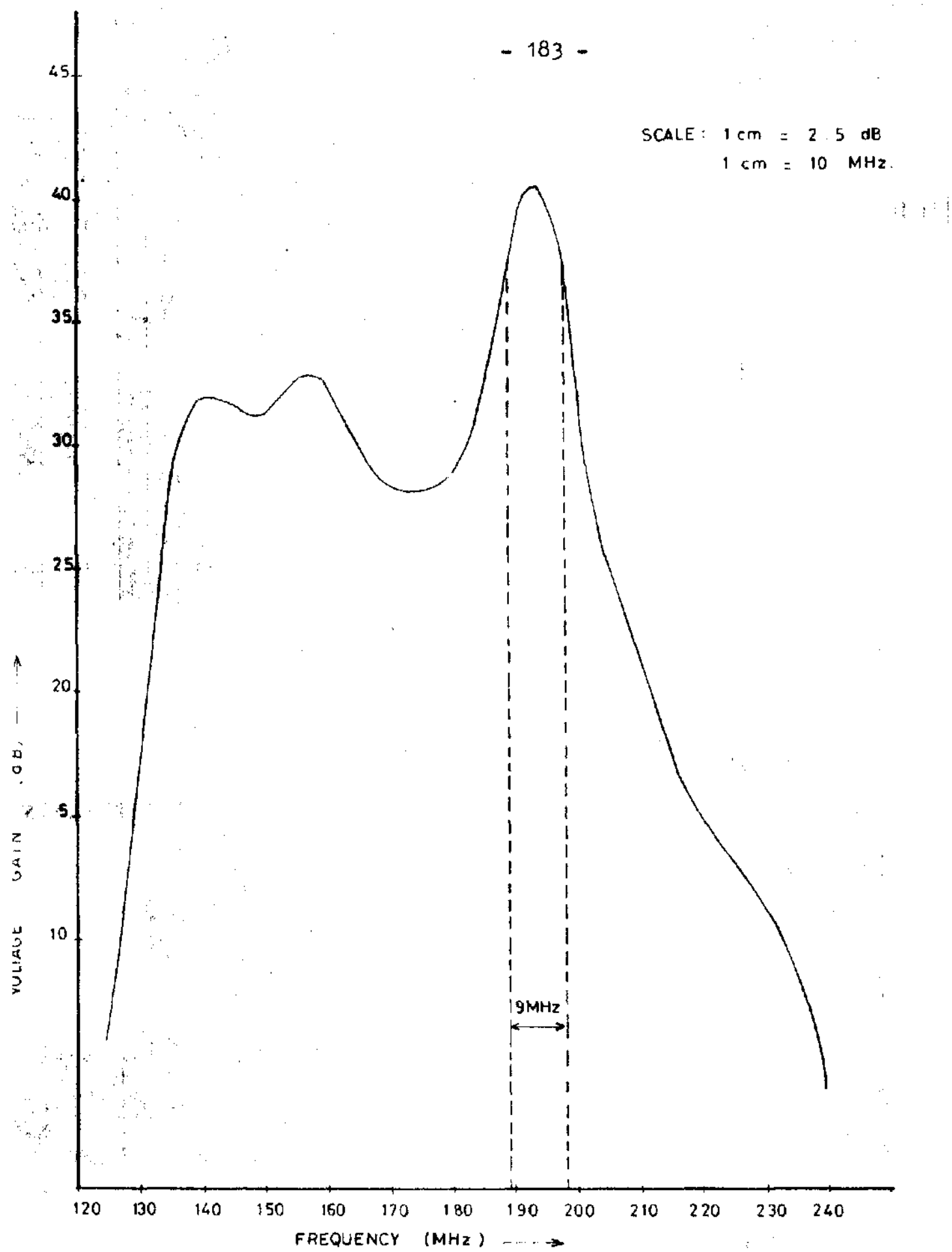


FIG. 40 — AMPLIFIER FREQUENCY RESPONSE WITH IMPROVED GAIN (R_E = 100 pF)

CHAPTER SIX

CONCLUSION

This research project primarily aims at two objectives: (1) To study the signal reaching Zaria from NTV Jos transmitter with a view to determining the major propagation mechanisms as well as highlighting the general signal behaviour. Thus contributing towards the collection of radio propagation data needed in Africa for checking out CCIR recommended curves on one hand, and possibly towards improvement of local Television services on the other; and (2) To actually design and construct a pre-amplifier which could be attached on a receiver antenna in Zaria so as to boost reception of NTV Jos signals with reasonable gain.

In line with these set goals NTV Jos signal was monitored in Zaria for a period of 13 months, and the statistical analysis of the field strength data has brought out some interesting results which will form a base for further investigations on the issue. A V.H.F. pre-amplifier capable of amplifying the 192 MHz NTV Jos carrier signal with a gain of over 40 dB has also been designed and constructed. Some of the more salient aspects of these results are discussed below.

Despite the fact that Zaria is far beyond the Jos transmitter horizon (about 200 km from Jos), strong field strength levels comparable with those of signals from Jaji (which is only 26 kilometres from Zaria) have been

received, and for reasonably long periods of time, especially during the rains. The main propagation mechanism has been identified as specular reflection. The increased impact of this mechanism due to the presence of thunderstorm cells in the troposphere explains the high correlation tendency observed between median signal levels and mean rainfall figures. It also explains the high median signal level of 30.5 dB (above 1 μV/m) obtained in more than 50% the reception time during the rainy season. Analysis based on the hourly median has also revealed that the intensity of thunderstorm activities - hence thunderstorm signal enhancement - falls sharply from October to November, and rises again from April to May.

The level of signal reaching Zaria from NTV Jos in the dry season is relatively much lower - being above 23.8 dB relative to 1 μV/m for 50% of the time - but still reasonably high. With little or no thunderstorm activities during this period, the propagation mechanism is predominantly scattering and/or diffuse reflection. The actual role of the high concentration of harmattan dust in the lower troposphere during the greater part of the dry season is yet to be exposed. The long distance from Jos to Zaria makes any positive contributions from the diffraction mode negligible. However, diffraction could account for a substantial amount of the attenuation of the transhorizon signals, especially in the region of

the Jos transmitter horizon (spherical diffraction) and inside Zaria (Knife-edge type of diffraction over buildings and trees).

In both wet and dry seasons signal level usually rise from the early evening hours into the night, with a rise rate of about 1 dB/hr higher in the rainy season than in the dry season; it then falls towards midnight, except for cases of abnormally high level of thunderstorm signal enhancement. The variation of daily median of signal level is higher in the wet season, and the statistical distribution of the 1.25 minutely medians approaches a log-normal distribution law.

One desirable effect of this signal behaviour is the fact that Zaria viewers can occasionally receive sufficiently strong signal from Jos, and thus for a while meet their desire for a multi-channel service. This situation can be made more permanent by coupling the receiving aerial to the receiver set via the low-noise booster amplifier attached to the former.

With the median signal level all through the period of measurement at 26.5 dB above 1 μV/m, such an amplifier can saturate a receiver set in Zaria with NTV Jos signal as high as 59.5 dB over 1 μV/m for more than 50% of the time. And even a better reception is possible if the receiving aerial itself is of reasonably high gain.

The other aspect of this signal behaviour is that it constitutes a potential interference source at Zaria, with

the proposed channel 7 from Funtua. Such a situation can be averted by re-allocating another channel to either of these stations, or by resorting to different polarization for the two.

As earlier pointed out, studies of this nature are usually carried out over extended periods of time for the results to be more reliable. It is therefore recommended that in such future work attempts be made towards exposing the actual role of the harmattan dust. It is also pertinent to monitor the humidity figures as well as cloud intensities so as to confirm that thunderstorm enhancement is more of a factor of atmospheric moisture content than of actual rainfall - a fact which will explain the observed high median signal levels even when the rainfall figures were low. Special attention should be given to the months of September and October to correct or confirm the result from the rather scanty data in September (that highest median signal levels are obtained in this month) and to establish whether the observed occurrence of very high level of thunderstorm activities around midnight in October was by chance of a normal trend. Variation in the surface value or the mean refractive index gradient can also be monitored to compare the monthly median of this gradient with the monthly median of signal level.

The effect of changing the height of the recieving antenna from 3 to 10 metres above the ground can be verified - CCIR* puts the expected values of

---

* (23), p.168

height gain in band III at 7 dB in flat terrain, and 4 - 6 dB in urban or hilly areas. This might shed some light on the role of the lower troposphere; Kühn et al* have suggested that it is erroneous to neglect this in radio propagation planning. Measurement of the ground constants around the Jos Transmitter horizon (about 40 km from Jos) will be complementary to this aspect of the study, as well as throw more light on the diffraction and ground-reflection losses in the radio path. And the need to extend field strength measurements to 24 hours of the day (where possible) cannot be overemphasized.

Further work is also anticipated towards improving the amplifier performance by including a third stage and hence further improving reception conditions for NTV Jos signals in Zaria. And until results have been accummulated and compiled from similar studies carried out at different times and different frequencies, reliable data for checking out CCIR recommended propagation curves for Africa would not be assumed to have been obtained.

APPENDIX A

THE COMPUTER PROGRAMS

A.1 Program For Data Conversion

This program converts each month's data into a form suitable for analysis by:

(1) adding to or subtracting the appropriate dB figure from each day's signal level, depending on whether the transmitted power for the day is less or greater than the nominal 7.5 kW value, and

(2) adding to each data a constant of 12.9 dB due to the antenna factor and extra cable loss.

The program is run with two other data files - one containing the data for a particular month (as extracted from the chart) and the other containing the daily power transmission (in dB) for the same month.

The example given here uses data file for the month of June 1980; for months ending in 31 days, all the 30's in the program must be changed to 31 accordingly, and the 10 in statement No.20 changed to 11:

```
Program N(Num, June 80, Output, tape 1 = Num,
tape 5 = June 80,  tape 6 = Output)

Dimension Umber  (30), Number (30), Line (30),
IROW(30)
```

```
      DO  10  I = 1,30
      IROW(I) = 0
      Number(I) = 0
10    Continue
      Read (1,20) (Umber(I), I = 1, 30)
20    Format (20 (F 3.1)/10 (F3.1) )
      DO 30 I = 1, 30
      Umber(I) = 10.0 * Alog 10(Umber(I)/7.5)
      Number(I) = Ifix (Umber(I) + Sign (0.5, Umber(I)))
30    Continue
40    Read (End = 99, 5, 50) (Line(I), I = 1,30)
50    Format (30(I 3, IX) )
      DO 60 K = 1, 30
      If (Line (K). GT . 800)  then
      IROW (K) = Line (K)
      Else
      IROW(K) = (Line(K) - Number(K) * 10) + 129
      End if
60    Continue
      Write (6, 70) (IROW(I), I = 1,30)
70    Format  (IX, 30(I3, IX))
      Go to 40
99    Stop
      End
```

After this conversion the output is re-named June 80, and the original June 80 file is replaced by this new one.

A.2 Program For Daily Median

This program is part of the Statistical Package for the Social Sciences (SPSS). Each line comprises two segements, the first of which must start from the first column and the second from column 16; also the 30's change to 31 for 31-day months:

Run name	Oyedum's Project
Pagesize	No eject
Variable List	Day 1 to day 30
Input Medium	Disk
Input Format	Fixed (30(IX, F 3.0))
N of Cases	Unknown
Missing Values	Day 1 to day 30 (970, 980, 990)*
Frequencies	General = ALL
Statistics	3
Read Input Data	
Finish	

This program is stored in a permanent file (called Median in this analysis) and is run with a copy of the converted monthly data file renamed and saved as Janc80. Use is made of the SPSS command after increasing the RFL and setting the Time Limit:

```
RFL , 65000
Settl, 7777
Get, Median, Janc 80
```

---

* SPSS may not accept more than 3 missing values.

```
Attach, Spss/un = Library
Spss, I = Median,  D = Janc 80 ,  L = 11.
Rewind, LL.
Dispose, LL = PR
Clear
Exit.
** Unsuccessful Run **
```

This command may be stored in a permanent file also (called DO) in this analysis because it is made use of many number of times. In that case, once Janc 80 has been replaced by a copy of the monthly data whose median is sought, all that is needed is a short command:

```
Call, DO.
```

A successful run is indicated by EXIT while an unsuccessful run is so indicated. Two common causes of unsuccessful runs are output limit and failure to change the 30's to 31's in the program (median) when handling a 31-day month or vice-versa.

A.3 Program Transforming Hourly Data Into a Column Matrix

The need to arrange all the data corresponding to an hour in a column arises due to the fact that Spss handles data in column wise.

Since each of the first six hours contains 48 rows, this program transforms a 48, 31 (or 30) matrix into a column matrix. The 7th hour usually contains a less number of rows.

The program is run with a local file containing only the data for a particular hour of a particular month. The procedure was to get a copy of the month's data into a local file (called A A) and edit this local file so that it contains only the required hourly data by deleting the unwanted parts. The output is also Janc 80 and must replace the already saved Janc 80 :

```
      Program Name (AA, Janc 80 , Tape 5 = AA, Tape 7 = Janc 80
      Dimension IROW (1488),  Line (31)
      DO  10  I = 1,  1488
      IROW(I)    = 0
  10  Continue
      I = 1
  66  Read (End = 99, 5, 40) (Line(N), N = 1, 31)
  40  Format (IX, 31 (I3, IX))
      DO 45 J = 1, 31
      IROW (I) = Line (J)
      I = I + 1
  45  Continue
      Go to 66
  99  Write (7, 50) (IROW (I), I = 1, 1488)
  50  Format (IX, I5)
      Stop
      End.
```

Although the 7th hour contains less than 1488 data, statement No.99 causes zeros to be written in the last rows of the output to bring up the number of lines to 1488;

this new Janc 80 must therefore be edited to remove these zeros before replacing the previous contents of the file with it.

For execution it is necessary to increase the line printer limit thus:

Mnf, i = HH, P = 10,000, L = LL
where HH is the name of the procedure file containing the program (A.3)

A.4 Program For Finding Hourly Median

This program is similar to A.2; the only difference is that the "Day 1 to day 31" now becomes "Hour 1", but the program runs successfully without making this change. It is in a permanent file (called Median 1) and may be run with the contents of the DO file if the term 'median' is changed to "Median 1". This modified DO is stored in another file called "Doforme" in this analysis, so that once the contents of Janc 80 is correct, all that is necessary is a "Call, Doforme" command.

A.5 Program For Transforming Monthly Data Into A Column Matrix

This program is a modified form of A.3. Since the program handles all the contents of a given month's data file at a time, all the 1488 in A.3 must now be replaced by a figure which corresponds to the total number of lines in the file multiplied by 31 (for a 31-day month) i.e. the number of data (T) in the file; this may be quickly verified

by finding the total number of lines (L) so that
T = L x 31.

The program is also run with a data file (called A A) which must now contain a local copy of all the data for the month in question. This replaces whatever the contents of A A were.

The line printer limit must also be further increased during the execution command:

mnf, i = HH 2 , P = 30,000, 1 = L L

and the output which is also Janc 80 must now replace the previous contents of this file.

A.6 Program For Finding Monthly Median

The program is exactly the same with A.4, except that 'hour 1' may now be changed to 'Month 1', still the program runs without this change. It also uses the "Call, Doforme" command, provided that the Janc 80 file has the right contents - i.e. the whole data of the right month arranged in a single column.

APPENDIX B(1)

TABLE OF DAILY RAINFALL IN ZARIA (mm), JULY 1979 - JULY 1980

DATE	JUL. 1979	AUG. 1979	SEP. 1979	OCT. 1979	NOV. 1979	DEC. 1979	JAN. 1980	FEB. 1980	MAR. 1980	APR. 1980	MAY 1980	JUN. 1980	JULY 1980
1	0	0.6	0	11.6	0	0	0	0	0	0	26.1	*	42.1
2	0	0	15.1	0	0	0	0	0	0	0	1.0	*	0.8
3	22.9	0	18.1	0	0	0	0	0	0	0	0	44	0.9
4	27.6	30.3	2.0	0	22.4	0	0	0	0	0	0	0	*
5	0.1	0	0	5.1	0	0	0	0	0	0	0	24	9.2
6	15.3	0	0	0	0	0	0	0	0	0	22.1	0	0
7	55.2	19.4	. 2	12.1	0	0	0	0	0	0	0	0	0
8	13.1	0	11.9	*	0	0	0	0	0	0	0	11.4	0.7
9	6.9	0.4	2.6	0	0	0	0	0	0	0	0	0	0
10	7.9	0	*	0	0	0	0	0	0	0	0	0	*
11	11	5.7	2.0	0	0	0	0	0	0	0	0	42.6	60.6
12	1.4	0.8	2.3	3.6	0	0	0	0	0	0	0	0	7.4
13	0	12.8	0	0	0	0	0	0	0	0	0	9.1	0
14	0	*	0	0	0	0	0	0	0	0	0	0	27.1
15	0.4	*	17.2	0	0	0	0	0	0	0	0	0	1.0
16	40.3	0	4.7	0	0	0	0	0	0	0	0	0	23.6
17	37	27.3	0	0	0	0	0	*	0	0	0	0	4.4
18	*	19.3	0	0	0	0	0	0	0	0	0	32.7	0
19	*	0	0	0	0	0	0	0	0	0	21.5	0	18.5
20	0	29.7	0	0	0	0	0	0	0	0	2.5	*	2.5
21	13.6	6.5	*	0	0	0	0	0	0	0	0.8	0	0
22	*	5.5	*	0	0	0	0	0	0	0	0	5.9	29.5
23	*	0	11.2	0	0	0	0	0	0	0	2.4	0	8.4
24	0	*	15.2	0	0	0	0	0	0	0	0	2.9	0
25	0	21.3	*	*	0	0	0	0	0	0	0	0	3.9
26	15.0	0	8.0	0	0	0	0	0	0	0	2.9	0	8.0
27	17.2	55	0.2	0	0	0	0	0	0	0	13.3	0	3.8
28	*	4.2	*	0	0	0	0	0	0	20.2	0.5	0	0
29	0	6.8	5.6	0	0	0	0	0	0	0	0	0	0
30	42.5	9.9	0.2	0	0	0	0	0	0	0	7.3	0	10.6
31	45.7	6.2	-	0	0	0	0	0	0	0	*	0	5.0
MEAN	11.7	8.4	3.9	1.1	0	0	0	0	0	7	3.3	3.7	8.7

* Trace Rainfall

APPENDIX B(2)

TABLE OF DAILY RAINFALL IN JOS (IN mm) JULY 1979 - JULY 1980

DATE	JULY 1979	AUG 1979	SEPT 1979	OCT 1979	NOV 1979	DEC 1979	JAN 1980	FEB 1980	MAR 1980	APR 1900	MAY 1980	JUNE 1980	JULY 1980
1	0	3.4	23.7	0	0	0	0	0	0	0	40.7	21.5	6.3
2	-	15.4	2.1	0	*	0	0	0	0	0	0	0	5.3
3	12.6	5.6	22.6	3.8	0	0	0	0	0	0	12.3	*	0
4	10.6	5.6	0	0	6.7	0	0	0	0	0	0	0	7.5
5	7.9	7.6	0	8.1	*	0	0	0	0	0	21.3	6.0	2.6
6	3.3	1.2	7.9	0	0	0	0	0	0	0	15.0	0	1.6
7	20.1	*	0	0	0	0	0	0	0	0	0	0	4.0
8	*	*	7.5	*	0	0	0	0	0	0	24.4	*	45.4
9	3.4	*	7.7	0	0	0	0	0	0	0	0	0	*
10	0	11.9	0	0	0	0	0	0	0	1.9	0	0	*
11	40.4	23.8	0	0	0	0	0	0	0	0	0	22.9	1.9
12	21.4	7.1	*	3.2	0	0	0	0	0		0	0	6.3
13	0	19.6	*	0	0	0	0	0	0		0	20.1	0
14	18.1	15.6	0	0	0	0	0	0	0		0	0	0
15	*	*	22	0	0	0	0	0	0		18.8	0	*
16	6.4	54.1	2.5	0	0	0	0	0	0		24.5	1.9	25.9
17	13.7	8.4	1.6	0	0	0	0	0	0		0	5.0	*
18	10.1	13.4	0	0	0	0	0	0	0		10.0	32.4	10.2
19	9.9	*	0	0	0	0	0	0	0		2.8	3.5	27.8
20	0	36.6	2.6	0	0	0	0	0	0	1.6	0	10.0	16.8
21	4.1	3.5	23.1	0	0	0	0	0	0	*	21.7	3.3	*
22	16.9	10.1	16.7	0	0	0	0	0	0.8	0	0	5.4	35.2
23	0	*	*	0	0	0	0	0	3.5	0	10.0	*	0.9
24	30.1	38.1	0	0	0	0	0	0	*	2.8	0	33.2	*
25	25	11.2	2.0	0	0	0	0	0	9.9	0	12.3	0	15.4
26	0	0	24.6	0	0	0	0	0	0	0	0	*	*
27	0	6.7	*	*	0	0	0	18.1	0	0	0	*	0
28	10.1	3.4	0	0	0	0	0	*	0	5.0	7.1	0	5.4
29	1.4	6.9	6.3	0	0	0	0	0	0	0	0	0	10.4
30	7.7	0	3.3	0	0	0	0	-	0	0	12.3	1.1	10.9
31	3.5	*	-	0	0	00	0	-	0	-	5.2	-	*
MEAN	8.2	10.0	5.2	.5	.2	0	0	.6	.5	.4	7.7	5.5	7.7

APPENDIX C

TABLE OF DAILY TRANSMITTED POWER (IN kW) FROM NTV JOS

JULY 1979 - JULY 1980

Day / Month/ Year	July '79	Aug. '79	Sept. '79	Oct. '79	Nov. '79
1	9.0	8.5	7.5	7.5	8.0
2	8.5	8.5	7.5	7.5	8.2
3	8.3	8.5	6.5	9.5	8.5
4	8.5	7.6	6.5	8.5	8.5
5	7.8	8.0	7.5	8.5	8.3
6	7.5	7.5	8.5	9.0	8.4
7	7.5	6.9	7.5	7.4	7.0
8	9.0	7.5	7.8	8.5	7.0
9	8.0	8.8	7.8	9.5	8.5
10	8.0	9.0	8.0	7.5	8.5
11	7.8	8.0	7.2	8.3	8.0
12	7.5	8.5	8.2	9.4	8.5
13	7.5	9.0	7.5	8.5	8.0
14	7.5	9.3	9.5	8.5	8.5
15	7.5	9.0	9.5	8.5	8.5
16	7.8	9.0	8.5	8.5	8.5
17	8.5	9.4	9.0	7.7	8.4
18	8.0	9.5	9.0	8.5	8.0
19	8.5	9.0	7.8	8.0	8.5
20	8.5	9.0	7.5	7.5	9.0
21	7.5	7.5	8.0	9.0	8.0
22	8.0	7.5	7.2	8.5	8.9
23	8.5	8.5	7.0	8.5	9.0
24	7.5	7.2	8.5	8.0	8.0
25	7.5	7.5	9.0	8.5	9.0
26	6.5	6.2	8.8	8.0	8.5
27	9.5	6.5	8.5	7.5	7.6
28	7.8	6.9	8.0	7.5	10.0
29	8.2	7.0	9.0	8.5	7.1
30	8.0	7.5	9.0	8.5	8.5
31	8.0	7.5	-	7.5	-

NTV JOS DAILY TRANSMITTED POWER CONTD.

Day / Month/ Year	Dec.'79	Jan.'80	Feb.'80	Mar.'80	Apr.'80	May'80	Jun.'80	Jul.'80
1	8.0	7.6	8.2	7.4	8.0	7.5	7.0	7.5
2	8.0	7.5	7.7	7.0	7.5	8.0	7.0	7.5
3	8.0	6.5	7.0	7.2	7.5	7.5	7.5	7.5
4	8.5	8.0	8.0	7.4	7.5	7.5	7.4	7.5
5	7.5	6.4	8.0	7.5	7.8	7.5	7.5	7.4
6	9.0	7.5	8.0	8.0	7.5	7.5	7.0	7.5
7	7.5	8.6	9.0	8.2	7.5	7.0	8.5	7.8
8	8.5	7.5	6.9	8.0	8.0	7.0	8.0	7.5
9	7.0	7.0	8.0	6.8	8.0	7.5	8.0	8.0
10	9.5	7.0	8.2	7.0	8.0	8.4	8.0	7.5
11	8.5	7.0	8.0	7.0	8.0	8.0	8.5	7.5
12	7.0	7.5	7.5	7.0	8.0	8.0	8.5	7.5
13	7.5	8.0	7.5	8.4	6.5	8.0	7.4	7.5
14	8.5	8.0	7.2	8.0	7.5	8.0	8.4	8.5
15	7.5	9.0	7.2	8.5	8.0	8.0	7.5	9.5
16	7.0	6.5	7.2	8.5	8.0	7.0	8.0	9.0
17	7.5	8.0	7.6	8.4	7.5	7.0	7.7	8.5
18	7.3	7.0	8.0	7.4	7.5	7.0	8.0	7.5
19	7.5	7.5	7.4	8.0	7.0	7.0	8.0	8.0
20	7.8	8.0	7.4	7.5	7.2	6.5	7.0	7.5
21	7.5	8.0	7.0	7.0	7.5	7.5	7.0	7.5
22	8.5	8.0	8.0	7.0	7.5	8.0	7.0	8.0
23	9.0	8.0	7.5	6.5	8.0	8.4	7.5	8.0
24	6.0	8.0	8.0	7.2	8.0	8.0	7.0	7.5
25	8.0	8.0	8.0	7.0	7.0	8.2	7.5	7.5
26	9.5	8.0	6.5	7.3	8.5	8.5	7.5	7.5
27	7.5	8.0	7.3	7.0	7.6	8.5	7.5	7.5
28	8.0	7.0	7.2	8.0	8.0	8.0	7.0	7.5
29	8.5	7.0	7.2	7.5	8.4	8.0	7.0	7.5
30	8.5	7.0		7.6	8.5	8.0	7.5	7.5
31	8.0	8.0				7.5		7.5

APPENDIX D

LISTS OF COMPONENTS USED AND THEIR SPECIFICATIONS

1. RESISTORS:

Resistance	Tolerance	Power Rating	Type
100 ohms	± 10%	½	Carbon
150 ohms	± 5%	½	Carbon
430 ohms	± 5%	½	Metal Film
1.1 kilo ohms	± 5%	½	Metal Film

2. CAPACITORS:

Capacitance	Voltage Rating	Type
15 pF	100 V d.c.	Ceramic
1000 pF	"	"
2 - 10 pF	-	Variable
5.5 - 65 pF	-	"
100 pF	-	Ceramic

3. INDUCTORS*

L (u H)	No. of Turns	Extension (mm)	Diameter (mm)	Q_u	S.W.G.
.0483	1½	4.6	12.3	250	16
.0454	1½	3.5	12.3	235	"
.0210	1	3.2	9.3	120	"
.010	¾	-	6.8	75	"

---

* See Table 5.2

LIST OF REFERENCES

1. Alley, Charles, L. and Atwood, Kenneth, W. (1973), Electronic Engineering. John Wiley and Sons Inc. pp. 123 - 154, 273 - 334.

2. Aurray, J. and Fourier, M. (1973), Problems In Electronics. Pergamon Press, Oxford, pp. 142 - 166, 246 - 160.

3. Bishop, G.D. David (1973), Electronics II. Macmillan Press Ltd. pp. 38 - 56.

4. Casasent, David (1973) Electronic Circuits. Quantum Publishers, Inc., New York, pp. 48 - 74.

5. Chipman, Robert, A. (1968), Transmission Lines. Schaum's Outline Series, McGraw Hill Book Company.

6. Dolukhanov, M. (1971), Propagation of Radio Waves. Mir Publishers, Moscow, pp. 9 - 356.

7. Du Castel, Francois, (1966), Tropospheric Radio Propagation Beyond The Horizon Pergamon Press, London, pp. 6 - 51, 62 - 97, 107 - 134, 139 - 202.

8. Graham, E.D. and Gwyn, C.W. (1975), Microwave Transistors. Artech House Inc. pp. 479 - 488.

9. Halkias, Christos, C. and Milman, Jacobe (1972), Integrated Electronics: Analog and Digital Circuits And Systems. McGraw-Hill, Kogakusha Ltd., pp. 447 - 482.

10. Hamsher (1967), Communication Systems Engineering Handbook. McGraw-Hill, U.S.A.

11. Jasik, Henry (1961). Antenna Engineering Handbook. McGraw-Hill Book Co., Inc., U.S.A., pp. 31 - 1 to 31 - 16, 33 - 1 to 33 - 27.

12. Kühn, U. and Täuma, F. (1974). "Some New Results of Propagation Measurements and Their Application for Planning Transmitter Networks", IEEE Transactions On Communications, Vol. COM - 22, No.9 pp. 1394 - 1402.

13. Lampitt, R.A. (1965), Network Analysis For Telecommunications and Electronics. Illife Books Ltd., London. pp. 35 - 45.

14. Lenk, John D. (1974), Handbook of Modern Solid State Amplifiers. Prentice-Hall Inc., New Jersey, pp. 14-33, 14 - 33, 141 - 152, 156 - 215.

15. Loveday, G.C. (1977). Electronics Fault Diagnosis. Pitman Publishing Ltd., London.

16. Norman, Lurch, E. (1981), Fundamentals Of Electronics, John Wiley and Sons.

17. Pannett, W.E. (1967),
Dictionary of Radio and Television. Butler and Tanner Ltd., London.

18. Peeran, S.M. (1980),
Computer Analysis of NTV Jos Field Strength Measurements Recorded at Zaria; Part III Project Thesis of the Department of Electrical Engineering, A.B.U., Zaria. pp. 1-24, 105 - 123.

19. Simpson, A. (1979).
Testing Methods and Reliability - Electronics, Macmillan Press Ltd.

20. Microwaves Associates: Transistor Designers Guide (1978), Bullettin No. 5210, U.S.A.

21. Texas Instruments Incorporated: Solid State Communications, (1966). McGraw-Hill Company, U.S.A.

22. CCIR Document on the Xth Plenary Assembly, Geneva, (1963) Vol.V, Rec. 418; pp. 58 - 68.

23. CCIR Document on the XIIIth Plenary Assembly, Geneva, (1974): Vol.V, pp. 39 - 41, 48 - 51, 55 - 79, 113 - 142, 155 - 176, 185 - 192, 209 - 245, 259 - 287.

24. Kluge, James E. (1977),
"Advanced Antenna Design and An Ultra Low-Noise Preamplifier Extend U.H.F. Viewing Area",
IEEE Transactions on Broadcasting, Vol. BC - 23, No.1, pp. 17 - 22.

25. Sears, W. et al (1980),
College Physics, Addison - Welsley Publishing Company,
London, pp. 4504 - 505.

26. Bolton, W. (1974),
Patterns in Physics McGraw-Hill Book Company (UK)
Ltd., London, p. 309.

27. Haltiner, G.J. and Martin, F.L., (1957)
Dynamic and Physical Meteorology McGraw-Hill Book
Company, New York, pp. 21 - 72, 125 - 141.

28. Hall, M.P.N. (1979),
Effects of The Troposphere On Radio Communication
Peter Peregrinus Ltd. (for IEEE London and New York).

29. Oyedum, O.D. (1977)
Atmospheric Temperature Structure Over Oshodi - Lagos
Final Year Project Thesis of the Department of Physics,
U.N.N., pp. 42 - 48, 65 - 66, 82 - 83.